COUPLED NUMERICAL ANALYSIS OF VARIATIONS IN THE CAPACITY OF AN ENERGY PILE IN CLAY SOIL

by

Daniel Patrick Zimmerman

A thesis

submitted in partial fulfillment

of the requirements for the degree of

Master of Science in Civil Engineering

Boise State University

December 2016

BOISE STATE UNIVERSITY GRADUATE COLLEGE

DEFENSE COMMITTEE AND FINAL READING APPROVALS

of the thesis submitted by

Daniel Patrick Zimmerman

Thesis Title: Coupled Numerical Analysis of Variations in the Capacity of an Energy Pile in Clay Soil

Date of Final Oral Examination: 21 October 2016

The following individuals read and discussed the thesis submitted by student Daniel Patrick Zimmerman, and they evaluated his presentation and response to questions during the final oral examination. They found that the student passed the final oral examination.

Arvin Farid, Ph.D.	Chair, Supervisory Committee
Chittoori Bhaskar, Ph.D.	Member, Supervisory Committee
Debakanta Mishra, Ph.D.	Member, Supervisory Committee

The final reading approval of the thesis was granted by Arvin Farid, Ph.D., Chair of the Supervisory Committee. The thesis was approved by the Graduate College.

ACKNOWLEDGMENTS

I would like to thank my advisor, Dr. Arvin Farid, for his guidance throughout this project. He has made himself available to me more times than I can count. He has patiently, and sometimes impatiently, walked me through concepts that I wouldn't have otherwise understood. I am grateful for the many opportunities he has offered to me. I have learned so much from him, and not all of it is academic. I doubt I could have succeeded without him.

I would also like to thank the other members of my thesis defense committee, Dr. Deb Mishra and Dr. Bhaskar Chittoori, for being a part of my committee under the circumstances.

Finally, I would like to thank my family for their love and support. I am especially indebted to my wife, Julie, for her seemingly limitless patience, love, and acceptance. This has been a journey of self-discovery for me. I have both expanded my limits and discovered my limitations. I would not give up, and I am grateful to you, Julie, for not giving up on me. I am eternally humbled.

ABSTRACT

Energy piles are an emerging alternative for the reduction of energy consumption to heat and cool buildings. The majority of the research to date focuses on thermodynamic properties or axial strain of piles. This paper concerns the effects of temperature fluctuation on the capacity of driven energy piles in clayey soils. Consolidation of clay (due to the dissipation of excess pore-water pressure in clay) surrounding piles affects the capacity of the pile (pile setup in clay). Reciprocally, it is reasonable to assume that heating and cooling periods will create or relax the excess pore-water pressure (EPWP) in clayey soils (due to the contraction and expansion of water) affecting the pile capacity. In the meantime, the thermal expansion and contraction of the pile also generates or relaxes the EPWP in the soil, which can be computed using the principle of cavity expansion theory. The resulting change in the EPWP due to the thermal cycle happens through day and night and is much faster than the drainage time required by the clay. This lack of time for dissipation of EPWP affects the effective stress and, hence, the capacity of the pile.

Hence, there is a need for an analysis that couples: (i) consolidation of clay, (ii) thermal expansion/contraction of pile and, in turn, the resulting relaxed/generated EPWP in clay, and (iii) thermal expansion/contraction of soil and, in turn, the resulting generated/relaxed EPWP in clay computed through cavity expansion theory. Therefore, a numerical analysis model was developed to analyze the generation and dissipation of

the EPWP resulting from all of these phenomena. This coupled analysis helps compute the variations of the generated EPWP and, in turn, its effect on the effective stress and, hence, pile capacity.

The numerical model also supports the hypothesis that the heating effect can accelerate the pile setup in clay. This flexible model can be used to estimate the ultimate capacity of energy piles, or even evaluate the possibility of using heating through construction to expedite pile setup in clay.

TABLE OF CONTENTS

LIST OF TABLES

LIST OF FIGURES

CHAPTER 1: INTRODUCTION

Motivation

Energy piles are an emerging alternative for the reduction of fossil-fuel energy consumption to heat and cool buildings. Energy piles combine ground-sourced heating and cooling systems with the building's foundation. In recent history, heat exchange within the soil had been accomplished by horizontal heating and cooling beds, or heat sinks outside of the building footprint. The use of ground-source heat pumps (GSHPs) requires additional ground surface outside of the building footprint. This requirement eliminates their use in most urban settings. While GSHPs require less energy to heat and cool structures, they have not been widely used in the United States due to higher installation costs than conventional heating and cooling methods (McCartney and Rosenberg, 2011). Building foundations that incorporate GSHPs (energy piles) may have advantages over separate foundation and GSHP systems including lower installation costs and no requirement for additional space. Energy piles serve the dual purpose of supporting the structure and serving as a heat exchange medium. Energy piles have been installed in Austria and Switzerland for the last 30 years and are gaining popularity in other parts of Europe (Brandl, 2009). Energy piles have not yet been embraced by the United States, mainly due to insufficient research concerning the effects of temperature fluctuation on the stress state of the foundation soils (McCartney and Rosenberg, 2011).

The adverse effect from energy piles may arise from the cyclic thermal loading of soils. In other words, the cyclic temperature change results in cyclic loading, which can,

in turn, result in a reduction of the pile capacity. The cyclic thermal loading in coarse-grained soils can affect the shear strength of soil, since shear strength can be temperature-dependent. However, in fine-grained soils such as clay, in addition to temperature-dependent shear strength, the thermal cyclic loading can cause cyclic variations of excess pore-water pressure (EPWP). Cyclic variations of EPWP cause cyclic variation of effective stress, which leads to fatigue and reduction of shear strength.

The focus of this thesis is on the latter effect, i.e., the effect of cyclic thermal loading on the capacity of energy piles embedded within fine-grained soils.

Background

There can be three types of energy-pile construction. Energy piles can be constructed from prefabricated concrete piles, drilled shafts, or auger-cast piles. In an energy pile, polyethylene tubing is laid in a continuous loop within the interior of the pile, usually attached to the reinforcing steel and extending the entire length of the pile. Polyethylene tubing is used because of its flexibility and corrosion-resistant characteristics (Ebnother, 2008). The tubing is filled with a conducting medium such as water, water mixed with antifreeze, or a saline solution (Brandl, 2009). During warm weather, excess heat from the building is collected and transferred to the subsurface soil via the energy pile. Conversely, during cold weather, heat is extracted from the ground and is used to heat the building.

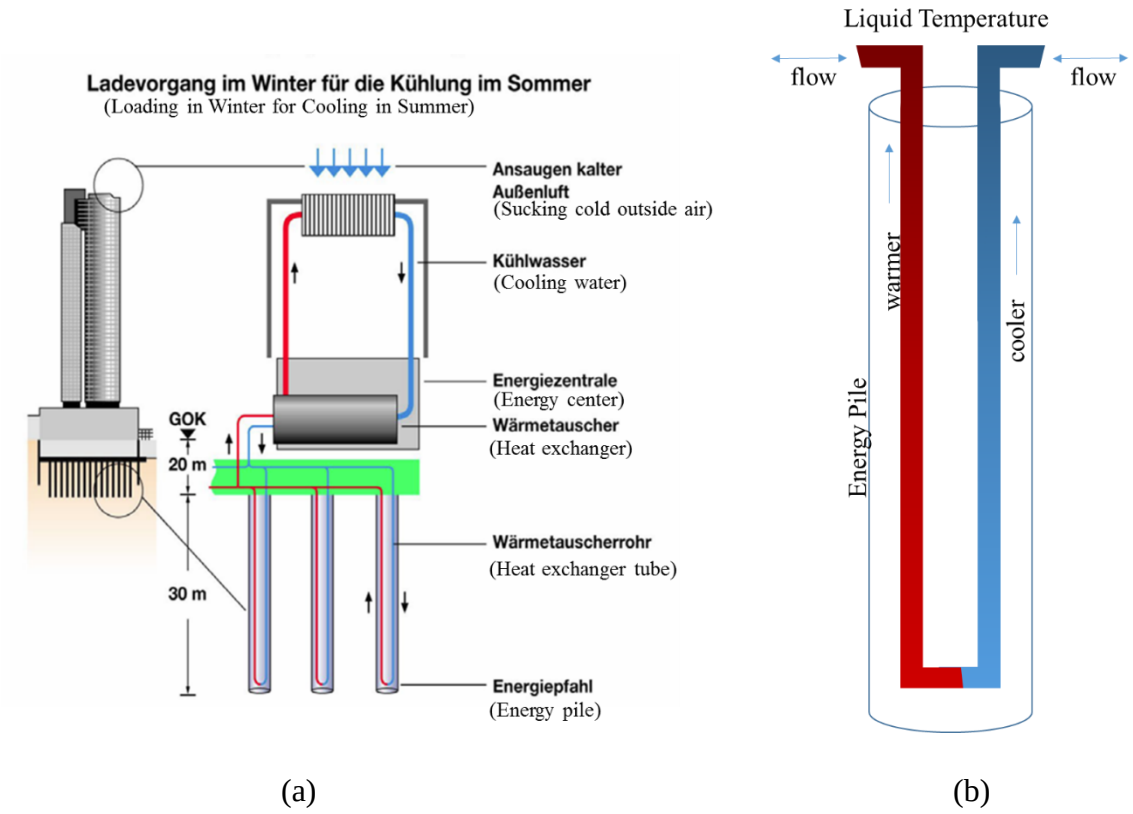

(a) (b)

Figure 1.1. (a) A schematic of a building's heating and cooling system with an energy pile system (Ebnother, 2008) and (b) A simple schematic of an energy pile with flow tubing.

Energy piles with diameters ranging from 0.3 to 0.5 m are assumed to extract 40 to 60 W/m (Watts per meter of depth), and energy piles with diameters greater than 0.6 m can extract 35 W/m^2 of earth-contact area for feasibility studies and pre-design (Brandl, 2009). Ebnother (2008) presented exchange rates between 20 and 100 W/m of depth.

Of the three types of energy pile installations described above, drilled shafts are likely the most versatile. Precast energy piles have load and length restrictions. Precast energy piles are likely to be up to 40 cm in width and have lengths of approximately 14 m. Precast piles are also not appropriate for some subsurface conditions such as soils with large gravel or cobbles present or for penetrating stiff or dense strata. While some precast

piles may be trimmed, precast energy piles cannot, due to the continuous tubing present. Therefore, precast energy piles are most suitable for use as friction piles. Precast energy piles may also be used as end-bearing piles under conditions where the penetration depth is predetermined or uniform.

Auger-cast piles are constructed with a hollow continuous-flight auger that serves as casing which is extracted while grout is injected into the auger hole. Steel reinforcement and the tubing for the GSHP are then lowered into the grouted hole (Coduto, 2001). The grout would likely have a high slump in order to allow the reinforcement and tubing to be correctly placed, or else voids could be created, affecting the structural integrity of the pile.

Drilled shafts allow the most versatility for use as energy piles. They can be drilled to any desired depth. They can also be constructed with larger diameters. The reinforcement can be properly installed prior to concrete placement, and concrete placement can also be controlled. Because of their versatility, higher potential capacity, and reduced uncertainty, drilled shafts can be used as GSHPs for large structures in a large variety of subsurface conditions.

The goal of this thesis is to help advance the understanding of energy pile performance. The majority of research on energy piles to date has focused on axial displacement of the pile due to thermal and mechanical loading. The piles may also be load tested during heating and cooling cycles. Little research has been performed to date that focuses on the spatial change of soil properties surrounding and in the vicinity of energy piles and the change in the pile capacity of an energy pile that results from cyclic thermal loading.

A numerical model analyzing the effects of temperature variation on pile capacity could help advance research on the feasibility of energy pile implementation in the United States and abroad. The work performed in this thesis is the result of only numerical simulation. Lab- and field-scale experimental simulations are also needed to achieve the certainty necessary to justify the efficacy of this model. However, it is hoped that this research will help researchers performing future lab- and field-scale experimental simulations.

Scope

This thesis focuses on the numerical analysis of the relationship between consolidation of clay around a cylindrical energy pile and the change in the temperature of the soil surrounding the energy pile, over time, resulting in variations in the pile capacity. A coupled numerical model has been developed using principles of axisymmetric (radial) and vertical primary consolidation of, and heat transfer through, saturated, slightly over-consolidated clay around both a drilled shaft and a driven circular energy pile. The increase / decrease of EPWP due to temperature variations in clay and the expansion or contraction of the pile will be modeled and analyzed in this work.

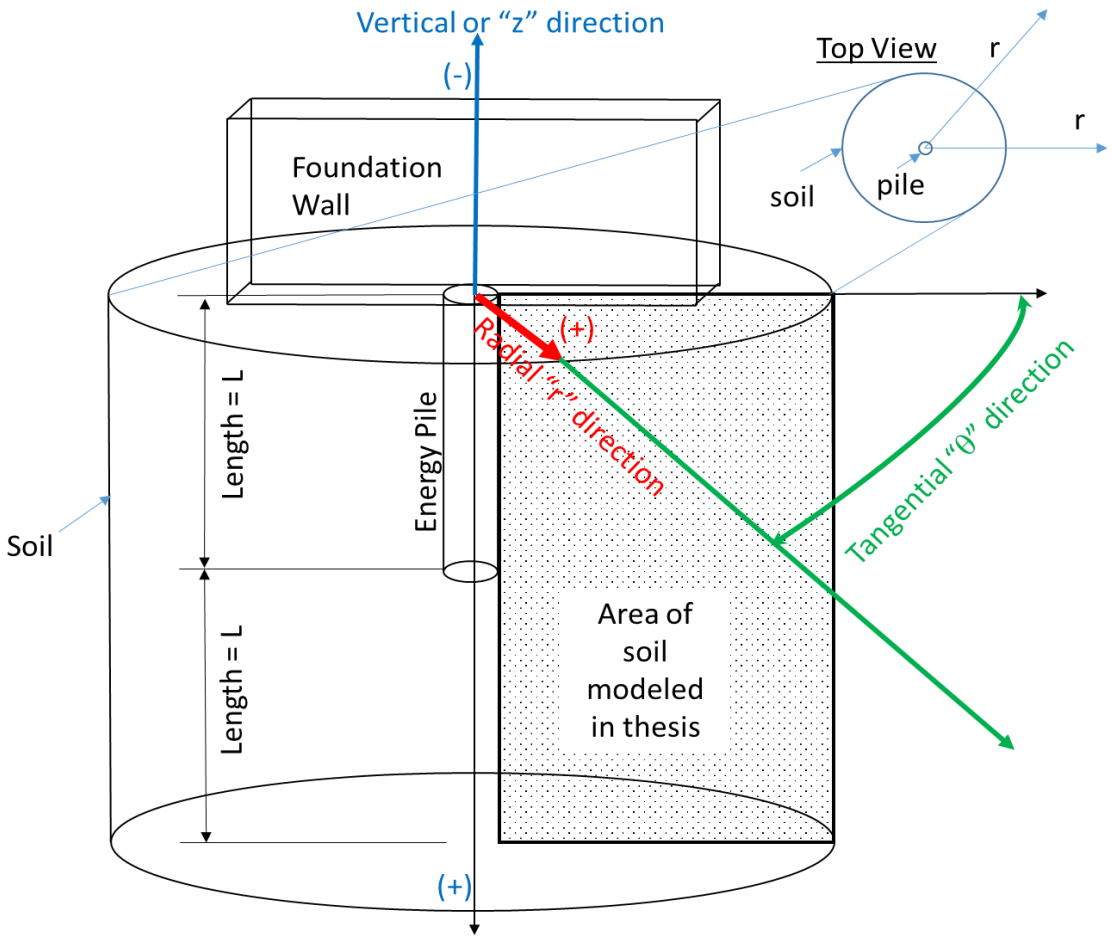

Figure 1.2. The layout of the model energy pile and simulated soil in cylindrical coordinates. Temperatures fluctuate between - 1 °C and + 51 °C in the soil adjacent to the energy pile over the course of a year in the model.

The objective of this numerical simulation is to estimate pile capacity variation in drilled shafts and driven piles utilized as GSHPs during heating and cooling cycles. The temperature of the soil surface adjacent to the energy pile was varied to simulate seasonal heating and cooling demands. Temperature changes adjacent to the pile were on the order of 52 °C (- 1 °C to + 51 °C) between peak heating and peak cooling temperatures. The model simulated the three-dimensional (3D) axisymmetric (i.e., radial and vertical) dissipation of the EPWP through the clay surrounding the pile. The resulting temporal and spatial variations of the pile capacity due to this cycling were computed. Thermal

conductivity coefficients and specific heat capacities for the soil matrix were estimated using accepted values for soil and water found in the literature. Coefficients of thermal expansion for the concrete piles, soil, and water were also assigned to the model according to accepted values found in the literature.

In subsequent chapters, this thesis will review some of the available literature on energy piles and engineering principles that are important for the understanding and development of this model. Next, the engineering principles used in the model will be discussed. Afterwards, the model itself will be described. This description includes the creation of the numerical-model structure as well as a description of the assumptions used to execute the model. Next, the results from three example problems will be presented and discussed. The three problems will include the following scenarios.

- A driven-pile energy pile that is modeled over a 2.5-year period with a constant-surface-temperature boundary condition.
- A driven-pile energy pile that is modeled over a 2.5-year period with a transient-surface-temperature boundary condition.
- A drilled-shaft energy pile that is modeled over a 2-year period with a constant-surface-temperature boundary condition. The reason behind the 6-month-shorter period is that, unlike driven piles, there is no pile driving and subsequent clay-setup period for drilled shafts.

The purpose of the transient-surface temperature iteration is to simulate an energy pile that is near an exterior wall that may be subjected to seasonal temperature changes of the ground surface. The purpose of the drilled-shaft iteration is to present the effects of EPWP changes due to temperature changes only, i.e., without EPWP generated from the installation of a driven pile.

Finally, conclusions will be discussed, and suggestions for further development of this model will be presented. The Appendices will present the derivation of the consolidation equation, the numerical model developed using Matlab, and additional results that were considered extraneous.

CHAPTER 2: LITERATURE REVIEW

Introduction

The model proposed in this thesis attempts to estimate the capacity values of both drilled-shaft energy piles and prefabricated driven energy piles. These strength values fluctuate due to the varying EPWP values caused by thermal changes in the surrounding soil. The major principles of science and engineering that are the basis of this model are consolidation and heat conduction. Consolidation occurs with the dissipation of EPWP, which is found to occur after pile driving and as a result of a temperature gradient. A review of energy-pile behavior literature is also necessary. Finally, soil behavior subjected to cyclic loading is of interest for the proposed model.

Pile Setup

Pile setup has been a subject of research for more than 50 years. Soderberg (1962) was among the first to study the problem of pile setup as one of consolidation. Soderberg (1962) defined pile set up as "increase in the driving resistance of a pile with time." Depending on the soil type, bearing-capacity values found immediately after pile driving may be as low as 10 percent of the maximum load value that can ultimately be reached. Soderberg described the results of a paper by Cummings, Kerkhoff, and Peck (1950) as referenced in Soderberg (1962). The paper showed "horizontal migration of the pore-water" that was "approximately constant with depth" and varied with time as a result of pile driving. Soderberg (1962) described the phenomenon as a gradual increase in the soil particle contact with the pile as the EPWP dissipates. Soderberg (1962) assumed pressure

did not vary in the direction tangent to the pile and that EPWP could be expressed as concentric circles. He defined the flow of water through an infinitesimal volume of soil, according to Darcy's Law, as follows in Equation (2.1).

$$\frac{\partial(dV_w)}{\partial t} = \frac{krd\theta dr}{\gamma_w} * \left(\frac{\partial^2 u}{\partial r^2} + \frac{\partial u}{r\partial r}\right) \qquad (\mathbf{2.1})$$

He also defined the volume of water in the soil element with respect to time as follows in Equation (2.2).

$$\frac{\partial(dV_w)}{\partial t} = \frac{rd\theta dr}{1 + e_0} * \frac{\partial e}{\partial t} \qquad (\mathbf{2.2})$$

After defining the horizontal coefficient of consolidation, c_h, Soderberg (1962) combined the previous two equations, Equations (2.1) and (2.2), to describe the dissipation of EPWP over time, as shown in Equation (2.3).

$$\frac{\partial u_e}{\partial t} = c_h \left(\frac{\partial^2 u_e}{\partial r^2} + \frac{\partial u_e}{r\partial r}\right) \qquad (\mathbf{2.3})$$

Soderberg assumed c_h was constant—although in reality it varies with the distance from the pile. Soderberg assumed c_h was an average value that did not change with the depth or distance from the pile. The equation is solved under the assumption that "the soil behaves as a viscous substance that will not support tension (Soderberg, 1962)."

Estimating pile capacity has been thoroughly researched. The Skov and Denver equation, presented in 1988, has been most widely used by engineers and researchers (Steward and Wang, 2011). Equation (2.4) utilizes site specific factors and restrike data, that is, data obtained from driving the pile some time after driving has initially ceased, whether a few hours or several days, and restriking is performed to either determine the capacity of the pile or to try to obtain additional penetration (Ng et al., 2013).

$$\frac{Q}{Q_0} = A \log_{10}\left(\frac{t}{t_0}\right) + 1 \qquad (\mathbf{2.4})$$

In Equation (2.4), Q is the capacity of the pile at time = t, Q_0 is the capacity of the pile at time = t_0, which is the time at which the dissipation of EPWP becomes linear with the log of time (Steward and Wang, 2011). The setup factor, *A*, is dimensionless and varies depending on soil conditions and type of pile (Steward and Wang, 2011). The setup factor can range from 0.2 to greater than 1, where *A = 0.6* is typically used for clay, and t_0 is typically valued at one day (Yang and Liang, 2006). However, the Skov and Denver equation is not used to predict ultimate pile capacity. The Skov and Denver equation assumes a linear increase in pile capacity, and since pile capacity does not increase to infinity, it is only valid for a limited time after pile installation (Wang et al., 2010).

Equation (2.5), from Bogard and Matlock (1990) as referenced in Mirza (2000), estimates the unit friction value of a driven pile as a percentage of degree of consolidation (Mirza, 2000). The unit friction value, *f*, is at least 20% of the ultimate value, f_{ult}.

$$\frac{f}{f_{ult}} = 0.2 + 0.8U \qquad (\mathbf{2.5})$$

This equation from Bogard and Matlock (1990) was developed using hollow, open and closed-end segment piles in highly plastic, normally-consolidated clay (Mirza, 2000). The equation allows the user to estimate the friction value at any time as a fraction of the ultimate value. The first step is to plot percent consolidation, *U*, versus time, *t*, divided by the radius of the pile, squared, on a logarithmic scale. The second step needed to find *f* is to create a graph similar to Figure 2.1.

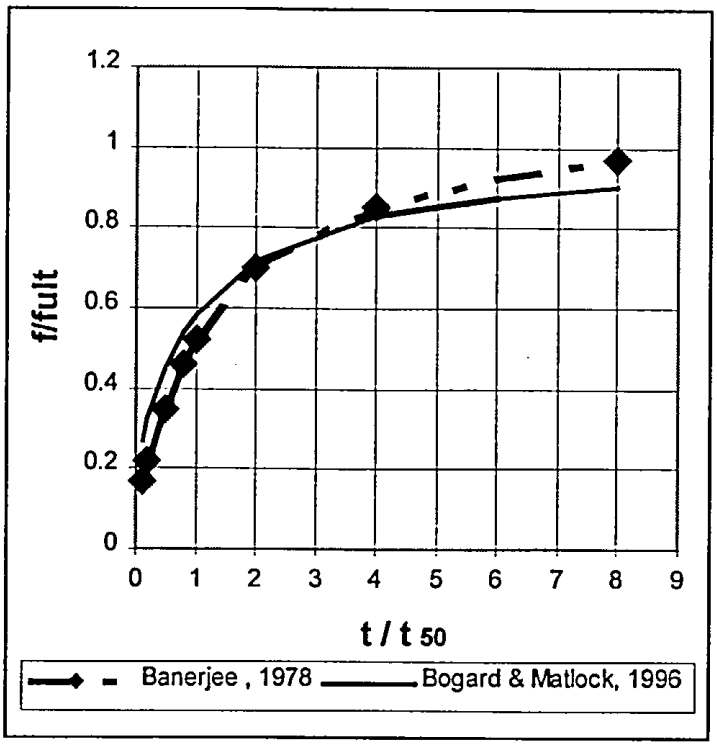

Figure 2.1 Graph comparing two methods for determining friction values versus time (Mirza, 2000).

Cavity Expansion Theory

Carter et al. (1979) presented a model to determine the stress and pore-water pressure (PWP) changes in clay after the expansion of a cylindrical cavity. The model proposed by Carter et al. (1979) simplified the behavior of soil in response to the cavity expansion, in that, vertical strains and deformations were neglected. Carter et al. (1979) assumed axial symmetry and plane strain conditions. They also assumed pore fluid would move through the saturated soil as a response to an applied stress, because of their earlier assumption that the pore fluid and soil skeleton were much less compressible than the saturated soil. This implies that any volume change in the saturated soil will be the result of pore fluid expulsion or absorption, and not a compression of the pore fluid or the soil skeleton (Carter et al., 1979). Additionally, they modeled the pore fluid to flow according

to Darcy's Law. The soil skeleton was modelled as an elastoplastic material. A schematic showing cavity expansion theory is presented in Figure 2.3.

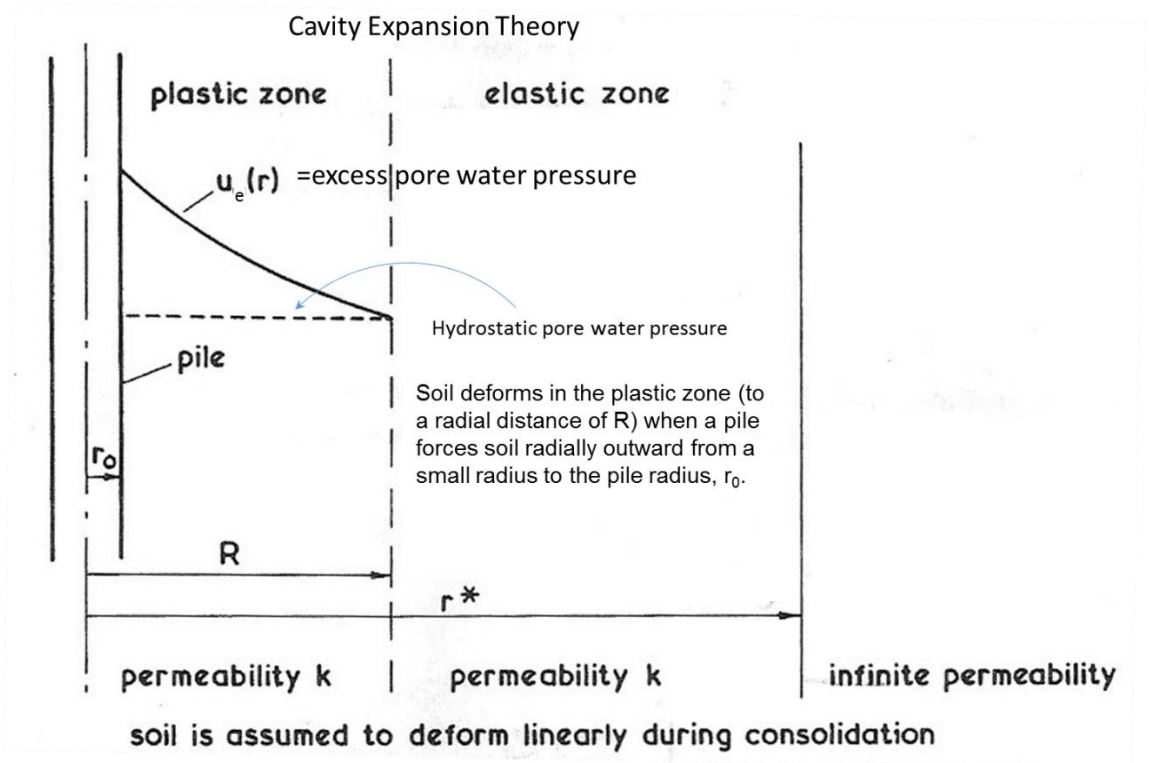

Figure 2.2. A schematic showing the relative dimensions of the pile, plastic zone, and elastic zone. *R* is calculated using Equation (3.6) below. (Adapted from Randolph and Wroth, 1979).

Values for the virgin compression line, the expansion coefficient, the value of the void ratio at the average value of effective stress at the point of failure, the slope of the failure envelope, the elastic shear modulus, values for soil permeability, the unit weight of the pore fluid, and in-situ stress values for the soil are needed for the analysis of the soil. Additionally, shear strength and effective Poisson's Ratio are required for analysis of the soil during cavity expansion.

Results of the numerical solutions to the model developed by Carter et al. (1979) indicated that cavity expansions on the order of five times the initial cavity radius could result in a radial-stress to shear-strength ratio, σ_r/c_u, of approximately eight. Cavity expansion on the order of 1.25 times the initial cavity radius would result in a radial-stress to shear-strength ratio of slightly more than four. However, the authors found that modeling a cavity expansion of up to twice the initial cavity radius proved sufficient. Additional cavity expansion only increased the length of soil deformed by the cavity expansion.

Randolph and Wroth (1979) presented an analytical closed-form solution for radial consolidation around a driven pile in elastic soil in response to expansion of a cylindrical cavity. Their work appears to have been published concurrently with the above paper by Carter et al. (1979). The authors presented field measurements of EPWP from different sources for different soils. The best-fit lines presented in Figure 2.3 show two soils with EPWP at the pile-soil interface of approximately 160 kN/m^2 and one soil with EPWP at the pile-soil interface of approximately 80 kN/m^2. For the soils with the larger initial EPWP values, the corresponding u_e/c_u values are approximately 5.3 and 8. The soil with the lower value had a u_e/c_u value of 5.3. The authors also provided the following equation to calculate the change in the radial stress at different radii within the plastic zone of the soil for a cavity having zero initial radius to a cavity having a radius equal to the radius of the pile.

$$\delta\sigma_r = c_u\left[1 + \ln\left(\frac{G}{c_u}\right) - 2\ln\left(\frac{r}{r_0}\right)\right] \qquad (\mathbf{2.6})$$

In Equation (2.6), r_0 is the pile radius and G is the shear modulus. The authors also assumed the mean effective stress remained constant under undrained conditions, i.e., the

above equation is also the distribution of EPWP when EPWP is added to c_u. In Figure 2.3, the authors graphed EPWP versus a non dimensionalized time representative for various values of G/c_u. On the horizontal axis, c represents c_v, the coefficient of consolidation.

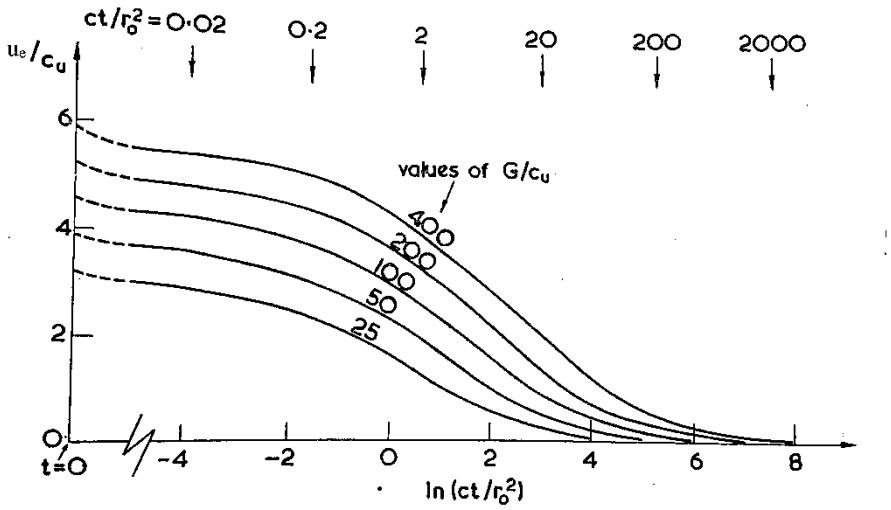

Figure 2.3. Variation of EPWP at the Pile Face with Time (Randolph and Wroth, 1979).

The value for initial EPWP at any radius within the plastic zone was found using Equation (2.7).

$$u_e = 2c_u ln\left(\frac{R}{r}\right) \qquad (\mathbf{2.7})$$

Azzouz et al. (1990) installed an instrumented test pile into Boston Blue Clay and compared the results to the cavity expansion theory proposed by Carter et al. (1979) and the strain-path method proposed by Baligh. The strain-path method accounts for vertical fluid flow and soil strain. The authors compared predictions of soil behavior between the cavity expansion theory method using the modified Cam-Clay Model, the strain-path

method also using the modified Cam-Clay Model, and the strain-path method using the MIT-E3 soil model. The strain-path method using the MIT-E3 soil model closely correlated to the values of lateral earth-pressure coefficient measured using the instrumented pile. The prediction of the initial lateral earth-pressure coefficient value indicated that the cavity-expansion theory value was approximately twice that of the strain-path method value, and three times greater than the value measured using the instrumented pile (Azzouz et al., 1990). Additionally, the cavity expansion theory method predicted consolidation occurring more quickly than the others. The cavity expansion method predicted a final lateral earth-pressure coefficient value approximately 25% greater than that of the strain-path method and greater than twice the measured value (Azzouz et al., 1990).

Zheng et al. (2010) analyzed the effects of variable consolidation coefficients on a cylindrical driven pile. The authors used the cavity expansion method and the initial EPWP predicted by Randolph and Wroth (1979). The model was discretized and solved using Matlab. The void ratio was related to the mean effective stress and the coefficient of permeability using Equations (2.8) and (2.9) shown below.

$$e = e_0 - C_p ln \frac{p'}{p'_0} \qquad (\mathbf{2.8})$$

$$e = e_0 - C_k log \frac{k_h}{k_{h0}} \qquad (\mathbf{2.9})$$

In Equations (2.8) and (2.9), C_p is the compressibility index, and C_k is the permeability index. Those are the slopes of the curve *e-log(k).* In addition, e, e_0, k_h, and k_{h0} are the void ratio and the coefficient of permeability corresponding to mean effective stress p' and p'_0, respectively (Zheng et al., 2010).” The initial values are represented by e_0 and k_{h0}, and

final values are represented by e_0 and k_{h0}. The mean effective stress (p') is the average of the radial, tangential, and vertical effective stresses (σ'_r, σ'_θ, and σ'_z), but since the authors chose to follow the model proposed by Randolph and Wroth (1979), the plane strain condition eliminates the vertical effective stress, σ'_z, the equation for p' reduces to Equation (2.10). Poisson's ratio for the soil is represented as v, and the tangential direction is represented by θ.

$$p' = \frac{(1+v)(\sigma'_r + \sigma'_\theta)}{3} \qquad (\mathbf{2.10})$$

Combining Equations (2.8) and (2.9) relating to void ratio, the authors derived the coefficient of permeability. The coefficient of volume compressibility, m_v, was also defined using Equation (2.11).

$$m_v = \frac{C_p}{p'_0(1+e)}\frac{p'_0}{p'} \qquad (\mathbf{2.11})$$

Zheng et al. (2010) compared consolidation data for values of C_p between 0.2 and 0.6 and C_p /C_k values of 0.5 to 1.5 and found that consolidation occurred at a markedly slower rate only when C_p was 0.6, indicating a lower limit for consideration.

Energy Piles

The majority of the energy-pile research to date focuses on the pile response to thermodynamic loading. These studies include load testing of existing piles, scale-model testing, and numerical analyses. Brandl (2009) presented design considerations and data on energy-pile usage in Europe. Laloui et al. (2006) both experimentally and numerically investigated the behavior of a heat-exchanger pile. Wang et al. (2011) performed a laboratory-scaled experiment of an energy pile subjected to thermal and mechanical loading. McCartney and Rosenberg (2011) performed experiments on 1:24 scale model

energy piles subjected to loading from a centrifuge to obtain load-displacement data under heated conditions.

Brandl (2009) outlined design considerations for energy foundations, including energy piles. He presented data for the amount of energy piles constructed in Austria from 1984 to 2004, then adds that between 2005 and 2009, "more than 6000 energy piles" had been installed annually, bringing the total number of energy piles installed in Austria to over 50,000 (Brandl, 2009). Brandl (2009) presented the mean daily outdoor temperatures for Vienna, Austria for the calendar year 2001. The data were then idealized to form a sinusoidal curve with a low temperature of 0° C and a high temperature of approximately 22° C. The annual mean was 11° C with amplitudes above and below the mean of 11° C. Brandl (2009) presents the sinusoidal curve as Equation (2.12).

$$\mathrm{T_{GS}} = \mathrm{T_{m,out}} + \Delta\mathrm{T_{out}} \cos\left[\frac{2\pi}{\bar{P}}\right](t - \varepsilon_t) \qquad (\mathbf{2.12})$$

In Equation (2.12), t is time, T_{GS} is the ground-surface temperature, $T_{m,\,out}$ is the average yearly temperature, ΔT_{out} is the temperature amplitude, $\bar{P}$ is the duration period, and ε_t is the phase displacement. Brandl (2009) also presented an example of heating and cooling loads compared to heating and cooling capacity over the course of a year, starting in January. The temperature of the heat-carrier fluid was also presented. The heat-carrier fluid's temperature ranged from 3°C in the third month to a high of 23°C in the eighth month of each year. Heating and cooling demands exceeded the capacity in Months 1 through 4 and Month 8.

Laloui et al. (2006) performed in-situ testing on an energy pile located in Switzerland. The pile was approximately 25 meters long with a nonuniform cross-sectional area varying between 7,200 and 10,800 cm^2 (square centimeters). Although not

described as such in the paper, the energy pile can probably be described as a drilled shaft because of the variable shaft diameter and description of the integrity test that was performed.

The drilled shaft was outfitted with a load cell at the bottom, 24 fiber-optic extensometers to measure the vertical strain and five fiber-optic extensometers to measure the radial strain, 24 vibrating-wire extensometers to measure the vertical strain and temperature, and four additional vibrating-wire extensometers located near the top of the shaft to measure the vertical strain to determine the axial load.

The drilled shaft was then subjected to both thermal and axial loading. The testing was performed as the building was being constructed. Hence, the mechanical loading was the dead load of each added story, and the thermal loading was also performed at the end of each floor's construction. The change in temperature for the first thermal test was 21°C, and the temperature change for the remaining tests was approximately 15°C. The first thermal loading was performed prior to any imposed dead load. Therefore, the drilled shaft was free to move vertically.

After installation, the drilled shaft was heated for 12 days during the initial thermal loading test. At the end of that time, the measured vertical strain ranged from approximately 0.00015 meter/meter (m/m) at a depth of 22 m to approximately 0.00019 m/m at a depth of 2 m. The radial strain measured 0.00056 m/m at the end of heating, and the vertical displacement of the top of the drilled shaft was between 3 and 4 millimeters (mm) at the end of the heating cycle. The authors found that a temperature increase of 1°C increases the vertical load on the drilled shaft by 100 kN; hence, the thermal load doubles the total axial load on the drilled shaft.

The authors also created a "thermo-hydro-mechanical model" to simulate the behavior of the drilled shaft and surrounding soil (Laloui et al., 2006). The model separated the soil into five layers to simulate the subsurface conditions surrounding the drilled shaft. The model assumed a constant surface temperature and incremental temperature changes within the drilled shaft.

Wang et al. (2011) performed a laboratory study on a scale-model energy pile that was loaded axially before and after a heating cycle. The model energy pile was a hollow steel rod with an outside diameter of one inch. The model pile was coated with epoxy and silica sand to simulate roughness. The model energy pile also had a heating element—as a heat source—inside. The experiment was performed three times with two different soils. The first soil was an "N50 silica sand". The other soil was a "300WQ silica flour" (Wang et al., 2011). The sand was loosely compacted and moisture conditioned with 0.5% moisture content, and the silica flour was moisture conditioned to 21.5% and 24% moisture content.

Results showed a reduction in the shaft resistance after heating. The silica sand showed an approximately 60% decrease in the maximum shaft capacity. The silica flour with 24% moisture content exhibited a 50% decrease in the maximum shaft resistance load, and the silica flour with 21.5% moisture content exhibited an approximate 11% decrease. Additionally, the sand sample exhibited very little rebound in displacement during loading/unloading cycles, while both of the silica flour samples demonstrated some rebound upon unloading.

McCartney and Rosenberg (2011) performed laboratory experiments on scale-model energy piles that were loaded using a centrifuge and then heated. The piles were

precast with wire mesh as reinforcement and an aluminum tube to circulate the heating fluid through the pile during the experiments. The piles were embedded within compacted silt. For all four of the tested piles, the centrifuge was accelerated to 24 times that of gravity, and then the piles were allowed to settle under their own weight until no more movement was detected at a constant temperature of 15 °C (McCartney and Rosenberg, 2011). Then, the piles were loaded at a constant rate of 0.2 mm/minute to a maximum of 5 mm. Thereafter, the temperature was raised to 50 °C for one sample and 60 °C for another sample. These piles were then loaded at a constant rate of 0.2 mm/minute. Based upon the load-settlement curves generated during the experiments, the authors fitted end-bearing versus pile tip displacement and side shear versus displacement curves to approximate the testing data. McCartney and Rosenberg (2011) proposed the equation below to estimate the shear capacity for drilled shafts exposed to thermal heating. The authors also stated the shear stress would increase due to heating in a drained condition.

$$Q_s = \beta A_s \sigma_v' \left(K_0 + \left(K_p - K_0\right) K_T\right) tan\varphi' \qquad (\mathbf{2.13})$$

In Equation (2.13), β is an empirical reduction factor representing the soil-interface behavior, A_s is the side surface area, σ_v' is the overburden pressure, K_0 and K_p are the at-rest and passive earth pressures, respectively, and K_T is a factor representing the mobilization of the lateral earth pressure with thermal strain (McCartney and Rosenberg, 2011). K_T is defined by Equation (2.14), where α_T is the coefficient of thermal expansion of reinforced concrete and κ is an empirical coefficient representing the soil resistance to expansion of the foundation (McCartney and Rosenberg, 2011). The diameter of the pile is represented by *D* and the length of the pile by *L*. The authors found that the values of κ

= 65 and β = 0.55 were a good fit for the load displacement curves for the test piles subjected to heating (McCartney and Rosenberg, 2011).

$$K_T = \kappa \alpha_T \Delta T \left(\frac{D/2}{0.02L} \right) \qquad (\mathbf{2.14})$$

Bourne-Webb et al. (2009) field tested a full-sized, drilled-shaft energy pile. The drilled shaft was loaded axially and subjected to a long-term heating and cooling cycle and then several short-term heating and cooling cycles. The drilled shaft was instrumented with vibrating-wire strain gauges and optical-fiber sensors to record mechanical data and thermistors and optical fiber sensors to record temperature data. Two of the four anchor piles and the heat sink pile were instrumented with optical-fiber sensors to record mechanical and temperature data. A borehole in close proximity to the drilled shaft was instrumented with thermistors and optical-fiber sensors to record temperature data. The test results provided the authors with likely responses to combined thermal and mechanical loading. When an energy pile is subjected to axial compression and cooling, the "…axial loads become less compressive and may become tensile, while the mobilized shaft resistance increases in the upper part of the pile and reduces in the lower part (Bourne-Webb et al., 2009)." When an energy pile is subjected to axial compression and heating, axial compression may increase, and shaft resistance may become "…reduced in the upper half of the pile and increased in the lower half (Bourne-Webb et al., 2009)." Bourne-Webb et al. (2009) also found that the axial load approximately doubled after heating. Soil temperatures were approximately 5 °C at a lateral distance of 0.5 m from the test pile at the end of the cooling period and approximately 23 °C at the same distance at the end of heating.

Abdelaziz et al. (2011) performed numerical analyses to investigate the heat-transfer behavior of an energy pile subjected to heating cycles of varying duration and embedded within sand or clay layers of varying moisture content. They assumed an initial ground temperature of 20 °C and a heat-exchanger fluid temperature of 40 °C. Simulations were run for one day, one week, and one month of heating, and the temperatures along the surface of the energy pile were plotted versus depth. The authors found that after one week of heating, temperatures were highest at the pile surface for partially saturated clay and lowest for both saturated clay and saturated sand. At a lateral distance of 0.5 m from the pile surface, temperatures were highest for saturated sand and lowest for dry sand. Temperatures at a distance of 0.5 m from the pile surface were similar for dry sand, partially saturated clay, and saturated clay. Temperatures were lower at a lateral distance of 0.5 m from the pile than they were along the pile for all four soil types. The effects of the flow rate and circulation-pipe diameter were also analyzed.

Thermal Effects

Under drained conditions, volume changes result from thermal expansion of soil and pore water (Campanella and Mitchell, 1968). For undrained conditions, the volume change of the soil mass due to temperature and pressure changes can be taken as the volume changes of the pore water and the soil particles (Campanella and Mitchell, 1968). The factors controlling pore-pressure changes for undrained conditions are "…the magnitude of the temperature change, the porosity, the difference between the coefficients of thermal expansion for soil grains and water, the volumetric strain due to physico-chemical effects, and the compressibility of the soil structure (Campanella and Mitchell, 1968)." For two samples of Illite clay, the authors found the value of physico-

chemical strain, α_{st}, to be -0.5×10^{-4}/ °C. Laboratory experiments by Campanella and Mitchell (1968) were performed using triaxial testing equipment that allowed temperature regulation of the soil samples. The samples were preconsolidated and then subjected to temperature changes from 65° F to 138 °F and back down to 40 °F. The temperature cycling was repeated, but incrementally. The results showed that the majority of the volume lost occurred during the initial temperature cycle. The incremental temperature change steps yielded minimal volumetric losses. The authors state that EPWP may develop due to the pore water expanding at a greater rate than the soil and a decrease in the shear strength between particles (Campanella and Mitchell, 1968). This latter development may cause a partial collapse of the soil structure and a decrease in void ratio. A temperature decrease causes a decrease in the particle size and causes the sample to absorb water (Campanella and Mitchell, 1968).

Demars and Charles (1982) observed a permanent decrease in the void ratio after a temperature cycling within a range of 25 °C. The authors subjected samples of normally consolidated and overconsolidated clay, a silt sample, and a sand sample to triaxial testing. The samples were kept at a constant temperature of 25 °C and consolidated. After the primary consolidation was completed, the samples were subjected to a temperature increase of 25 °C—reaching a temperature of 50 °C—and observed without additional stress until the volume changed ceased again. Then, the samples were cooled back to 25 °C and observed while cooling. The authors observed that a portion of the volume lost to heating returned upon cooling, referred to as the reversible volume change. The authors termed the other portion of the volume lost to heating that was not recovered irreversible volume change (Demars and Charles, 1982). The authors found a relationship between

the irreversible volume change and plasticity. For normally consolidated soils, the authors presented the relationship in the equation below.

$$\Delta e_{st} = \left(0.00048 + 0.00000 I_p\right)\Delta T \qquad (\mathbf{2.15})$$

In Equation (2.15), Δe_{st} is the permanent change in the void ratio, I_p is the plasticity index, and ΔT is the change in temperature in degrees Celsius. The authors concluded that the irreversible volume change was independent of the effective confining pressure (Demars and Charles, 1982). In addition, the volume change was soil-dependent. Finally, the value of Δe_{st} for overconsolidated soils depends upon the stress level as measured in terms of OCR as well as the soil type and plasticity (Demars and Charles, 1982).

Demars and Charles (1982) also demonstrated that the change in the void ratio results in a linear change in the plasticity index for normally consolidated clays.

Abe (2001) presented a thermo-viscoplastic numerical model for soft clays. In that model, the author discretized the top quarter of a triaxial compression test specimen's vertical cross-section into one hundred elements as shown in Figure 2.4. The author states the surface temperature of the sample was raised from 20 °C to 80 °C for 1 minute under drained conditions, but based upon an accompanying figure, it appears that the temperature of the surface was raised over the first minute of the simulation and stayed at 80 °C for the remainder of the simulation (Abe, 2001). The author demonstrated that when clays are heated, clay particles and pore water expand, but the clay skeleton contracts (Abe, 2001). Therefore, clays initially expand upon heating, generating EPWP, then volumetric strain develops as the EPWP dissipates (Abe, 2001). In addition, negative pore-water pressure is briefly generated as the soil matrix expands during heating.

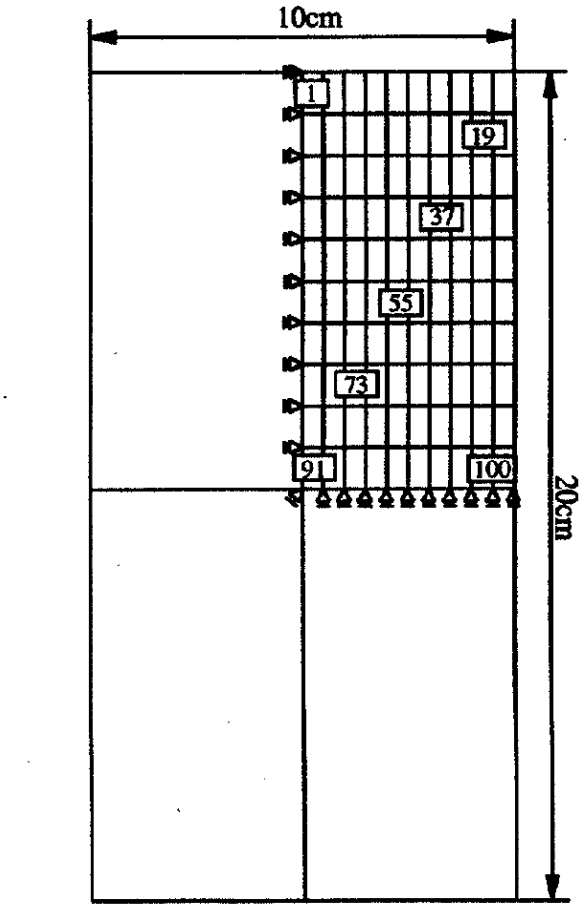

Figure 2.4 Finite-Element Mesh for Triaxial Specimen (Abe, 2001).

Cyclic Loading

Li et al. (2011) found that cyclic failure of clay occurs at approximately 3% single amplitude shear strain for clay samples with a cyclic stress ratio of 0.3 or larger, and that EPWP continuously increases with the number of cycles. Clays with a cyclic stress ratio less than 0.3 do not reach cyclic failure. Samples tested at a frequency of 0.01 Hz with a cyclic stress ratio less than 0.3 incur a degradation of undrained shear strength up to approximately 12%. Accumulative pore-water pressure (PWP) increased to approximately 24 kPa throughout the testing duration.

Wang et al. (2005) performed both static and cyclic triaxial tests on soft clay. The triaxial tests were performed under unconsolidated-undrained (UU) conditions at various confining pressures. Wang et al. (2005) observed a slight decrease in the undrained shear strength for clays with increasing cyclic-loading duration.

CHAPTER 3: PHENOMENA CONSIDERED FOR THE MODEL

Introduction

The numerical model employed in this work couples several phenomena of geotechnical engineering and thermodynamic scientific principles. In the model, the installation of a driven pile generates EPWP, which reduces the skin friction, temporarily reducing the capacity of the pile. The soil is displaced during pile driving, and the resulting stresses are computed based on the Cavity-Expansion Theory. After pile driving into the clayey soil has occurred, EPWP gradually decreases during a process known as pile setup in clay. The EPWP dissipates as a result of consolidation of the clayey soil. Darcy's Law helps define the process of consolidation. Heat transfer occurs through a material in a process called conduction. Thermal expansion of the material also occurs when heat is added into the system. Chapter 3 briefly presents the major physical processes that will be modeled within this energy pile model. The following describes the background material.

Darcy's Law

Darcy's law governs seepage through soils where the discharge velocity, v, for water flowing through saturated soil is a function of the hydraulic gradient, i, by the coefficient of hydraulic conductivity, or permeability of the soil to water, k**.** In Equation (3.1), *Q* is the volume of flow, and *A* is the gross cross-sectional area of the soil sample. The hydraulic gradient is equal to the gradient of total head, i.e., the hydraulic-head

difference, *dh*, divided by the length of flow over which the head loss occurred, *dL*, also shown in Equation (3.1).

$$\frac{Q}{A} = \vec{v} = -k\vec{\imath} = -k\vec{\nabla}h = -k\frac{dh}{dL} \qquad (\mathbf{3.1})$$

Darcy made the following assumptions:

- Flow through the porous media is laminar;
- *Porosity is determined using the average properties of the porous media;*
- *Fluid properties are spatially and temporally constant.*

The coefficient of permeability is related to the properties of the water, such as viscosity and unit weight, as well as the intrinsic permeability of the soil, $\overline{K}$, as shown in Equation (3.2).

$$k = \frac{\gamma_w}{\mu_w}\overline{K} \qquad (\mathbf{3.2})$$

In Equation (3.2), γ_w is the unit weight of water and μ is the dynamic viscosity of water. The intrinsic permeability of granular soils is also dependent upon their pore size, grain-size distribution, and roughness of mineral particles (Das, 1990). The permeability of clayey soils is dependent upon mineral structure, ionic concentration, and the thickness of the double-diffuse bound-water layer (Das, 1990).

Equation (3.2) is valid at a constant temperature. A temperature change will alter the dynamic viscosity and density of the soil. In order to account for the change in temperature, Equation (3.2) may be rewritten as Equation (3.3). Equation (3.3) is valid for constant absolute permeability, which assumes the soil structure does not change.

$$k_T = K\frac{\gamma_T}{\mu_T} = \left(k_{20^\circ C}\frac{\mu_{20^\circ C}}{\gamma_{20^\circ C}}\right)\frac{\gamma_T}{\mu_T} \qquad (\mathbf{3.3})$$

Therefore, Darcy's assumptions, above, were violated so that the changes in permeability due to temperature changes could be examined in the model.

Dynamic Viscosity

Dynamic viscosity is the measure of a fluid's resistance to deformation by shear or tensile stresses. The Vogel-Fulcher-Tammann (VFT) model for dynamic viscosity, μ, was used to find values for the variation of the dynamic viscosity of water with temperature. The general form of the VFT model is shown in Equation (3.4).

$$\mu = e^{\left(A+\frac{B}{C+T}\right)} \qquad (\mathbf{3.4})$$

The coefficients A, B, and C for water were obtained from *http://ddbonline.ddbst.de/VogelCalculation/VogelCalculationCGI.exe?component=Wate*r that is a VFT-equation viscosity calculator for a variety of fluids. The VFT equation for the dynamic viscosity of water, with coefficients, is presented in Equation (3.5).

$$\mu = e^{\left(-3.7188+\frac{578.919}{-137.546+T^{oK}}\right)} \qquad (\mathbf{3.5})$$

Cavity-Expansion Theory

Cavity Expansion Theory was presented in Chapter 2 as part of the literature review. The theory used in the model, developed by Randolph and Wroth (1979), states that a rapidly expanding cavity of an assumed initial radius will develop EPWP. The change in the horizontal total stress will increase based upon Equation (2.4). The clay will deform within the plastic zone, which is defined as that area where the soil reaches shear failure during pile driving (Randolph and Wroth, 1979). The initial EPWP will be zero beyond the plastic zone. The radius of the plastic zone, R, can be found using Equation (3.6)

$$R = r_0\left(\frac{G}{c_u}\right)^{0.5} \qquad (\mathbf{3.6})$$

where r_0 is the pile radius, G is the shear modulus, and c_u is the unconfined compressive strength. Under undrained conditions, the change in effective stress is equal to zero, which means the increase in the total stress is equal to the increase in the EPWP.

Bearing Capacity

The vertical capacity of a pile is comprised of the tip resistance and skin (i.e., side / circumferential area) friction. The method for calculating tip resistance in clay is similar for driven piles and drilled shafts. The undrained shear strength at the tip is higher for driven piles because pile driving compacts the soil (Coduto, 2001). Skin friction in drilled shafts and driven piles may be evaluated using effective- or total-stress methods. Effective-stress analysis may be used to evaluate side-friction resistance when it is assumed that little or no E.P.W.P. is generated (Coduto, 2001). Total-stress analyses, while more widely used, are less accurate (Coduto, 2001).

Shear Capacity (Skin Friction)

Shear capacity for a drilled shaft may be evaluated using a sliding-friction model using the lateral earth-pressure coefficient, K. The simplest model is shown as Equation (3.7), where f_s is the unit side-friction value, σ_h' is the effective horizontal stress, and φ' is the effective stress friction angle (Coduto, 2001).

$$f_s = \sigma_h' \tan \varphi' \qquad (\mathbf{3.7})$$

Due to the changes in stress onto the surrounding soil caused by deep foundation installation, the K may be different from the at-rest earth-pressure coefficient, K_0. Lateral earth-pressure coefficient may be difficult to evaluate; hence, the friction equation has been modified to a form referred to as the β-method. Generally, unit skin-friction resistance, f_s, is calculated using Equation (3.8) where β is given by Equation (3.9).

$$f_s = \beta \sigma_z' \qquad (3.8)$$

$$\beta = K_0 \left(\frac{K}{K_0}\right) \tan\left[\varphi' \left(\frac{\delta}{\varphi'}\right)\right] \qquad (3.9)$$

where φ' is the effective stress friction angle, and δ is the soil-foundation friction angle. For silts and clays, the value of β is given by Figure (3.1).

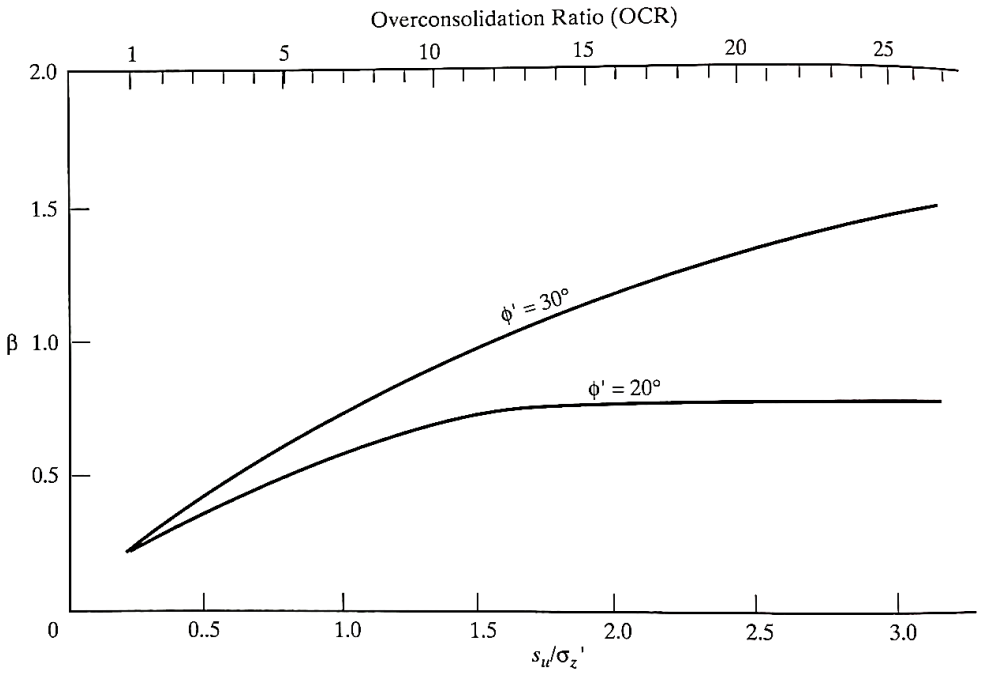

Figure 3.1. β value for normally to slightly over-consolidated silts and clays (Coduto, 2001) where s_u and σ_z' are undrained shear strength and effective vertical stress, respectively.

Total-stress analysis of skin friction is most commonly performed using the α-Method. The α–method computes the unit side-friction resistance by multiplying an adhesion factor, α_f, with the undrained shear strength, s_u, in the soil adjacent to the foundation (Coduto, 2001), as shown in Figure (3.10).

$$f_s = \alpha_f s_u \qquad (3.10)$$

Values for α_f range from 1.0 for soft, relatively insensitive clays to 0.5 for stiff, relatively insensitive clays. Sensitive clays require full-scale static load tests or special lab tests to determine appropriate values for α_f (Coduto, 2001). Similar values for α_f are appropriate for computing unit skin-friction capacity for drilled shafts (Coduto, 2001).

Appropriate values for α_f are determined empirically from pile load-test results (Coduto, 2001). The total-friction method is not likely to be an appropriate method for estimating unit skin-friction values immediately after pile installation, given the large value of EPWP. The value of undrained shear strength deteriorates rapidly with increasing the degree of saturation (Das, 2007), which suggests that for an unsaturated soil, the value of undrained shear strength would be much lower after pile driving and before setup than the value obtained during laboratory testing.

End Bearing (Tip Resistance)

End-Bearing resistance is assumed to occur under undrained conditions in clays (Coduto, 2001). The equation for net unit toe-bearing resistance is given by Equation (3.11), where q_t' is the net unit toe-bearing resistance, N_c^* is the bearing capacity factor, and s_u is the undrained shear strength of the soil between the toe and two times the width of the pile/shaft below the toe.

$$q_t' = N_c^* s_u \qquad (\mathbf{3.11})$$

With an assumed undrained shear strength value of 75 kPa, $N_c^* = 8.5$ for the clay in the model (Coduto, 2001).

The above equations provide unit resistance values. These values should be multiplied by the effective area of the pile or drilled shaft to find allowable capacities.

For the purpose of this thesis, tip resistance is beyond the scope of this work, because the model was created to find the effects temperature has on frictional resistance.

Consolidation

Terzaghi's definition of consolidation is a change in the volume of soil by a net volumetric outflow of water (Das, 1990). The derivation of the time rate of consolidation is based upon the following assumptions.

- The clay-water system is homogeneous;
- Complete water-saturation exists;
- Compressibility of soil grains is negligible;
- The flow of water is in the direction of the compression;
- *Compressibility of water is negligible;*
- *Darcy's law is valid.*

Terzaghi considered one-dimensional consolidation in the vertical direction of a volume of soil in his derivation of consolidation, as shown in Equation (3.12) governing 1D, one-dimensional, vertical consolidation

$$\frac{\partial u_e}{\partial t} = c_v \left(\frac{\partial^2 u_e}{\partial z^2} \right) \qquad (\mathbf{3.12})$$

where c_v is the coefficient of volumetric consolidation. The equation for c_v is presented in Equation (3.13) where k is the coefficient of hydraulic conductivity, m_v is the volumetric compressibility, and γ_w is the unit weight of water.

$$c_v = \frac{k}{m_v \gamma_w} \qquad (\mathbf{3.13})$$

In this model, consolidation can occur in three dimensions. In other words, in addition to the vertical consolidation, consolidation can also occur in the radial

(axisymmetric horizontal) direction, about a cylindrical drilled shaft or driven pile, as opposed to Terzaghi's one-dimensional vertical consolidation, which he assumed would occur in the vertical direction, as shown in Equation (3.12). The general equation for three-dimensional consolidation was converted from the Cartesian coordinate system to the cylindrical coordinate system using the Laplace transform. Thus, the general equation for consolidation in this model is shown in Equation (3.14).

$$\frac{\partial u_e}{\partial t} = c_v\left(\frac{\partial^2 u_e}{\partial r^2} + \frac{1}{r}\frac{\partial u}{\partial r} + \frac{1}{r^2}\frac{\partial^2 u_e}{\partial \theta^2} + \frac{\partial^2 u_e}{\partial z^2}\right) \qquad (\mathbf{3.14})$$

Terzaghi's assumptions were violated within the model. A detailed derivation of consolidation may be found in Appendix A.

Conduction

The general energy equation for a volume can be written as Equation (3.15). In Equation (3.15), ρ is the density, c is the specific heat, q'' is heat flux, and q''' is the internal heat source vector.

$$\int_V \left(\rho c \frac{\partial T}{\partial t} + \nabla \cdot q'' - q'''\right) dV = 0 \qquad (\mathbf{3.15})$$

Conduction is the transfer of heat between molecules where a temperature gradient exists. Conduction, $\boldsymbol{q''}$, through a medium can be described by Fourier's Law, shown in Equation (3.16), where k_H is the thermal conductivity, and ∇T is the temperature gradient.

$$q'' = -k_H \nabla T \qquad (\mathbf{3.16})$$

A general conduction equation for a volume with no internal heat energy may be written in cylindrical coordinates as shown in Equation (3.17), where the diffusivity, d, is equal to Equation (3.18).

$$\frac{\partial T}{\partial t} = d\left(\frac{\partial^2 T}{\partial r^2} + \frac{1}{r}\frac{\partial T}{\partial r} + \frac{1}{r^2}\frac{\partial^2 T}{\partial \theta^2} + \frac{\partial^2 T}{\partial z^2}\right) \quad (\mathbf{3.17})$$

$$d = \frac{k_H}{\rho c_p} \quad (\mathbf{3.18})$$

where k_H is the coefficient of conductivity, ρ is the density, and c_p is the specific heat.

When the transient-conduction equation has a time-harmonic heating source, the boundary condition may be written as shown in Equations (3.19) and (3.20)

$$T(L, t) = T_1 \quad (\mathbf{3.19})$$

$$T(0, t) = T_1 + \Delta T \cos(2\pi t / t_1) \quad (\mathbf{3.20})$$

where T_1 is the temperature at location x = L (far-side soil with ambient soil temperature), and at time, t. At location $x = 0$ (pile side) and at time, t, the temperature, T, is equal to temperature, T_1, plus or minus an amplitude, ΔT, that fluctuates over a period, t_1. In this model, this boundary condition is used to show the fluctuation of the ground-surface temperature. This equation is adapted, in the model used for this work, to vary the temperature generated by the heating and cooling of the energy pile.

Thermal Expansion

As matter heats, its molecules become more excited. This excitement causes the molecules to vibrate farther apart. As the molecules vibrate farther apart, the matter expands its shape. Thermal expansion in one dimension is linear. Thermal expansion of an area is two-dimensional. And thermal expansion of a volume is three-dimensional. Since the matter does not gain mass during heating, the increase in dimension results in a decrease in density. Conversely, cooling of the matter tends to have the opposite effect. One exception is ice, which is less dense than water since water expands during freezing. In order to find the change in the radius of the concrete pile or drilled shaft in the model

for this work, the thermal expansion of the pile in radial direction is calculated using the equation for the thermal expansion of an area, Equation (3.21)

$$\Delta A = 2\alpha_T A_0 \Delta T \qquad (\mathbf{3.21})$$

where ΔA is the change in area, A_0 is the original area, α_T is the coefficient of thermal expansion, and ΔT is the change in temperature. The new radius, R_1, may be calculated based on the initial radius, *R*, using Equation (3.22).

$$R_1 = [R^2 \times (1 + 2\alpha_T \Delta T)]^{0.5} \qquad (\mathbf{3.22})$$

CHAPTER 4: METHODS

Introduction

The model developed for this thesis is designed to calculate the transient excess pore-water pressure (EPWP) and temperature values within an axisymmetric slice of homogeneous, anisotropic clay that is affected by the installation and thermodynamic properties of a single driven energy pile or drilled-shaft energy pile. Axisymmetry allows analyzing a 2D grid in cylindrical coordinates instead of the axisymmetric 3D problem. The energy pile is assumed to be located along the perimeter of the building's footprint. The axisymmetric area of soil is presented in Figure 4.1. In Figure 4.1, the depth of the modeled soil is twice the length of the modeled pile. The radius, or width, of the modeled soil is approximately 2.5 times greater than the plastic zone calculated for the soil by Equation (3.6).

This chapter contains information pertaining to the creation of the model based upon the scientific and engineering principles described in previous chapters. First, the creation of the discretized, truncated mesh, used to model the clay. This will include the description of governing equations for interior nodes and boundary conditions. Then the model will be described in detail. The next section, "Inputs and Model Conditions," will describe the inputs and their values used to analyze the sample problems. Afterwards, the methods and calculations that are exclusive to the driven-pile iterations are explained, including the effects of cavity expansion and friction calculation for the driven pile. The next section, "Combined Consolidation and Conduction," details the iteration process

pertaining to combined heat conduction and consolidation in the modeled soil. The next section "Transient Ground-Surface Temperature," describes how transient ground-surface temperatures were implemented for one of the driven-pile scenarios. The last section "Drilled-Shaft Model," describes how the drilled-shaft iteration differs from the two driven-pile iterations.

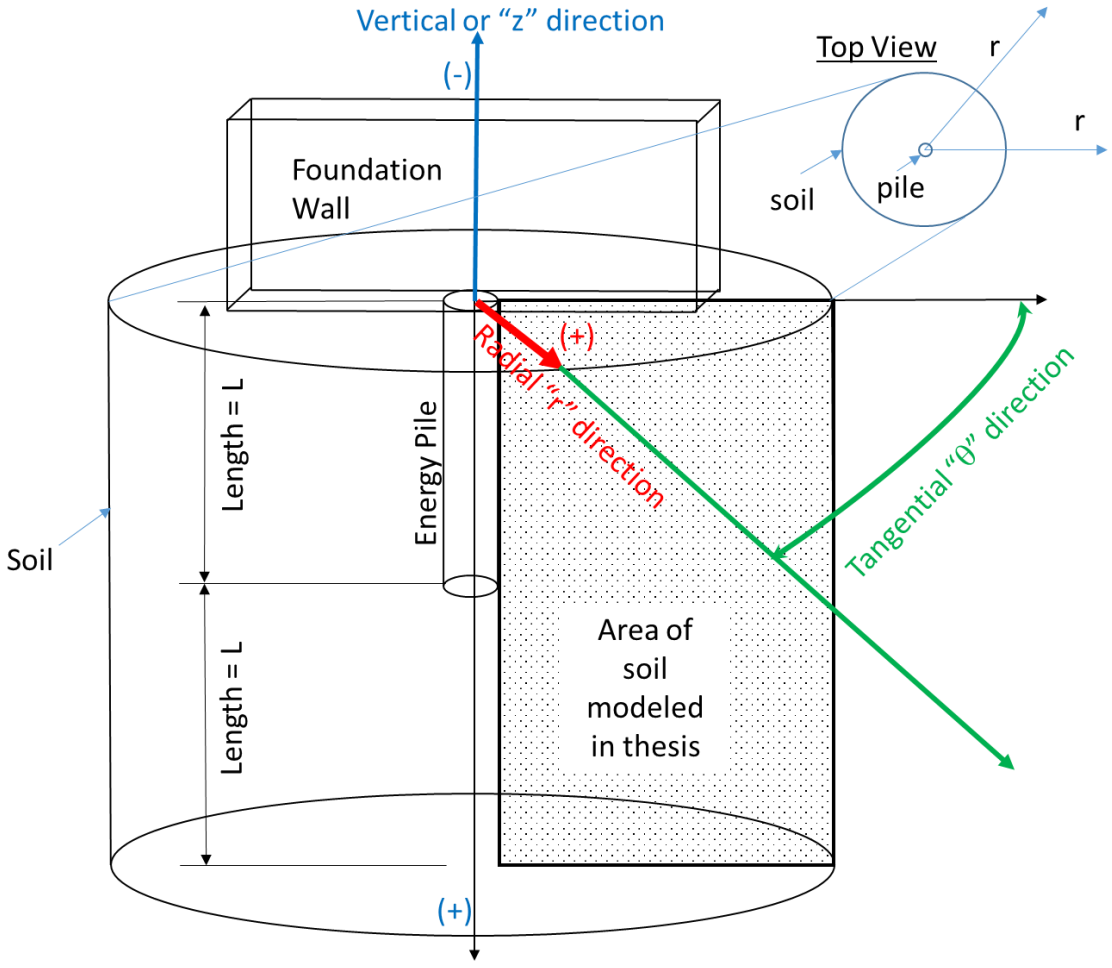

Figure 4.1. The layout of the model energy pile and simulated soil in cylindrical coordinates.

Matrix-Based Model

The numerical model used in this work was created using the MATLAB platform and language. The model was created to solve transient, second-order, partial differential equations (PDEs) of consolidation and conduction. These PDEs were solved using central-difference approximations. For a function, $z_i = f(x_i)$, and its derivative, $z_i' = f'(x_i)$, central-difference approximations for higher order derivatives are shown in Equations (4.1 and 4.2), where *s* is the spacing between nodes, or difference between the values of x_i and x_{i+1}.

$$z_i' = \frac{1}{2s}(z_{i+1} - z_{i-1}) \qquad (\mathbf{4.1})$$

$$z_i'' = \frac{1}{s^2}(z_{i+1} - 2z_i + z_{i-1}) \qquad (\mathbf{4.2})$$

The model was designed to consider consolidation and conduction about a cylindrical pile or drilled shaft in cylindrical coordinates. The PDEs were further reduced to two dimensions, based upon the assumption that both consolidation and conduction will be axisymmetric.

When discretizing a two-dimensional PDE for the *(i, j)* node, values of *i* increase to the right and values of *j* increase vertically upward. A central-difference approximation for a second-order PDE is shown in Equation (4.3).

$$\frac{\partial^2 f}{\partial x^2} = \frac{\partial}{\partial x}\left(\frac{\partial f}{\partial x}\right) = \frac{\partial}{\partial x}(f_x') = \frac{f(x_{i+1}, y_j) - 2f(x_i, y_j) + f(x_{i-1}, y_j)}{dx^2} \qquad (\mathbf{4.3})$$

A central-difference approximation of the second-order partial differential derivative with respect to the *Y*-coordinate for the function, *f(x, y),* would be found in a similar fashion where x_i remains constant. The 2D grid would naturally be defined using *N* nodes in the width and *M* nodes in the height directions.

In this model, however, nodes of the discretized 2D grid were numbered in a one-dimensional array to reduce the system of equations to be solved from a 3D matrix equation to a 2D matrix equation. Central-difference approximations were completed in the manner shown in Equation (4.3) in the radial direction, where the discretized node was located at *(ii)*, and relocating vertically one row, the node's location became *(ii+N)*, for example. This type of approximation was used to solve for interior nodes. The layout for the truncated, discretized mesh used to model the soil, as well as how the adjacent nodes relate to generic node a_{ii} are shown in Figure 4.2. The one-dimensional (1D) node numbering for the two-dimensional grid results in a 2D coefficient matrix [a] and two 1D vectors $\{x\}$ and $\{b\}$ for the variable coefficient *a* used in the equation *[a]{x} = {b}*. A generic vector equation *[a]{x} = {b}* is shown in Equation (4.4) where $p = M.N$ and *x* is scalar.

$$[A]_{p\times p}\{x\}_{p\times 1} = \{b\}_{p\times 1} \qquad (\mathbf{4.4})$$

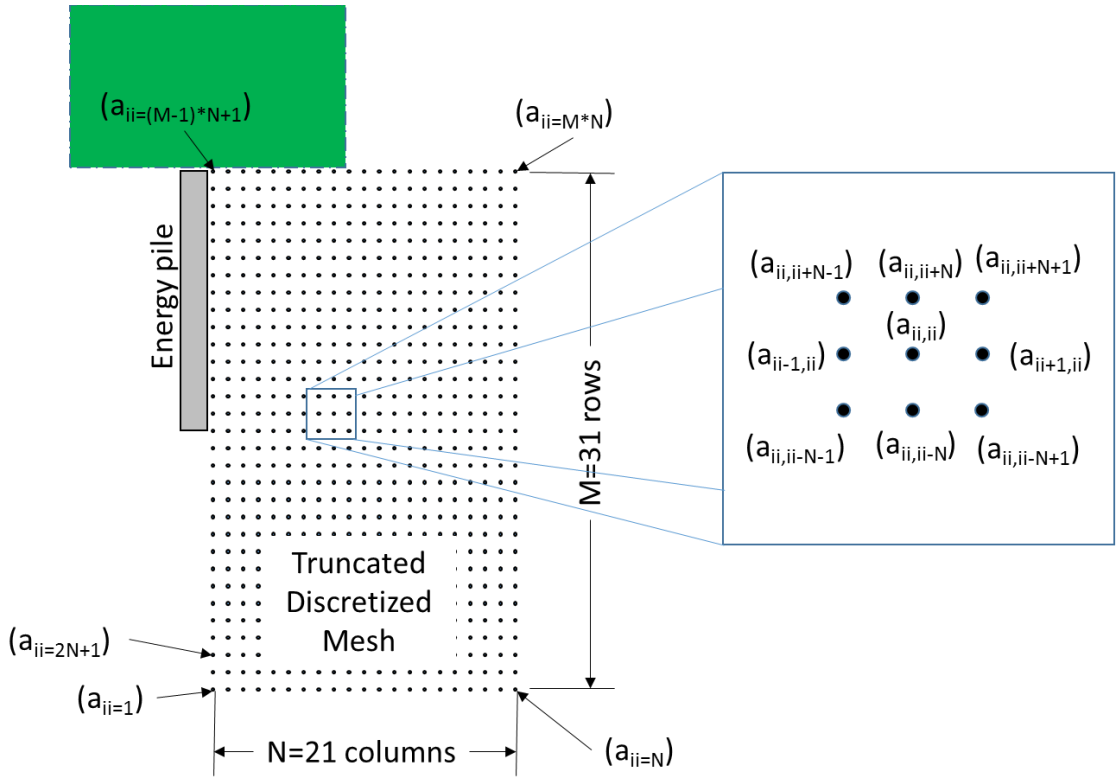

Figure 4.2. The layout of the truncated, discretized mesh and the relationship of adjacent nodes to node a_{ii}.

The Crank-Nicolson method was used to solve the interior (i.e., core) nodes to avoid instability and provide better accuracy and improve the speed and probability of convergence. This method is used in conjunction with the central-difference method. A general form for the Crank-Nicolson method is shown in Equation (4.5)

$$\frac{\partial u}{\partial t} = a\frac{\partial^2 u}{\partial r^2} =>$$

$$\frac{u_i^{k+1}-u_i^k}{\Delta t} = \frac{a}{2(\Delta r)^2}\left[\left(u_{i+1}^{k+1} - 2u_i^{k+1} + u_{i-1}^{k+1}\right) + \left(u_{i+1}^{k} - 2u_i^{k} + u_{i-1}^{k}\right)\right] \quad (\mathbf{4.5})$$

where the superscript *k* is the time step.

Nodes around the perimeter of the discretized mesh are considered boundary nodes. The governing for these boundary node, i.e., boundary conditions, indicate equations necessary to truncate the grid. For example, the soil does not exist beyond the

ground surface, so consolidation cannot continue beyond that surface, but the soil does exist in a radial direction beyond the border of the soil modeled by the truncated mesh. General boundary conditions are presented in Figure 4.3.

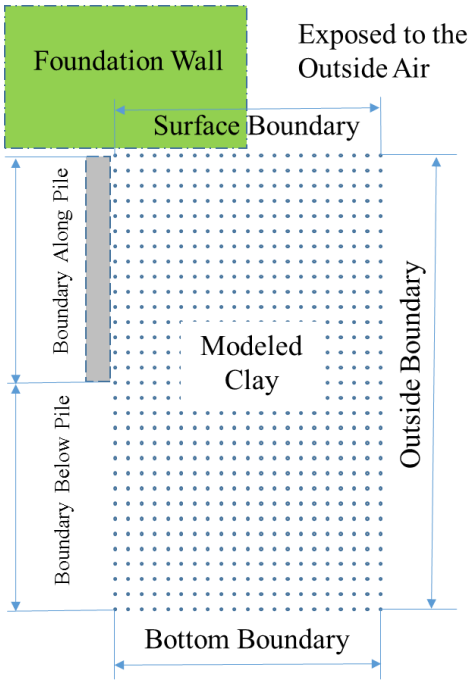

Figure 4.3. The general boundary conditions used for the modeled soil.

These boundary conditions may be either Dirichlet- or Neumann-type boundary conditions. Dirichlet or Neumann boundary conditions were applied correspondingly to boundary nodes and approximated using the forward-difference or backward-difference methods. Dirichlet boundary conditions are boundary conditions that have a discrete value. On the other hand, Neumann boundary conditions are boundary conditions where values are not known but the variation (derivative) values are forced. In the model, Dirichlet boundary conditions were used along the pile or drilled shaft face, along the bottom of the soil, and along the ground surface where a forced value for EPWP or temperature exists. In certain instances, the boundary condition was transient in nature,

but at a given time, had a discrete value. As mentioned, Neumann boundary conditions are boundary conditions where values are not known but the variation (derivative) values are forced. An example is the impermeable boundaries where the derivative is forced to be zero, resulting in an assumption that boundary values are the same as the virtual nodes on the other side of the boundary, that is, symmetrical about the boundary. An example of a Neumann boundary condition is $\frac{\partial u}{\partial r} = b$. Neumann boundary conditions were used below the pile, and on the side opposite the pile face. Boundary-condition equations and constants are presented in Figure 4.4.

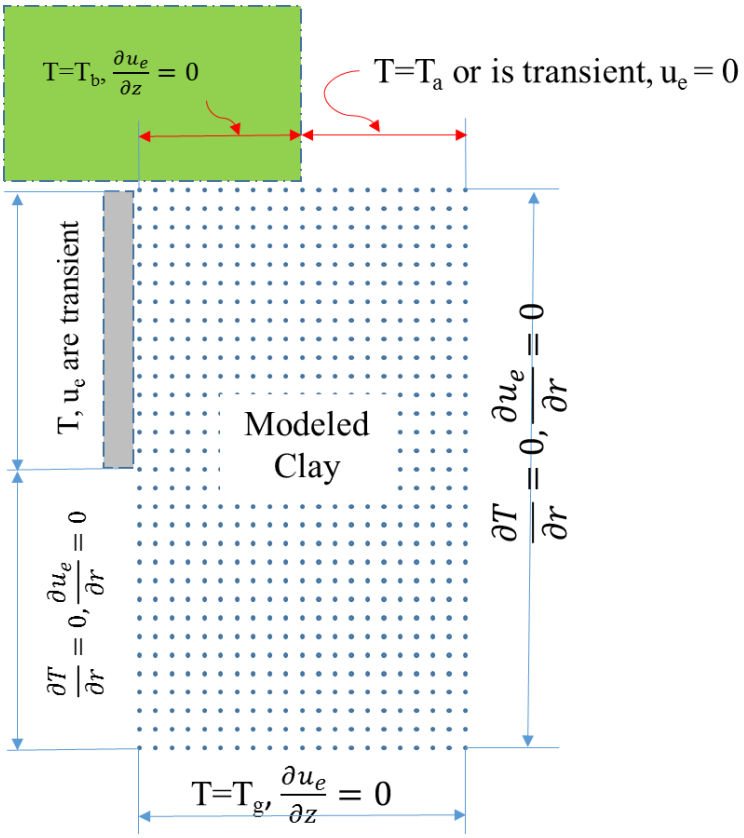

Figure 4.4. Boundary condition equations and values used in the model.

Model Overview

The model was designed to allow for user input for almost all situations. The user may specify the length and radius of the pile or drilled shaft. The dimensions of the rectangular matrix for the finite-difference analysis is not included on the "Inputs" file but is easily changed in the "Constants" file. The user may input a large variety of values for the physical and thermodynamic characteristics of the clay. At this time, the model defaults to a single, homogeneous layer of saturated clay. The model results presented below assume the clay is anisotropic for vertical and radial permeability; however, these values can also be defined by user input. The user may input initial values for soil temperature and range values for transient surface temperature. The user may also input the number of years the model may be run. However, the time interval between pile installation and the beginning of transient heat (i.e., when HVAC is initiated) emanating from the energy pile is set to default at six months. In addition, the temperature-range driving conduction from the pile or drilled shaft is not part of the user input at this time.

The model consists of three related but stand-alone models. The three models all use common lines of code and function files but are separated partly by necessity and partly for convenience. Two of the models analyze a driven energy pile. One of these models includes transient ground-surface temperatures, and one assumes a constant surface soil temperature. Both of these driven-pile models assume the pile is driven six months before the HVAC system is turned on, as stated above. The third model analyzes a drilled shaft that is subjected to heat from the HVAC system immediately, since there is no driving period, and hence setup, for drilled shafts. Therefore, all three models are the same once the HVAC system starts, with the exception of the initial EPWP.

Inputs and Model Conditions

The soil was modeled as a saturated, slightly over-consolidated clay of medium to high plasticity. The characteristics of the clay were similar to the Illite tested by Campanella and Mitchell (1968). The value of horizontal or radial hydraulic conductivity, k_{rr}, is 7 $\times 10^{-7}$ m/s, and the vertical hydraulic conductivity, k_{zz}, is 4 $\times 10^{-7}$ m/s at 20 °C. The saturated unit weight, γ_{sat}, is approximately 17 kN/m^3 but changes as the void ratio is readjusted after the pile is driven or after soil expansion or contraction. The initial void ratio, e_0, was set to 1.1, but it is also readjusted by the model as a result of the cavity expansion due to pile driving and soil expansion and contraction. The Young's modulus for the soil, E_s, was set to 20,000 kN/ m^2. The specific gravity of the soil, G_s, is 2.75. The Poisson's ratio of the soil, ν, was set to 0.3. The undrained shear strength of the clayey soil, s_u, was set to 75 kN/ m^2. The angle of effective internal friction of the clay, ϕ', was set to 20°. The over-consolidation ratio, *OCR*, is 1.1. The liquid and plastic limits were set to 52 and 17, respectively.

The heat conductivity coefficient, *K*, is equal to 365 J/day.m.^{o}K for both vertical and radial directions. The coefficient of thermal expansion for the saturated soil, α_s, is 3.3 $\times 10^{-7}$ / °C. The specific heat for the clay, c_p, is 2,462 J/kg. °C at 20 °C. The physico-chemical coefficient of structural volume change, α_{st}, is -0.5 $\times 10^{-4}$/ °C after Campanella and Mitchell (1968).

The coefficient of thermal expansion, α_{pile}, of the concrete for both the driven pile and the drilled shaft is 14.5 $\times 10^{-6}$/ °C. The Young's Modulus for the concrete is 25 MN/m^2. The coefficient of thermal expansion for water, α_{H2O}, is 0.207 $\times 10^{-3}$/ °C but is calculated within the model. Water density, ρ_ω, is 999.973 kg/m^3 at 4 °C but is

continually recalculated based upon the current temperature within the model. The dynamic viscosity for water, μ, is computed based upon Equation (3.4). Because the hydraulic conductivity changes when temperature changes, it is adjusted continuously within the model, using Equation (3.3).

The coefficient of volumetric compressibility for water, m_v, was set at -0.364×10^{-3} m^2/kg. The coefficient of compressibility was set at this value so that the EPWP would dissipate within the 910-day model run and also so that the clay being modeled would have physical characteristics similar to the Illite used in the study performed by Campanella and Mitchell (1968). Consolidation was set to update on a daily basis within the model. The initial temperature of the soil was set to 15 °C (288 °K).

The finite-difference mesh used to model the soil is a rectangular grid of 21 nodes wide and 31 nodes high, for a total of 651 nodes, as shown in Figure 4.2. The width of the mesh is modeled at approximately 3.33 m (dr = 0.167 m), and the height of the mesh is modeled at 30 m (dz = 1 m). The incremental distances, dr and dz, are the modeled distance divided by the number of nodes minus one. The driven pile or drilled shaft is represented as a boundary condition from the top left corner of the mesh to mid-height. The pile is assumed to be 15 m long. The boundary condition below the pile to the bottom left corner is soil that is assumed to be symmetrical to the soil below the pile. The bottom row of mesh is modeled to be impermeable if the modeled soil is clay or symmetrical if the model soil is sand. This selection is made based upon the hydraulic conductivity of the soil. The top of the mesh is assumed to have a concrete cover or pile cap over the left half of the surface. The right half of the top of the mesh is assumed to be exposed to the air.

Driven Energy-Pile Models

The driven-pile versions of the model assume that the structure built upon the energy piles will be built and operational, at least from the standpoint of HVAC system operation, exactly six months after pile installation. The modeled pile is representative of a typical pile, and no distinction is made between an interior pile and exterior, or perimeter pile, except for the transient ground-surface temperature iteration of the model, which may be interpreted for an exterior pile. Consideration of the specifics of the construction of the building's foundation are beyond the scope of the model.

The model establishes a loop through the initial six-month period prior to HVAC introduction, which allows for dissipation of EPWP and consolidation of the modeled soil. Both versions of the driven-pile model also calculate EPWP dissipation for a period of two years plus six months, or 910 days, without HVAC system introduction, so that consolidation without conduction may be compared to consolidation with conduction.

As the six-month period begins within the time loop, density and coefficient of thermal expansion of the water is calculated based upon in-situ temperature. Next, the physical state of the soil is changed due to pile driving. The initial void ratio, e_0, is recalculated to in-situ values using Equation (4.6). In Equation (4.6), C_c is the compression index, K_o is the at-rest lateral earth-pressure coefficient, γ_{sat} is the initial saturated unit weight, and σ_v is the total vertical stress.

$$e_1 = e_0 - C_c[\log_{10}(K_o.\gamma_{sat}.z) - \log_{10}(K_o * \gamma_{sat}.(1))] \qquad (\mathbf{4.6})$$

The installation of the pile will increase the radial stress based on Equation (2.4). The model recalculates the void ratio within the plastic zone based upon the increase in stress. Once the void ratio and porosity are recalculated, γ_{sat} is also recalculated. After the

density of water is calculated based upon temperature, its dynamic viscosity is calculated according to Equation (3.5), and the absolute hydraulic conductivity is calculated according to Equation (3.3). The next values to be calculated by the model were the radial and vertical coefficients of consolidation, c_{rr} and $c_{zz,}$ respectively. This calculation was performed using Equation (4.7), and the value of c_{rr} was converted to days.

$$c_{rr} = \frac{k_{rr}(86{,}400)}{m_v \rho_w g} \qquad (\mathbf{4.7})$$

The EPWP is then calculated. The boundary condition along the pile face is calculated using the logarithmic decay shown in Figure 2.1. This logarithmic decay is rewritten in Equation (4.8). Once the value of u_e in Equation (4.8) reaches zero, the model limits the value of this boundary u_e to zero for cavity expansion.

$$u_e = 4.5 \cdot c_u \left[1 - \frac{\ln\left(\frac{c_r t}{R^2}\right)}{6}\right] \qquad (\mathbf{4.8})$$

Finally, the unit skin-friction resistance is calculated according to Equation (3.9), the $\boldsymbol{\beta}$ Method, presented in Chapter 3. The effective vertical stress, σ_z', is calculated for each one-meter thickness of soil using Equation (4.9). In Equation (4.9), for a calculation of unit friction for a 1m thick slice of soil at a depth of *x* m to a depth of *(x+1)* m, the value of the effective vertical stress is the overburden above *(x)* m plus the effective vertical stress if the midpoint between *(x)* m and *(x+1)* m.

$$\sigma_z' = \gamma_{sat} \cdot (z - 1) + 0.5(\gamma_{sat} - \rho_w \cdot g) \qquad (\mathbf{4.9})$$

$$K_0 = (1 - \sin\varphi')OCR^{\sin\varphi'} \qquad (\mathbf{4.10})$$

$$\mathrm{K} = 1.5 \cdot K_0 \qquad (\mathbf{4.11})$$

In Equation (3.9), $\left(\frac{K}{K_0}\right)$ values for a large displacement, driven pile range from 1.0 to 2.0 (Coduto, 2001). Values for the $\left(\frac{\delta\prime}{\varphi'}\right)$ ratio are given at 0.8 to 1.0 for smooth concrete, such as that seen in a precast pile, and 1.0 for rough concrete (Coduto, 2001). In the model, $\left(\frac{K}{K_0}\right)$ is calculated using Equations (4.10) and (4.11), where φ' is 20°. The ratio $\left(\frac{\delta\prime}{\varphi'}\right)$ is assumed to be equal to 0.8 in the model. Unit-circumference-friction is calculated using a ratio of EPWP to initial EPWP, with the assumption that EPWP at Day 1 is equal to 1.25 times the deviator stress, $\delta\sigma_r$, as shown in Equation (4.12). The unit friction calculated using Equation (3.8) equals the friction along a unit length of the pile. Because the model calculates friction along the entire effective length of the pile, the frictional capacity calculation only requires multiplying the results by the perimeter of the pile. Therefore, the friction value computed by the model will, here on, be referred to as the unit-circumference friction value.

$$f = \left(\sum K_0.\sigma'_{z(ii)} \cdot \frac{K}{K_0} \cdot \tan\left[\varphi'\left(\frac{\delta}{\varphi'}\right)\right]\right) * \left\{0.2 + 0.8\left[1 - \left(\frac{u_{e(ii)}}{\left(\frac{\delta\sigma_r}{0.8}\right)}\right)\right]\right\} \quad (\mathbf{4.12})$$

Unit-circumference-friction for the drilled shaft will be computed according to Equation (3.7).

After the six-month construction period, all three versions of the model loop through two years of simulated seasonal heating and cooling cycles. The heating and cooling cycles are cyclical in nature and separated into thirteen week seasons. The details of this portion of the model are presented below in Figure 4.5.

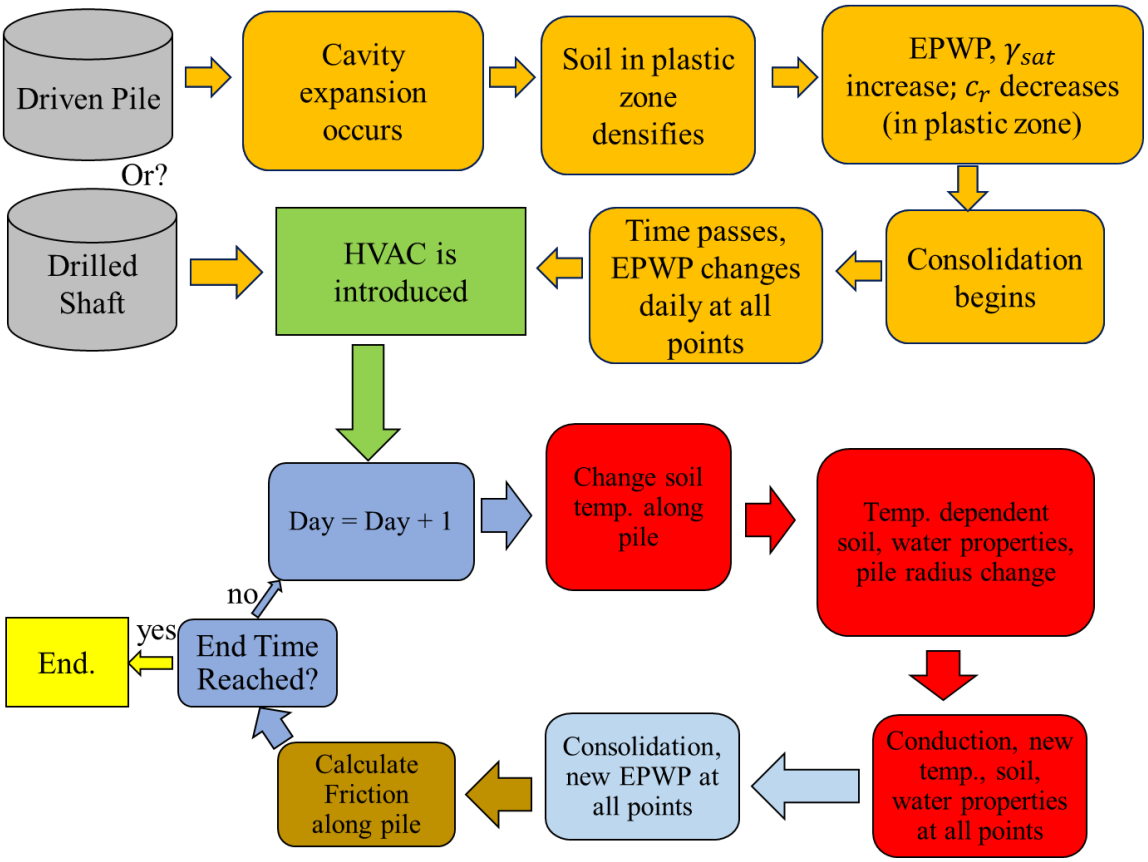

Figure 4.5. The process that is followed by the model for both the driven-pile and the drilled-shaft iterations.

Combined Consolidation and Conduction

After the initial six months, the EPWP values are augmented by heat generated from the HVAC system. The HVAC system begins adding heat at the pile surface at the first day of summer. Heating of the energy pile through the convection of the heat carrying fluid, as described by Brandl (2009), is beyond the scope of this thesis. Researchers such as Laloui et al. (2006) and Brandl (2009) present heating and cooling cycles that reach their maximum differential in a matter of days. The heat energy was added to and removed from the soil gradually in this model. In order to keep the quantity of heat added to the soil out of the model, a method of representing the gradual change in heat energy was devised. This gradual change in heat energy introduced or removed from

the soil is represented in a gradual change in surface temperature of the soil adjacent to the energy pile. In addition, the gradual nature of the temperature change along the pile or drilled shaft is meant to simulate the change in demand of the occupants of the theoretical building on the HVAC system throughout the calendar year. In the model, the highest demand on the cooling system would occur when the outside temperature was hottest. This time period is modeled to be in the middle of the summer season. Cooling of the building would pull heat from the occupied space and transfer that heat into the soil via the energy piles. This would then heat the soil. Conversely, the highest demand for heat would occur in the middle of the winter season, requiring the greatest amount of heat to be removed from the soil. The change between demand for cooling and heating the building occurs gradually and linearly, with a week in the middle of autumn and another in the middle of spring where neither heating nor cooling is required for the building.

The summer season consists of 13 weeks and begins the first day of summer. There are four 13-week seasons in a year, totaling 364 days. Heat is added for 6 hours per day, initially, for the first week. An additional two hours of heating are added per day for each successive week until the seventh week of the summer season, which has heat added for 18 hours per day. The heating is then reduced two hours per day, per week, until at the end of the quarter, six hours of heat is added per day. During the autumn season, heat is reduced one hour per day/per week until no heat is added on the seventh week of the quarter, or 20th week of the model run. Heat is then removed from the soil at a rate of one hour per day per week, until heat is removed at a rate of six hours per day per week at the end of the quarter. During the winter quarter, heat is removed at the same rate that it is added during the summer quarter, until heat is removed at six hours per day per week at

the end of the quarter. The spring quarter is modeled similar to the fall quarter, such that heat is removed in a decreasing fashion until no heat is added nor subtracted in the middle of the quarter, and then, heat is added at a rate of one hour per day per week until the end of the first year at which point, the model is returned to the summer quarter. The model is run through this cycle two times, i.e., for two years. A chart summarizing the model described above for HVAC demand is presented in Figure 4.6.

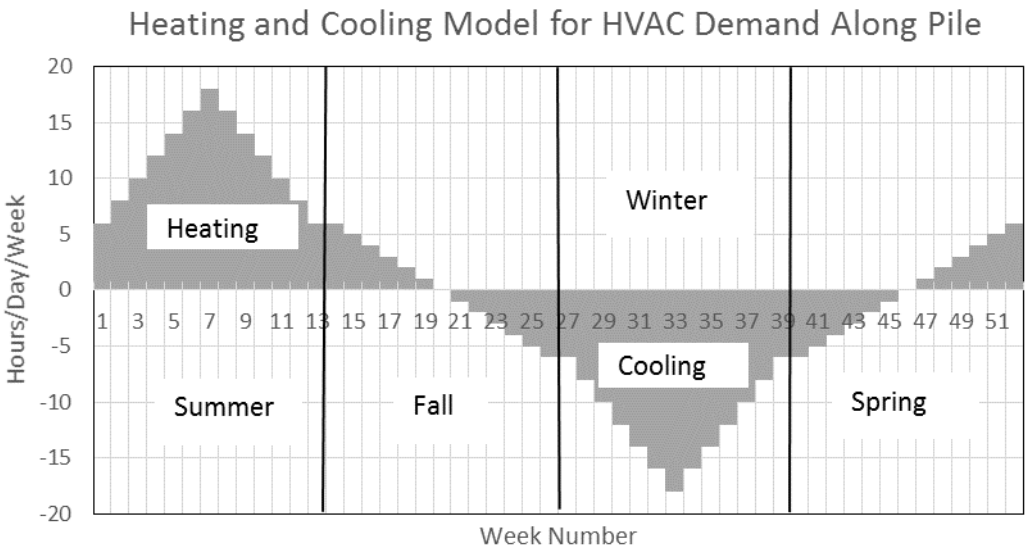

Figure 4.6. A chart modeling the seasonal heating and cooling demand that was used to model temperature change for the temperature boundary condition along the pile.

The total number of heating hours is calculated and then proportioned so that it could be distributed as described above. The total range of temperature that the soil would see was decided upon prior to the creation of the model. The energy-pile face reaches a maximum temperature of slightly more than 50 °C and a minimum temperature of slightly less than 0°C. The number of hours of heating was calculated using the method described above. Heat was to be added to the soil for one hour per day, each day for the first week of heating (Week 8 of the spring season), for a total of seven hours for

the first week. During the second week, heat was added to the soil two hours per day per week, for a total of 14 hours for the second week. At the end of the spring season, heat was modeled to be added to the soil for six hours per day for a total of 42 hours for that week. Heat was added for a total of 42 hours the first week of the summer season. By Week 7 of the summer season, heating was modeled for a total of 18 hours per day. Then the number of heating hours per day per week was reduced by two hours per day until the end of the summer season and, then, one hour per day per week until the end of Week 6 of the autumn season. The total number of heating hours was calculated to be 1,344 heating hours.

When heat is added to the energy pile, the pile undergoes volumetric strain. However, the vertical dimension may be ignored in order to find the effect thermal expansion has upon the horizontal cross-sectional area of the pile, and pile radius. The increase in the pile radius will result in increased total stress on the soil, in the form of increased EPWP. The change in temperature between the in-situ temperature and the maximum soil temperature is 35°C. Using the modulus of elasticity for concrete and coefficient of thermal expansion for concrete presented above and Equation (32), the pile radius will expand 0.000076105 m during a change in temperature of 35°C. Using Equation (4.13) for a linear, compressive stress-strain relationship and assuming that since the stiffness of the concrete is much greater than that of the clay, the entirety of the strain from the thermal expansion of the energy pile is assumed to be transferred to the clay. The strain, ε, caused by the thermal expansion of the energy pile, represented by the right-hand side of Equation (4.13), is equal to the strain due to linear compression of the clay, represented by $\frac{\sigma}{E_s}$ in Equation (4.13).

$$\varepsilon = \frac{\sigma R_{clay}}{E_s} = R_{pile}\alpha_c \Delta T \qquad (\mathbf{4.13})$$

where it is assumed that the radius of the energy pile, R_{pile}, is equal to the length of clay being compressed, R_{clay}. Assuming that the stress created by the thermal expansion of the energy pile is then equal to the strain multiplied by the modulus of elasticity of the clay, and that also assuming that the stress, σ, is equal to an increase of EPWP, the EPWP created by a temperature increase of 1 °C is calculated using Equation (4.14).

$$u_{heat} = \frac{\varepsilon E_s}{\Delta T} = \frac{(7.6105 \times 10^{-5})20{,}000\ kN/m^2}{35℃} = 0.0435\ \frac{kN}{m^2 \cdot ℃} \qquad (\mathbf{4.14})$$

At this point in the model, the 182 day "construction phase" is over, and the model starts calculating temperature change to the pile-soil boundary. This portion of the model consists of nested "for-loops," with the outermost loop the current year, the next level of loop is the current week. The "week" loops are divided into the first seven weeks of the 13-week season, and then the remaining six weeks of the season. Within the "week" loops, the final layer of for-loops is the current day. For example, as this portion of the model starts, the time, *t*, is at Day 183, which is Year 1, Week 1, Day 1. After Day 7, the week turns to Week 2. The model assumes consolidation will occur as it would without the addition of the changing temperature components and, then, adds or subtracts EPWP created by the changing temperatures.

The value of u_{heat} in Equation (4.14) is multiplied by the change in temperature calculated for that day to obtain the amount of EPWP caused by the thermal expansion of the pile. This temperature change is added to the previous temperature, and the density and coefficient of thermal expansion values of water are then recalculated. At this point in the loop, the model starts to account for the changes to the soil characteristics caused

by the change in temperature that was not required during the "construction phase" because the temperature was constant. The model then recalculates the density of the soil, ρ_{clay}, and $\gamma_{sat,\ clay}$. The specific heat is, thereafter, recalculated. The incremental temperature added to the previous day's temperature is then removed, because the temperature is added to the previous day's temperature value in the part of the model that calculates conduction as a boundary condition along the pile face. This was necessary to prevent the change in temperature from being counted twice. Next, the EPWP caused by thermal expansion of the soil is calculated. The values of dynamic viscosity and thermal expansion of water are then calculated, which are in turn used to calculate the hydraulic conductivity and coefficient of consolidation. EPWP is thus calculated for the day, and then the values of EPWP caused by thermal expansion of the pile and thermal expansion of the soil are added. This totals the EPWP value for the day. The unit-circumference skin friction is then calculated and recorded, and the time value advances afterwards. A chart summarizing the model process, with attention given to those parts of the model that are specific to thermal, soil, and water properties as well as the model type, is presented in Figure 4.7.

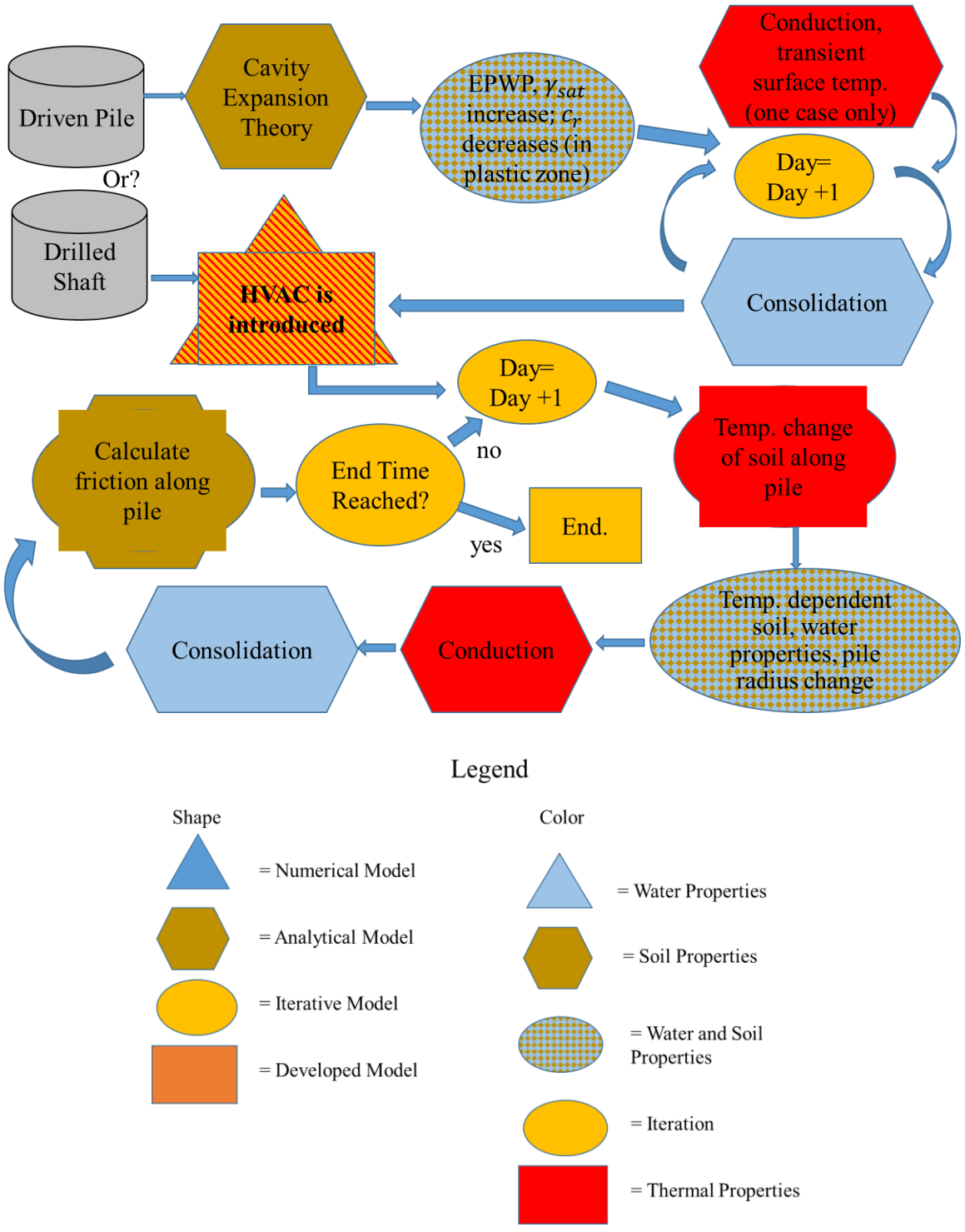

Figure 4.7. Schematic showing model process, with detail given to model type and the properties affected.

Transient Ground-Surface Temperature

The transient ground-surface temperature version of the model varies the temperature of the top right boundary of the grid according to Equation (2.12). Equation (2.12) is modified according to Equation (4.15) where T_{med} is the median surface soil temperature, equal to 16°C, T_h is the highest temperature (36°C), T_l is the lowest temperature (-4°C). The phase shift is 212 days, making the peak surface-soil temperature occur approximately 30 days after the beginning of the summer season. The transient ground-surface temperature is introduced into the time loop at the beginning of the model, after the pile has been installed.

$$T = T_{med} + \left(\frac{T_h - T_l}{2}\right) * \cos\left[\frac{2\pi(t-212)}{364}\right] \qquad (\mathbf{4.15})$$

where time, *t*, is in days.

Drilled-Shaft Model

The drilled-shaft model assumes drilled-shaft construction does not create a cavity expansion; hence, no EPWP is created during the construction of the drilled shaft. The drilled-shaft model also assumes no decrease in the static pore-water pressure (PWP) that may be caused by the relaxation of the clay along the excavation. The drilled shaft version of the model assumes the EPWP will be caused only by the transient temperatures at the energy-pile face. Therefore, the first day of the time loop is the first day of HVAC usage, i.e., the first day of summer. Other than this difference, this version of the model runs very similar to the drilled-shaft model for 728 days.

CHAPTER 5: RESULTS AND DISCUSSION

Introduction

The results of each iteration of the model are presented in this chapter. An emphasis has been placed upon values of the excess pore-water pressure (EPWP) and temperature at a variety of locations within the soil stratum that were most affected by the simulation of heating and cooling of the soil from the energy pile. Results for temperature and EPWP data were obtained for both vertical and horizontal slices of the soil. The figures presented in this chapter show the values of EPWP and temperature over the course of the model run with vertical slices of the soil. The data presented in the figures that show horizontal slices of soil is data presented in the figures with vertical slices of soil from a different perspective. Because the figures with horizontal slices do not present new or different data, these figures will be placed in Appendix C with little or no additional commentary. The locations are summarized in Table 5.1. Each figure also has a thumbnail-sized key located in the lower left corner. This key has a faint outline of the soil grid, with a heavy line representing the energy pile or drilled shaft, and a light solid line representing the vertical or horizontal locations from which the data points were taken. If no location line is present, the data points are located along the pile or drilled-shaft face.

Table 5.1. Different locations.

Figure Types	Distances from Pile/Drilled Shaft (m)		Depths (m)	
Vertical Slices in this Chapter	*Slice along*	0 (At Pile Edge)	*Shows results at*	3, 6, 9, 12, 15
		1/6		3, 6, 9, 12, 15
		1		3, 6, 9, 12, 15
		2		3, 6, 9, 12, 15
		3		3, 6, 9, 12, 15
Horizontal Slices in Appendix C	*Shows results at*	0, 1/6, 1, 2, 3	*Slice along*	5
		0, 1/6, 1, 2, 3		10
		0, 1/6, 1, 2, 3		15

The results are grouped by energy-pile type. Driven energy-pile results are presented first, followed by drilled-shaft results. The figures are grouped by their proximity to the pile. For each type of graph presented, the transient ground-surface temperature iteration follows the constant surface-soil temperature iteration so that differences in the graphs are more easily compared.

For each vertical slice of soil, the figures show the EPWP and temperature at the various lateral distances from the pile shown in Table 5.1 for the total elapsed time in the model. Next will be the difference in EPWP between the model with HVAC running and the model without HVAC running for the total elapsed time. These results are also displayed in figures according to the locations presented in Table 5.1. Following each set of differential EPWP figures, one figure shows the percent of initial EPWP along the pile surface for the total time. Afterwards, EPWP normalized to peak EPWP is presented. Following the results displaying the normalized EPWP, results showing the contribution to EPWP from pile expansion is presented. In addition, the contribution to EPWP from thermal expansion of the soil is presented for the various vertical distances from the pile only, as presented in Table 5.1. Finally, the unit-circumference-friction values over time for various depths are presented. Percent-initial EPWP and EPWP due to the thermal

expansion of the pile are only presented in the section of results that are adjacent to the pile.

For the drilled-shaft iteration of the model, fewer types of results are presented. Temperature and EPWP are presented according to the array presented in Table 5.1, but only for the two years of HVAC activity, since no setup period is necessary. In drilled-shaft construction, soil is removed from the ground, creating a void, and reinforced concrete fills that void—no EPWP is created. In contrast, a driven-pile creates a cavity without removing soil. The soil is disturbed and compressed, and in a soil with low hydraulic conductivity, the pore water cannot immediately find a path to dissipate. Normalized EPWP is next, presented with the combinations shown in Table 5.1. Then figures are presented showing EPWP due to thermal expansion of the drilled shaft and the soil. Finally, the unit-circumference-friction along the side of the drilled shaft over time is presented.

Following the series of results for the drilled-shaft iteration, several graphs are presented that demonstrate why the model results behaved the way they did. These graphs present radial and vertical coefficients of consolidation, the changes of the ratio of water density over dynamic viscosity as the temperature changes, and the saturated unit weight of the soil. In addition, a discussion is presented comparing the results of unit-circumference side friction calculated in the model with two methods presented in Chapter 2.

Variations of Temperature and Excess Pore-Water Pressure Results Adjacent to a Driven Energy-Pile

This section presents temperature and excess pore-water pressure (EPWP) results along the pile face over the period of time input into the model. Soil next to the pile has been densified due to cavity expansion from installation of the pile. Cavity expansion has been represented in the model as an increase in saturated unit weight and decreased void ratio. The void ratio decreased by assuming a coefficient of compression, C_c, and a stress increase of $\delta\sigma_r$, according to Equation (2.6). EPWP values begin near their peak values and then eventually decrease. Temperatures of the soil remain constant along the pile face, except for the influence of transient surface temperatures, until the introduction of temperature variations from HVAC activity. Figure 5.1 presents a schematic view to emphasize that, within this section, values are calculated on the face of the pile.

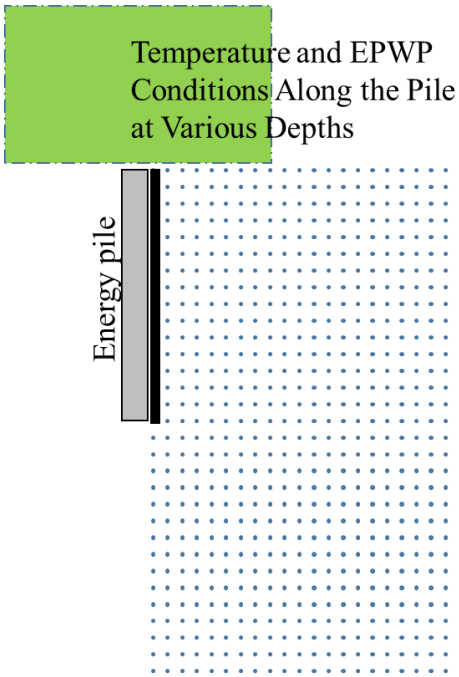

Figure 5.1. Figures in this chapter that present results from points along the face of the pile will be identified with this symbol.

Temperature Variations Over Time at Various Depths

The temperature along the pile face is presented over the course of the model period in Figures 5.2 and 5.3. All five of the depths shown in Figure 5.2 are initially at the same temperature because the model assumes the entire depth of the pile has the same daily temperature. The temperature at every depth along the pile begins at 15 °C and rises to just above 50 °C during the summer and drops to approximately 6 °C in the winter. The temperatures decrease more than they increase due to an assumption in the model. It is not a result but a reflection of input parameters. The temperatures in the second year rise and fall as much as they do in the first year, which is, again, a reflection of the assumptions in the model. Near the end of the second year, the temperature reaches a minimum value of approximately 1 °C.

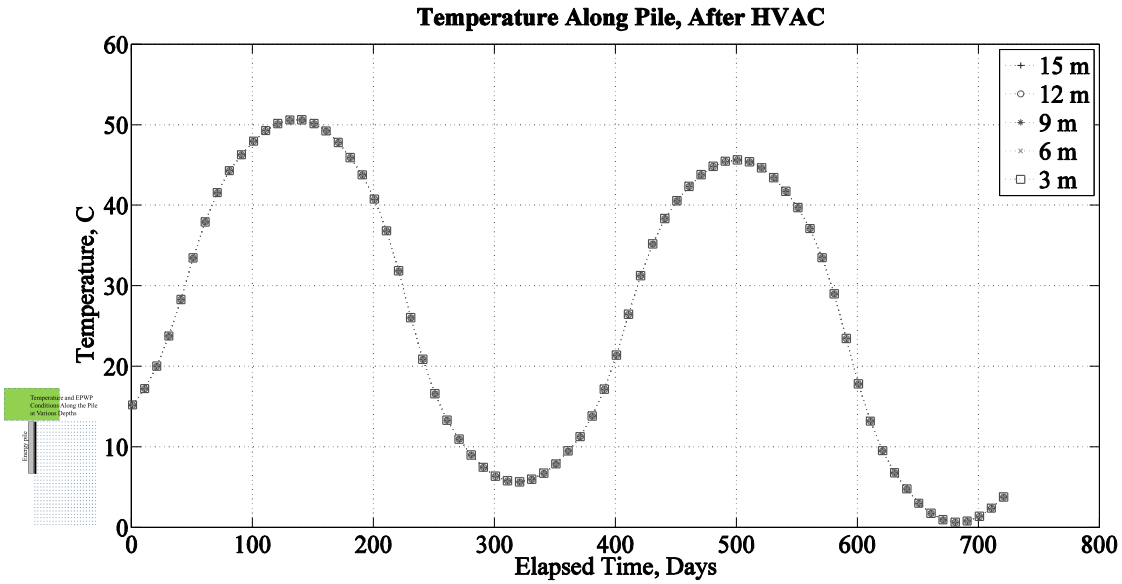

Figure 5.2. Temperature at the pile surface at various depths shown in Table 5.1, from the time of the beginning of HVAC introduction until the end of the model run. The ground-surface temperature is a constant 15 °C.

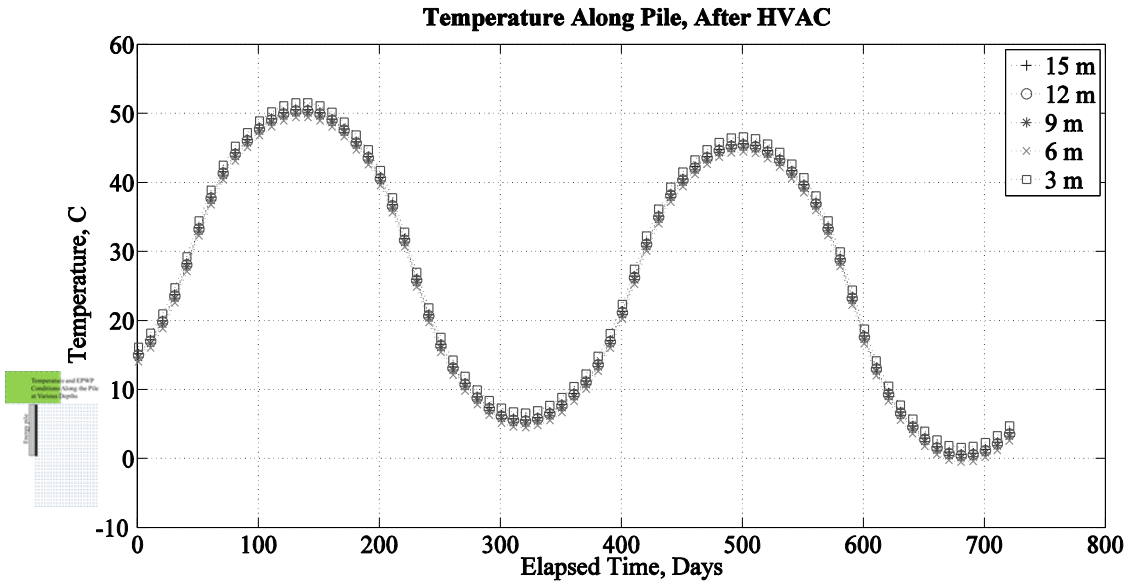

Figure 5.3. Temperature at the pile surface at various depths shown in Table 5.1, from the time of the beginning of HVAC introduction until the end of the model run, with transient ground-surface temperatures.

In Figure 5.3, the temperature of the soil at a depth of 3 m is consistently higher by approximately 1 °C than the other depths. Temperatures at a depth of 6 m are consistently lower by approximately 1 °C than the other depths as the temperatures reach maxima and minima.

Excess Pore-Water Pressure (EPWP) Variations Over Time at Various Depths

Figures 5.4 and 5.5 present EPWP data along the pile face at various depths. Figure 5.4 shows that the EPWP at various depths experiences an initial rise in value of approximately 14% immediately after pile installation. During this period, EPWP values increase before consolidation begins—a dilatory response of the soil that is similar to that described in Burns and Mayne (1999). The EPWP decreases more rapidly around Day 200. This coincides with the beginning of soil heating. The increased soil temperature increases the hydraulic conductivity of the soil.

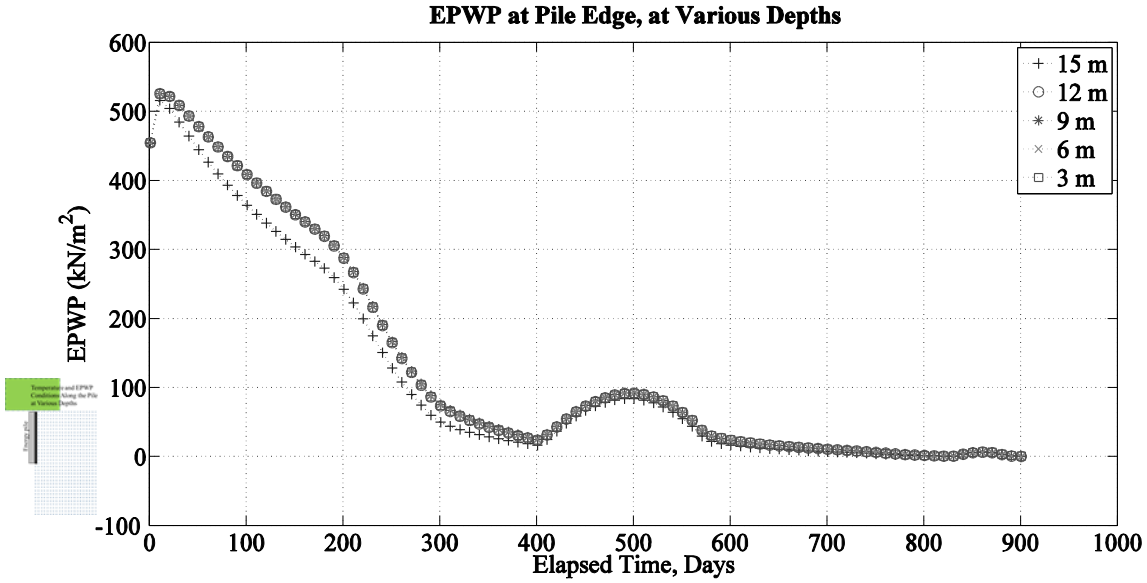

Figure 5.4. Excess pore-water pressure (EPWP) at the pile surface at various depths shown in Table 5.1, from the time of pile installation to the end of the model run. The ground-surface temperature is a constant 15 °C.

On Day 402, and peaking on Day 497, the EPWP increases 67 kN/m^2. This increase coincides with soil cooling during the winter season. There is another smaller increase in EPWP toward the end of Year 2. Figure 5.4 also shows EPWP values are equal along the pile face, with the exception of the 15m depth. This difference is likely due to the proximity of soil that has not undergone deformation due to cavity expansion within the assumptions of the model. In Figure 5.5, the influence of the ground-surface temperature has caused greater separation of the EPWP values at the 3m depth from the values at the other depths.

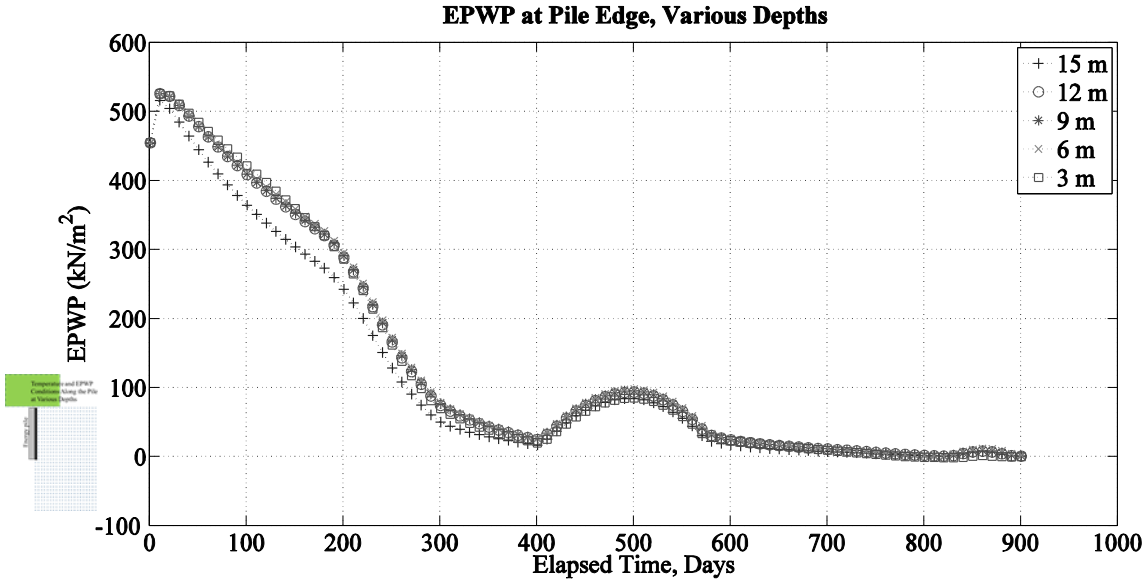

Figure 5.5. EPWP at the pile surface at various depths shown in Table 5.1, from the time of pile installation to the end of the model run, with transient ground-surface temperatures.

Comparison of EPWP Values Over Time With and Without HVAC

Figures 5.6 and 5.7 present the effect that temperature has on the value of EPWP at the side of the energy pile. The EPWP values over time without heating and cooling the soil at each depth shown in Figures 5.6 and 5.7 were subtracted from the EPWP values over time with the HVAC system heating and cooling the soil. Figures 5.6 and 5.7 show no difference until Day 183, when the HVAC is turned on, as expected. The EPWP value subject to temperature change remains lower than EPWP without temperature change until Day 485, when the EPWP increases due to soil cooling and peaks on Day 525, for all depths but the 15 m depth. The EPWP differential becomes negative once again on Day 563 and remains negative until the second spike near the end of Year 2. The greatest differential occurs on Day 309 at almost -139 kN/m^2.

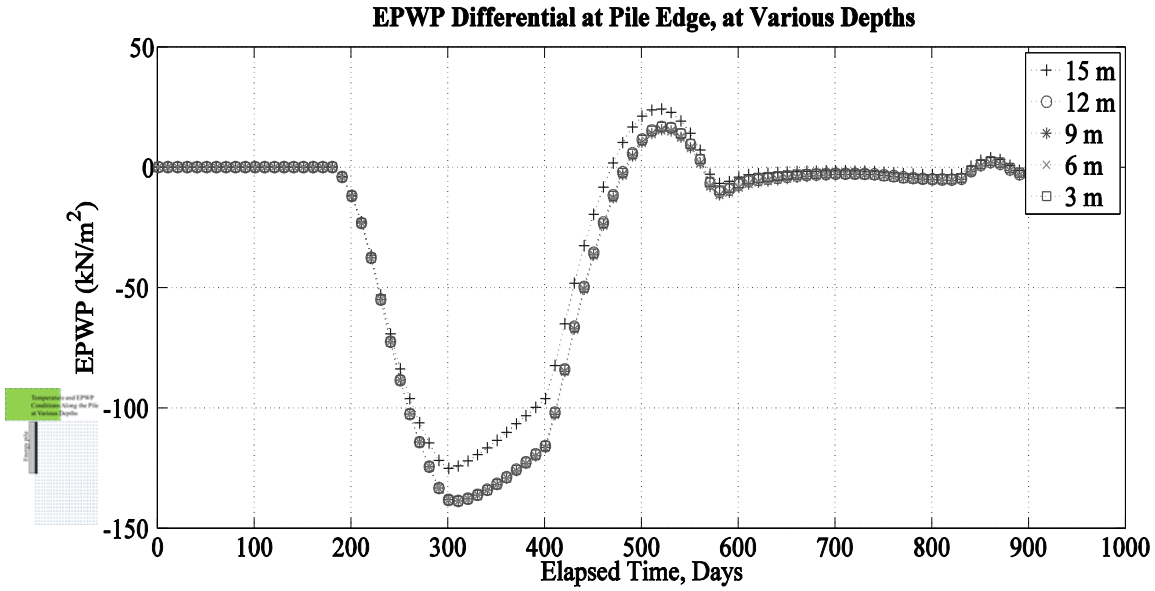

Figure 5.6. EPWP differential between model runs with and without HVAC introduction, along the pile surface at various depths. The ground-surface temperature is a constant 15 °C.

In Figure 5.7, greater variability of the EPWP values from each depth are evident, compared to Figure 5.6. In addition, the warmer surface temperature has lessened the positive differential values at the 3m depth between Days 508 and 567, and prevented the EPWP from becoming positive during Year 2. The differential value at the 3m depth reaches its minimum value around Day 300, but the differential is smaller in Figure 5.7 than in Figure 5.6. In addition, the minimum differential value at a depth of 3 m remains relatively constant for a duration of approximately 100 days in Figure 5.7.

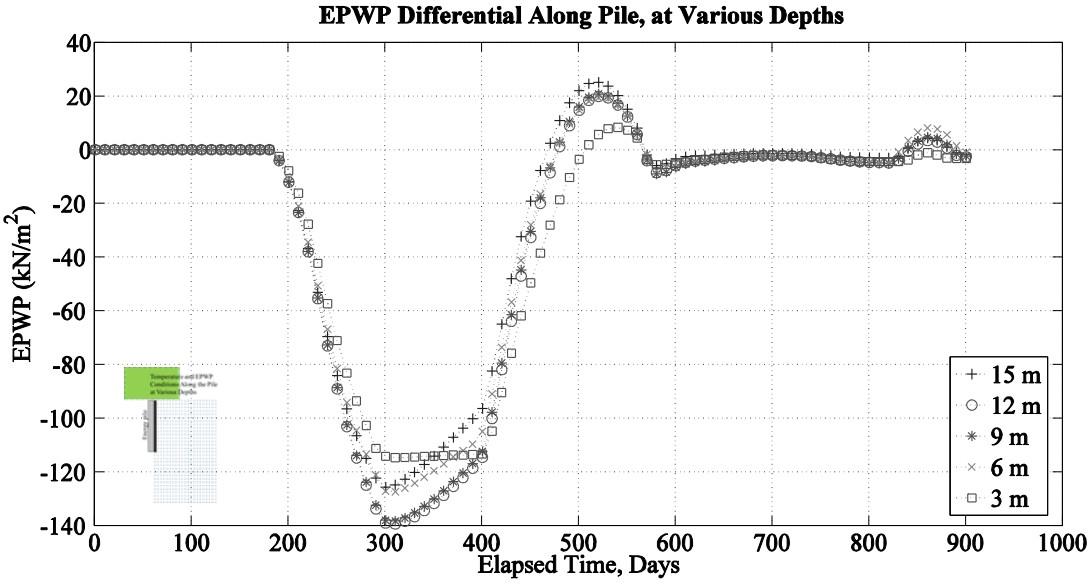

Figure 5.7. EPWP differential between model runs with and without HVAC introduction, along the pile surface at various depths, with transient ground-surface temperatures.

Percent of Initial EPWP at Various Depths

Figures 5.8 and 5.9 present the EPWP as a percentage of the initial EPWP at the pile face. The EPWP rises to approximately 116% of the original value before dissipation begins. The figure also shows that the increase in the EPWP due to the decrease in soil temperature is approximately 15%. In Figure 5.9, EPWP at the 3m depth is slightly lower than the depths in the middle of the pile.

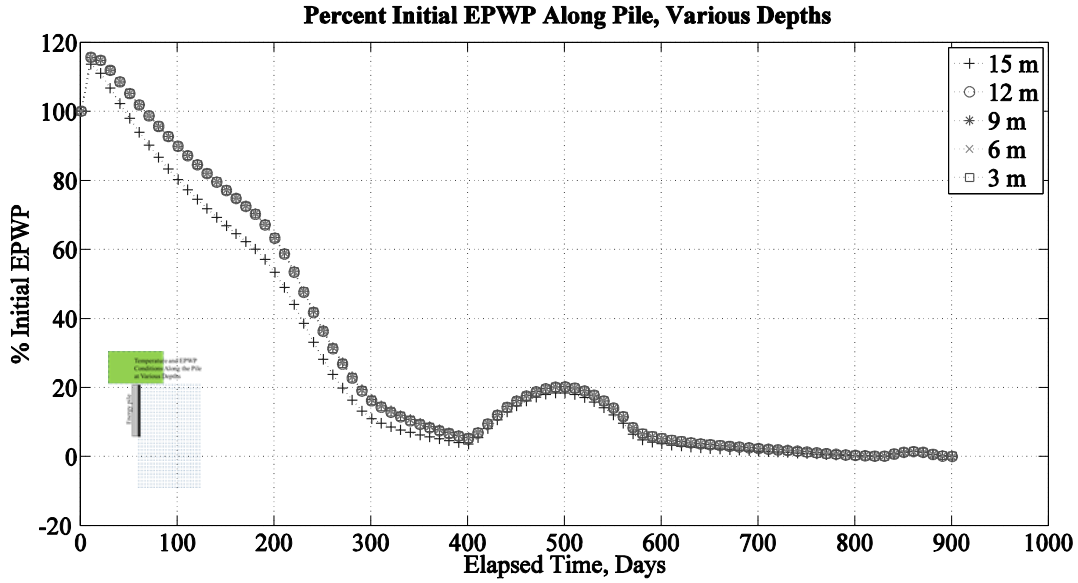

Figure 5.8. Percent Initial EPWP at the pile surface at various depths, from the time of pile installation to the end of the model run. The ground-surface temperature is a constant 15 °C.

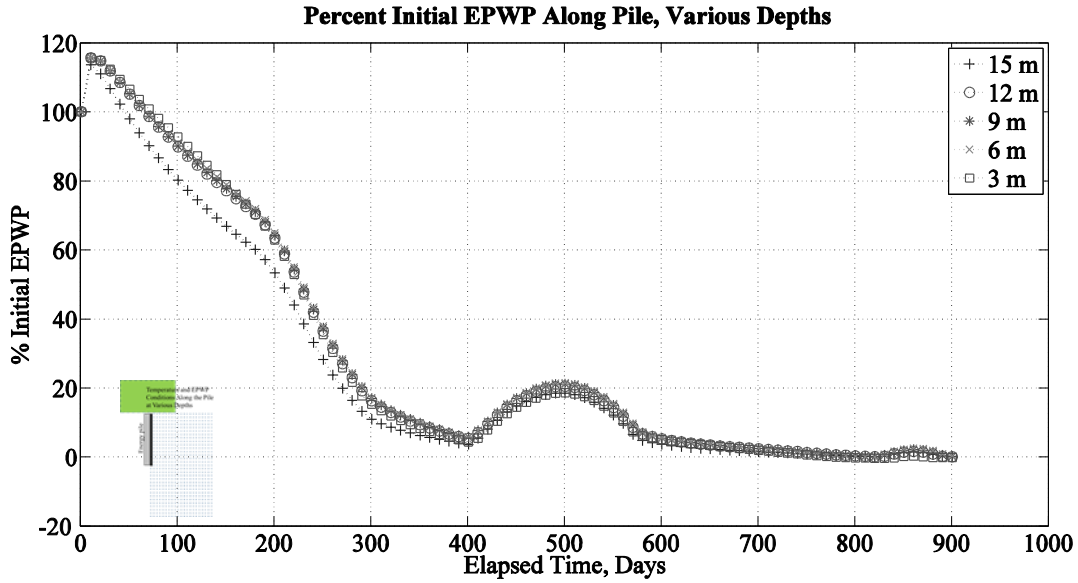

Figure 5.9. Percent Initial EPWP at the pile surface at various depths, from the time of pile installation to the end of the model run, with transient ground-surface temperatures.

EPWP Normalized to Peak EPWP at Various Depths

Figures 5.10 through 5.11 present the normalized EPWP at various horizontal distances from the energy pile as presented in Table 5.1. The initial EPWP is approximately 86% of the peak value and this value is reached 13 days after the model begins at the pile surface, as shown in Figure 5.10. Figure 5.11 differs slightly from Figure 5.10, because the EPWP at the 3m depth dissipates faster. The EPWP decreases at a rate of approximately 0.24% per day until the HVAC system starts, then decreases at a rate of approximately 0.38% per day until around Day 274. At this time the EPWP has dissipated to 20% of its peak value. By Day 400, the EPWP is down to approximately 5% of the peak value, but increases to 17% by Day 500.

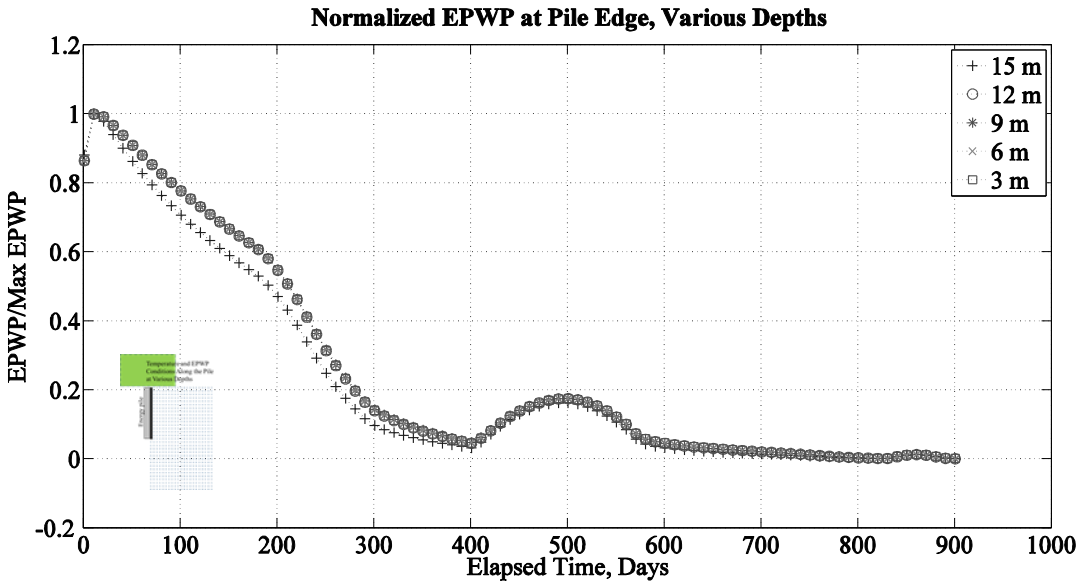

Figure 5.10. Normalized EPWP at the pile surface at various depths, from the time of pile installation to the end of the model run. The ground-surface temperature is a constant 15 °C.

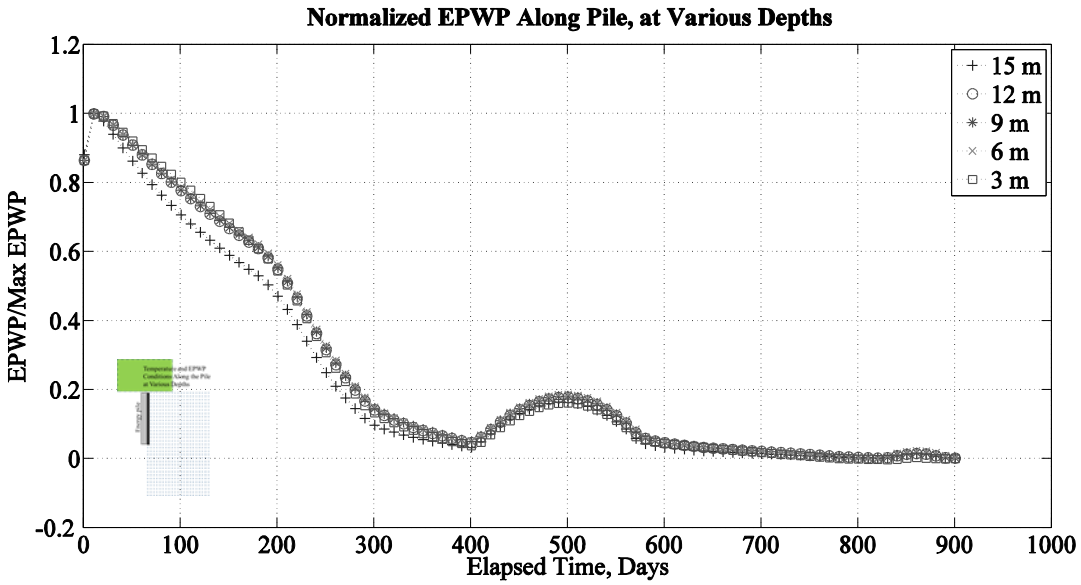

Figure 5.11. Normalized EPWP at the pile surface at various depths, from the time of pile installation to the end of the model run, with transient ground-surface temperatures.

EPWP Due to Thermal Expansion of the Pile

The contribution to the EPWP, by thermal expansion of the pile, is presented in Figures 5.12 and 5.13. The EPWP is slightly higher, again, at the 3m depth, in Figure 5.13, due to the influence of the higher ground-surface temperatures. The elapsed time begins after HVAC is started. The EPWP reaches a peak of approximately 0.43 kN/m^2 shortly after the amount of heat added to the system per day reaches its peak, i.e., after seven weeks. The EPWP due to thermal expansion of the pile decreases but remains positive until Day 134. The EPWP due to thermal expansion of the pile reaches its lowest value of -0.44 kN/m^2 on Day 211. The value of EPWP reaches a peak value of 0.33 kN/m^2 during the middle of summer of the second year, and a minimum Year 2 value of -0.34 kN/m^2.

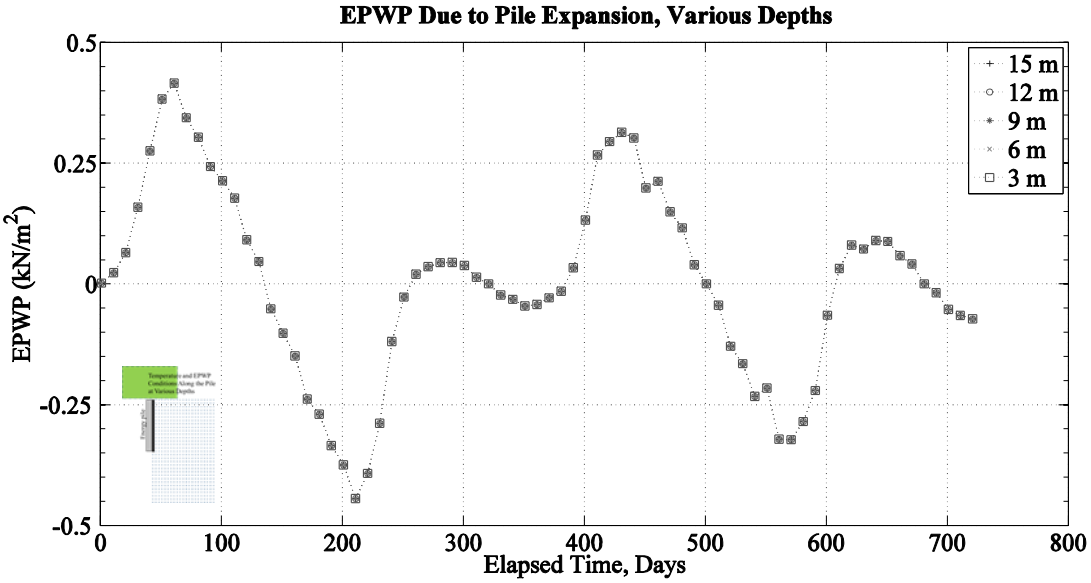

Figure 5.12. EPWP due to thermal expansion of the pile along the pile surface at various depths from the beginning of heating to the end of the model run. The ground-surface temperature is a constant 15 °C.

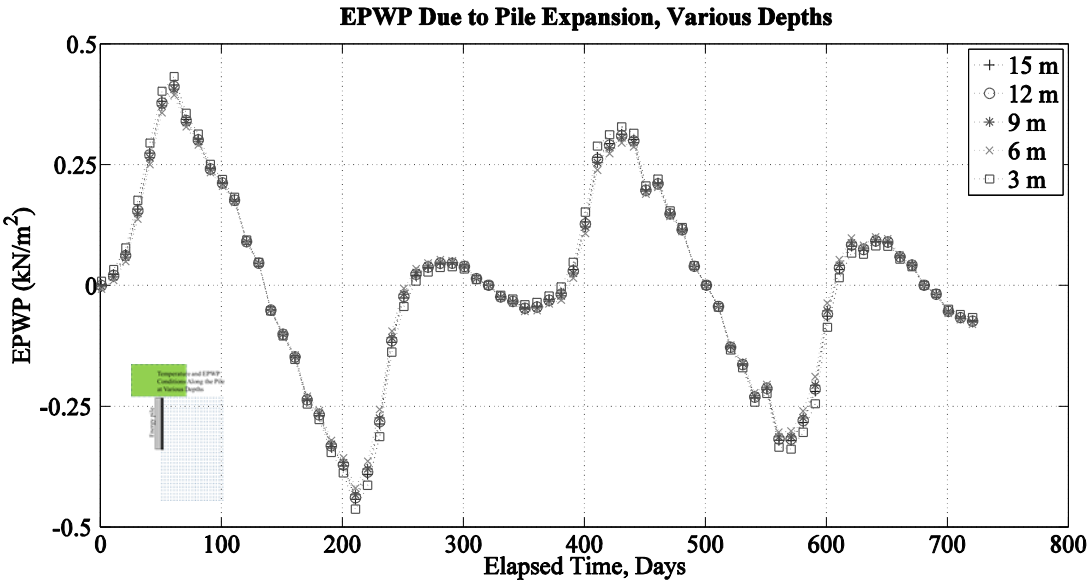

Figure 5.13. EPWP due to thermal expansion of the pile along the pile surface at various depths from the time of pile installation to the end of the model run, with transient ground-surface temperatures.

EPWP Due to Thermal Expansion of the Soil

EPWP along the pile ranges from approximately 0.24 kN/m^2 to -0.26 kN/m^2 in the model iteration with transient ground-surface temperatures in Figures 5.14 and 5.15. The range is slightly smaller with a constant surface temperature, because of elevated temperature values in the transient ground-surface model iteration that increase thermal expansion values at the 3m depth.

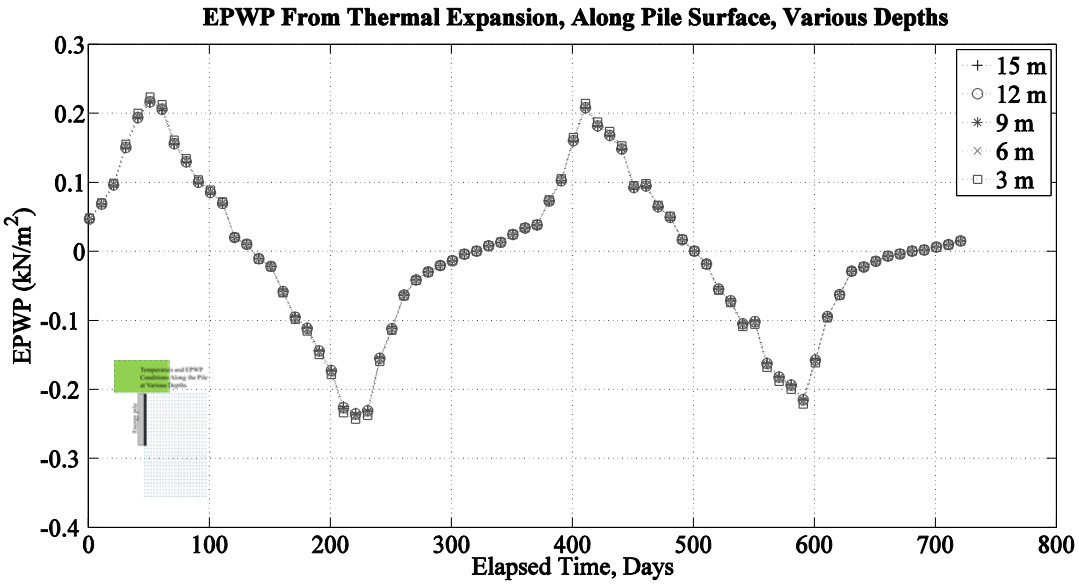

Figure 5.14. EPWP due to thermal expansion of the soil along the pile surface at various depths from the beginning of heating to the end of the model run. The ground-surface temperature is a constant 15 °C.

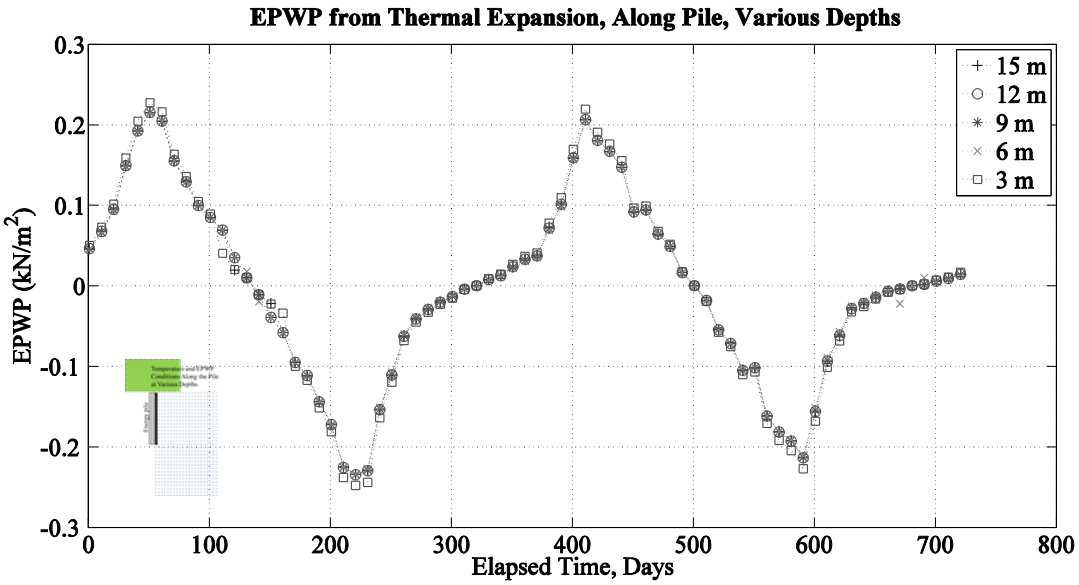

Figure 5.15. EPWP due to thermal expansion of the soil along the pile surface at various depths from the time of pile installation to the end of the model run, with transient ground-surface temperatures.

Variations of Temperature and EPWP at a Lateral Distance of 1/6 m from the Pile Face

The soil at this distance from the pile face is slightly less dense than that soil adjacent to the pile face. The EPWP and temperature differences between soil at this distance and the soil adjacent to the pile face will be small. Figure 5.16 indicates the lateral distance from the pile from which the results in this section were presented along the depth.

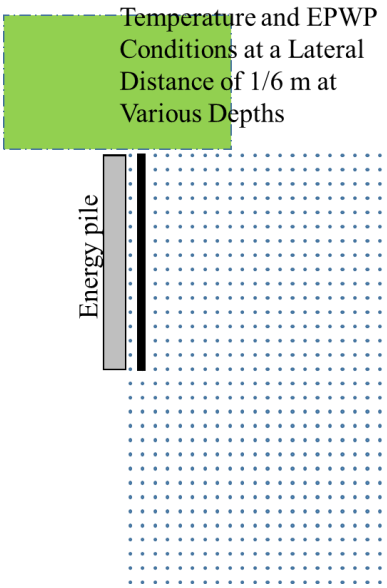

Figure 5.16. Figures in this chapter that present results from points at a lateral distance of 1/6 m from the pile will be identified with this symbol.

Temperature Variations at Various Depths

The temperature never rises above 44 °C at a lateral distance of 1/6 m from the pile, according to Figure 5.17. Similarly, the temperature never goes below 5 °C at the end of the modeled time period. The temperatures at the various depths also show more variance compared to each other than to those temperatures along the pile face. The temperatures at depths of 3 m and 15 m are usually lower than the other depths, most likely because they are closer to constant temperatures of 15 °C at the ground surface and below the pile.

In Figure 5.18, the temperatures for the 3m depth are slightly higher than in Figure 5.17. In addition, temperatures at the 6m depth are the lowest when temperatures reach their minimums near Day 330. Temperatures for the 3m depth are approximately two degrees higher with the warmer ground-surface temperatures in Figure 5.18 compared to those in Figure 5.17.

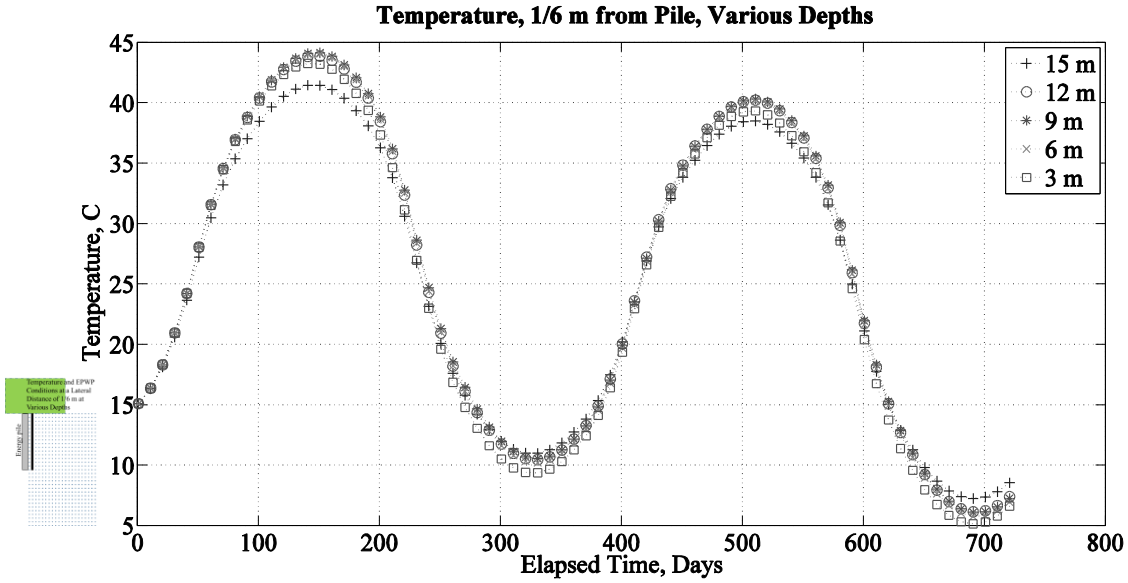

Figure 5.17. Temperature at various depths at a lateral distance of 1/6 m from the pile, from the time of pile installation to the end of the model run. The ground-surface temperature is a constant 15 °C.

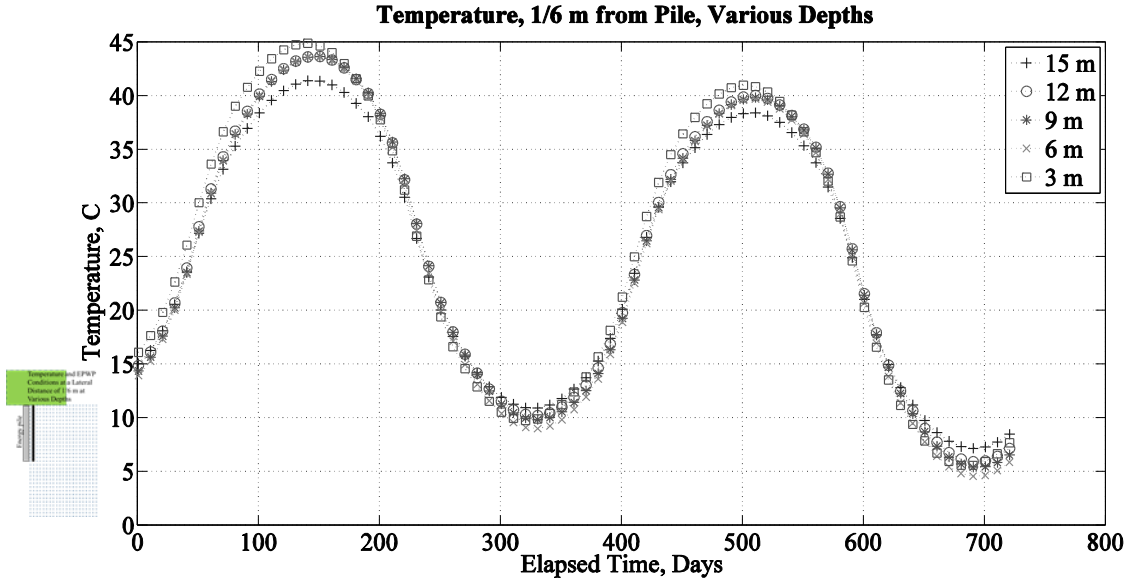

Figure 5.18 Temperature at various depths at a lateral distance of 1/6 m from the pile, from the time of pile installation to the end of the model run, with transient ground-surface temperatures.

Excess Pore-Water Pressure (EPWP) Values Over Time at Various Depths

The results displayed in Figure 5.19 appear to be similar to those in Figure 5.4 but are lower in magnitude. The initial EPWP value is approximately 94 kN/m^2 and rises to approximately 342 kN/m^2 by Day 37.

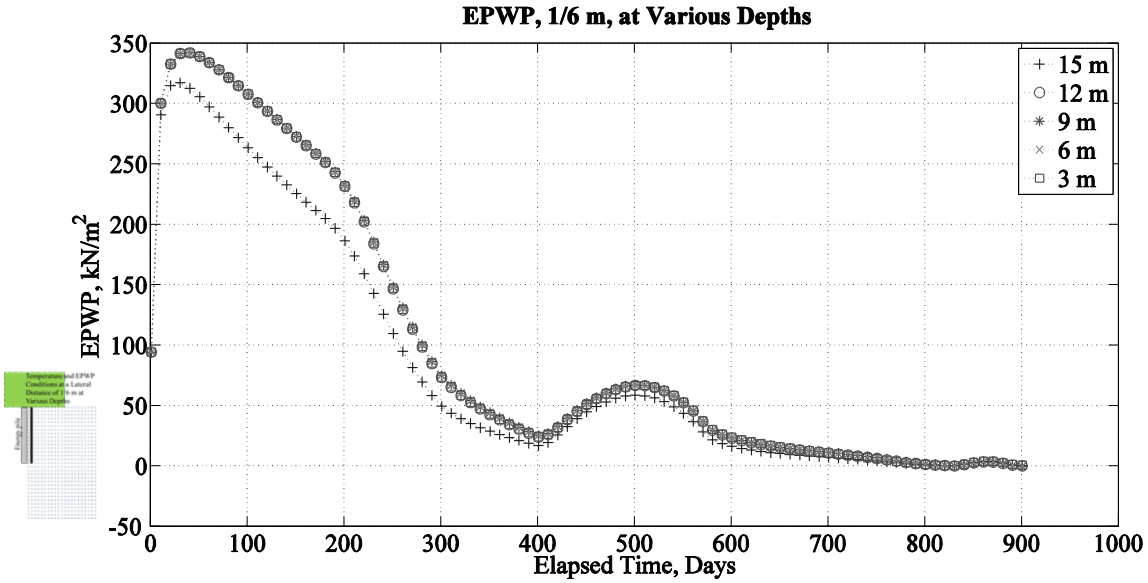

Figure 5.19. EPWP at a lateral distance of 1/6 m from the pile surface at the various depths shown in Table 5.1, from the time of pile installation to the end of the model run. The ground-surface temperature is a constant 15 °C.

Figure 5.20 shows similar results to Figure 5.19, with similar separation of the 3 m depth observed in Figure 5.5.

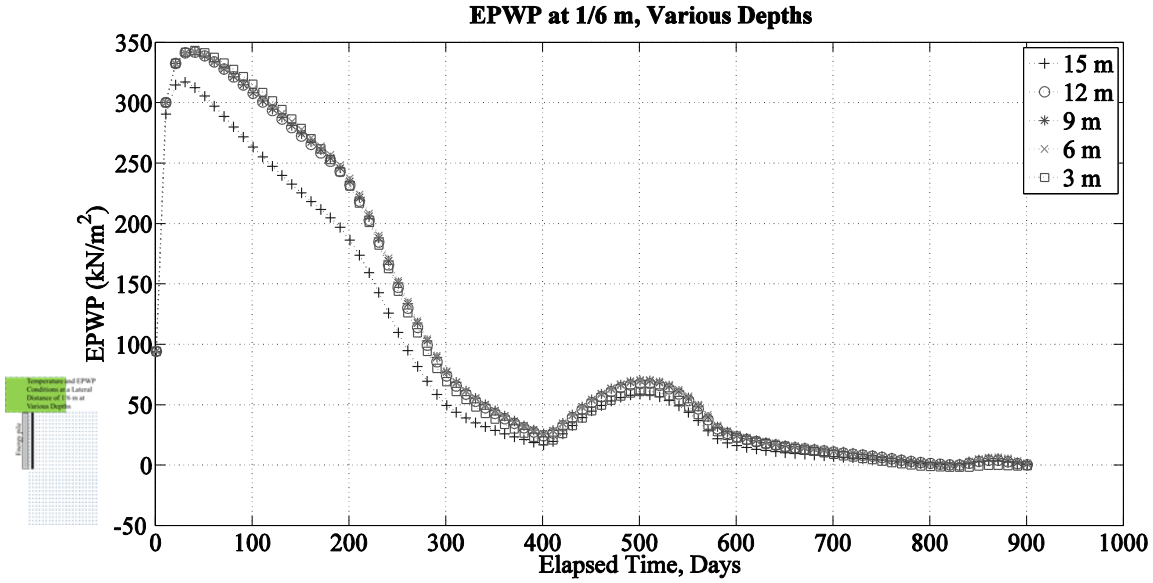

Figure 5.20. EPWP at a lateral distance of 1/6 m from the pile surface at various depths from the time of pile installation to the end of the model run, with transient ground-surface temperatures.

Comparison of EPWP Values Over Time With and Without HVAC

The differences in EPWP at a lateral distance of 1/6 m from the pile shown in Figures 5.21 and 5.22 are similar to those in Figures 5.6 and 5.7, but the magnitude of the differential is lower. In Figure 5.22, the effect of surface temperature becomes apparent—the 3m depth becomes briefly positive, but is less than the EPWP at that depth in Figure 5.21.

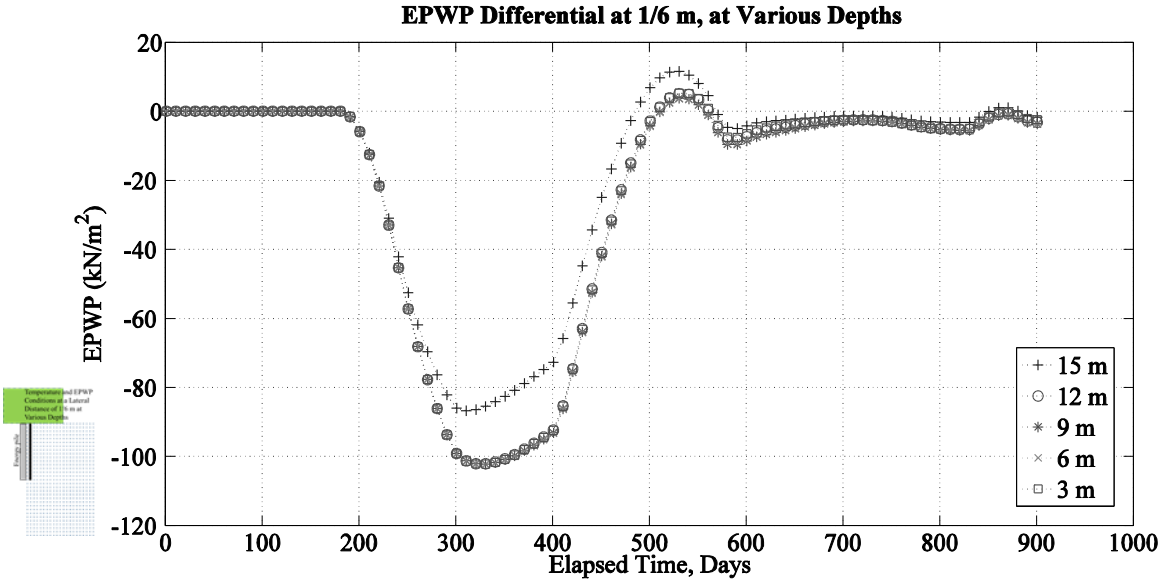

Figure 5.21. EPWP differential between model runs with and without HVAC introduction, at a lateral distance of 1/6 m from the pile surface at various depths. The ground-surface temperature is a constant 15 °C.

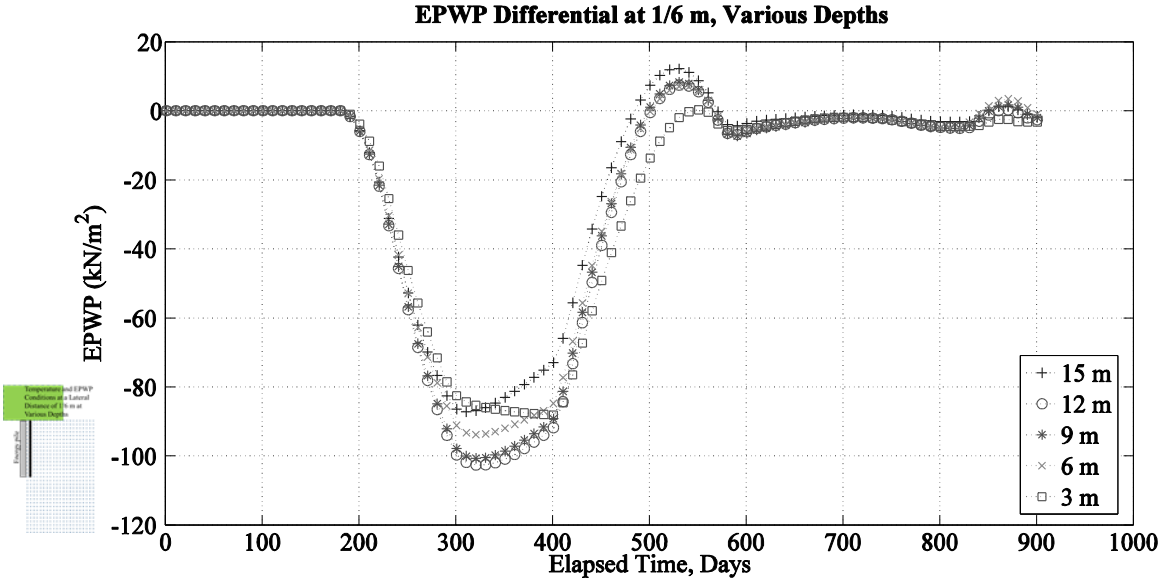

Figure 5.22. EPWP differential between model runs with and without HVAC introduction, at a lateral distance of 1/6 m from the pile surface at various depths, with transient ground-surface temperatures.

EPWP Normalized to Peak EPWP at Various Depths

As the distance from the pile increases, the time to reach the peak EPWP increases. In Figures 5.23 and 5.24, the peak is not reached until Day 37. The initial EPWP value is 27.5% of the peak value. After the peak EPWP value is reached, the initial rate of dissipation is approximately 0.2% per day and is lower than that present near the pile face. From Day 220 to Day 280, the rate of decrease of EPWP (dissipation) is approximately 0.59% per day. By Day 400, EPWP is approximately 7% of the peak value.

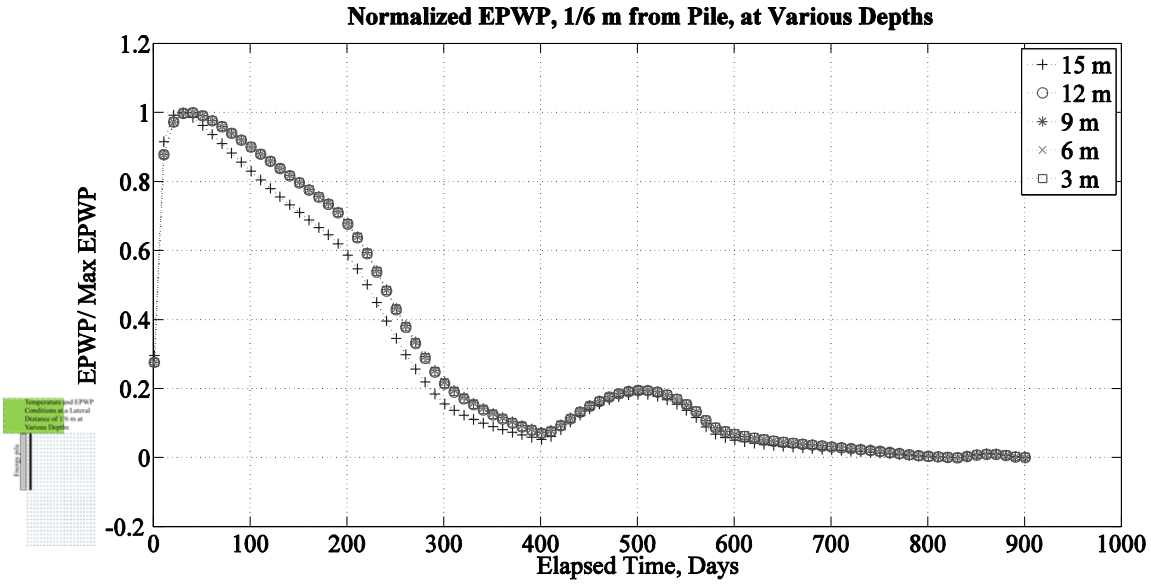

Figure 5.23. Normalized EPWP at a lateral distance of 1/6 m from the pile surface at various depths, from the time of pile installation to the end of the model run. The ground-surface temperature is a constant 15 °C.

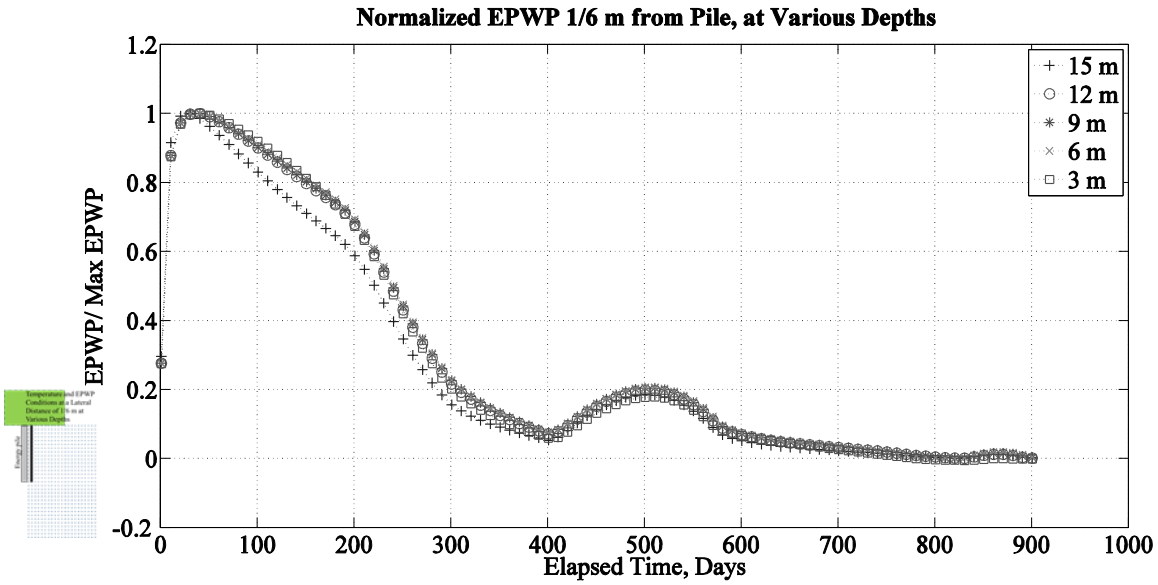

Figure 5.24. Normalized EPWP at a lateral distance of 1/6 m from the pile surface at various depths, from the time of pile installation to the end of the model run, with transient ground-surface temperatures.

EPWP Due to Thermal Expansion of the Soil

EPWP near the pile ranges from approximately 0.15 kN/m^2 to -0.19 kN/m^2 in the model iteration with transient ground-surface temperatures in Figures 5.25 and 5.26. The range is slightly less with a constant surface temperature, because of elevated temperature values in the transient ground-surface model iteration that increase thermal expansion values at the 3m depth.

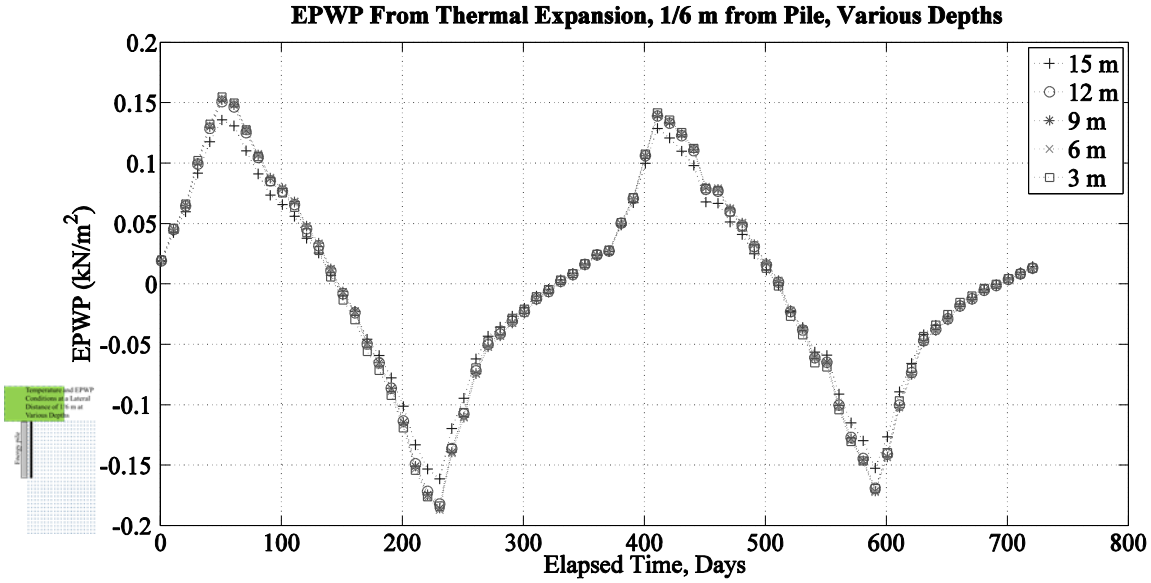

Figure 5.25. EPWP due to thermal expansion of the soil at a lateral distance of 1/6 m at various depths from the beginning of heating to the end of the model run. The ground-surface temperature is a constant 15 °C.

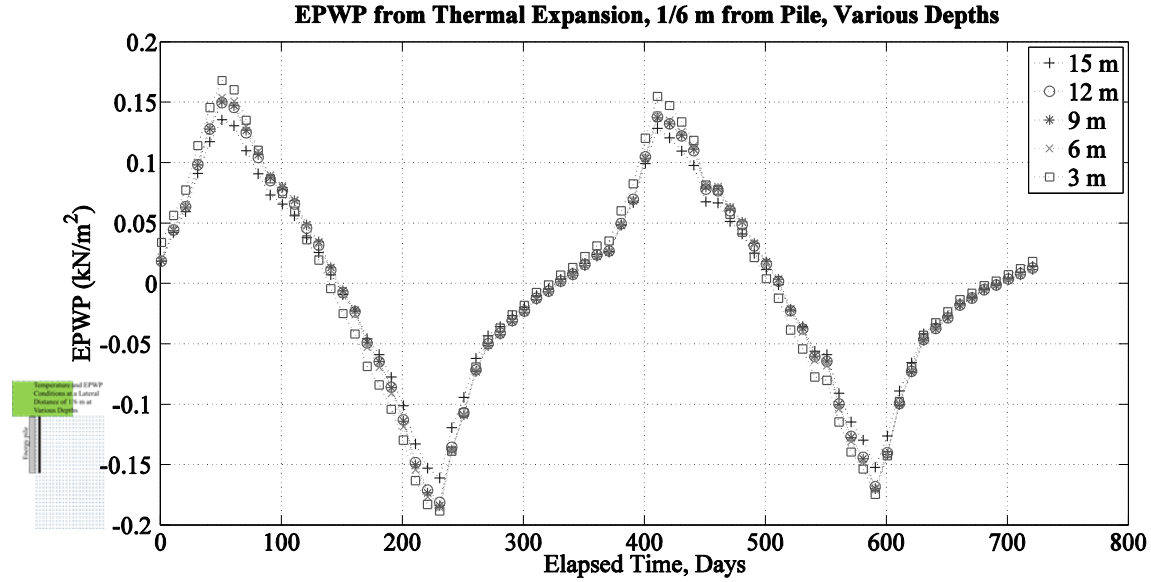

Figure 5.26. EPWP due to thermal expansion of the soil at a lateral distance of 1/6 m at various depths from the time of pile installation to the end of the model run, with transient ground-surface temperatures.

Variations of Temperature and EPWP at a Lateral Distance of 1 m from the Pile Face

At a distance of 1 m from the pile face, delays in the time for the EPWP and temperature values to reach their peaks and minimums are apparent. Soil at this distance from the pile face are less dense and are near the far edge of the plastic deformation zone. The peak EPWP and temperature values at this distance do not reach those values observed near the pile. Figure 5.27 indicates the relative distance from the pile face where the results in this section are presented along the depth.

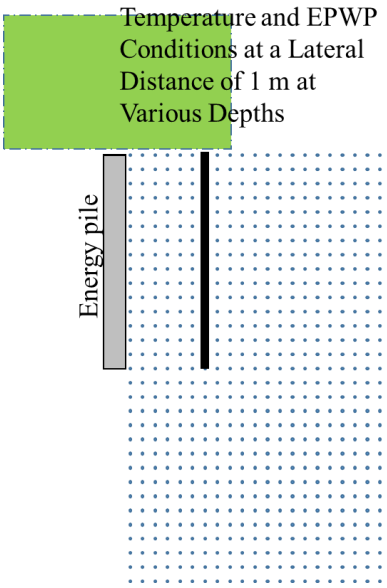

Figure 5.27. Figures in this chapter that present results from points at a lateral distance of 1 m from the pile will be identified with this symbol.

Temperature Values Over Time at Various Depths

The temperatures shown in Figure 5.28 show greater variation than at the previous distances from the pile. Again, the interior depths see higher temperatures than the 3m and 15m depths. The 3m depth is out of phase compared to the other depths, showing peak and minimum yearly temperatures 15 days earlier than the remaining

depths because the ground-surface temperature is lower than the soil at 3 m, preventing it from rising as high as the soil below, which is less affected by the cooler ground-surface temperature.

The temperatures at the 3m depth in Figure 5.29 are more out of phase with the other depths than they are in Figure 5.28. The soil temperature is approximately 16 °C at the start of HVAC usage, due to the influence of the ground-surface temperature. As a result, the 3m depth reaches peak and minimum temperatures approximately 43 days earlier than the other depths during the first year, and that number is closer to 39 days during the second year.

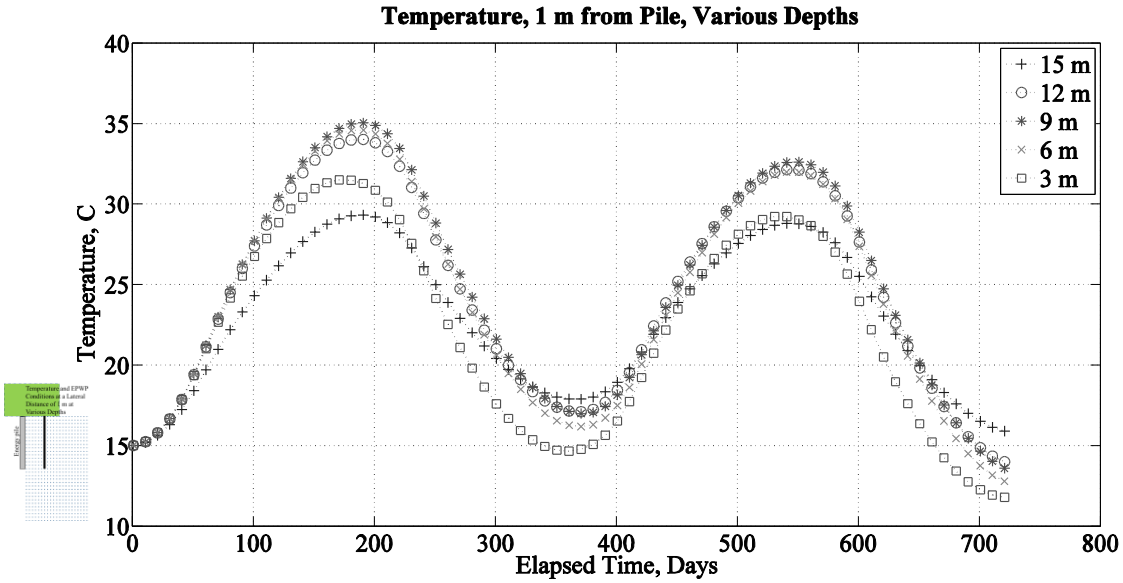

Figure 5.28. Temperature at various depths at a lateral distance of 1 m from the pile, from the time of pile installation to the end of the model run. The ground-surface temperature is a constant 15 °C.

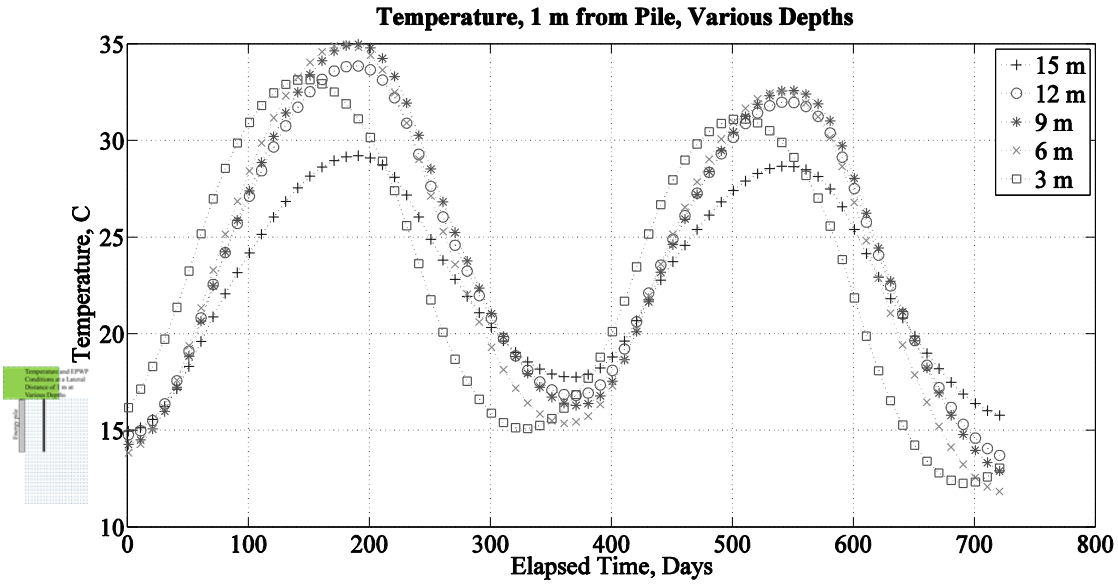

Figure 5.29. Temperature at various depths at a lateral distance of 1 m from the pile, from the time of pile installation to the end of the model run, with transient ground-surface temperatures.

Excess Pore-Water Pressure (EPWP) Values Over Time at Various Depths

Figure 5.30 presents EPWP at various depths at a lateral distance of 1 m from the pile. The depths shown, with the exception of the 15m depth, reach peak EPWP values of approximately 126 kN/m^2 about four months after pile installation. At this distance, there is still an increase in the EPWP due to soil cooling, but the increase is lower and does not peak until Day 535. The soil at a depth of 15 m reaches a peak EPWP value of approximately 94 kN/m^2 on Day 114.

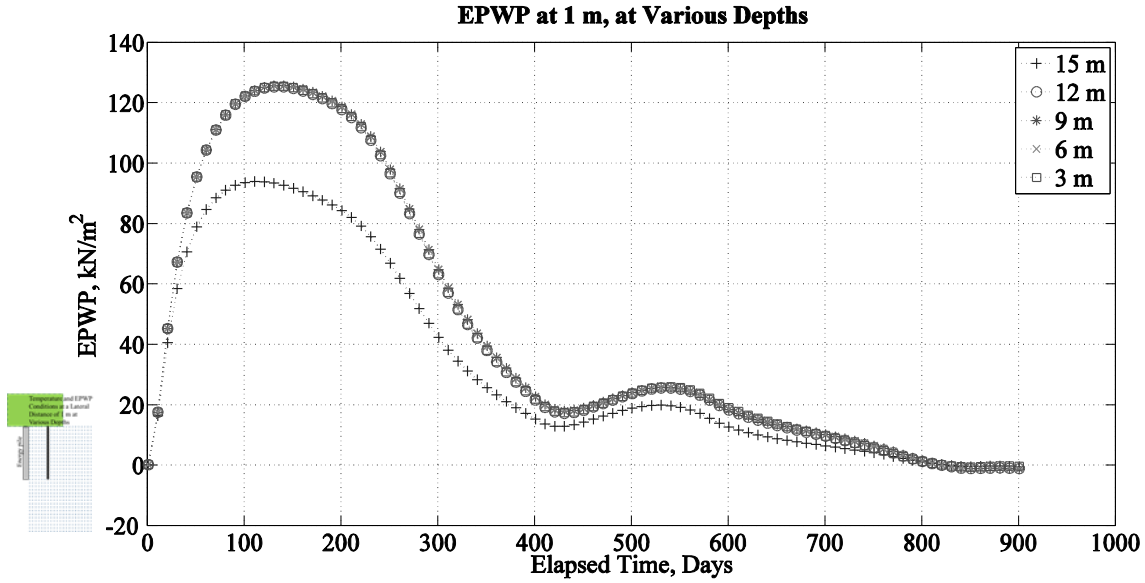

Figure 5.30. EPWP at a lateral distance of 1 m from the pile surface at various depths from the time of pile installation to the end of the model run. The ground-surface temperature is a constant 15 °C.

The 3m depth exhibits lower EPWP in Figure 5.31 than in Figure 5.30.

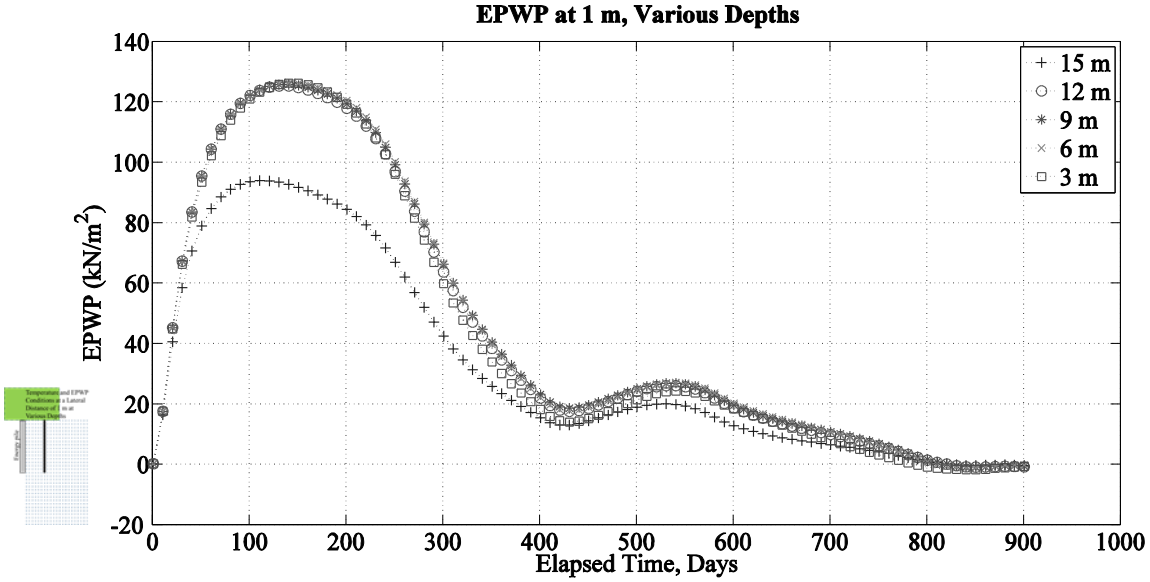

Figure 5.31. EPWP at a lateral distance of 1 m from the pile surface at various depths from the time of pile installation to the end of the model run, with transient ground-surface temperatures.

Comparison of EPWP Values Over Time With and Without HVAC

At a lateral distance of 1 m from the pile, as presented in Figures 5.32 and 5.33, the same differential remains nonexistant until after Day 200, and never becomes positive. The peak negative differential is -47 kN/m^2. In Figure 5.33, the EPWP values at depths other than at 15 m show greater variability. EPWP differential values at the 3m and 6m depths decrease more slowly with higher surface temperatures, suggesting some influence at the 6m depth.

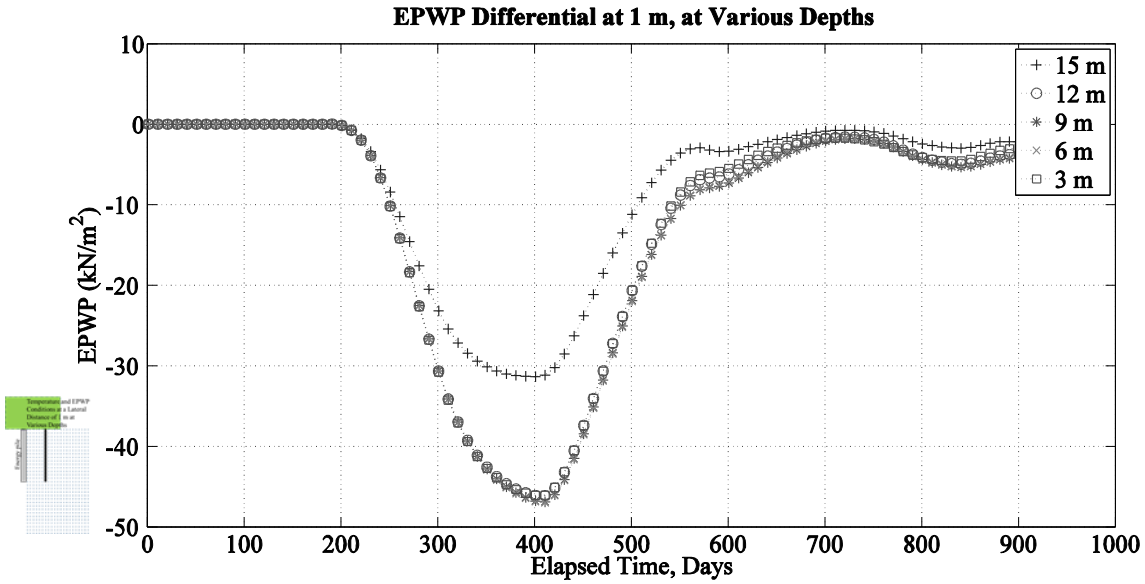

Figure 5.32. EPWP differential between model runs with and without HVAC introduction, at a lateral distance of 1 m from the pile surface at various depths. The ground-surface temperature is a constant 15 °C.

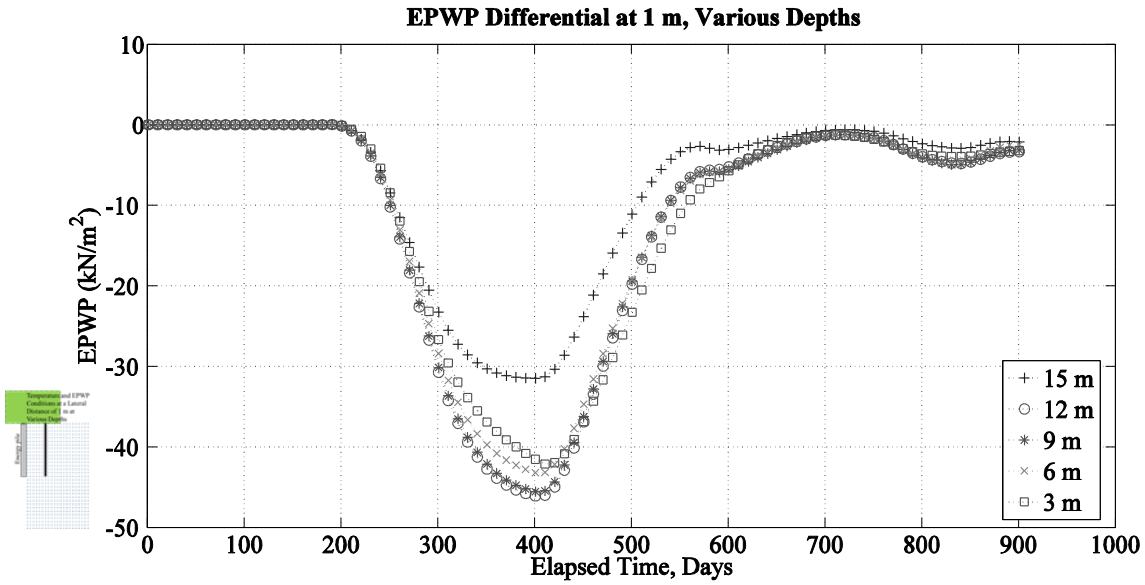

Figure 5.33. EPWP differential between model runs with and without HVAC introduction, at a lateral distance of 1 m from the pile surface at various depths, with transient ground-surface temperatures.

EPWP Normalized to Peak EPWP at Various Depths

The initial EPWP is zero at 1 m from the pile face. The time to reach the peak EPWP increases as the distance from the pile increases, and is 113 days at the 1m distance. By the end of the model run, the EPWP values are below zero at all depths. This is likely due to the soil temperature. The rates of change near the peak EPWP are lower at this distance from the pile than at or near the pile face. After the peak EPWP values are reached, the rates of dissipation from 80% of peak EPWP down to 40% of the peak EPWP for the distances are around 0.5% per day (shown in Figures 5.34 and 5.35).

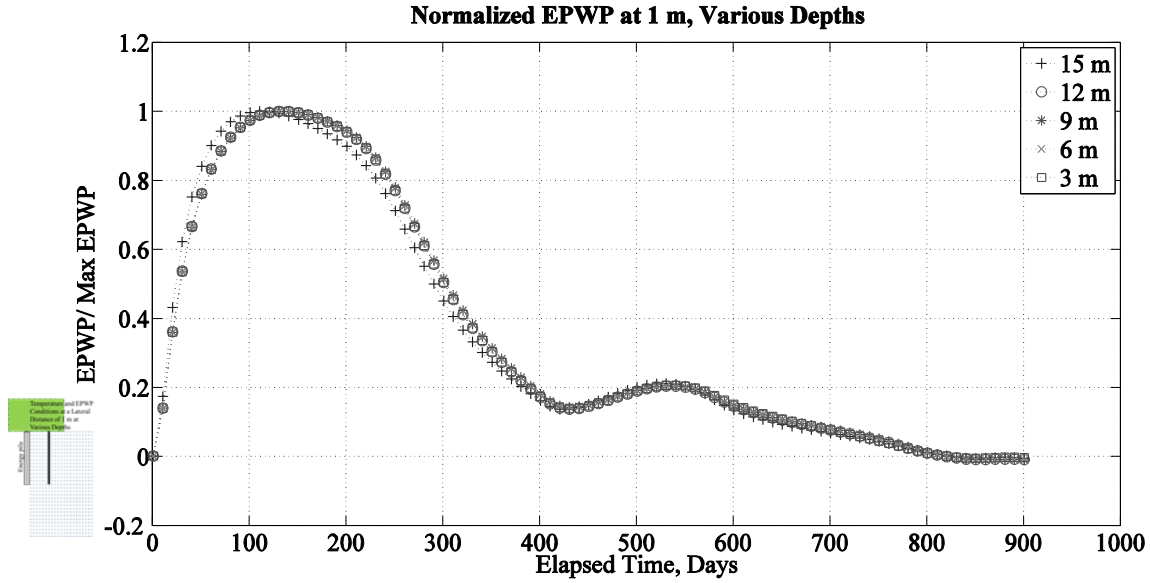

Figure 5.34. Normalized EPWP at a lateral distance of 1 m from the pile surface at various depths, from the time of pile installation to the end of the model run. The ground-surface temperature is a constant 15 °C.

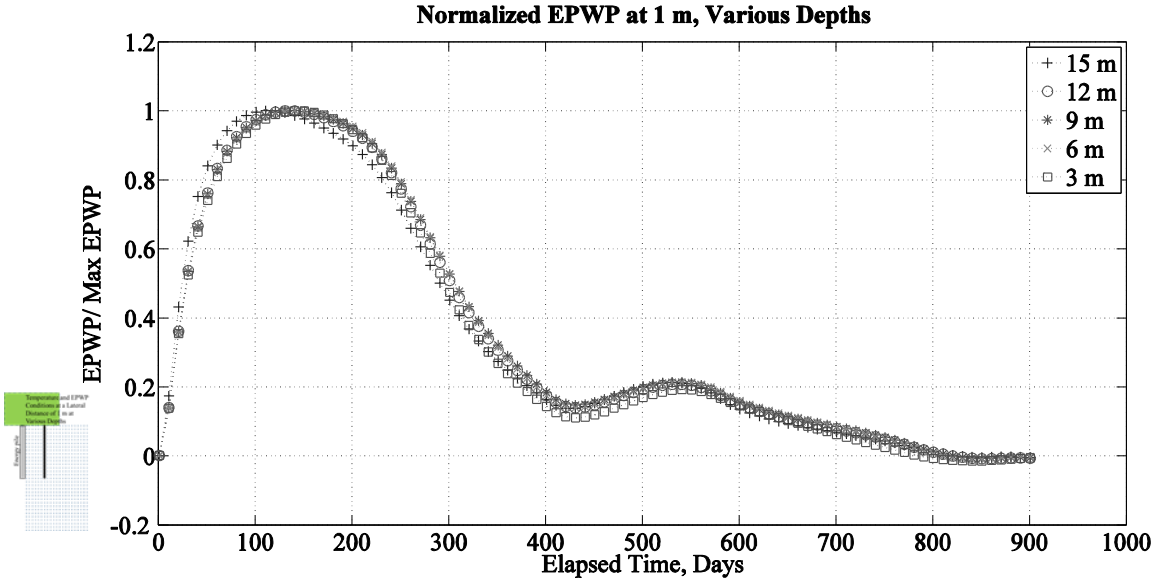

Figure 5.35. Normalized EPWP at a lateral distance of 1 m from the pile surface at various depths, from the time of pile installation to the end of the model run, with transient ground-surface temperatures.

EPWP Due to Thermal Expansion of the Soil

Figures 5.36 and 5.37 present the contribution of EPWP from thermal expansion of the soil. EPWP along the pile ranges from approximately 0.08 kN/m^2 to -0.09 kN/m^2 in the model iteration with transient ground-surface temperatures in Figure 5.37. The range of EPWP is slightly lower in Figure 5.36 because of elevated temperature values in the transient ground-surface model iteration that increase thermal expansion values at the 3m depth.

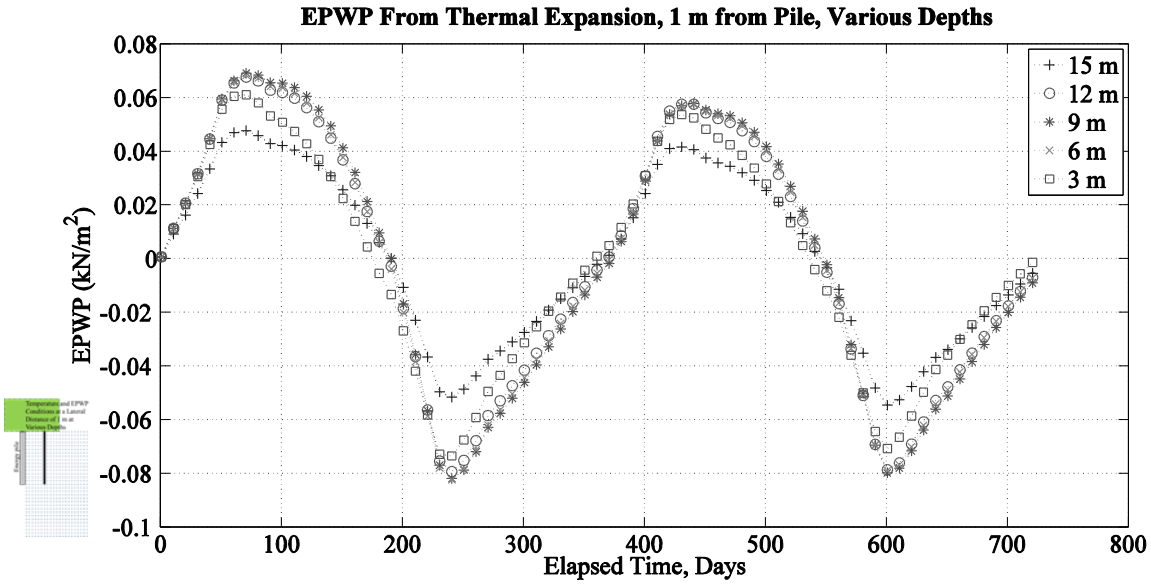

Figure 5.36. EPWP due to thermal expansion of the soil at a lateral distance of 1 m at various depths from the beginning of heating to the end of the model run. The ground-surface temperature is a constant 15 °C.

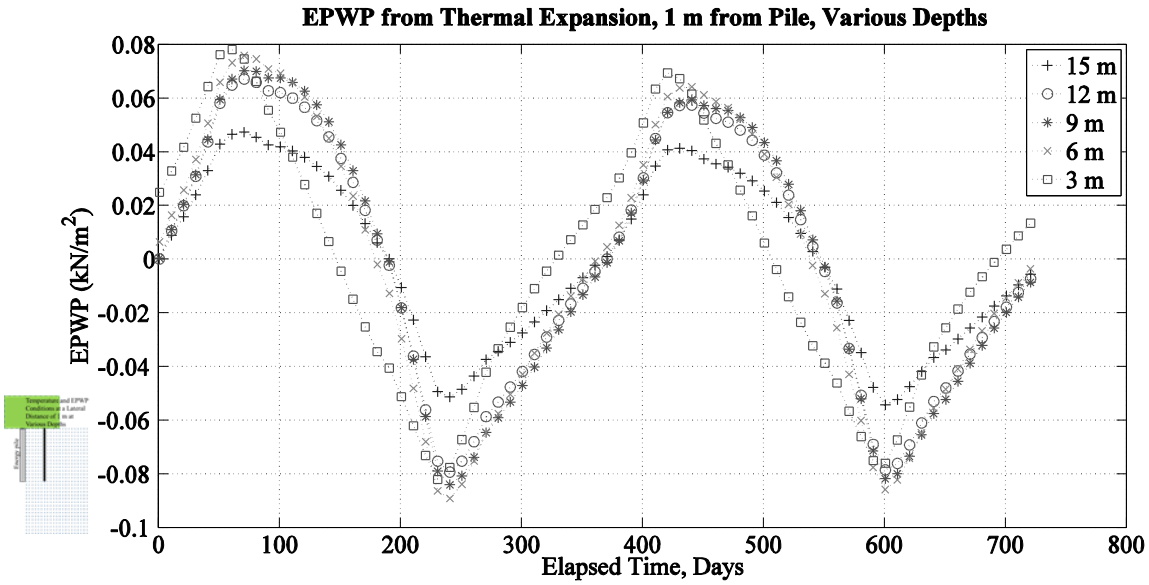

Figure 5.37. EPWP due to thermal expansion of the soil at a lateral distance of 1 m at various depths from the time of pile installation to the end of the model run, with transient ground-surface temperatures.

Variations of Temperature and EPWP at a Lateral Distance of 2 m from the Pile Face

The soil at this distance from the pile face is out of the plastic zone that was created by cavity expansion of the soil from pile installation. EPWP and temperature values are lower than those closer to the pile. The influence of transient ground-surface temperatures is greater. Figure 5.38 presents the relative location where the results of this section are presented along the depth.

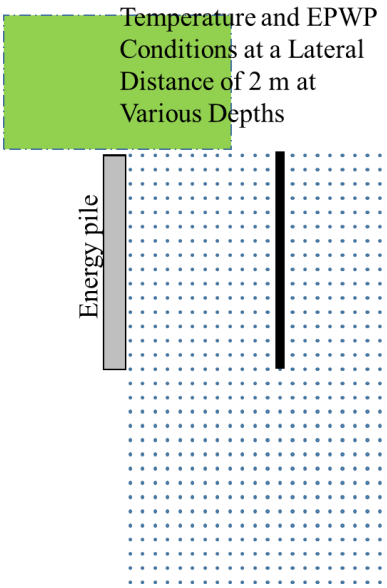

Figure 5.38. Figures in this chapter that present results from points at a lateral distance of 2 m from the pile will be identified with this symbol.

Temperature Values Over Time at Various Depths

The temperatures at a lateral distance of 2 m from the pile, shown in Figures 5.39 and 5.40, reach peak values 25 days later than the temperatures shown in Figures 5.28 and 5.29. The different depths show additional separation from each other in the cases of Figures 5.39 and 5.40 as well.

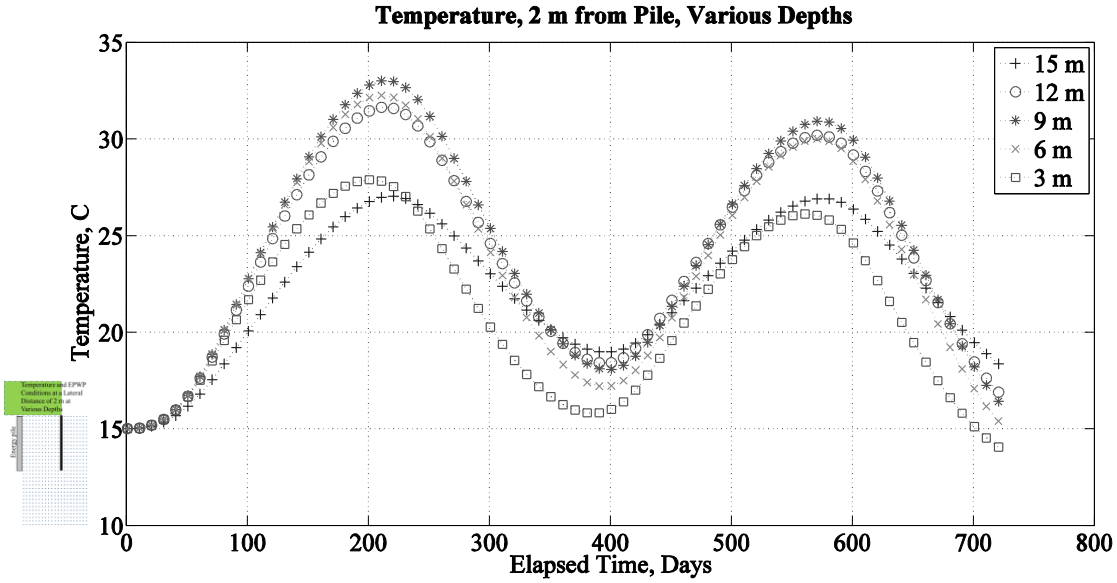

Figure 5.39. Temperature at various depths at a lateral distance of 2 m from the pile, from the time of pile installation to the end of the model run. The ground-surface temperature is a constant 15 °C.

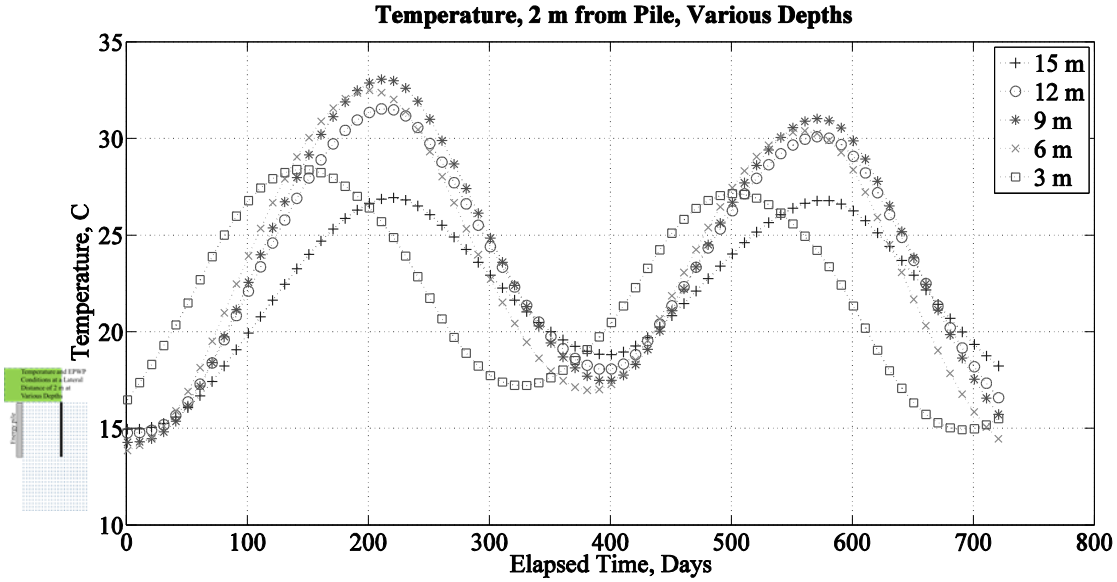

Figure 5.40. Temperature at various depths at a lateral distance of 2 m from the pile, from the time of pile installation to the end of the model run, with transient ground-surface temperatures.

Excess Pore-Water Pressure (EPWP) Values Over Time at Various Depths

At a lateral distance of 2 m from the pile, Figure 5.41 shows peak EPWP of approximately 53 kN/m^2 after 194 days, with the 15 m depth showing EPWP values of approximately 17 kN/m^2 less. The effect of soil cooling is less pronounced in this case and does not peak until Day 579.

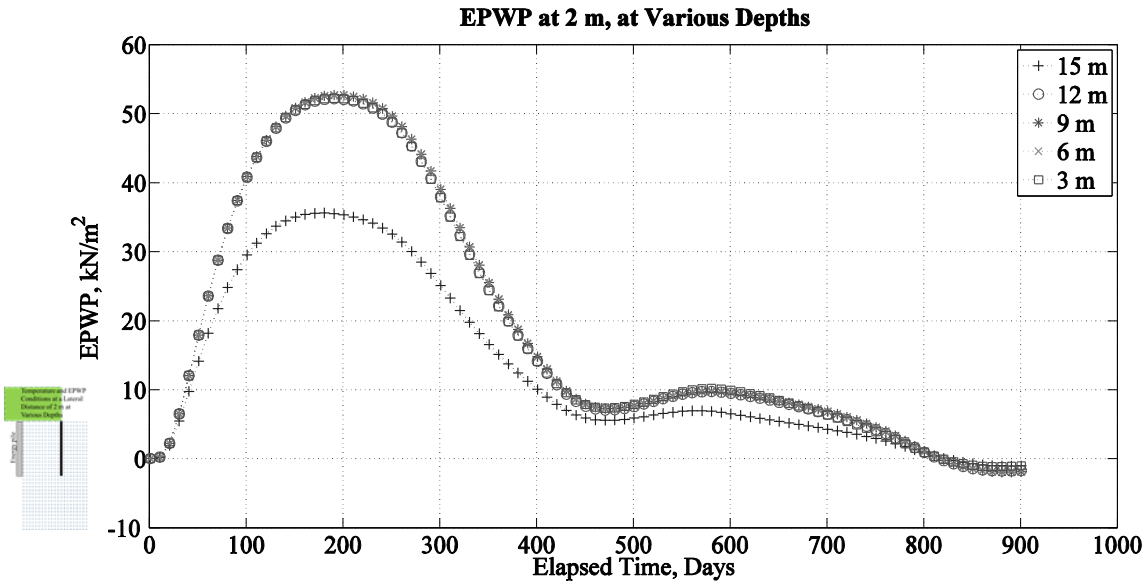

Figure 5.41. EPWP at a lateral distance of 2 m from the pile surface at various depths from the time of pile installation to the end of the model run. The ground-surface temperature is a constant 15 °C.

In Figure 5.42, EPWP at the 3m depth dissipates more quickly after reaching peak values in both Years 1 and 2 than it does with the cooler surface soil temperature presented in Figure 5.41. Toward the end of Year 2, EPWP at a depth of 3 m reaches a minimum 38 days earlier in Figure 5.42 than in Figure 5.41, although that is not the case during the first year, where a peak EPWP is reached at approximately the same time as the other depths.

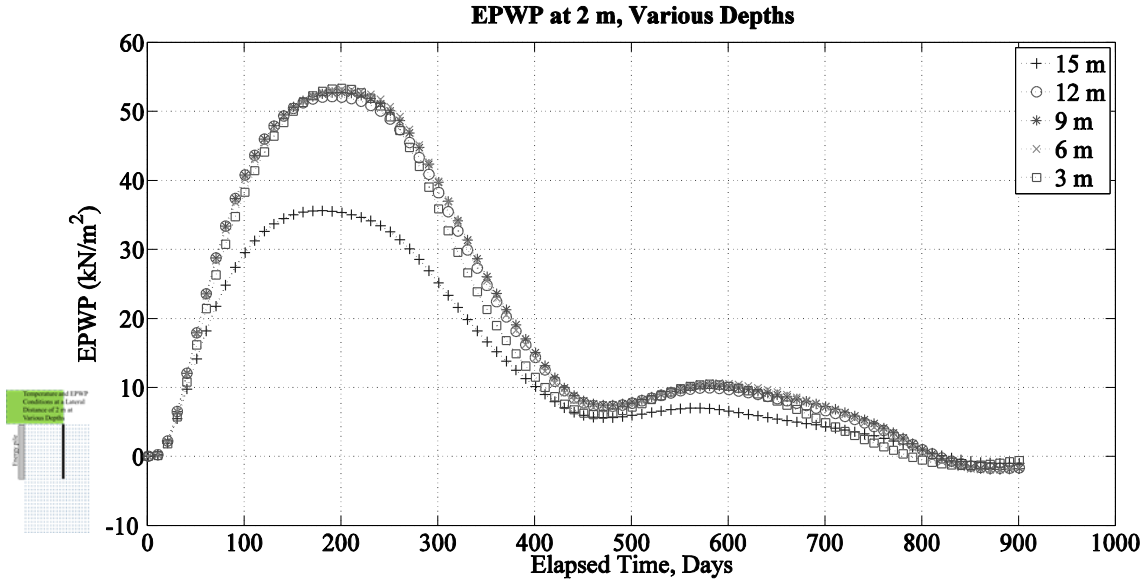

Figure 5.42. EPWP at a lateral distance of 2 m from the pile surface at various depths from the time of pile installation to the end of the model run, with transient ground-surface temperatures.

Comparison of EPWP Values Over Time With and Without HVAC

The EPWP differential at 2 m does not change until Day 187, and unlike the differential EPWP at the lateral distance of 1 m from the pile, the differential becomes slightly larger than zero until Day 234 and approaches but is never larger than zero around Day 727 at the depth of 15 m, as seen in Figure 5.43. In Figure 5.44, EPWP is slightly positive during Year 2, with a peak EPWP value of 57.2 N/m^2 at 15 m. Once again the differential values at 3 m and 6 m are slightly less negative because of the transient surface temperatures.

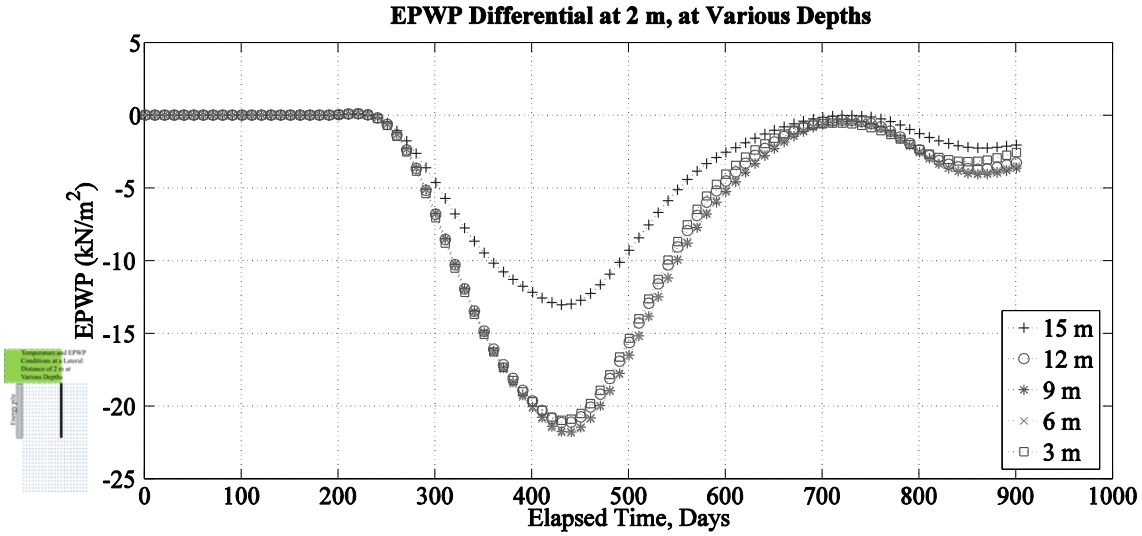

Figure 5.43. EPWP differential between model runs with and without HVAC introduction, at a lateral distance of 2 m from the pile surface at various depths. The ground-surface temperature is a constant 15 °C.

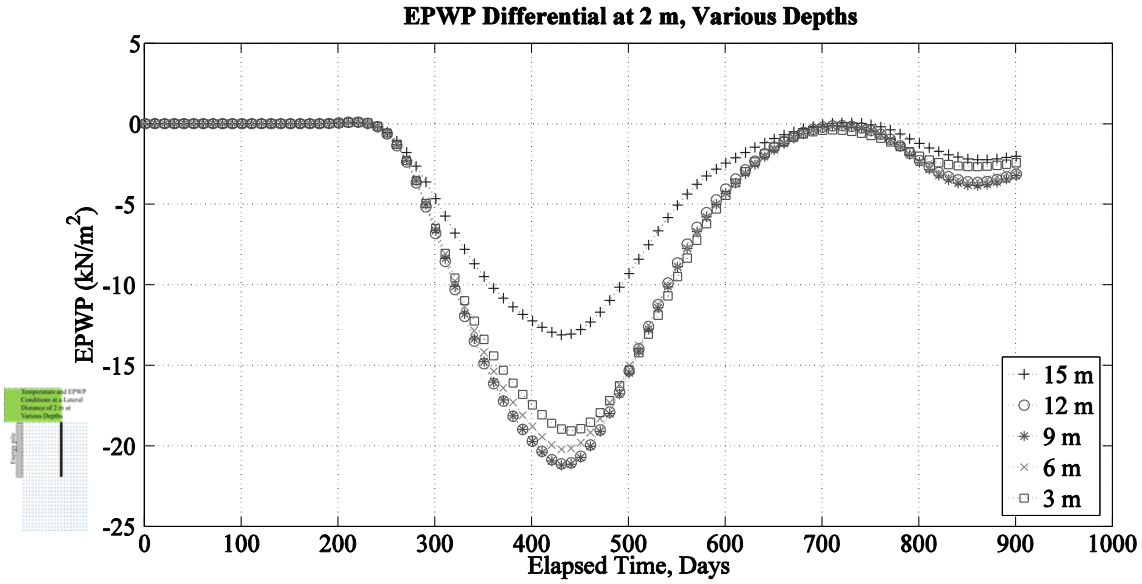

Figure 5.44. EPWP differential between model runs with and without HVAC introduction, at a lateral distance of 2 m from the pile surface at various depths, with transient ground-surface temperatures.

EPWP Normalized to Peak EPWP at Various Depths

The initial EPWP is zero at a lateral distance of 2 m from the pile face. The time to reach the peak EPWP increases as the distance from the pile increases, and is 177 days

for the 2m distance. By the end of the model run, the EPWP values are below zero, likely because of the soil temperature. The rates of change near the peak EPWP are lower than at or near the pile face. After the peak EPWP values are reached, the rates of dissipation from 80% of peak EPWP down to 40% of the peak EPWP for the distances are around 0.5% per day (shown in Figures 5.45 and 5.46).

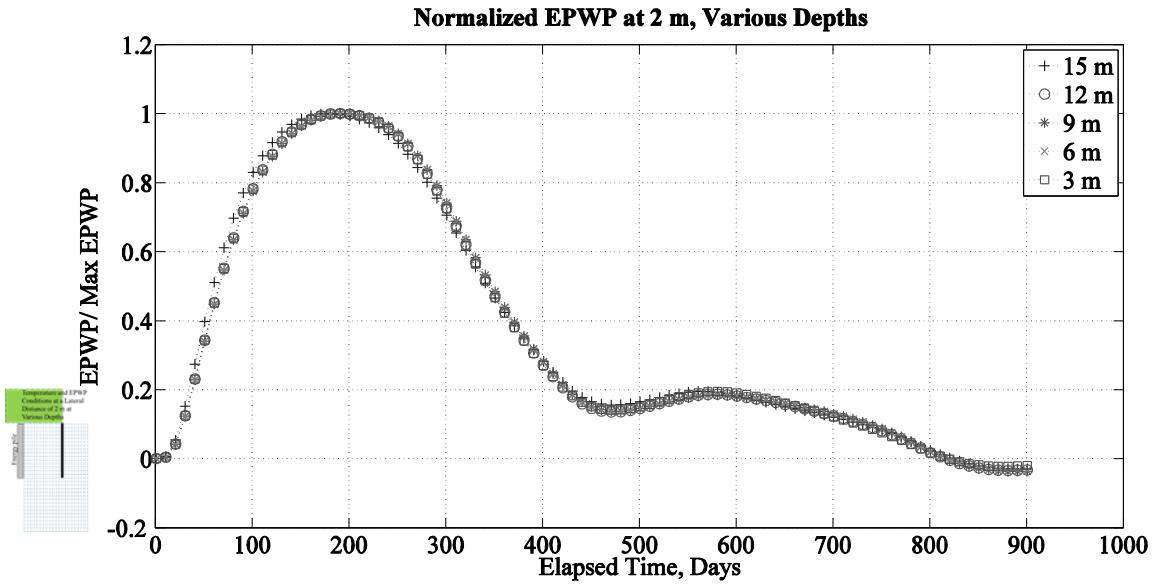

Figure 5.45. Normalized EPWP at a lateral distance of 2 m from the pile surface at various depths, from the time of pile installation to the end of the model run. The ground-surface temperature is a constant 15 °C.

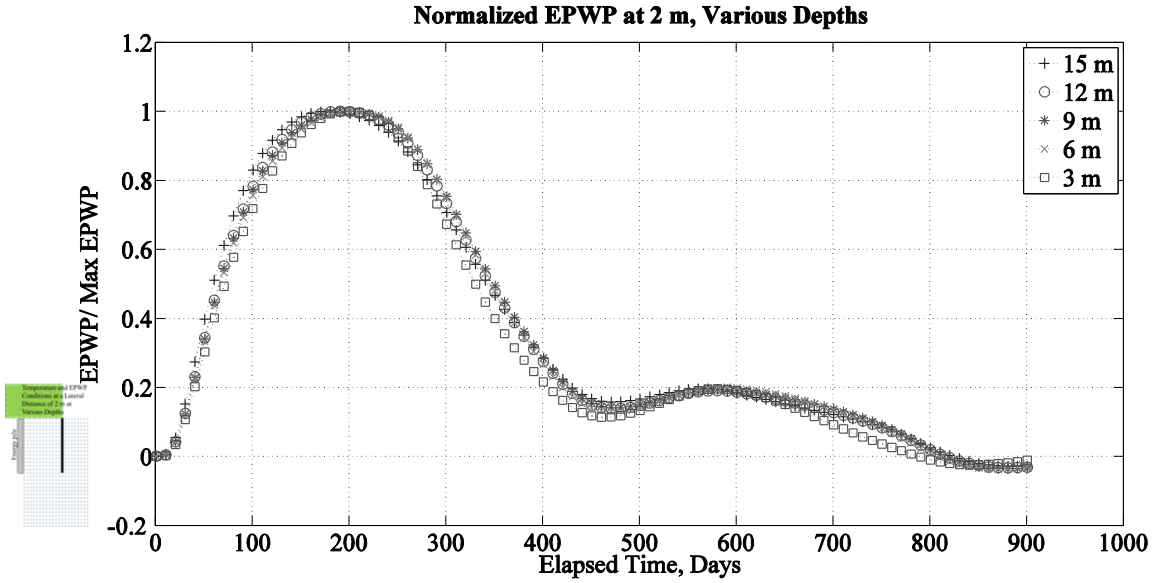

Figure 5.46. Normalized EPWP at a lateral distance of 2 m from the pile surface at various depths, from the time of pile installation to the end of the model run, with transient ground-surface temperatures.

EPWP Due to Thermal Expansion of the Soil

At a lateral distance of 2 m from the pile, the EPWP, due to thermal expansion of the soil, ranges from 0.055 kN/m^2 to -0.055 kN/m^2 in Figure 5.47 and 5.48, with slightly higher values at a depth of 3 m in Figure 5.48. Figure 5.48 also shows greater variation among the values at each depth. In Figure 5.48, the EPWP values become increasingly out of phase due to the influence of transient ground-surface temperatures.

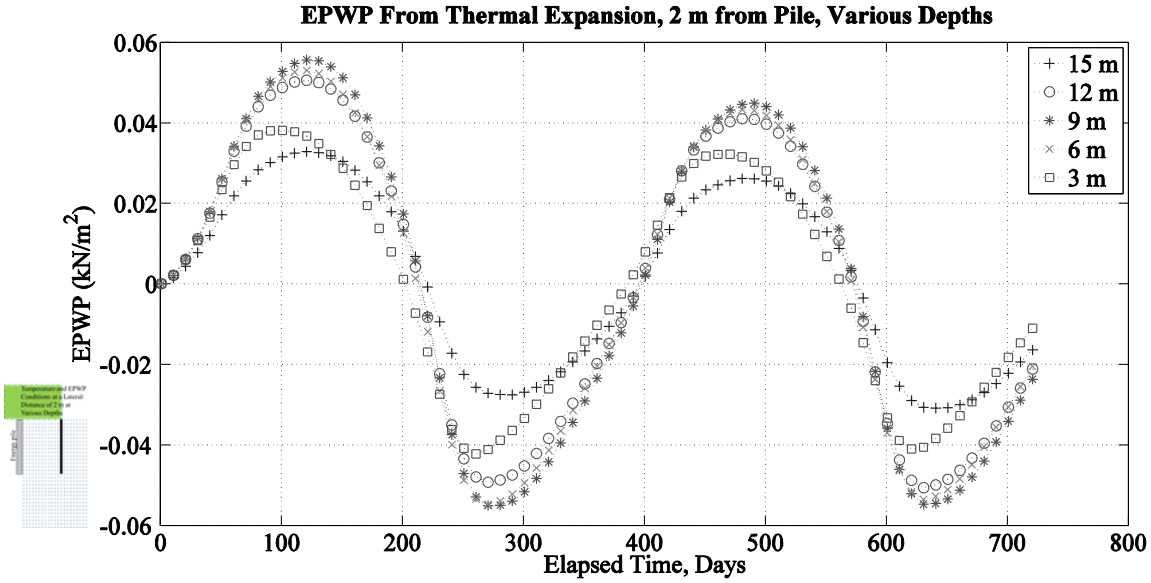

Figure 5.47. EPWP due to thermal expansion of the soil at a lateral distance of 2 m at various depths from the beginning of heating to the end of the model run. The ground-surface temperature is a constant 15 °C.

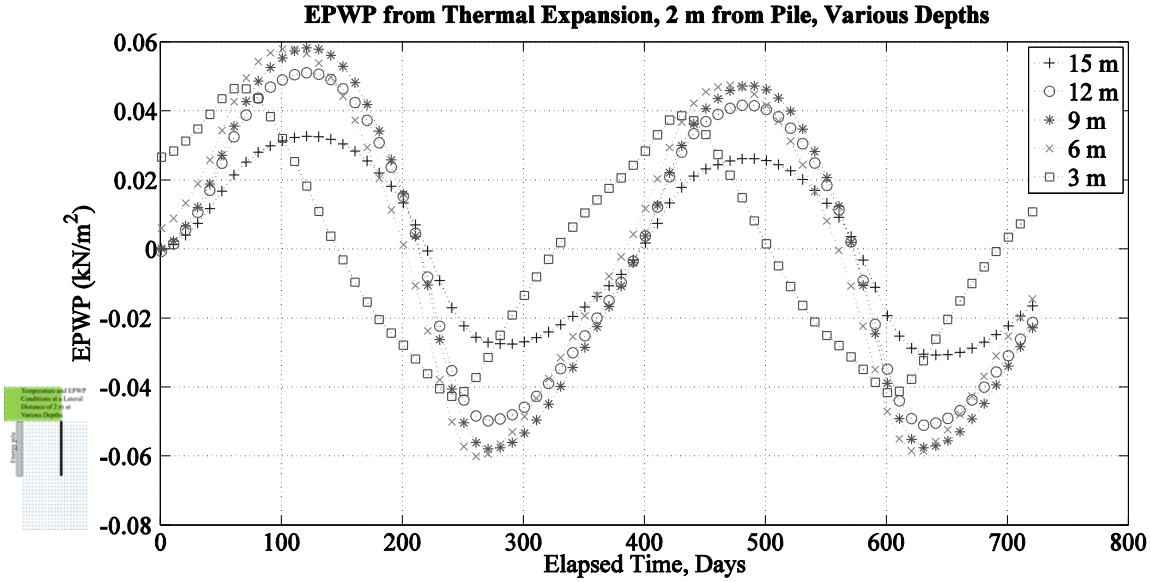

Figure 5.48. EPWP due to thermal expansion of the soil at a lateral distance of 2 m at various depths from the time of pile installation to the end of the model run, with transient ground-surface temperatures.

Variations of Temperature and EPWP at a Lateral Distance of 3 m from the Pile Face

The EPWP values at this distance are insignificant. Temperatures rarely ever drop below the ambient soil temperature. Transient ground-surface temperatures influence EPWP values. Figure 5.49 indicates the distance from the pile where the results in this section are presented along the depth.

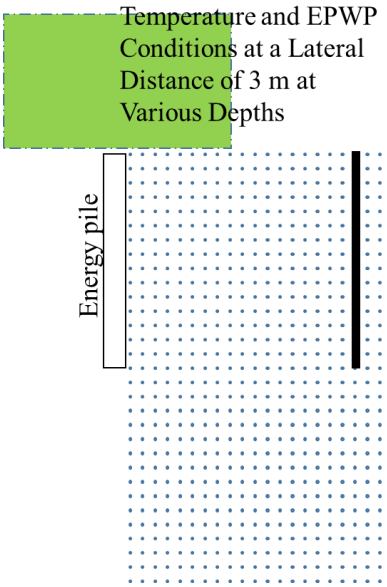

Figure 5.49. Figures in this chapter that present results from points at a lateral distance of 3 m from the pile will be identified with this symbol.

Temperature Values Over Time at Various Depths

The temperature peaks between 32 °C and 33 °C 225 days after pile installation at a depth of 9 m as shown in Figures 5.50 and 5.51. At a depth of 15 m, temperatures peak approximately ten days after temperatures in the middle depths. Interestingly, the low temperature for the 15 m depth remains approximately 2 °C warmer than soil at the 6m depth after 400 days. The temperatures at the 3m depth in Figure 5.51 begin at slightly more than 16 °C and are out of phase with the remaining depths by at least 67 days.

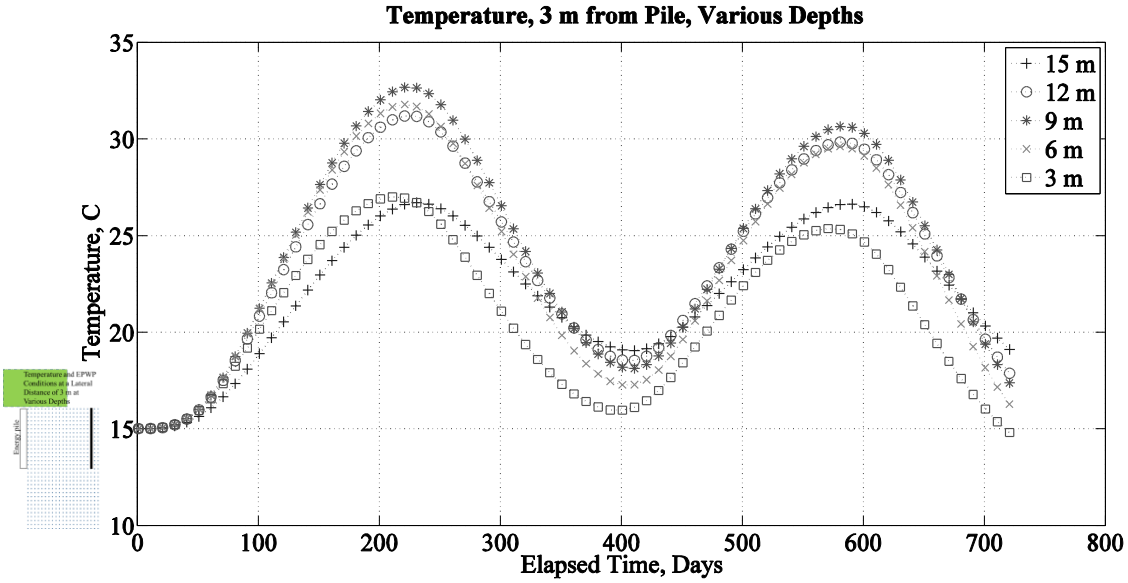

Figure 5.50. Temperature at various depths at a lateral distance of 3 m from the pile, from the time of pile installation to the end of the model run. The ground-surface temperature is a constant 15 °C.

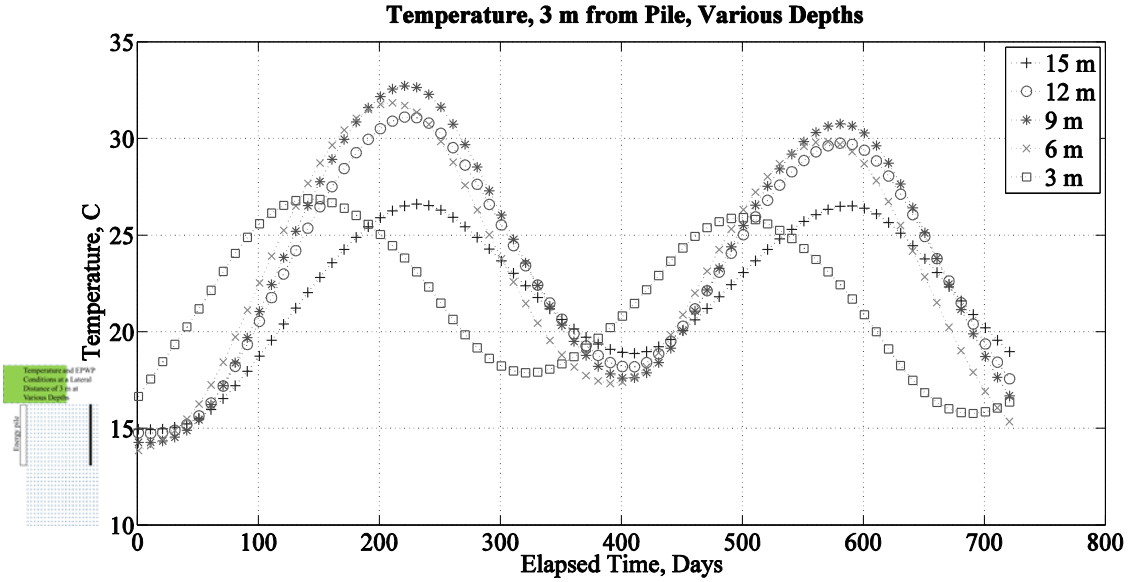

Figure 5.51. Temperature at various depths at a lateral distance of 3 m from the pile, from the time of pile installation to the end of the model run, with transient ground-surface temperatures.

Excess Pore-Water Pressure (EPWP) Values Over Time at Various Depths

Figures 5.52 and 5.53 presents EPWP values at a lateral distance of 3 m from the pile. The values peak 229 days after pile installation at just over 11 kN/m^2. The EPWP values drop below 0 kN/m^2 after 800 days for all depths except the 3m depth in Figure 5.53. The EPWP at the 3m depth, at a lateral distance of 3 m from the pile, decreases after pile installation, because of the assumption that the piles are installed during the winter season. During Year 2, the peak EPWP value and the minimum value occurs 32 and 46 days before the other depths, respectively.

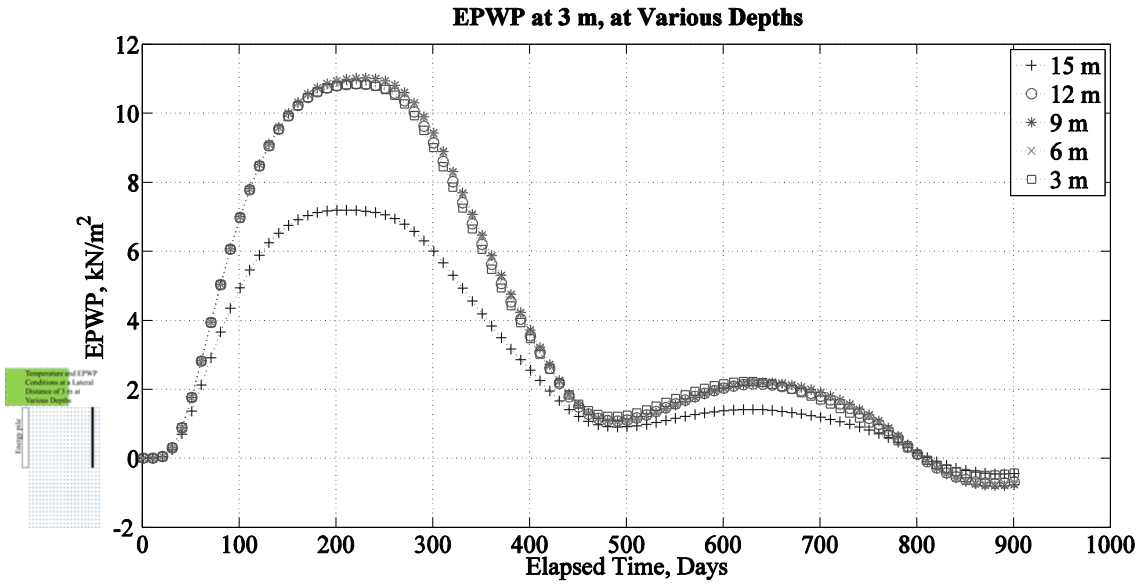

Figure 5.52. EPWP at a lateral distance of 3 m from the pile surface at various depths from the time of pile installation to the end of the model run. The ground-surface temperature is a constant 15 °C.

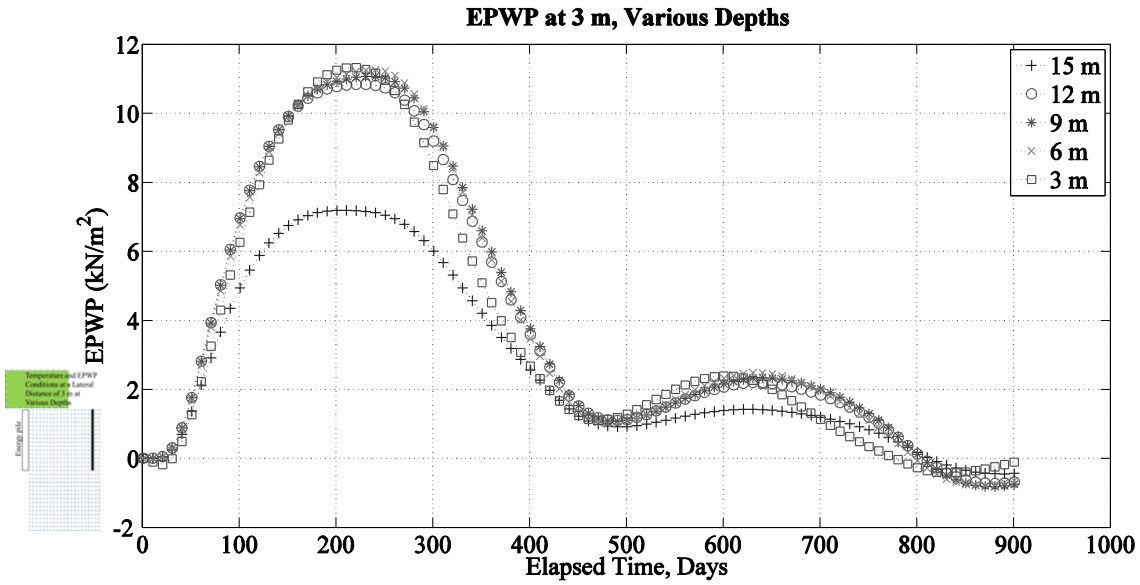

Figure 5.53. EPWP at a lateral distance of 3 m from the pile surface at various depths from the time of pile installation to the end of the model run, with transient ground-surface temperatures.

Comparison of EPWP Values Over Time With and Without HVAC

In Figures 5.54 and 5.55, the differential at a lateral distance of 3 m from the pile is positive between Day 191 and Day 283 and positive again between Day 671 until after Day 767 at a depth of 15 m. It is also positive between Day 684 and Day 728 for the 3m depth. The differential values at depths between 3m and 15 m fall within this range. The differential magnitude is between -3 kN/m^2 and -5 kN/m^2.

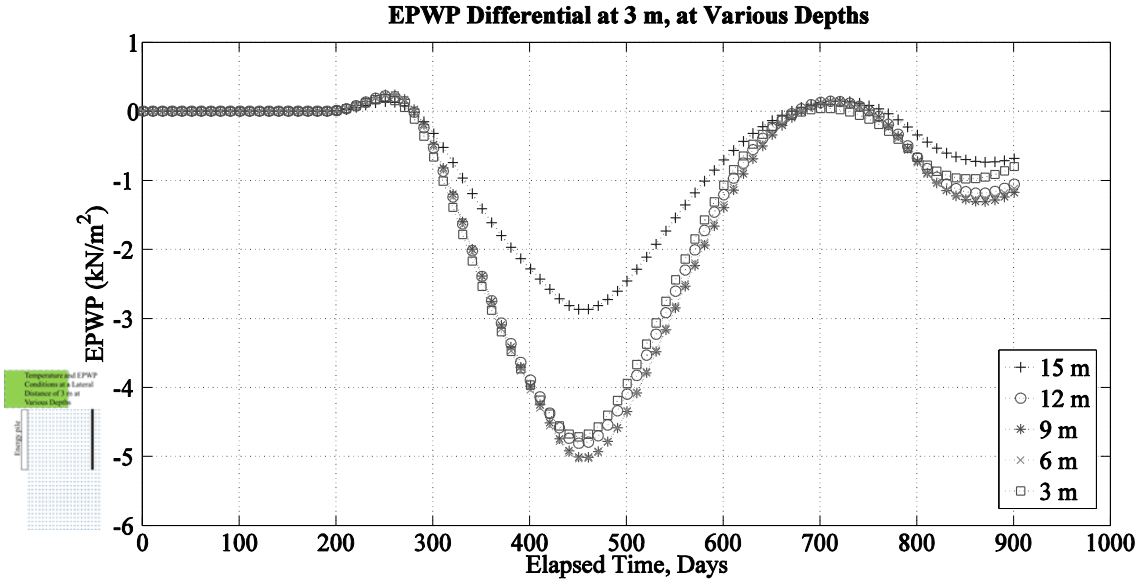

Figure 5.54. EPWP differential between model runs with and without HVAC introduction, at a lateral distance of 3 m from the pile surface at various depths. The ground-surface temperature is a constant 15 °C.

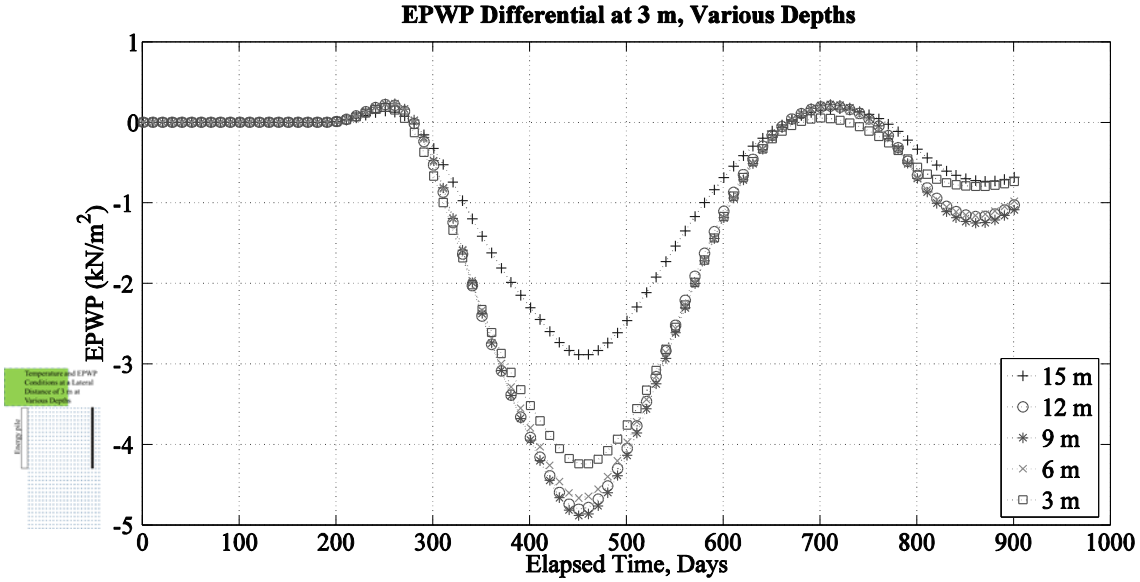

Figure 5.55. EPWP differential between model runs with and without HVAC introduction, at a lateral distance of 3 m from the pile surface at various depths, with transient ground-surface temperatures.

EPWP Normalized to Peak EPWP at Various Depths

The initial EPWP is zero at 3 m from the pile face. The time to reach the peak EPWP increases as the distance from the pile increases, and is 208 days for the 3m distance. By the end of the model run, the EPWP values are below zero. This is likely due to the soil temperature. The rates of change near the peak EPWP are lower than those at or near the pile face. After the peak EPWP values are reached, the rates of dissipation from 80% of peak EPWP down to 40% of the peak EPWP for the distances are around 0.5% per day (shown in Figures 5.56 and 5.57).

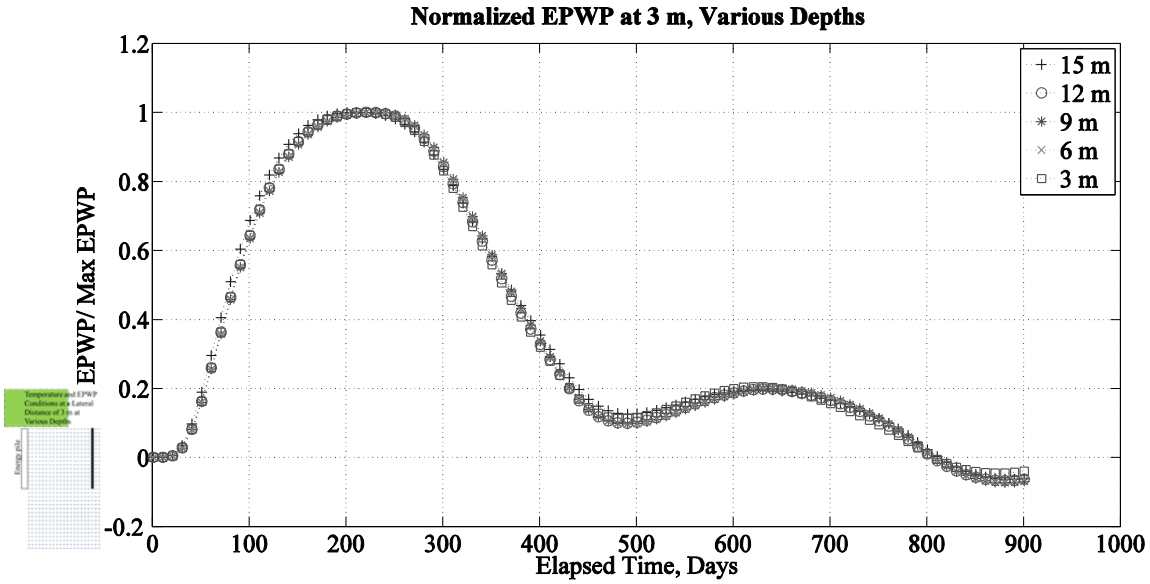

Figure 5.56. Normalized EPWP at a lateral distance of 3 m from the pile surface at various depths, from the time of pile installation to the end of the model run. The ground-surface temperature is a constant 15 °C.

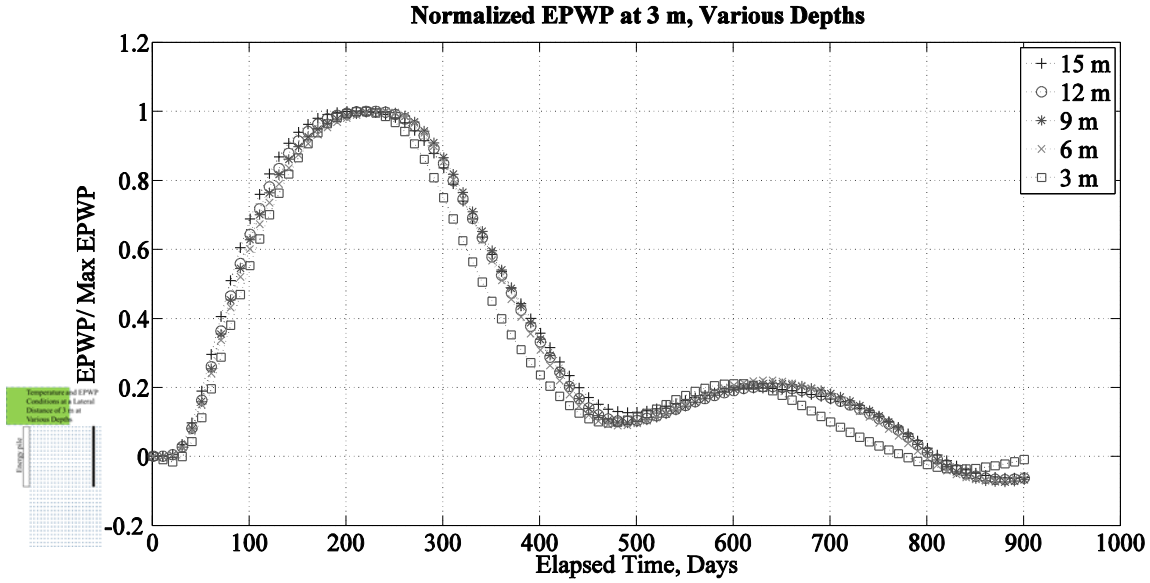

Figure 5.57. Normalized EPWP at a lateral distance of 3 m from the pile surface at various depths, from the time of pile installation to the end of the model run, with transient ground-surface temperatures.

EPWP Due to Thermal Expansion of the Soil

At a lateral distance of 3 m from the pile, the EPWP, due to thermal expansion of the soil, ranges from 0.05 kN/m^2 to -0.05 kN/m^2 in Figure 5.58 and 5.59, with slightly higher values at a depth of 3 m in Figure 5.59. There is little difference between EPWP values due to thermal expansion of the soil at a lateral distance of 2 m and 3 m from the pile. Figure 5.59 also shows greater variation among the values at each depth. In Figure 5.59, the EPWP values become increasingly out of phase due to the influence of transient ground-surface temperatures.

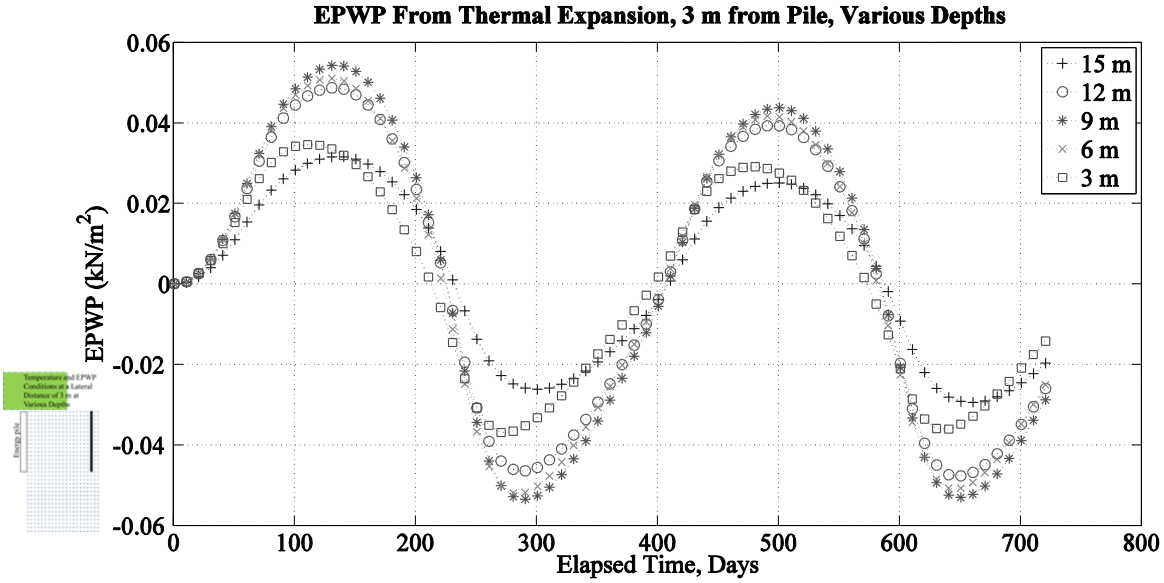

Figure 5.58. EPWP due to thermal expansion of the soil at a lateral distance of 3 m at various depths from the beginning of heating to the end of the model run. The ground-surface temperature is a constant 15 °C.

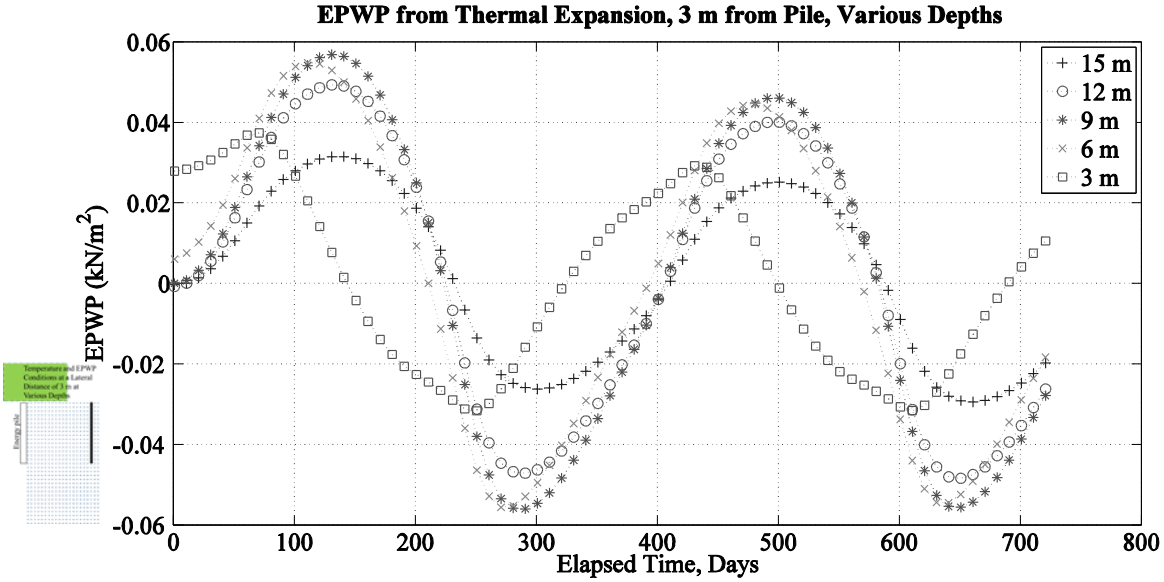

Figure 5.59. EPWP due to thermal expansion of the soil at a lateral distance of 3 m at various depths from the time of pile installation to the end of the model run, with transient ground-surface temperatures.

Unit-Circumference Frictional Capacity

The unit-circumference friction values are presented in Figures 5.60 and 5.61. Friction values drop after Day 1 until approximately Day 10, then rise until approximately Day 400, and then decrease due to the increased EPWP. The initial decreased-friction values coincide with the period of dilation in the soil, where the EPWP values rise for a period of time before decreasing. Friction values drop slightly again due to soil heating during the spring of Year 2. Unit-circumference-friction values are slightly higher in Figure 5.61 due to higher ground-surface temperatures. Although friction capacity continues to increase until the end of the model run, the recommended unit-radius friction value is that value observed at the local minimum caused by soil cooling near the end of the first year of HVAC usage. The justification for this as well as the discussion of these results are discussed below. This value is site and soil dependent, obviously.

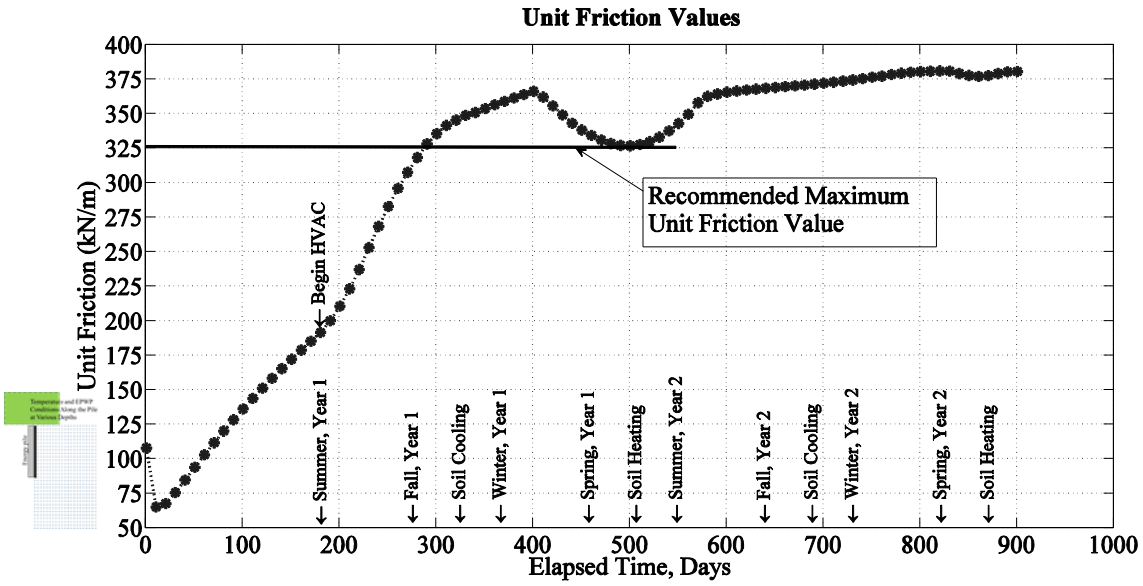

Figure 5.60. Unit-circumference-friction values from the time of pile installation to the end of the model run. The ground-surface temperature is a constant 15 °C.

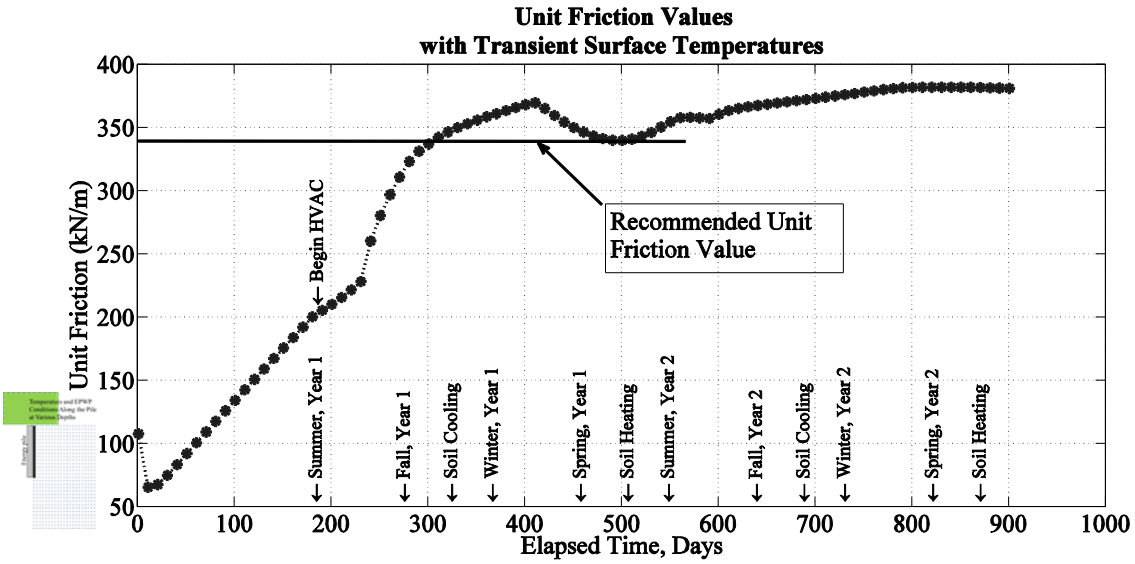

Figure 5.61. Unit-circumference-friction values from the time of pile installation to the end of the model run, with transient ground-surface temperatures.

Variations of Temperature and Excess Pore-Water Pressure Results Adjacent to a Drilled-Shaft Energy-Pile

Figures 5.62 through 5.88 present the results for the drilled-shaft iteration of the model. Without the EPWP from cavity expansion, EPWP is produced completely from thermal expansion of both the drilled shaft and the soil. The radius of the drilled shaft is 0.45 m instead of 0.15 m for the driven piles, so it is easily predictable that EPWP due to thermal expansion of the drilled shaft will be slightly larger. The figures presented in this section present results for the same array of lateral distances from the shaft and depths below the ground surface that were presented in Table 5.1.

Variations of Temperature and Excess Pore-Water Pressure Conditions Adjacent to the Drilled Shaft

Figure 5.62 indicates the distance from the drilled shaft where the results in this section are presented along the depths presented in the figure's legend.

Temperature Values Over Time at Various Depths

The temperatures along the drilled shaft presented in Figure 5.63 are all equal and fluctuate between than 10 °C and more than 51 °C.

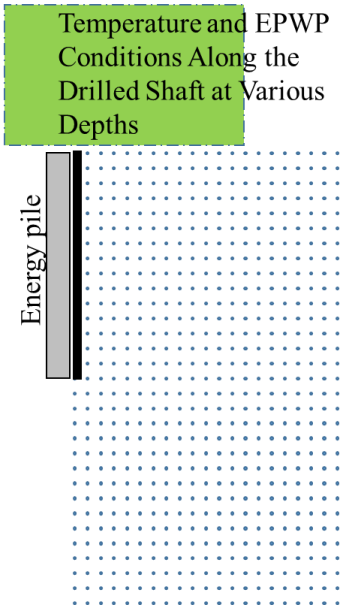

Figure 5.62. Figures in this chapter that present results from points along the face of the drilled shaft will be identified with this symbol.

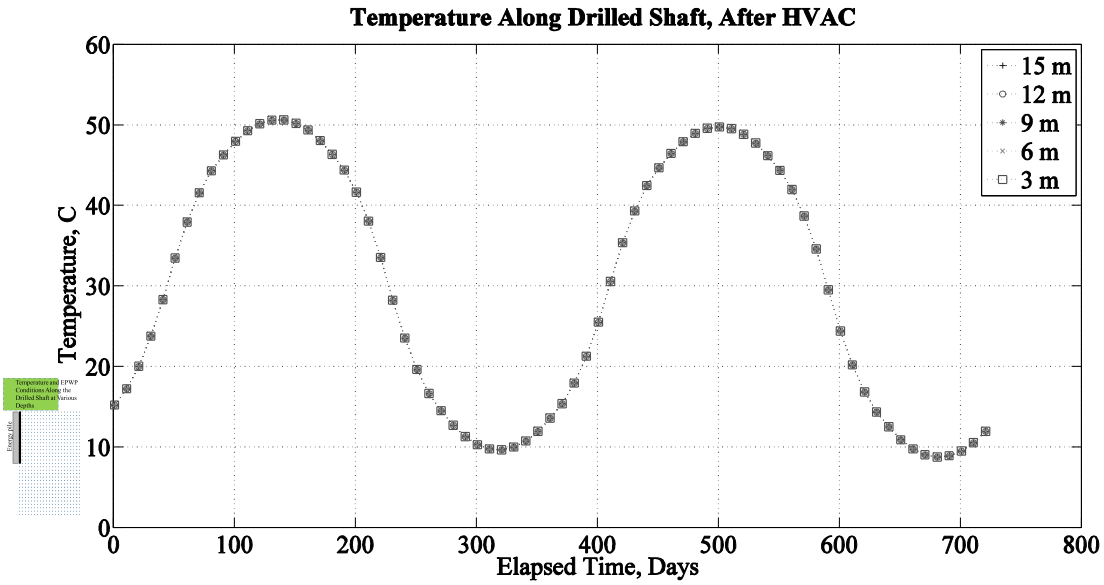

Figure 5.63. Temperature at the drilled shaft surface at various depths for the two-year model run.

Excess Pore-Water Pressure (EPWP) Values Over Time at Various Depths

Figure 5.64 presents the EPWP along the side of the shaft. There is greater variability between the various depths than those observed for the driven piles. The peak EPWP is greater than 5 kN/m^2 for all depths except the 15 m depth, and the minimum is less than -2 kN/m^2 for all depths except the 15 m depth near the end of Year 2.

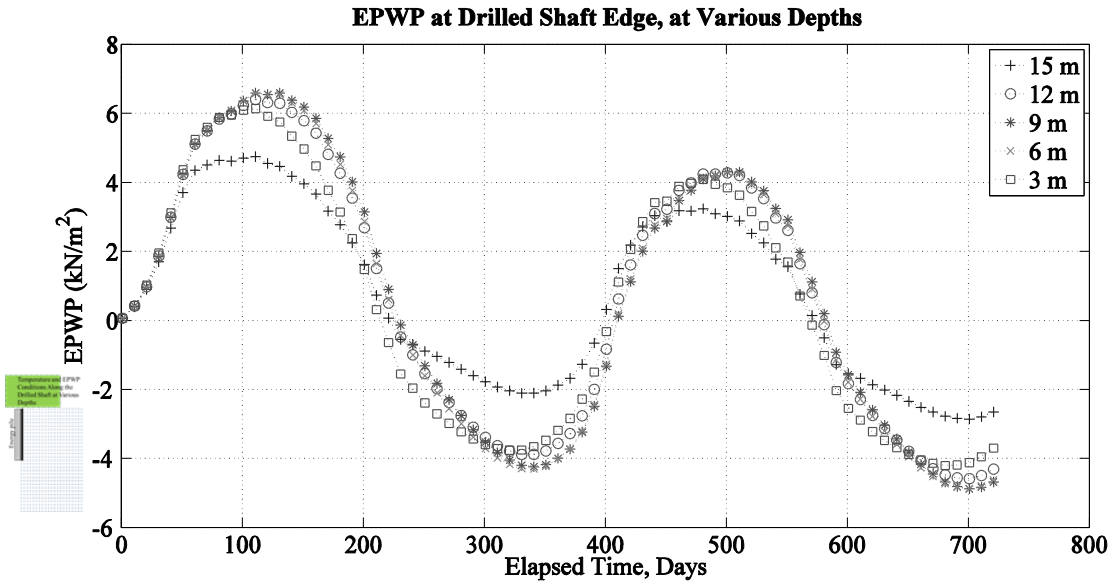

Figure 5.64. EPWP at the drilled-shaft surface at various depths for the two-year model run.

EPWP Normalized to Peak EPWP at Various Depths

The EPWP, normalized to the peak EPWP is presented in Figure 5.65. The peak EPWP occurs at a depth of 15 m along the face of the drilled shaft during the second year in Figure 5.65, but the peak EPWP occurs during the first year of the model run at the other depths and lateral distances from the drilled shaft. As the lateral distance from the side of the shaft increases, the time to reach the peak EPWP increases, as observed in Figures 5.72, 5.77, and 5.82.

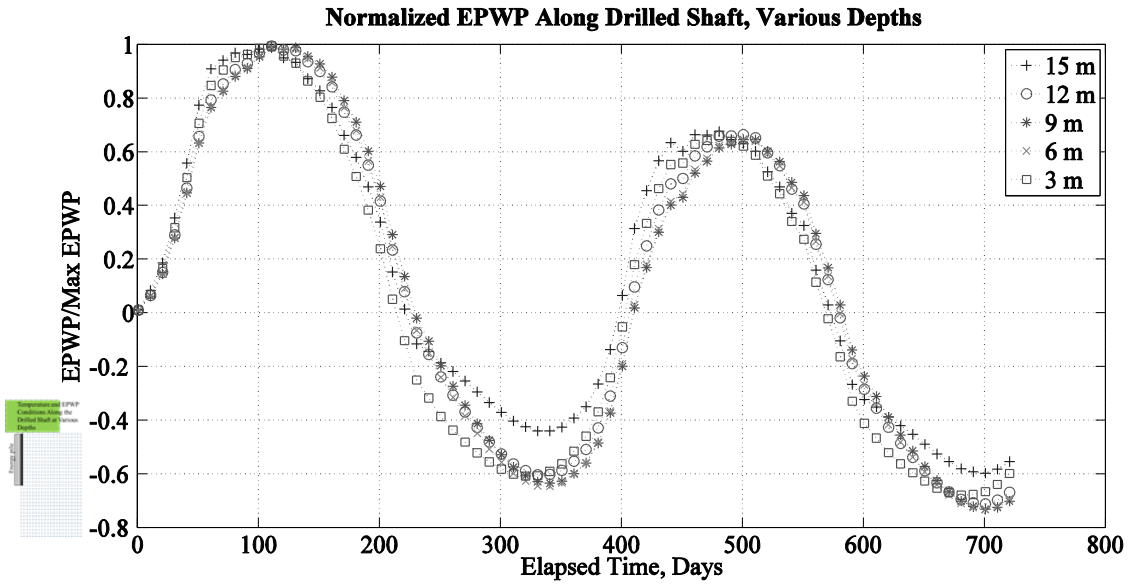

Figure 5.65. EPWP, normalized to the peak EPWP, along drilled shaft at depths shown for the two-year model run.

EPWP Due to Thermal Expansion of the Drilled Shaft

Figure 5.66 presents the EPWP along the side of the shaft due to thermal expansion of the drilled shaft. The peak EPWP occurs approximately 60 days after the start of the model and reaches a value of approximately ±1.3 kN/m^2 during the first year.

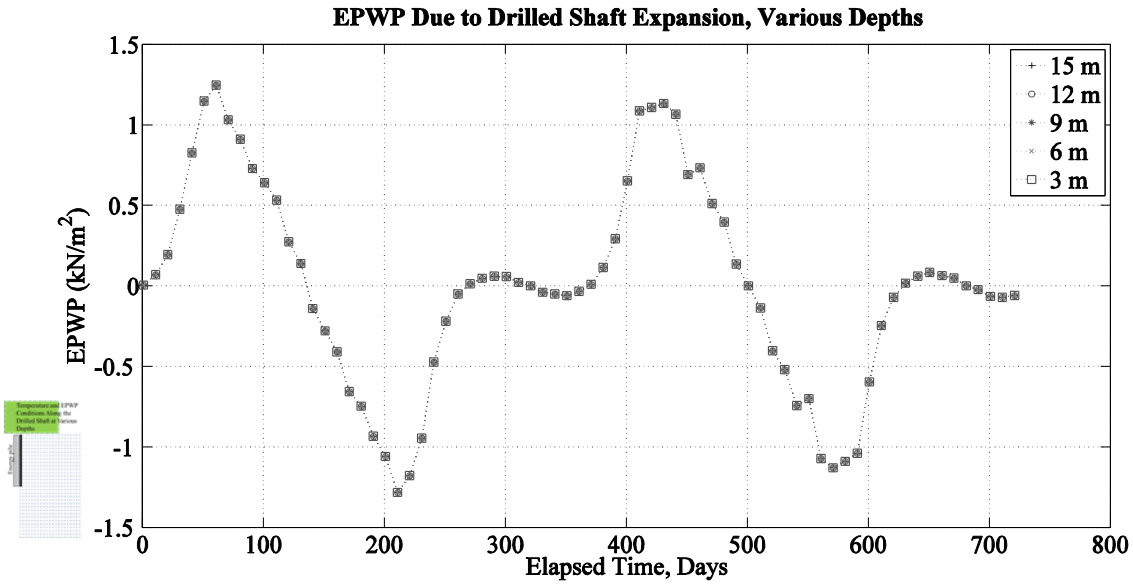

Figure 5.66. EPWP due to thermal expansion of the drilled shaft at the drilled shaft surface for the depths shown for the two-year model run.

EPWP Due to Thermal Expansion of the Soil

EPWP due to thermal expansion of the soil along the shaft is presented in Figure 5.67. The overall peak and minimum value of approximately ±0.275 kN/m^2 occur during the second year and are higher than Year 1 because of a change to the temperature range input into the model. The changes before and after the maxima become more gradual as the lateral distance from the drilled shaft increases. Peak values also decline as the distance from the drilled shaft increases.

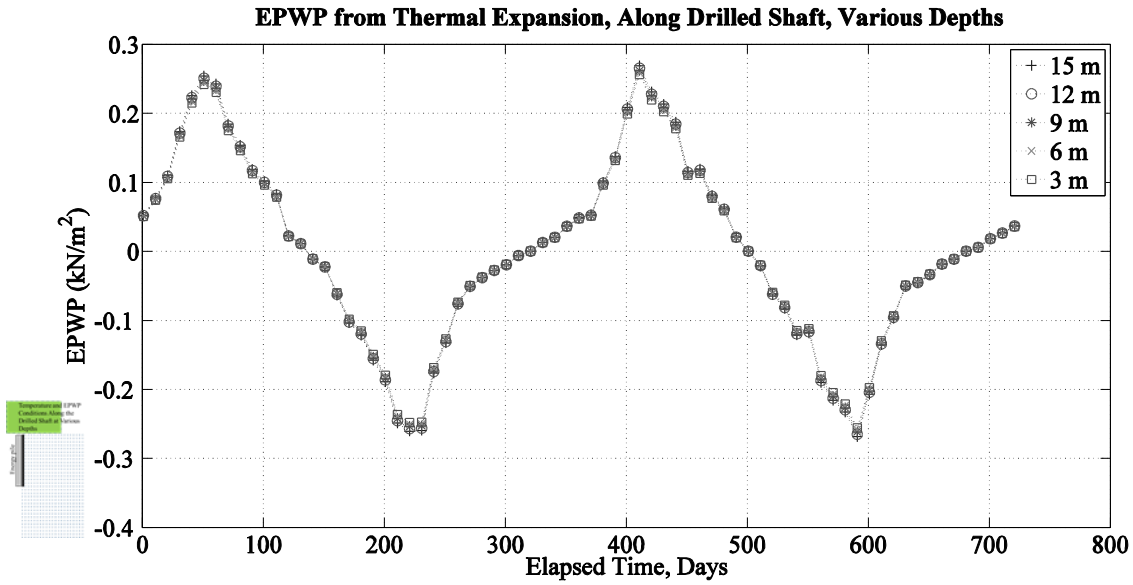

Figure 5.67. EPWP due to thermal expansion of the soil at the drilled shaft surface for the depths shown for the two-year model run.

Unit-Circumference-Friction Values

The unit-circumference-friction value over the modeled time period is presented in Figure 5.68 for the drilled shaft. These unit-circumference-friction values are calculated for the length of the drilled shaft, less the first meter. The friction capacity would be calculated by multiplying the unit-circumference-friction value by the perimeter of the drilled shaft. It is apparent that unit-circumference-friction values decrease during periods of soil heating and increase during periods of soil cooling. The beginning unit-circumference-friction value is approximately 447 kN/m. The unit-circumference-friction value decreases to 421 kN/m at Day 112 and increases to 460 kN/m on Day 337. The unit-circumference-friction value increases slightly a year later, due to the way the temperature fluctuation was set up in the model. It is recommended that the allowable frictional capacity for the drilled shaft should be calculated using the minimum value observed on the unit-circumference-friction plot. In Figure 5.68, this value is 421 kN/m.

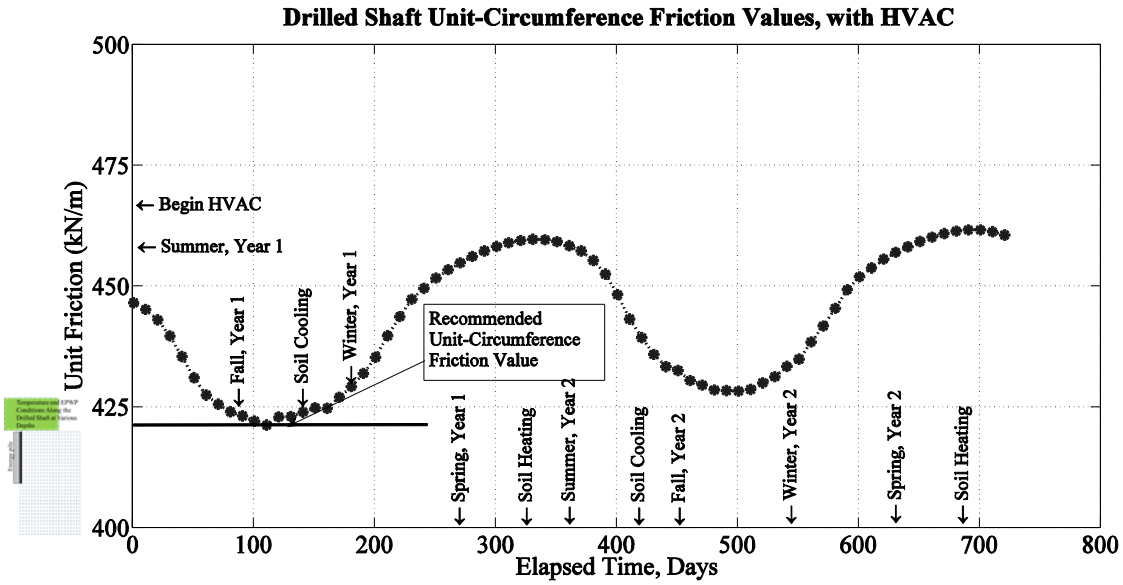

Figure 5.68. Unit-circumference friction values shown for the two-year model run.

Variations of Temperature and EPWP at a Lateral Distance of 1/6 m from the Drilled Shaft

Figure 5.69 indicates the distance from the drilled shaft where the results in this section are presented along the depths presented in the figure's legend.

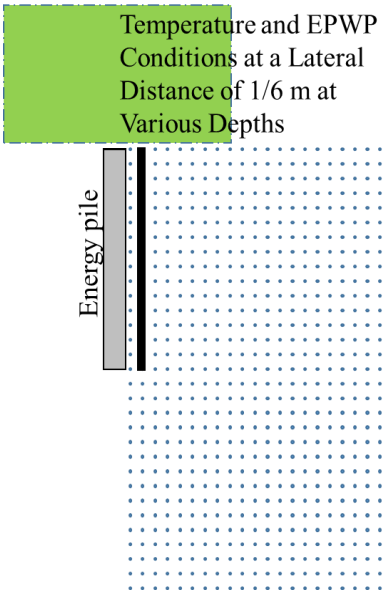

Figure 5.69. Figures in this chapter that present results from points at a lateral distance of 1/6 m from the drilled-shaft face will be identified with this symbol.

Temperature Values Over Time at Various Depths

Temperatures presented in Figure 5.70 reach peak values around 45 °C and minimums just below 15 °C. Temperatures at the bottom and the top of the drilled shaft are lower than those in the middle of the drilled shaft. Peak temperatures during the second year are slightly greater than those of the first year. This trend becomes more exaggerated as the distance from the drilled shaft increased, as seen in Figures 5.75, 5.80, and 5.85.

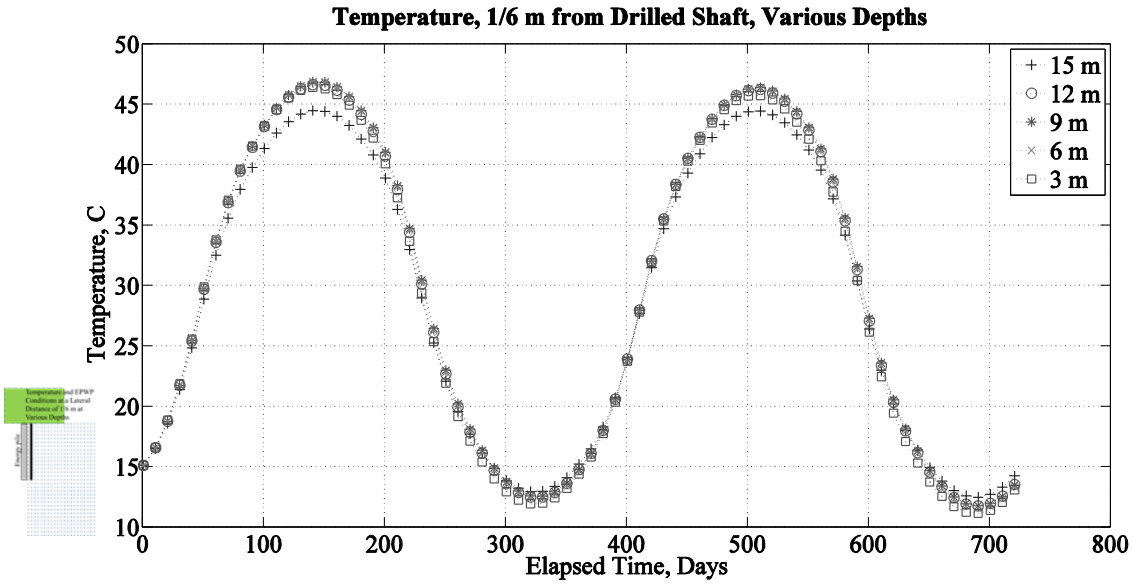

Figure 5.70. Temperature at a lateral distance of 1/6 m from the drilled shaft at various depths for the two-year model run.

Excess Pore-Water Pressure (EPWP) Values Over Time at Various Depths

The EPWP presented in Figure 5.71 is slightly lower in magnitude than at the side of the drilled shaft and exhibits greater variability between the depths. This trend also continues as the distance from the drilled shaft increases, as presented in Figures 5.76, 5.81, and 5.86. The majority of depths extend below -2 kN/m^2 at all distances from the drilled shaft except at a lateral distance of 2 m.

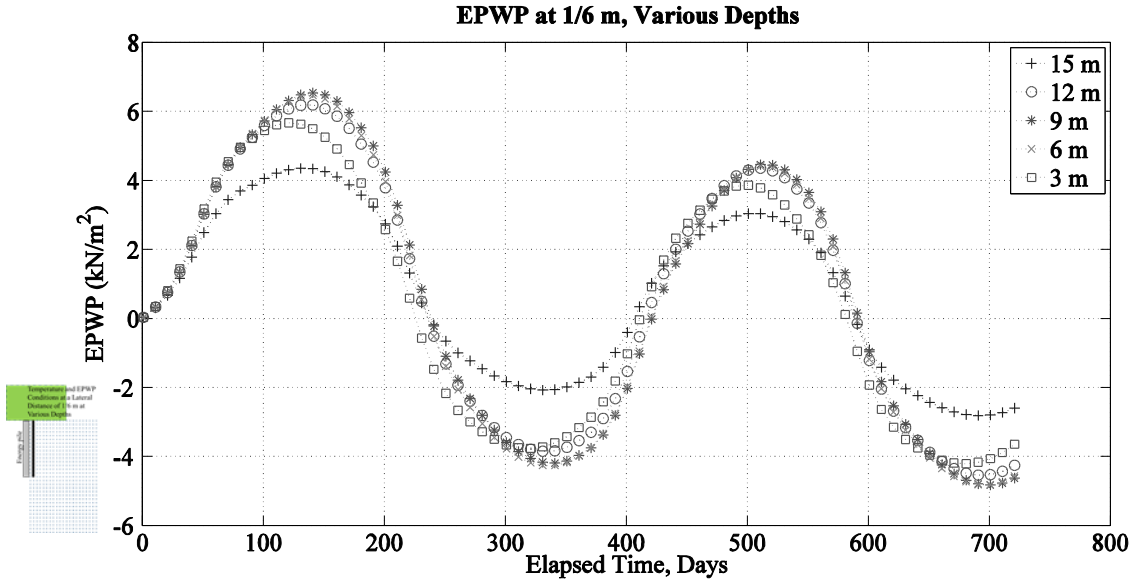

Figure 5.71. EPWP at a lateral distance of 1/6 m from the drilled shaft at various depths for the two-year model run.

EPWP Normalized to Peak EPWP at Various Depths

Excess Pore-Water Pressure reaches a peak at the end of the heating cycle of the soil, as would be expected. The peak is reached approximately 20 days later than along the drilled-shaft face.

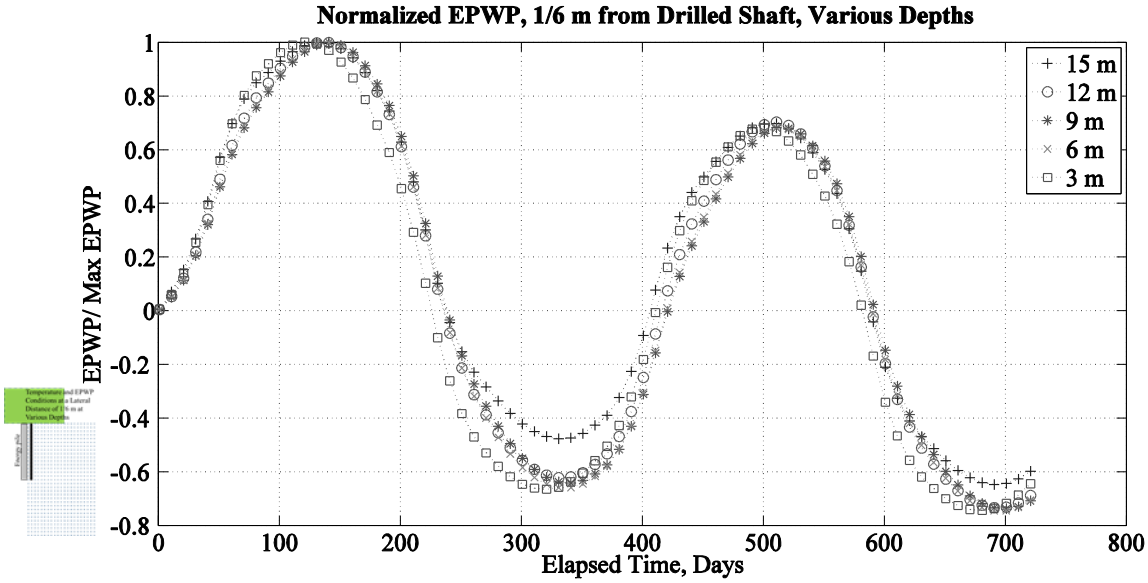

Figure 5.72. EPWP, normalized to the peak EPWP, at a lateral distance of 1/6 m from the drilled shaft at various depths for the two-year model run.

EPWP Due to Thermal Expansion of the Soil

A peak value of 0.2 kN/m^2 is reached during each year of the modeled time period. Minimum values of slightly less than -0.2 kN/m^2 are reached approximately 160 days after the peak value is reached in Year 1, but the minimum values aren't reached until approximately 200 days after the peak is reached in Year 2, as shown in Figure 5.73.

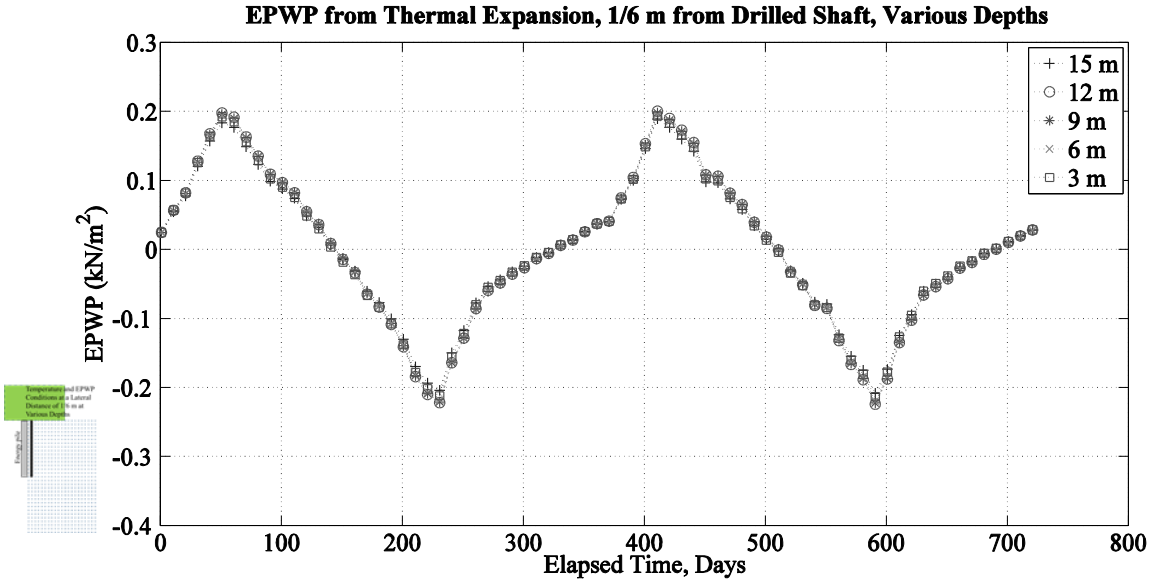

Figure 5.73. EPWP due to thermal expansion of the soil at a lateral distance of 1/6 m for the depths shown for the two-year model run.

Variations of Temperature and EPWP at a Lateral Distance of 1m from the Drilled Shaft

Figure 5.74 indicates the distance from the drilled shaft where the results in this section are presented along the depths presented in the figure's legend.

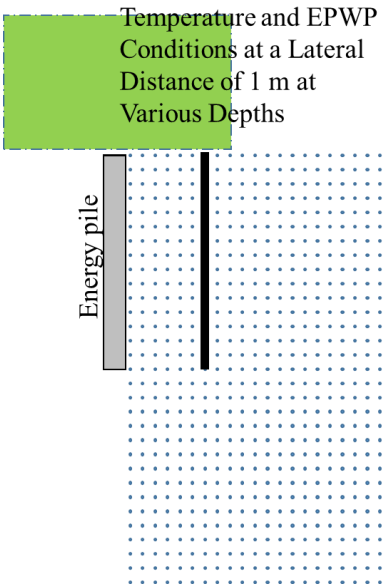

Figure 5.74. Figures in this chapter that present results from points at a lateral distance of 1 m from the drilled-shaft face will be identified with this symbol.

Temperature Values Over Time at Various Depths

Temperatures range from 15 °C at the beginning of the modeled time period to a peak of approximately 39 °C. The peak temperatures are reached approximately 30 days later than those at a lateral distance of 1/6 m from the drilled shaft face.

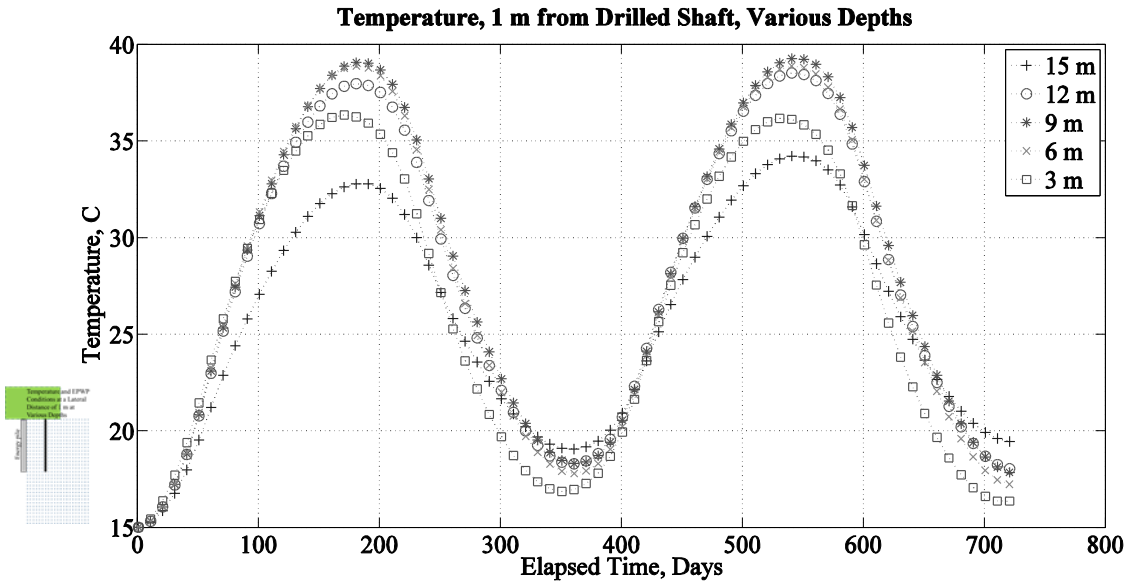

Figure 5.75. Temperature at a lateral distance of 1 m from the drilled shaft at various depths for the two-year model run.

Excess Pore-Water Pressure (EPWP) Values Over Time at Various Depths

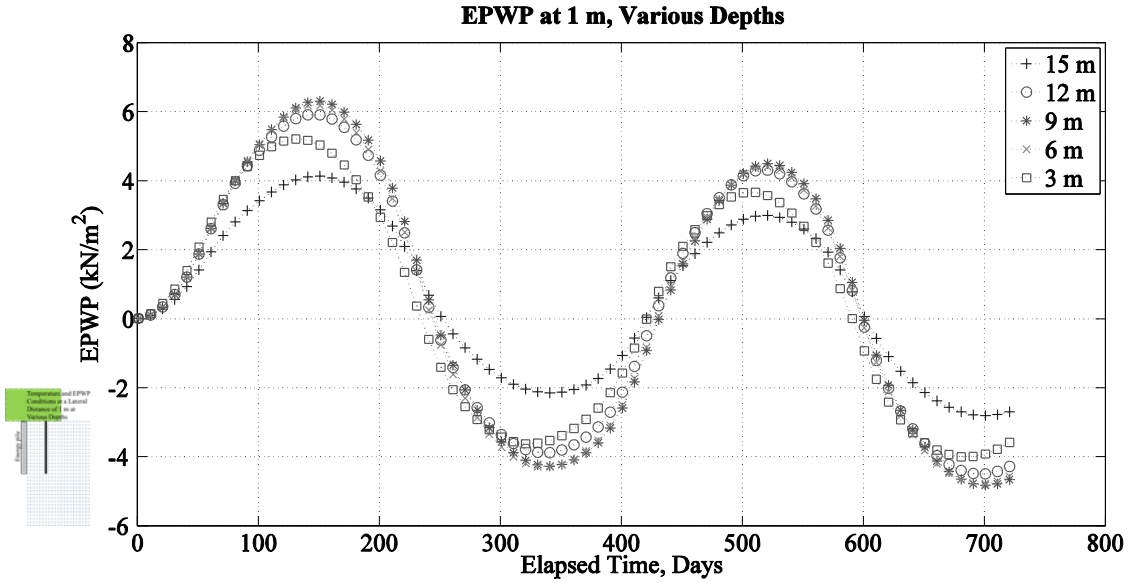

Figure 5.76. EPWP at a lateral distance of 1 m from the drilled shaft at various depths for the two-year model run.

EPWP Normalized to Peak EPWP at Various Depths

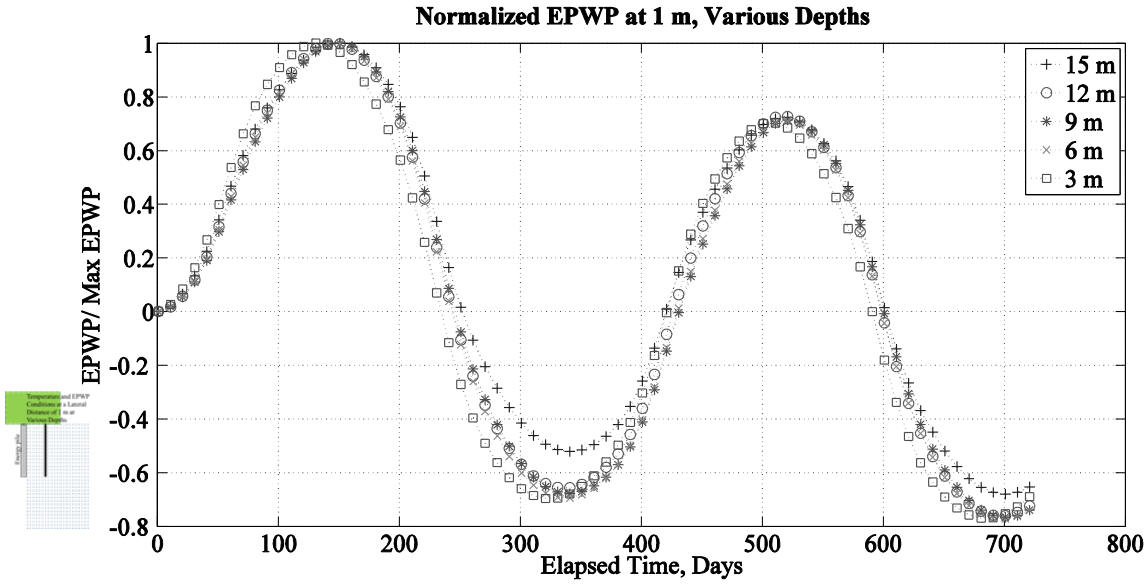

Figure 5.77. EPWP, normalized to the peak EPWP, at a lateral distance of 1 m from the drilled shaft at various depths for the two-year model run.

EPWP Due to Thermal Expansion of the Soil

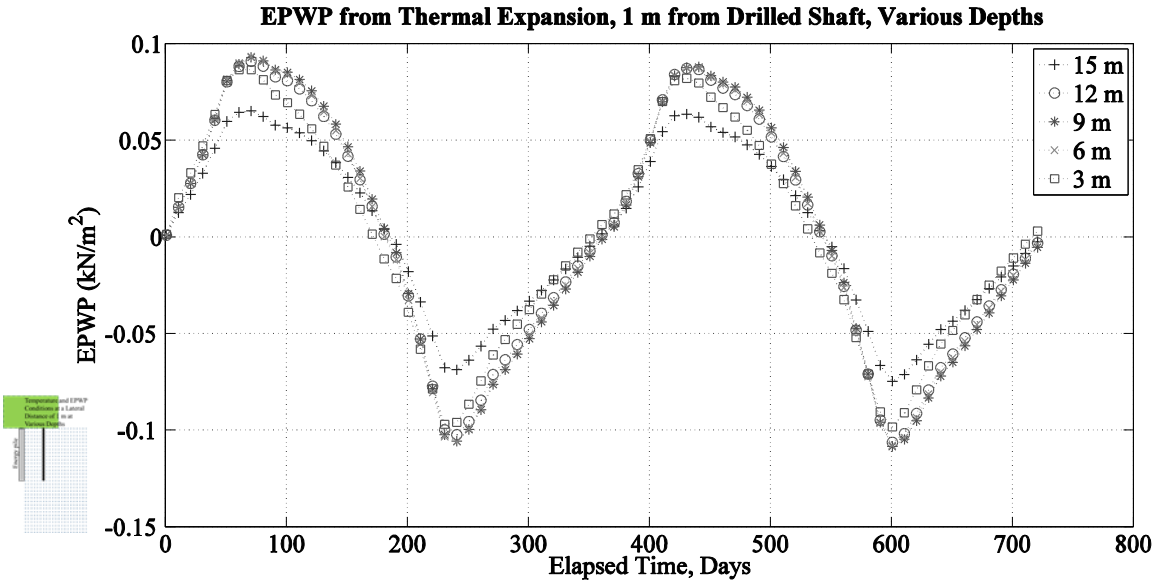

Figure 5.78. EPWP due to thermal expansion of the soil at a lateral distance of 1 m for the depths shown for the two-year model run.

Variations of Temperature and EPWP at a Lateral Distance of 2 m from the Drilled Shaft

Figure 5.79 indicates the distance from the drilled shaft where the results in this section are presented along the depths presented in the figure's legend.

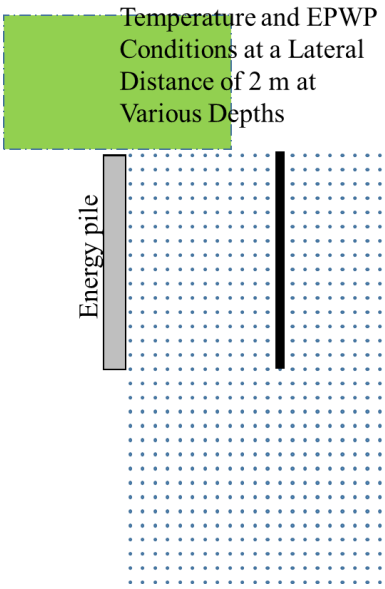

Figure 5.79. Figures in this chapter that present results from points at a lateral distance of 2 m from the drilled-shaft face will be identified with this symbol.

Temperature Values Over Time at Various Depths

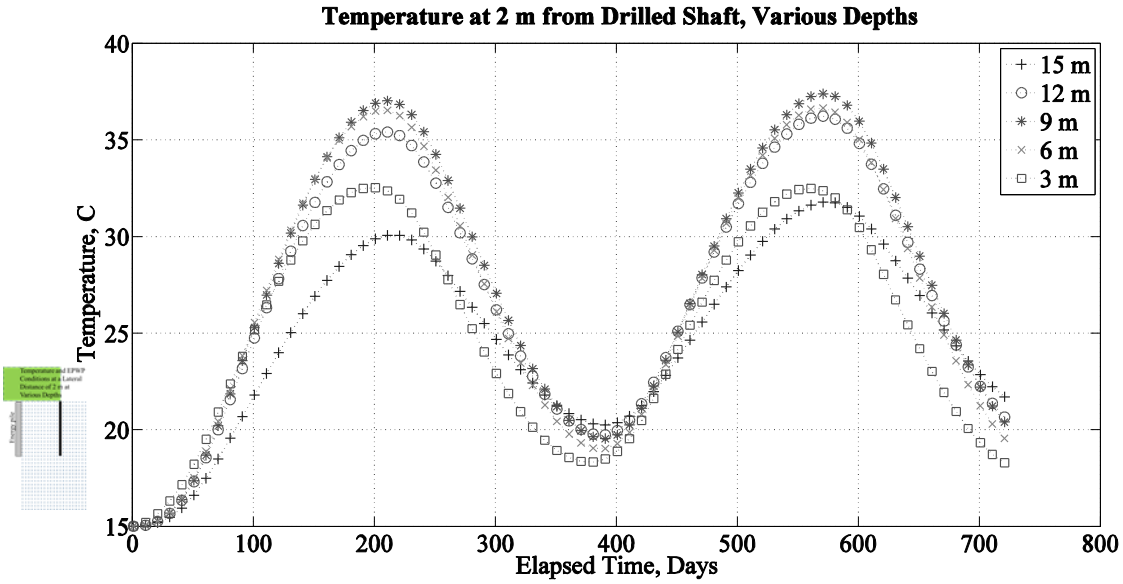

Figure 5.80. Temperature at a lateral distance of 2 m from the drilled shaft at various depths for the two-year model run.

Excess Pore-Water Pressure (EPWP) Values Over Time at Various Depths

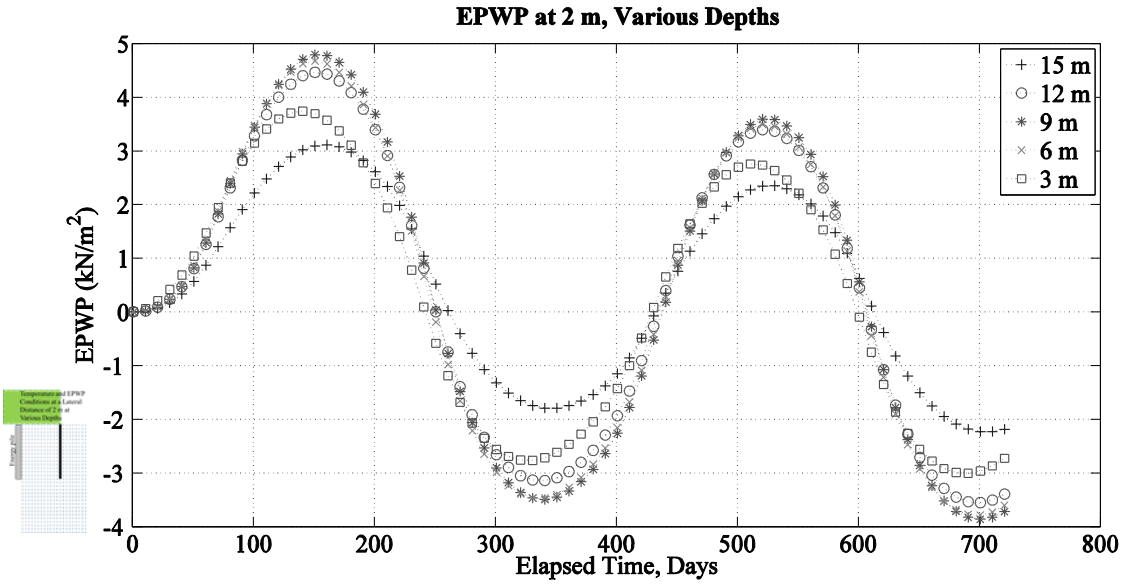

Figure 5.81. EPWP at a lateral distance of 2 m from the drilled shaft at various depths for the two-year model run.

EPWP Normalized to Peak EPWP at Various Depths

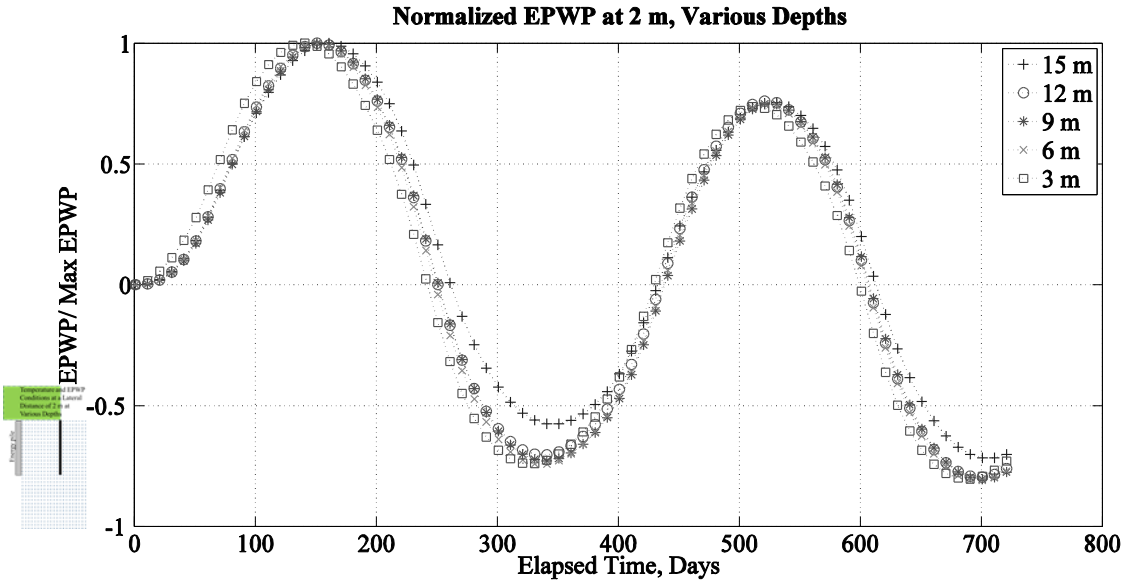

Figure 5.82. EPWP, normalized to the peak EPWP, at a lateral distance of 2 m from the drilled shaft at various depths for the two-year model run.

EPWP Due to Thermal Expansion of the Soil

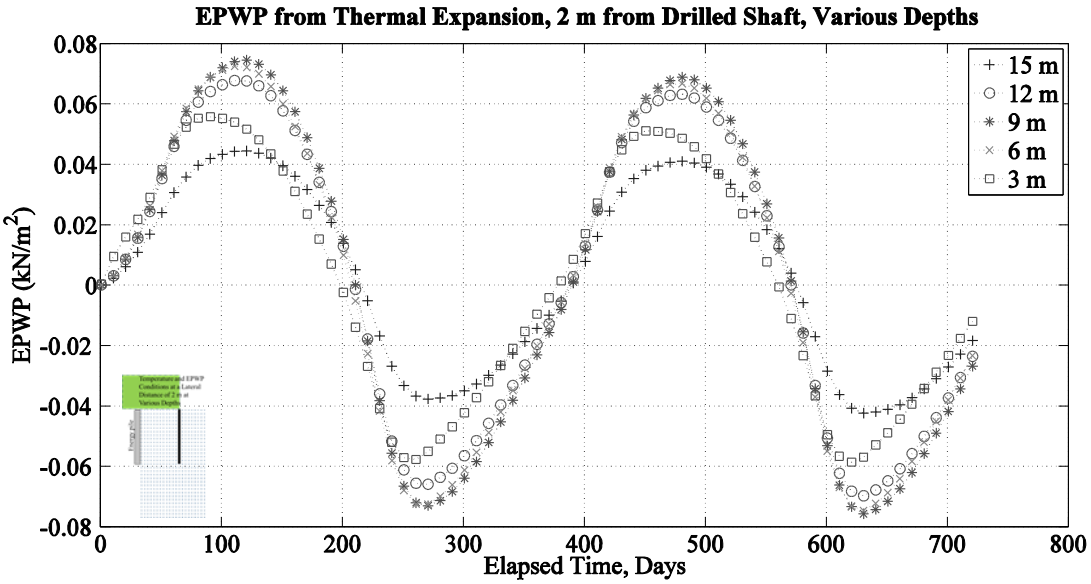

Figure 5.83. EPWP due to thermal expansion of the soil at a lateral distance of 2 m for the depths shown for the two-year model run.

Variations of Temperature and EPWP at a Lateral Distance of 3 m from the Drilled Shaft

Figure 5.84 indicates the distance from the drilled shaft where the results in this section are presented along the depths presented in the figure's legend.

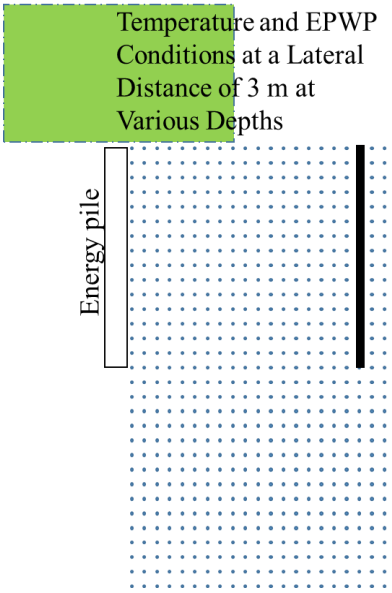

Figure 5.84. Figures in this chapter that present results from points at a lateral distance of 3 m from the drilled-shaft face will be identified with this symbol.

Temperature Values Over Time at Various Depths

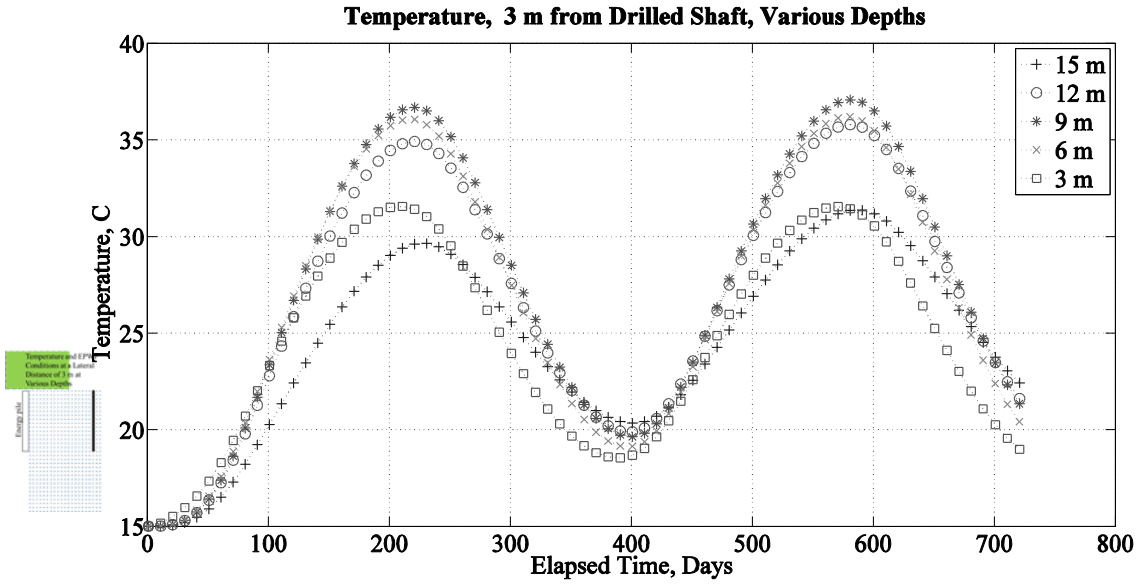

Figure 5.85. Temperature at a lateral distance of 3 m from the drilled shaft at various depths for the two-year model run.

Excess Pore-Water Pressure (EPWP) Values Over Time at Various Depths

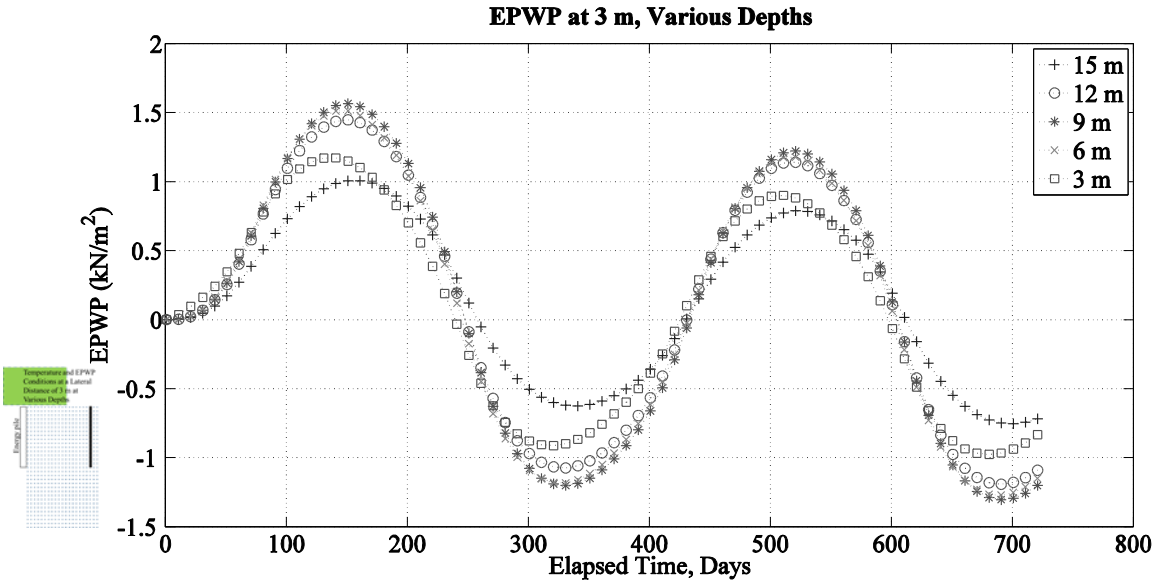

Figure 5.86. EPWP at a lateral distance of 3 m from the drilled shaft at various depths for the two-year model run.

EPWP Normalized to Peak EPWP at Various Depths

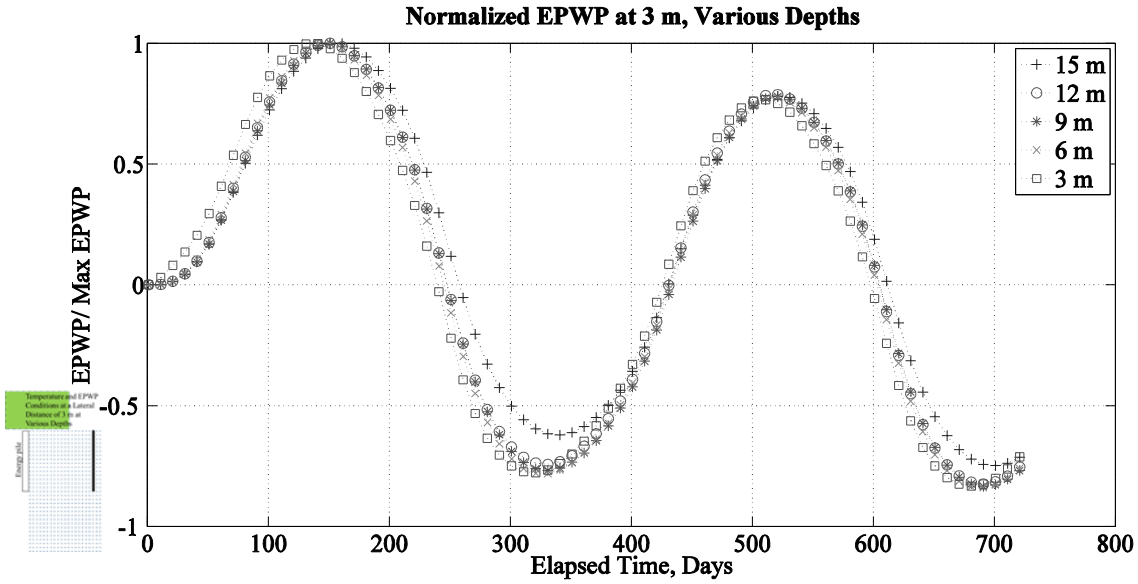

Figure 5.87 EPWP, normalized to the peak EPWP, at a lateral distance of 3 m from the drilled shaft at various depths for the two-year model run.

EPWP Due to Thermal Expansion of the Soil

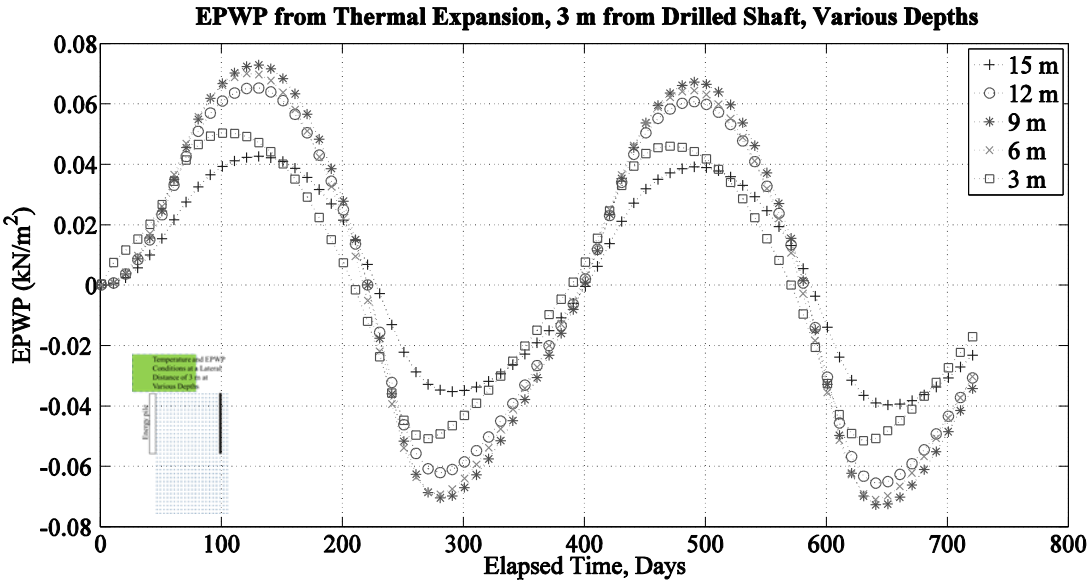

Figure 5.88. EPWP due to thermal expansion of the soil at a lateral distance of 3 m for the depths shown for the two-year model run.

Summary of Results and Discussion

The consolidation modeled in this work differs from Terzaghi's model for one-dimensional, vertical consolidation. Terzaghi's model was discussed in Chapter 3 and was based upon Darcy's Law, which was also briefly discussed in Chapter 3, but both are summarized again below.

Darcy made the following assumptions:

- Flow through the porous media is laminar;
- Porosity is determined using the average properties of the porous media; and
- Fluid properties are spatially and temporally constant.

The derivation of Terzaghi's model for time rate of consolidation is based upon the following assumptions.

- The clay-water system is homogeneous;
- Complete water saturation exists;
- Compressibility of soil grains is negligible;
- Compressibility of water is negligible;
- The flow of water is in the direction of the compression;
- Darcy's law is valid.

In this work, temperature fluctuation has been introduced, both within the soil and outside of the soil matrix. This temperature fluctuation violates Darcy's law because the fluid properties vary as a result of temperature change. In addition, porosity is allowed to change with temperature change. The assumptions that are violated in Terzaghi's model include compressibility of the soil grains and water, and, of course, Darcy's law. The compressibility of soil grains is addressed via the constant, α_{st}, the coefficient of physico-

chemical strain. The compressibility of water is addressed with a variable coefficient of thermal expansion.

The effect temperature has on the consolidation rate of the soil is presented in Figures 5.90 through 5.99. While the ideas presented in the following figures are valid for both driven piles and drilled shafts, Figures 5.90 through 5.93 and 5.95 through 5.99 are presented using values obtained during the driven pile iteration of the model for illustrative purposes. The results shown in previous figures indicate that consolidation rates are greater during periods of relatively lower temperatures than during periods of relatively higher temperatures. Figures 5.90 through 5.93 present coefficients of radial consolidation, c_r, and of vertical consolidation, c_v, along the pile face, in model runs where temperature fluctuations from the introduction of HVAC are both present and not present. Figure 5.90 presents fluctuation of c_r and Figure 5.92 presents fluctuation of c_v that decreases with increasing depth. This change can be attributed to the difference between the value of the surface temperature and the value of the soil temperature along the pile. Once HVAC is introduced, as shown in Figures 5.91 and 5.93, values of c_r and c_v vary with soil temperatures, and are more than double initial values at their peak. Figure 5.89 indicates the distance from the driven pile where the results are presented at the depths indicated in the graph legend.

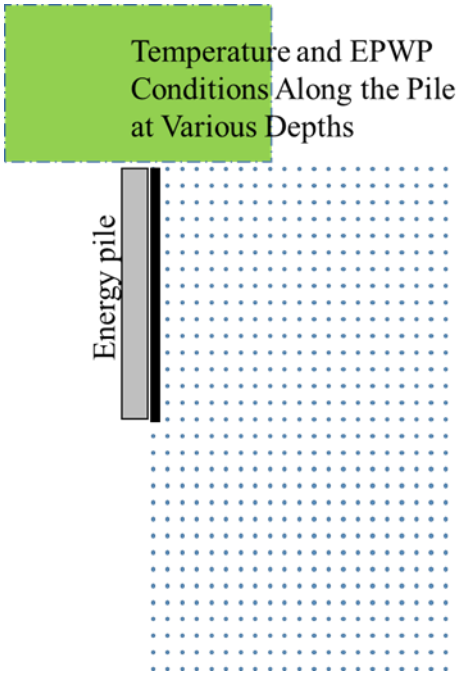

Figure 5.89. Figures in this chapter that present results from points along the face of the driven-pile face will be identified with this symbol.

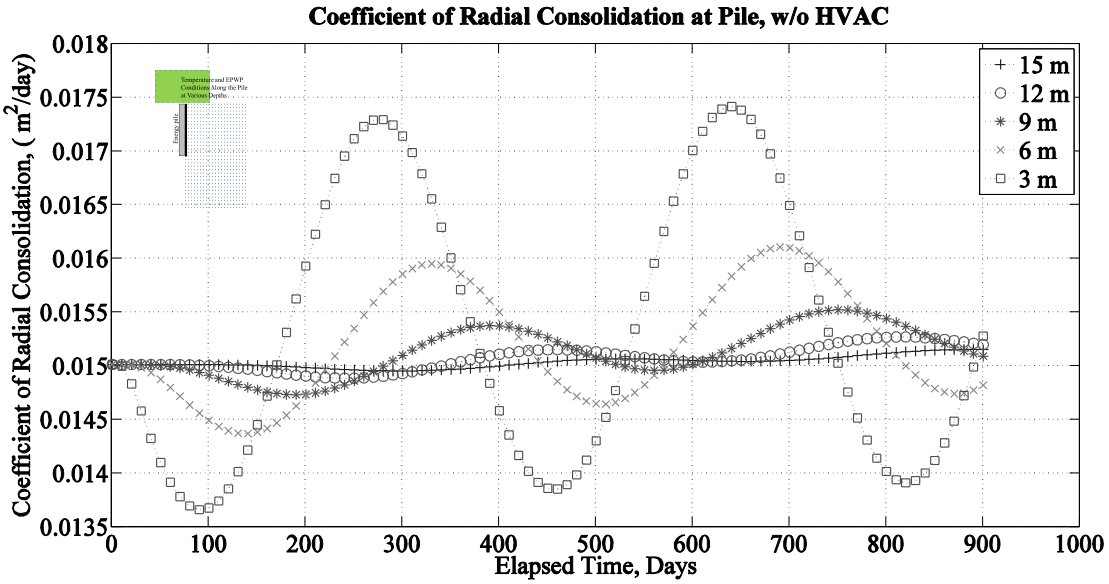

Figure 5.90. Coefficient of radial consolidation along pile with transient ground-surface temperatures at various depths, without HVAC.

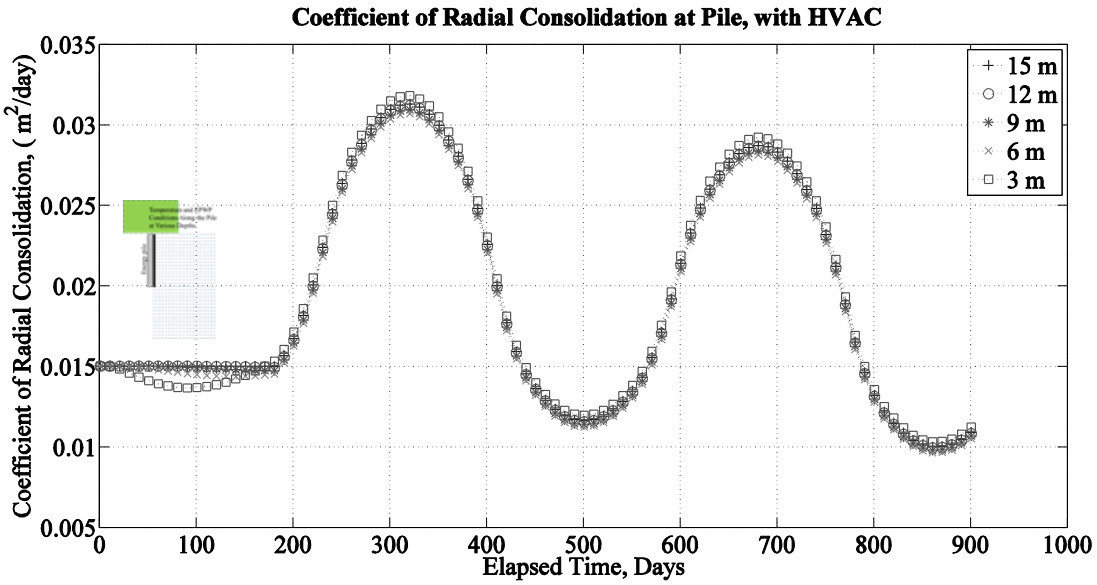

Figure 5.91. Coefficient of radial consolidation along pile with transient ground-surface temperatures at various depths, with HVAC.

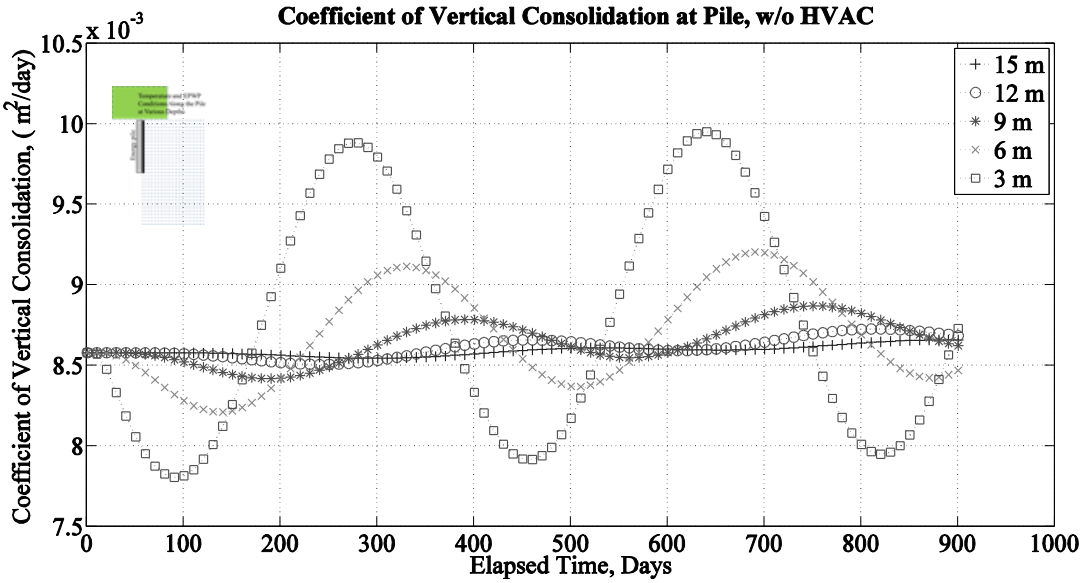

Figure 5.92. Coefficient of vertical consolidation along pile with transient ground-surface temperatures at various depths, without HVAC.

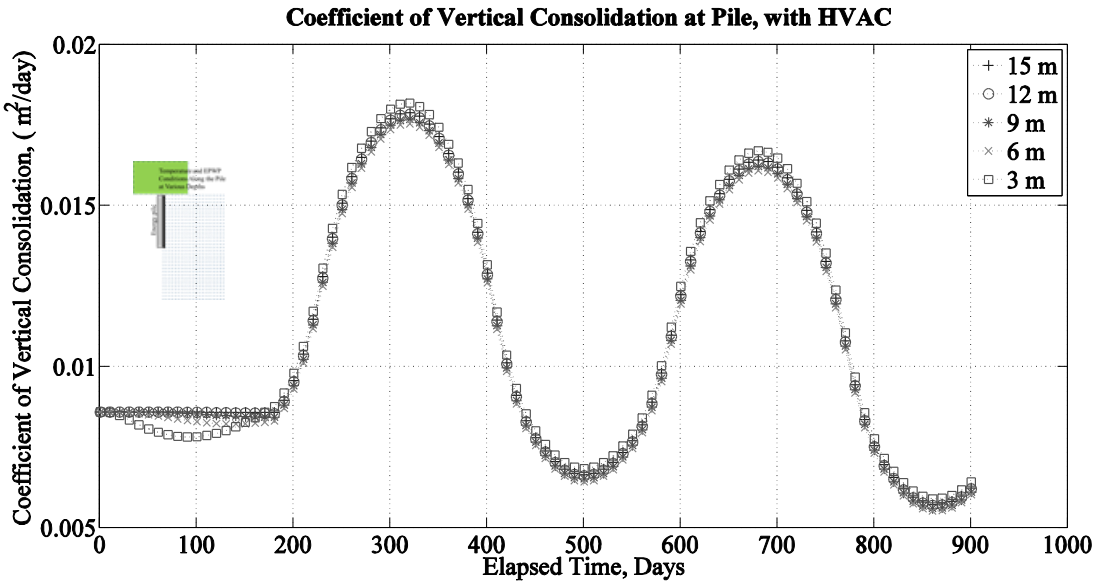

Figure 5.93. Coefficient of vertical consolidation along pile with transient ground-surface temperatures at various depths, with HVAC.

Figure 5.95 presents the correlation between the ratio that differentiates the intrinsic permeability from hydraulic conductivity, which is a function of the permeant fluid properties, i.e., $\frac{\gamma_T}{\mu_T}$, which is the unit weight of water divided by the dynamic viscosity at a temperature other than the standard 20 °C presented in Equation (3.3) and the daily temperature over the model period. It is because of this portion of the permeability equation that consolidation occurs more rapidly in periods of lower temperatures than periods of higher temperatures. The density of water decreases with increasing temperature as does the dynamic viscosity. However, the dynamic viscosity decreases more rapidly than the density, increasing this ratio with increasing temperatures, resulting in increased hydraulic conductivity of the soil with increasing temperatures. According to Equation (4.7), a larger permeability results in a higher coefficient of consolidation.

Figure 5.94 indicates the results in the graph were obtained along the face of the driven pile at a depth of 6 m.

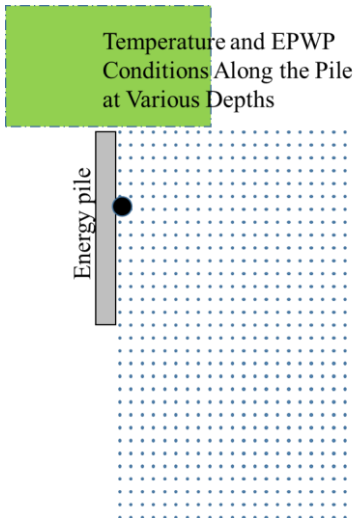

Figure 5.94. Figures in this chapter that present results from a depth of 6 m along the face of the driven-pile face will be identified with this symbol.

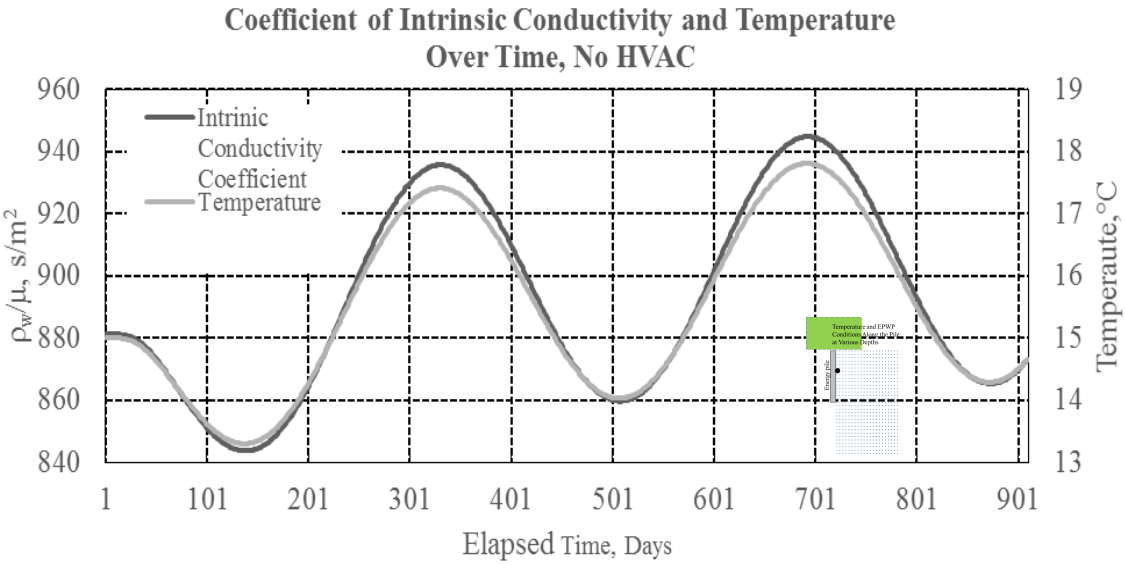

Figure 5.95. Coefficient of intrinsic permeability and temperature at pile surface at 6 m depth with transient surface temperatures, without HVAC.

To further demonstrate the effect temperature variations have on consolidation, Figure 5.96 presents the differential between EPWP values with and without the effects

of HVAC. The period of time presented in Figure 5.96 begins when HVAC begins and lasts for two years. Figure 5.96 is an overlap of Figures 5.3 and 5.7 and clearly shows that when temperature increases, EPWP levels are lower with the presence of HVAC than without; and during low temperature periods, when the soil is cooler with HVAC than without, EPWP values are higher with HVAC than without.

Figures 5.97 and 5.98 present water-saturated unit-weight values over time. Figure 5.97 presents values along the pile surface, and Figure 5.98 presents values at a lateral distance of 2 m from the pile, beyond the plastic zone. Both figures include transient ground-surface temperatures. The values are not calculated until HVAC is turned on in Figure 5.98.

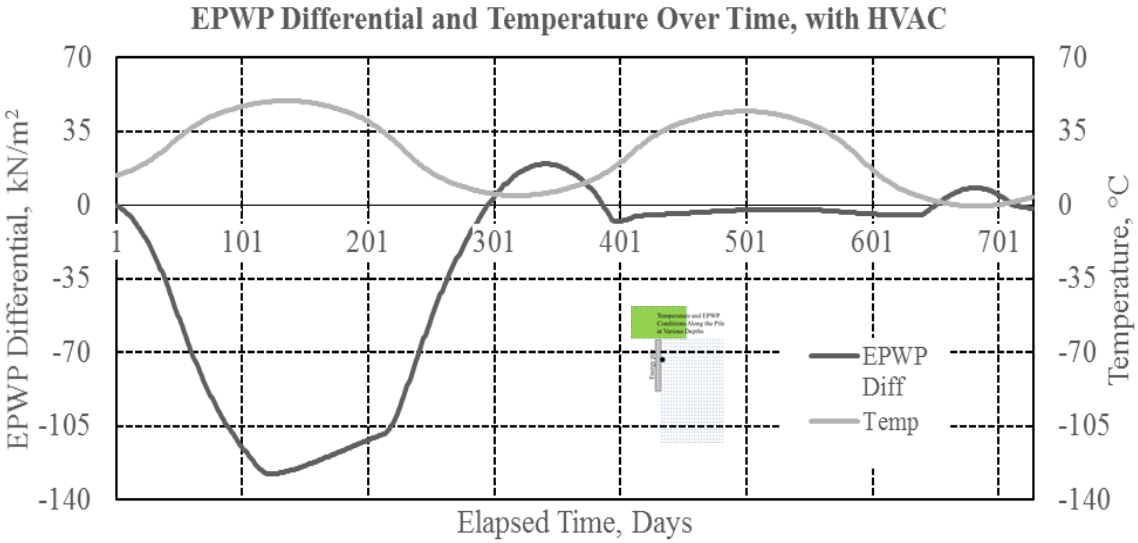

Figure 5.96. Differential EPWP and temperature with transient ground-surface temperatures on pile face at depth=6 m.

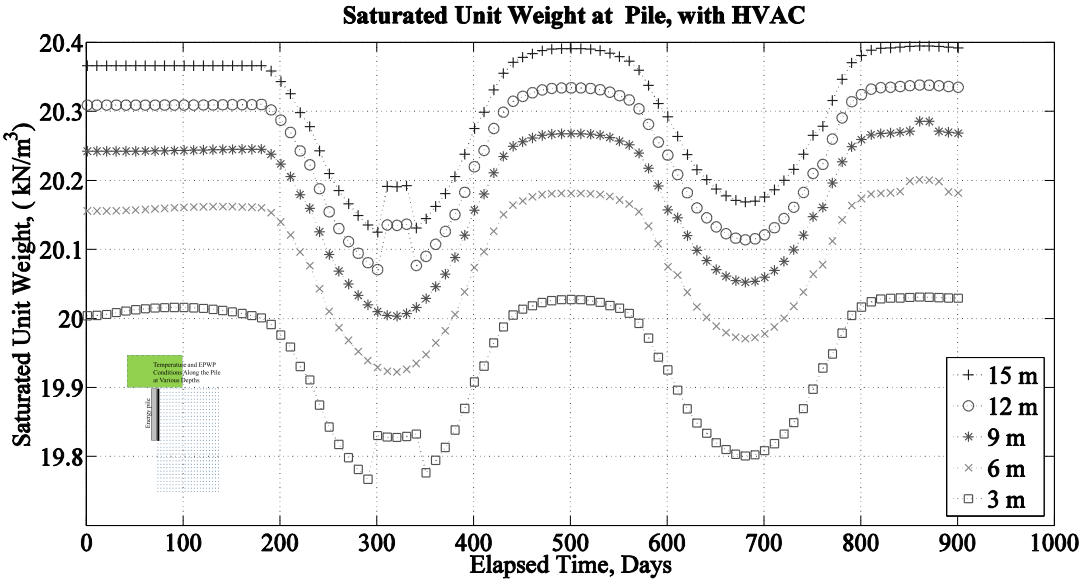

Figure 5.97. Water-saturated unit weight of soil along pile face, at various depths, with transient ground-surface temperatures and HVAC.

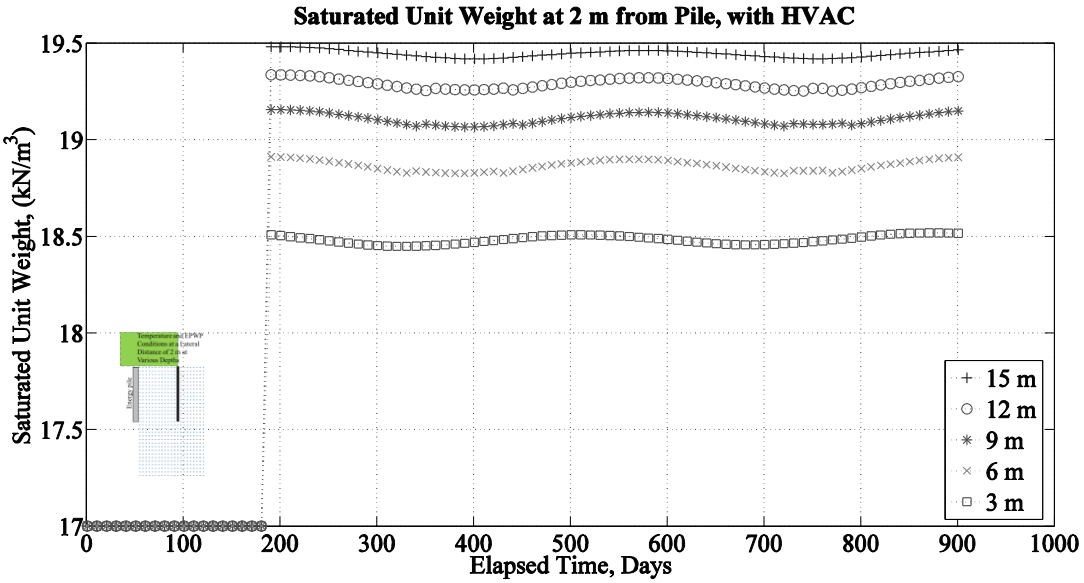

Figure 5.98. Water-saturated unit weight of soil at a lateral distance of 2 m from the pile face, at various depths, with transient ground-surface temperatures and HVAC.

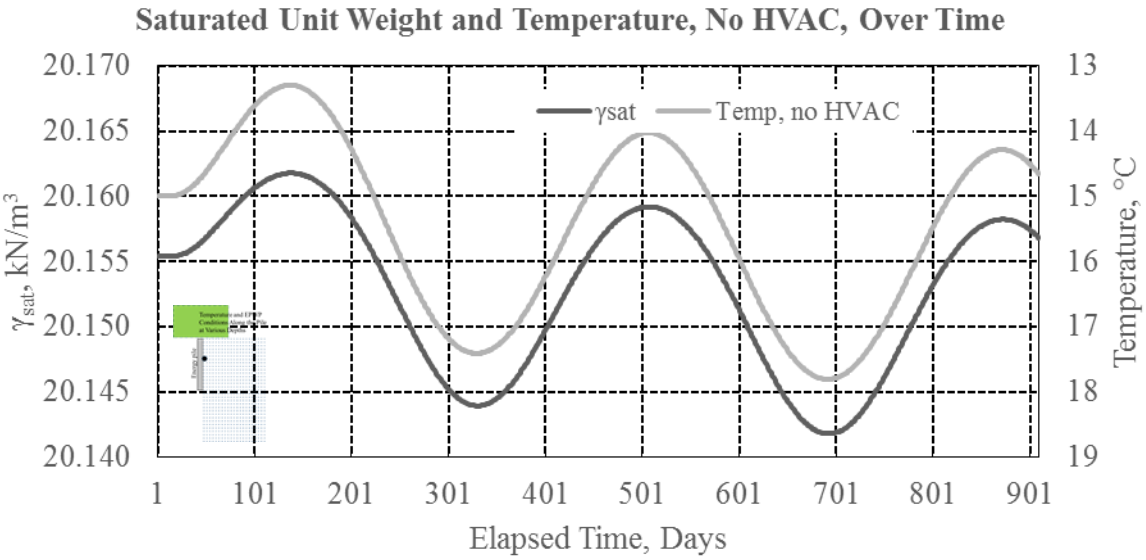

Figure 5.99. Correlation between γ_{sat} and temperature along pile face at a depth of 6 m with transient ground-surface temperatures, but without HVAC. Note that the temperature scale is flipped.

Figures 5.99 and 5.100 focus on a node along the pile face at a depth of 6 m from the ground surface. Transient surface-temperature conditions are present in both figures. Figure 5.99 presents values of water-saturated unit weight over the modeling period without the presence of HVAC while Figure 5.100 includes HVAC. Note that the temperature values are in reverse order for these two figures in order to show the correlation between temperature and water-saturated unit weight.

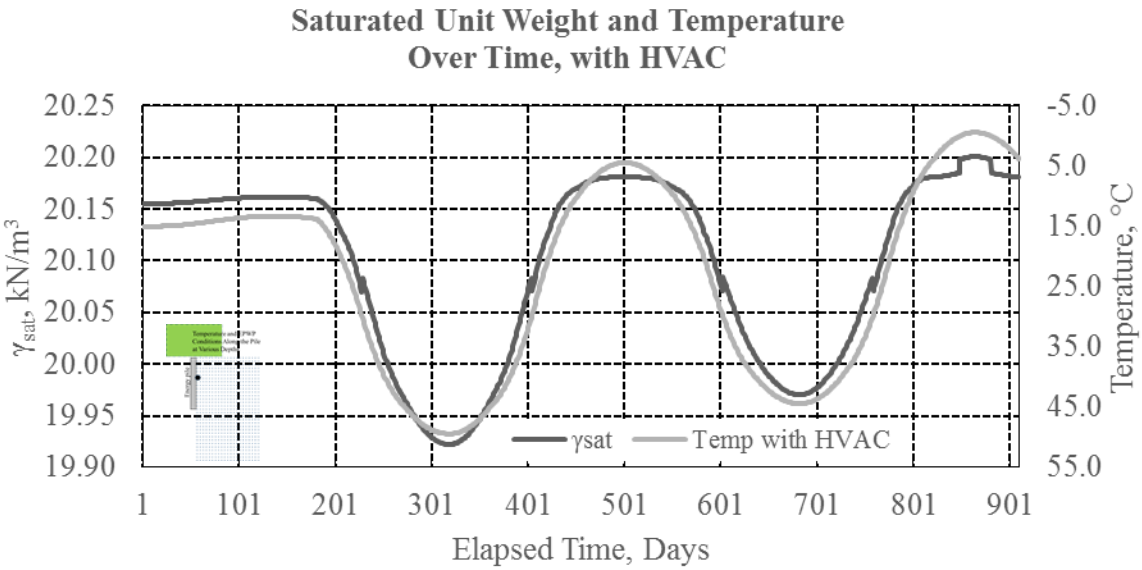

Figure 5.100 Correlation between γ_{sat} and temperature along pile face at a depth of 6 m with transient surface temperatures, with HVAC. Note that the temperature scale is flipped.

Unit-Circumference Friction Value Adjustment

The unit-circumference-friction values for driven energy piles were calculated based upon Equations (4.10) through (4.12). The vertical effective stress, σ_z', was calculated for each 1m increment of the pile using Equation (4.10).

The deviator stress, $\delta\sigma_r$ in Equation (2.6), and has a peak value of 422.26 kN/m^2, which is less than the value of EPWP during the dilation that occurs in the first 75 days after the pile was assumed to be driven. This negative differential appears as a decreasing unit-circumference-friction value in Figures 5.60 and 5.61. A negative value of unit-circumference-friction was avoided by combining Equations (4.10) through (4.12) with an initial friction value of 20% of the ultimate value, as presented in Equation (2.5). Strictly speaking, a negative value of side friction is possible and would be acting to resist upward motion by the pile.

The unit-circumference-friction values calculated in the model can be compared to historical methods such as the Skov and Denver equation and the equation from Bogard and Matlock (1990) as referenced by Mirza (2000), both of which were presented in Chapter 2 of this work. If pile capacity and frictional capacity are assumed to be proportional, the equation can be appropriated to estimate frictional capacity in the first one hundred days of the model if the friction resistance from Figures 5.60 and 5.61 is assumed to be linear from Day 1 to Day 100. To accomplish this, the value of the parameter *A* was calculated from data used to create Figure 5.60. Figure 5.101 presents unit-friction values versus log time.

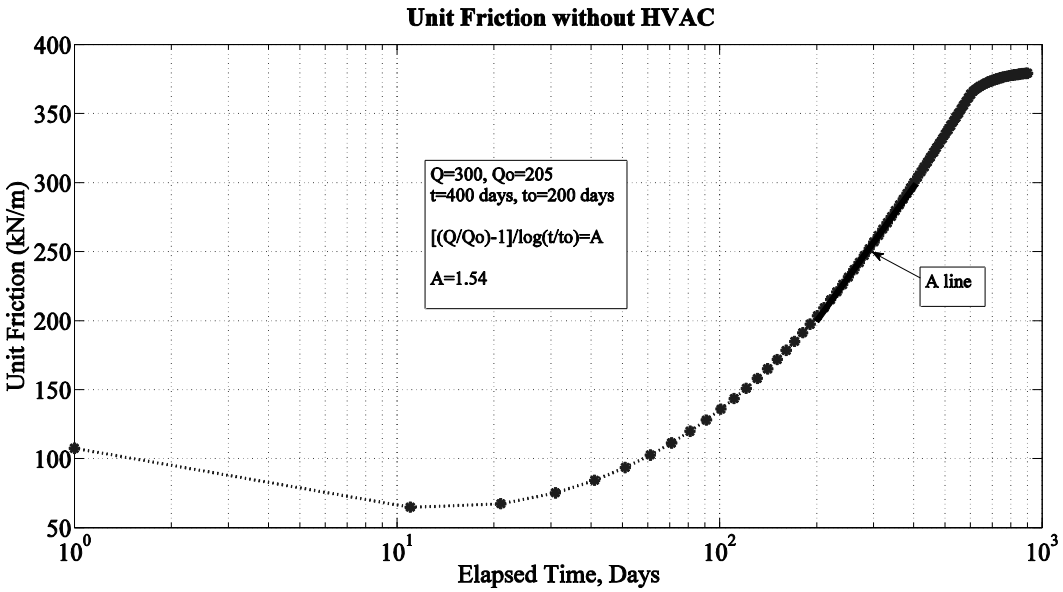

Figure 5.101. Unit-friction values versus log time for soil along the pile. Surface soil temperature is 15 °C.

If unit-friction values versus time are assumed to be linear between Day 200 and Day 400, *A* is approximately 1.54, based upon a unit- friction value of approximately 205 kN/m at Day 200 and a unit friction value of 300 kN/m at Day 400. Q_o is then 45.1 kN/m

at Day 1 and approximately 140 kN/m on Day 100. According to Figure 5.101, the unit friction value is very close to 140 kN/m on Day 100.

In order to compare the frictional capacity equation used in the model to the equation from Bogard and Matlock (Mirza, 2000), Figure 5.102 was created using the EPWP results from Figure 5.4.

The degree of consolidation, *U*, is related to normalized EPWP, as shown in Equation (5.1).

$$U = 1 - \frac{EPWP_t}{Max\ EPWP} \qquad (\mathbf{5.1})$$

Referring to Figure 5.102, $U = 0.5$ at EPWP = 263 kN/m^2. Therefore, the time to 50% consolidation is approximately 230 days.

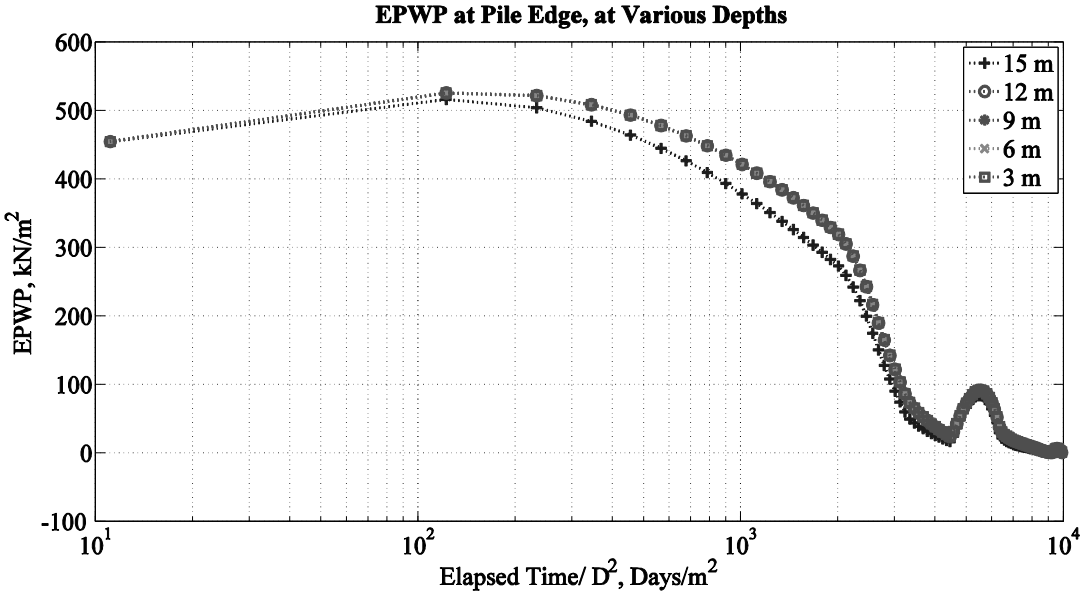

Figure 5.102 Time to 50% consolidation plot, based upon work by Bogard and Matlock (1990) as referenced in Mirza (2000).

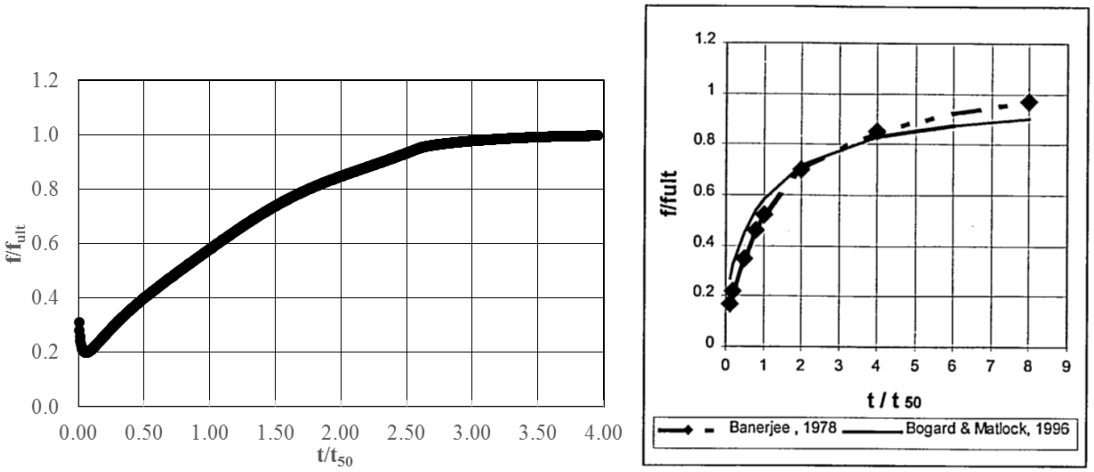

Figure 5.103. Comparison between a graph of unit friction ratio versus normalized time for soil in this model, without HVAC, to the soil graphed by Bogard and Matlock (1996) method as referenced in Mirza (2000).

The difference between the two graphs in Figure 5.101 is due to the difference between the coefficients of consolidation of the two soils. Note that the two horizontal axes have different ranges and the time to $\frac{f}{f_{ult}} = 1$ occurs more rapidly with the example from the model. Information about the soil in the graph on the right was not provided by Mirza (2000). Without a way to normalize the parameters, the two graphs are not directly comparable. The graph on the left, presented in Figure 5.103, shows that unit side friction ranges between 20% and 40% of the ultimate unit side friction value in the first 100 days. The side friction presented on the left in Figure 5.103 assumes consolidation is allowed to progress without the introduction of heat into the soil. Unit side friction reaches a peak value on Day 870. If the unit-circumference-friction values presented on Figure 5.60 are used to find the ultimate unit-circumference-friction, which is estimated to be 380 kN/m, then unit-circumference-friction values would range from 76 kN/m to 152 kN/m during the first 100 days. However, the peak EPWP was not used in the model to calculate unit-circumference-friction because the peak EPWP is not known until after the model has

finished computing. Therefore, unit-circumference-friction is calculated using Equation (4.12). The result of this difference in computing methods is that the minimum unit-circumference-friction value would not be lower than 20% of the peak if Equation (4.12) was constructed using Equation (2.5).

The β-method, presented in Equations (3.8) and (3.9), may be used to calculate total side friction for the pile. Assuming the ratio, $\frac{\delta}{\varphi'}$, is equal to 0.8, and the lateral earth pressure coefficients are the same as before, $\beta = 0.29$ for the model pile. The unit-circumference friction value calculated in the model assumes 1m thick layers of soil. The soil in the model is a single layer of clay. Therefore, the β-method may be calculated by finding the effective vertical stress at the midpoint of the effective length of the soil layer. In the modeled soil layer, disregarding the top 1.5 meters of the pile, the effective length is 13.5 m, and the total friction for the pile is approximately 295 kN.

The frictional capacity of the model pile is approximately 306 kN, as computed using Equations (2.13) and (2.14), the method proposed by McCartney and Rosenberg (2011). The overburden value was calculated using a depth of 15 m of pile embedment. The remaining variables were obtained from the literature and from assumptions made for the model.

The unit-circumference-friction value proposed in this work for capacity calculations is the value, presented in Figures 5.60 and 5.61, that is equal to the minimum unit-circumference-friction value computed during the decrease due to soil heating during Year 1. The value may be found within the model, or located on Figures 5.60 and 5.61, by drawing a horizontal line tangent to bottom of the localized curve and connecting it to the vertical axis. Using a unit-circumference friction value of 325 kN/m, the

recommended value for the constant surface temperature iteration of the model, the total friction value is equal to 306.3 kN, which is comparable to both the β-method and the method presented by McCartney and Rosenberg (2011).

The unit-circumference-friction value for the modeled drilled shaft was selected to be 421 kN/m, as presented in Figure 5.92. Using the α-method for the drilled shaft, an unconfined shear strength of 75 kN/m^2, a value of $\alpha = 0.4$ (Coduto, 2001), and an effective shaft length of 13 m, the unit-circumference friction value calculated using the α-method is 390 kN/m. The method used in the model is therefore less conservative than the α-method but provides comparable results. The allowable skin-friction values are calculated by multiplying the unit-circumference friction value by the perimeter of the drilled shaft. For the model, this value is 1190 kN, and using the α-method, the allowable friction capacity is 1103 kN.

CHAPTER 6: CONCLUSIONS

The purposes of this work, both the written thesis and finite-difference model, were to understand some of the physical processes relating to the soil-pile interaction of energy piles and to model the effects of temperature fluctuation on the capacity of driven energy piles in clayey soils. These physical processes include the consolidation of clay around energy piles as well as conduction through the saturated clay soil. The consolidation of clay (due to the drainage of excess pore-water pressure (EPWP) in clay) surrounding piles affects the capacity of the pile (pile setup in clay). This work modeled how temperature fluctuations within the soil surrounding the energy pile and fluctuations of the ground-surface temperature affected the drainage of EPWP and thus the shear capacity of the energy pile.

The hypothesis for this model was that an increase in soil temperature would cause thermal expansion of the water within the soil and of the soil itself, causing an increase in EPWP and, thus, a reduction in shear capacity of the pile; or, conversely, that cooling of the soil would accelerate the dissipation of EPWP.

The change in EPWP due to the thermal expansion and contraction of the energy pile and thermal expansion and contraction of the soil matrix was included in the model as well as the dissipation of EPWP generated by cavity expansion during pile driving. The model analyzed the effect that variable temperature had on the shear capacity of both driven energy piles and drilled-shaft energy piles. The temperatures of both the soil at the surface of the pile or drilled shaft and the ground surface were varied sinusoidally to

simulate seasonal demands on the energy pile and seasonal temperature changes, respectively.

Temperature Effects

Generally, the hypothesis stated in this work was found to be true. An increase in temperature tends to increase the rate of consolidation, and therefore, increase the shear capacity of the pile. This relationship is in agreement with the findings of McCartney and Rosenberg (2011), as stated in Chapter 2.

The model assumed that the pile was driven on the first day of winter and the energy pile began operation on the first day of summer. As shown in Chapter 5, EPWP dissipated at an increased rate during the period of time when the soil was heating. The peak differential was approximately 140 kN/m^2. When the EPWP was nearly dissipated, around Day 400, the soil cooling cycle raised the EPWP 67 kN/m^2 and the EPWP didn't reach its pre-cooling-cycle value for 195 days. If the model conditions were flipped, that is, the energy pile was constructed on the first day of summer and operational on the first day of winter, the EPWP values would dissipate more slowly, likely leading to a longer period of consolidation.

The influence of cyclical surface temperatures can be observed in the results of the model. As presented in Chapter 4, the offset in the cyclical surface temperature equation placed the highest surface temperature in the middle of the summer, thus exaggerating the influence higher temperatures have on increasing consolidation rates, because additional heat is present at the surface and is being conducted down into the soil at the same time the soil is heating due to HVAC usage. Consolidation rates would likely

decrease more slowly if surface soil temperatures peaked during the period prior to operation of the energy pile and during the period of soil cooling.

Side Friction Capacity

A comparison between the shear capacity of the energy pile using an equation that considered the degree of consolidation that was modeled in this work and both the shear capacity calculate using the β–method (Equation (4.8)) and the equations by McCartney and Rosenberg (2011), (Equation (2.13)) was presented in Chapter 5. The unit-circumference-friction values computed by the model were calculated by using the β–method where the effective vertical stress was calculated using 1m-thick layers of clay that were then modified to consider degree of consolidation over the modeled time period. The unit-circumference-frictional values computed in the model were shown to lead to allowable side-friction-capacity values that were similar in value to the allowable capacities that were calculated using the β–method, where the effective vertical stress was calculated as a single full-depth clay layer, and the method by McCartney and Rosenberg (2011).

In hindsight, the driven-energy-pile timeline was not the best example to show the benefit of using the model to estimate allowable frictional capacity. Assuming a time-to-finished-construction timeline of six months, the unit-circumference frictional capacity is approximately 190 kN/m, compared to the recommended value of 325 kN/m. However, the data obtained from the example should be viewed as evidence of a properly working model, and not a design problem. The model was developed to input a variety of conditions, assumptions, and timelines.

Cyclic Loading

Cyclic loading is not expected to be of a magnitude or frequency to cause additional EPWP in the soil surrounding the energy pile.

Limitations

A sincere effort was put into incorporating realistic values of soil and water characteristics into the model for the example scenarios presented in this work. The Vogel-Fulcher-Tammann (VFT) model is suitable for fluids in the temperature range presented here. The Cavity-Expansion Theory model was used because it suggested greater generated excess-pore-water pressure (EPWP) values than other models. Other models may also provide acceptable results.

As stated in Chapter 4, convection within the energy pile was not included within the scope of this work. Temperature variations with depth, inside or on the surface of the energy pile, were likewise not considered in this work. Instead, a simplified assumption that the heat from the energy pile directly led to a uniform soil temperature along the face of the pile was used to represent the transfer of heat from the building (and energy pile) to the soil. In addition, the model used to represent HVAC demand assumes heat will be added to the soil for a limited number of hours per day. The temperature of the soil will remain constant until it is changed due to assumed HVAC demand the next day. This was an assumption and may not reflect actual conditions. In reality, temperature and EPWP values are changing continuously, but as a practical matter, given the time period of the model, daily changes were deemed more appropriate. The temperature range for the soil along the surface of the energy pile is believed to be realistic and within the temperature range used experimentally by others. Actual temperature and EPWP values may not be

exactly as presented in simulated scenarios. However, the code is capable of simulating other more realistic scenarios. The model, developed for this work, uses approximations to estimate values at discrete points. The values presented here are approximations only, and it is assumed that this model should be compared with experimental data at some future time.

CHAPTER 7: FUTURE WORKS

The objective of this work was to create a model that analyzed the effect that temperature had on the consolidation of soil surrounding an energy pile. The model used multi-physics to solve second-order differential equations of transient consolidation and conduction. It is understood that while the model is versatile, as general conditions were incorporated into it wherever possible, it is also simplistic, and there are many directions to go in order to analyze energy piles for which this work could serve as a basis.

This work analyzes a single pile or drilled shaft in a single layer of relatively homogeneous, saturated clayey soil. The water level is assumed to be at the ground surface. The deformation of the soil due to pile driving at the pile tip is not considered. The convection within the energy pile is not within the scope of this work. Thermal expansion of the pile has been covered extensively by many authors cited in this work (Bourne-Webb et al., 2009, Laloui et al., 2006, Laloui and Cekerevac, 2008), but was not part of the scope of this work. The heating and cooling cycles in this model are simplistic.

The model could be amended to consider layered soil. To accomplish this, characteristics of the different soils would have to be incorporated into the model. Consolidation and conduction would be evaluated in the radial direction with soil characteristics assigned to rows of nodes.

The model could analyze a situation where the groundwater surface is not at the ground surface or the groundwater level suddenly drops. The soil above the groundwater

level might be experiencing negative pore-water pressure prior to the beginning of the model. Perhaps the soil above the groundwater level is not saturated, and consolidation and conduction analyses incorporate unsaturated soil conditions.

The soil grid could be reshaped to include a boundary condition that represents the bottom of the pile or drilled shaft from the centerline to the edge, to show consolidation and conduction occurring below the pile. Deformation of the soil below the pile tip could be examined using spherical cavity expansion.

More in-depth analysis could be given to how the heating fluid changes the temperature of the energy pile and how the temperature changes reach the soil. This work effectively bypassed the heat transfer occurring within the energy pile itself. In addition, the temperature cycle incorporated into this work probably does not reflect reality. A few of the works cited in this thesis (Bourne-Webb et al., 2009, Laloui et al., 2006), present in situ temperature recordings of energy piles subjected to heating and cooling cycles that change the soil temperature much more rapidly than was modeled in this work. Perhaps this model could be redone with either a much more rapid temperature change period or redone using a more real realistic model for the input and extraction of heat from the soil.

Lastly, in this work, a single driven pile or drilled shaft was analyzed. The model conditions were such that EPWP and temperature were effectively dissipated within the 3.3 meter width of the modeled soil space. A model could be created that analyzes the effects of adjacent piles. A pile spacing of four to 5 m might create a hot or cold spot that delays dissipation of EPWP or limits the effectiveness of individual piles.

REFERENCES

Abdelaziz, S.L., Olgun, C.G., and Martin II, J.R. 2011. Design and Operational Considerations of Geothermal Energy Piles. *Geotechnical Special Publication No. 211*. ASCE. 450-459.

Abe, N. 2001. Thermo-Viscoplastic Model for Soft Clays. Proceedings of the Eleventh (2001) International Offshore and Polar Engineering Conference. 417-424.

Azzouz, A.S., Baligh, M.M., and Whittle, A.J. 1990. Shaft Resistance of Piles in Clay. *Journal of Geotechnical Engineering*, **116**(2), 205-221.

Bourne-Webb, P.J., Amatya, B., Soga, K., Amis, T., Davidson, C., and Payne, P. 2009. Energy Pile Test at Lambeth College, London: Geotechnical and Thermodynamic Aspects of Pile Response to Heat Cycles. *Geotechnique*, **59**(3), 237-248.

Brandl, H. 2009. Energy Pile Concepts. *Deep Foundations on Bored and Auger Piles*. 77-95.

Burns, S., and Mayne, P. 1999. Pore Pressure Dissipation Behavior Surrounding Driven Piles and Cone Penetrometers. *Transportation Research Record.* **1675**. 17-23.

Campanella, R.G., and Mitchell, J.K. 1968. Influence of Temperature Variations on Soil Behavior. *Journal of the Soil Mechanics and Foundations Division.* ASCE. **94**(3). 709-734.

Carter, J.P., Randolph, M.F., and Wroth, C.P. 1979. Stress and Pore Pressure Changes in Clay During and After the Expansion of a Cylindrical Cavity. *International journal for numerical and analytical methods in geomechanics (0363-9061).* **3**(4), 305-322.

Coduto, D. 2001. Foundation Design: Principles and Practices, Second Edition. Prentice Hall. 402-558.

Das, B. 1990. Principles of Geotechnical Engineering, Second Edition. PWS-Kent. 95-98, 249-251.

Das, B. 2007. Principles of Foundation Engineering, Sixth Edition. PWS-Kent. 491-639.Website that had coefficients for Vogel dynamic viscosity model (http://ddbonline.ddbst.de/VogelCalculation/VogelCalculationCGI.exe?component=Acetone)

Demars, K.R., and Charles, R.D. 1982. Soil Volume Changes Induced by Temperature Cycling. *Canadian Geotechnical Journal*. **19**, 188-194.

Ebnother, A. 2008. Energy Piles: The European Experience. *Geo Drilling*. http://www.docstoc.com/search/geodrilling-international.

Laloui, L., Nuth, M., and Vulliet, L. 2006. Experimental and Numerical Investigations of the Behavior of a Heat Exchanger Pile. *International Journal of Numerical and Analytical Methods in Geomechanics.* **30**, 763-781.

Laloui, L., and Cekerevac, C. 2008. Numerical Simulation of the Non-Isothermal Mechanical Behavior of Soils. *Computers and Geotechnics.* **35**, 729-745.

Li, L., Dan, H., and Wang, L. 2011. Undrained Behavior of Natural Marine Clay Under Cyclic Loading. *Ocean Engineering*, **38**, 1792-1805.

McCartney, J.S., and Rosenberg, J.E. 2011. Impact of Heat Exchange on Side Shear in Thermo-Active Foundations. *Geotechnical Special Publication No. 211*. ASCE. 488-498.

Mirza, U.A.A.. 2000. Consolidation Parameters from Axial Pile Load Tests. Proceedings of The Tenth (2000) International Offshore and Polar Engineering Conference. 395-402.

Ng, K., Roling, M., AbdelSalam, S., Suleiman, M., Sritharan, S. 2013. Pile Setup in Cohesive Soil. I: Experimental Investigation. *Journal of Geotechnical and Geoenvironmental Engineering.* **139**(2). ASCE. 199-209.

Randolph, M.F. and Wroth, C.P. 1979. An Analytical Solution for the Consolidation Around a Driven Pile. *International Journal for Numerical and Analytical Methods in Geomechanics*. **3**, 217-229.

Soderberg, L.O. 1962. Consolidation Theory Applied to Foundation Pile Time Effects. *Geotechnique*. **12**, 217-225.

Steward, E.J., and Wang, X. 2011. Predicting Pile Setup (Freeze): A new approach considering soil aging and pore pressure dissipation. *Geotechnical Special Publication No. 211*. ASCE. 11-19.

Wang, B., Bouazza, A., Haberfield, C. 2011. Preliminary Observations from Laboratory Scale Model Geothermal Pile Subjected to Thermo-mechanical Loading. *Geotechnical Special Publication No. 211*. ASCE. 430-439.

Wang, J., Li, C., and Moran, K. 2005. Cyclic Undrained Behavior of Soft Clays and Cyclic Bearing Capacity of a Single Bucket Foundation. *Proceedings of The Fifteenth (2005) International Offshore and Polar Engineering Conference.* 392-399.

Wang, X., Verma, N., Tsai, C., and Zhang, Z. 2010. Setup Prediction of Piles Driven into Louisiana Soft Clays. *GeoFlorida 2010: Advances in Analysis, Modeling & Design.* GSP 199. ASCE. 1573-1582.

Yang, L., and Liang, R. 2006. Incorporating Set-up into Reliabilty-Based Design of Driven Piles in Clay. *Canadian Geotechnical Journal.* **43**(9). 946-955.

Zheng, J., Lu, Y., Yin, J., and Guo, J. 2010. Radial Consolidation with Variable Compressibility and Permeability Following Pile Installation. *Computers and Geotechnics*. **37**, 408-412.

APPENDIX A

APPENDIX A: DERIVATIONS

The derivation has been converted to consider a unit volume of soil undergoing consolidation in the horizontal direction. Consider a unit volume of saturated soil in cylindrical coordinates. The volume of soil is given as follows.

$$dV_o = rdrd\theta dz \qquad \textbf{(A.1)}$$

The change in volume of the soil is equal to the change in the volume of water flowing through the soil.

$$q_{out} - q_{in} = \frac{\partial(dV_o)}{\partial t} \qquad (\mathbf{A.2})$$

For a saturated soil, the volume of voids is equal to the volume of water. A partial change in volume is equal to the partial change in water volume, as follows.

$$\partial(dV_o) = \partial(dV_w) = \partial(dV_V) \qquad (\mathbf{A.3})$$

For a saturated soil, the volume of voids is equal to the volume of water. If the partial differential with respect to volumetric strain is defined as follows, then a relationship can be developed for the change in water volume.

$$\partial\varepsilon_V = \frac{\partial(dV_o)}{dV_o} = \frac{\partial(dV_w)}{dV_o} \rightarrow \partial(dV_w) = \partial\varepsilon_V \cdot dV_o = \partial\varepsilon_V(rdrd\theta dz) \qquad (\mathbf{A.4})$$

The void ratio is defined as the volume of voids divided by the volume of solids.

The total volume, V_t, is equal to the volume of solids, V_s, plus the volume of voids, V_v.

$$V_V + V_S = V_t$$

$$\frac{V_s}{V_t} + \frac{V_v}{V_t} = \frac{V_t}{V_t} = 1 \qquad (\mathbf{A.5})$$

The porosity is defined as follows.

$$n = \frac{V_v}{V_t} \qquad (\mathbf{A.6})$$

The relationship between void ratio, e, and porosity can be seen in the series of equations below.

$$\frac{V_s}{V_t} = 1 - \frac{V_v}{V_t} \rightarrow e = \frac{V_v/V_t}{1 - V_v/V_t} \rightarrow \frac{V_v}{V_t} = e\left(1 - \frac{V_v}{V_t}\right) = e - e\frac{V_v}{V_t} \rightarrow e = \frac{V_v}{V_t} + e\frac{V_v}{V_t}$$

$$= \frac{V_v}{V_t}(1 + e) \rightarrow \frac{V_v}{V_t} = \frac{e}{(1 + e)} = n$$

For a saturated soil, $V_v = V_w$

$$\frac{V_V}{V_S} + \frac{V_S}{V_S} = \frac{V_t}{V_S}$$
$$e_0 + 1 = \frac{V_o}{V_S}$$

$$V_S = \frac{V_o}{1 + e_0}$$
$$dV_o = dV_v$$
$$dV_V = de \cdot V_S$$

Volumetric strain is defined as follows.

$$\varepsilon_V = \frac{dV_o}{V_o} = \frac{dV_V}{V_o} = \frac{de \cdot V_S}{V_o} = \frac{de}{V_o} \cdot \frac{V_o}{1 + e_0} = \frac{de}{1 + e_0}$$

$$\partial\varepsilon_V = \frac{\partial(de)}{1 + e_0} = \frac{\partial e}{1 + e_0} \qquad (\mathbf{A.7})$$

$$\left(v_z + \frac{\partial v_z}{\partial z}dz\right)dx \cdot dy - v_z \cdot dx \cdot dy = \frac{\partial V_z}{\partial t}$$

$$\left(v_y + \frac{\partial v_y}{\partial y}dy\right)dx \cdot dz - v_y \cdot dx \cdot dz = \frac{\partial V_y}{\partial t}$$

$$\left(v_x + \frac{\partial v_x}{\partial x}dx\right)dy \cdot dz - v_x \cdot dy \cdot dz = \frac{\partial V_x}{\partial t}$$

$$\frac{\partial V_z}{\partial t} + \frac{\partial V_y}{\partial t} + \frac{\partial V_y}{\partial t} = \frac{\partial V_o}{\partial t}$$

$$\frac{\partial v_x}{\partial x}dx \cdot dy \cdot dz + \frac{\partial v_y}{\partial y}dy \cdot dx \cdot dz + \frac{\partial v_z}{\partial z}dz \cdot dx \cdot dy = \frac{\partial V_o}{\partial t}$$

$$\left(\frac{\partial v_x}{\partial x} + \frac{\partial v_y}{\partial y} + \frac{\partial v_z}{\partial z}\right)dx \cdot dy \cdot dz = \frac{\partial V_o}{\partial t}$$

$$\left(\frac{\partial v_x}{\partial x} + \frac{\partial v_y}{\partial y} + \frac{\partial v_z}{\partial z}\right) = \frac{\partial V_o}{dx \cdot dy \cdot dz}\frac{1}{\partial t} = \frac{\partial V_o}{dV_0}\frac{1}{\partial t} = \frac{\partial \varepsilon_V}{\partial t} = \frac{1}{1 + e_0}\frac{\partial e}{\partial t}$$

Darcy's Law states that the discharge velocity, v, of water flowing through a "unit gross cross-sectional area of soil at right angles to the direction of flow" (Das, 1990) equals the change in head divided by the change in distance times the coefficient of permeability of the soil.

$$\partial e = \frac{\partial V_v}{\partial V_s}$$

$$v = -ki$$

$$\vec{v} = \vec{\nabla} \cdot (q_{out} - q_{in}) = \frac{\partial (dV_o)}{\partial t} = \frac{\partial \varepsilon_V}{\partial t}$$

$$\vec{\nabla} \cdot (q_{out} - q_{in}) = \frac{\partial (dV_o)}{\partial t} = \frac{\delta (dr \cdot rd\theta \cdot dz)}{\partial t} = \frac{\partial \varepsilon_V \cdot \delta (rdrd\theta dz)}{\partial t} = \vec{v} = \frac{\partial \varepsilon_V}{\partial t}$$

$$= \frac{\partial (dV_w)}{\partial t} = \frac{drrd\theta dz}{1 + e_0} * \frac{\partial e}{\partial t}$$

$$h = h_e + \frac{u}{\gamma_w} = h_e + \frac{u_0 + u_e}{\gamma_w} \text{ and } h_e \& \, u_0 \; are \; constant, so \; \partial h = \frac{\partial u_e}{\gamma_w}$$

$$\sigma' = \sigma - u = \sigma - (u_0 + u_e) \rightarrow \partial\sigma' = -\partial u_e$$

$$\frac{\partial}{\partial x} v_x = \frac{\partial}{\partial x}\left(-k\frac{\partial h}{\partial x}\right) = \frac{\partial}{\partial x}\left(-\frac{k}{\gamma_w}\frac{\partial u_e}{\partial x}\right)$$

$$\frac{\partial}{\partial y} v_y = \frac{\partial}{\partial y}\left(-k\frac{\partial h}{\partial y}\right) = \frac{\partial}{\partial y}\left(-\frac{k}{\gamma_w}\frac{\partial u_e}{\partial y}\right)$$

$$\frac{\partial}{\partial z} v_z = \frac{\partial}{\partial z}\left(-k\frac{\partial h}{\partial z}\right) = \frac{\partial}{\partial z}\left(-\frac{k}{\gamma_w}\frac{\partial u_e}{\partial z}\right)$$

$$\frac{\partial v_x}{\partial x} + \frac{\partial v_y}{\partial y} + \frac{\partial v_z}{\partial z} = -\left(\frac{k}{\gamma_w}\frac{\partial^2 u_e}{\partial x^2} + \frac{k}{\gamma_w}\frac{\partial^2 u_e}{\partial y^2} + \frac{k}{\gamma_w}\frac{\partial^2 u_e}{\partial z^2}\right) = \frac{\partial V_o}{\partial t}$$

$$\frac{\partial V_o}{\partial t} = \frac{\partial \varepsilon_V}{\partial t} = \frac{1}{1+e_0}\frac{\partial e}{\partial t}$$

$$a_v = -\frac{\partial e}{\partial \sigma'} \rightarrow \partial e = -a_v \partial\sigma'$$

$$\frac{\partial \varepsilon_v}{\partial t} = \frac{1}{1+e_0}\frac{\partial e}{\partial t} = -\frac{a_v}{1+e_0}\frac{\partial \sigma'}{\partial t} = -\frac{a_v}{1+e_0}\frac{\partial u_e}{\partial t} = -m_v\frac{\partial u_e}{\partial t}$$

$$-m_v\frac{\partial u_e}{\partial t} = -\left(\frac{k}{\gamma_w}\frac{\partial^2 u_e}{\partial x^2} + \frac{k}{\gamma_w}\frac{\partial^2 u_e}{\partial y^2} + \frac{k}{\gamma_w}\frac{\partial^2 u_e}{\partial z^2}\right)$$

$$c_v = \frac{k}{m_v\gamma_w}$$

$$\frac{\partial u_e}{\partial t} = c_v\left(\frac{\partial^2 u_e}{\partial x^2} + \frac{\partial^2 u_e}{\partial y^2} + \frac{\partial^2 u_e}{\partial z^2}\right)$$

$$\frac{\partial^2 u_e}{\partial x^2} + \frac{\partial^2 u_e}{\partial y^2} + \frac{\partial^2 u_e}{\partial z^2} = \frac{\partial^2 u_e}{\partial r^2} + \frac{1}{r}\frac{\partial u_e}{\partial r} + \frac{1}{r^2}\frac{\partial^2 u_e}{\partial \theta^2} + \frac{\partial^2 u_e}{\partial z^2}$$

$$(v_r(r+dr)rd\theta dz + \frac{\partial v_r}{\partial r}dr(r+dr)rd\theta dz + v_\theta drdz + \frac{\partial v_\theta}{r\partial\theta}rd\theta drdz + v_z drrd\theta$$

$$+ \frac{\partial v_{\theta z}}{\partial z}dzrd\theta dr) - (v_r rd\theta dz + v_\theta drdz + v_z drrd\theta) = \frac{d\forall}{dt}$$

$$\frac{\partial V_o}{\partial t} = \frac{\partial(dV_w)}{\partial t} = \frac{drrd\theta dz}{1+e_0} * \frac{\partial e}{\partial t}$$

$$= \left(v_r(r+dr)rd\theta dz + \frac{\partial v_r}{\partial r}dr(r+dr)d\theta dz + v_\theta drdz + \frac{\partial v_\theta}{r\partial\theta}rd\theta drdz + v_z drrd\theta\right.$$

$$\left. + \frac{\partial v_z}{\partial z}dzrd\theta dr\right) - (v_r rd\theta dz + v_\theta drdz + v_z drrd\theta)$$

$$= \left[(v_r)(r+dr)d\theta dz + (\frac{\partial v_r}{\partial r}dr)(r+dr)d\theta dz + (v_\theta)drdz + (\frac{\partial v_\theta}{r\partial\theta}rd\theta)drdz\right.$$

$$\left. + (v_z)drrd\theta + (\frac{\partial v_z}{\partial z}dz)rd\theta dr\right] - [(v_r)rd\theta dz + (v_\theta)drdz + (v_z)drrd\theta]$$

$$= \left[(v_r)rd\theta dz + (v_r)drd\theta dz + (\frac{\partial v_r}{\partial r}dr)(r+dr)d\theta dz + (v_\theta)drdz + (\frac{\partial v_\theta}{r\partial\theta}rd\theta)drdz\right.$$

$$\left. + (v_z)drrd\theta + (\frac{\partial v_z}{\partial z}dz)rd\theta dr\right] - [(v_r)rd\theta dz + (v_\theta)drdz + (v_z)drrd\theta]$$

$$\frac{\partial V_o}{\partial t} = \frac{\partial(dV_w)}{\partial t} = \frac{rdrd\theta dz}{1+e_0} * \frac{\partial e}{\partial t}$$

$$= (v_r)drd\theta dz + (\frac{\partial v_r}{\partial r}dr)(r+dr)d\theta dz + (\frac{\partial v_\theta}{r\partial\theta}rd\theta)drdz + (\frac{\partial v_z}{\partial z}dz)rd\theta dr$$

$$\frac{\cancel{rdrd\theta dz}}{1+e_0} * \frac{\partial e}{\partial t}$$

$$= (v_r)\cancel{drd\theta dz} + \left(\frac{\partial v_r}{\partial r}\right)\cancel{rdrd\theta dz} + \left(\cancel{\frac{\partial v_r}{\partial r}}\right)\cancel{drdrd\theta dz} + (\frac{\partial v_\theta}{r\partial\theta}\cancel{rd\theta)drdz}$$

$$+ (\frac{\partial v_z}{\partial z}\cancel{dz)rd\theta dr}$$

$$dV_o = dzrd\theta dr, and\ dr^2\ is\ too\ small\ to\ matter$$

$$m_v\frac{\partial u_e}{\partial t} = v_r + \left(\frac{\partial v_r}{\partial r}\right)r + \frac{\partial v_\theta}{r\partial\theta} + \frac{\partial v_z}{\partial z}$$

$$v_r + \left(\frac{\partial v_r}{\partial r}\right) r = v_r + \frac{\partial}{\partial r} v_r r = \frac{v_r}{r} + \frac{\partial v_r}{\partial r}$$

$$\vec{\nabla} q = \frac{v_r}{r} + \frac{\partial v_r}{\partial r} + \frac{\partial v_\theta}{r \partial \theta} + \frac{\partial v_z}{\partial z}$$

$$\vec{v} = -k\vec{\nabla} h = -\left[\vec{r}\frac{k_r}{\rho g}\frac{\partial u_e}{\partial r} + \vec{\theta}\frac{k_\theta}{\rho g}\frac{1}{r}\frac{\partial u_e}{\partial \theta} + \vec{z}\frac{k_z}{\rho g}\frac{\partial u_e}{\partial z}\right]$$

$$\vec{\nabla} \cdot \vec{v} = \nabla(\vec{\nabla} q) = -\begin{Bmatrix} \left(\frac{1}{r} + \frac{\partial}{\partial r}\right)\vec{r} \\ \left(\frac{1}{r}\frac{\partial}{\partial \theta}\right)\vec{\theta} \\ \left(\frac{\partial}{\partial z}\right)\vec{z} \end{Bmatrix} \begin{bmatrix} \frac{k_{rr}}{\rho g} & \frac{k_{r\theta}}{\rho g} & \frac{k_{rz}}{\rho g} \\ \frac{k_{\theta r}}{\rho g} & \frac{k_{\theta\theta}}{\rho g} & \frac{k_{\theta z}}{\rho g} \\ \frac{k_{zr}}{\rho g} & \frac{k_{z\theta}}{\rho g} & \frac{k_{zz}}{\rho g} \end{bmatrix} \cdot \left\{\vec{r}\frac{\partial}{\partial r} \quad \vec{\theta}\frac{1}{r}\frac{\partial}{\partial \theta} \quad \vec{z}\frac{\partial}{\partial z}\right\}$$

$$= -\begin{Bmatrix} \left(\frac{1}{r} + \frac{\partial}{\partial r}\right)\vec{r} \\ \left(\frac{1}{r}\frac{\partial}{\partial \theta}\right)\vec{\theta} \\ \left(\frac{\partial}{\partial z}\right)\vec{z} \end{Bmatrix} \begin{bmatrix} \frac{k_{rr}}{\rho g}\left(\frac{\partial}{\partial r}\right)\vec{r} + \frac{k_{r\theta}}{\rho g}\left(\frac{1}{r}\frac{\partial}{\partial \theta}\right)\vec{\theta} + \frac{k_{rz}}{\rho g}\left(\frac{\partial}{\partial z}\right)\vec{z} \\ \frac{k_{\theta r}}{\rho g}\left(\frac{\partial}{\partial r}\right)\vec{r} + \frac{k_{\theta\theta}}{\rho g}\left(\frac{1}{r}\frac{\partial}{\partial \theta}\right)\vec{\theta} + \frac{k_{\theta z}}{\rho g}\left(\frac{\partial}{\partial z}\right)\vec{z} \\ \frac{k_{zr}}{\rho g}\left(\frac{\partial}{\partial r}\right)\vec{r} + \frac{k_{z\theta}}{\rho g}\left(\frac{1}{r}\frac{\partial}{\partial \theta}\right)\vec{\theta} + \frac{k_{zz}}{\rho g}\left(\frac{\partial}{\partial z}\right)\vec{z} \end{bmatrix}$$

$$= -\left[\left(\frac{1}{r} + \frac{\partial}{\partial r}\right)\frac{k_{rr}}{\rho g}\left(\frac{\partial}{\partial r}\right) + \left(\frac{1}{r} + \frac{\partial}{\partial r}\right)\frac{k_{r\theta}}{\rho g}\left(\frac{1}{r}\frac{\partial}{\partial \theta}\right) + \left(\frac{1}{r} + \frac{\partial}{\partial r}\right)\frac{k_{rz}}{\rho g}\left(\frac{\partial}{\partial z}\right)\right.$$

$$+ \left(\frac{1}{r}\frac{\partial}{\partial \theta}\right)\frac{k_{\theta r}}{\rho g}\left(\frac{\partial}{\partial r}\right) + \left(\frac{1}{r}\frac{\partial}{\partial \theta}\right)\frac{k_{\theta\theta}}{\rho g}\left(\frac{1}{r}\frac{\partial}{\partial \theta}\right) + \left(\frac{1}{r}\frac{\partial}{\partial \theta}\right)\frac{k_{\theta z}}{\rho g}\left(\frac{\partial}{\partial z}\right) + \left(\frac{\partial}{\partial z}\right)\frac{k_{zr}}{\rho g}\left(\frac{\partial}{\partial r}\right)$$

$$\left. + \left(\frac{\partial}{\partial z}\right)\frac{k_{z\theta}}{\rho g}\left(\frac{1}{r}\frac{\partial}{\partial \theta}\right) + \left(\frac{\partial}{\partial z}\right)\frac{k_{zz}}{\rho g}\left(\frac{\partial}{\partial z}\right)\right]$$

$$= \frac{k_{rr}}{\rho g}\left(\frac{1}{r}\frac{\partial}{\partial r} + \frac{\partial^2}{\partial r^2}\right) + \frac{k_{r\theta}}{\rho g}\left(\frac{1}{r^2}\frac{\partial}{\partial \theta} + \frac{\partial}{\partial r}\frac{1}{r}\frac{\partial}{\partial \theta}\right) + \frac{k_{rz}}{\rho g}\left(\frac{1}{r}\frac{\partial}{\partial z} + \frac{\partial}{\partial r}\frac{\partial}{\partial z}\right) + \frac{k_{\theta r}}{\rho g}\frac{1}{r}\frac{\partial}{\partial \theta}\frac{\partial}{\partial r}$$

$$\left. + \frac{k_{\theta\theta}}{\rho g}\frac{1}{r^2}\frac{\partial^2}{\partial \theta^2} + \frac{k_{\theta z}}{\rho g}\frac{1}{r}\frac{\partial}{\partial \theta}\frac{\partial}{\partial z} + \frac{k_{zr}}{\rho g}\frac{\partial}{\partial z}\frac{\partial}{\partial r} + \frac{k_{z\theta}}{\rho g}\frac{\partial}{\partial z}\frac{1}{r}\frac{\partial}{\partial \theta} + \frac{k_{zz}}{\rho g}\frac{\partial^2}{\partial z^2}\right]$$

$$= -\left[\frac{k_{rr}}{\rho g}\left(\frac{1}{r}\frac{\partial}{\partial r}+\frac{\partial^2}{\partial r^2}\right)+\frac{k_{r\theta}}{\rho g}\left(\frac{1}{r^2}\frac{\partial}{\partial \theta}+\frac{1}{r}\frac{\partial}{\partial r}\frac{\partial}{\partial \theta}-\frac{1}{r^2}\frac{\partial}{\partial \theta}\right)+\frac{k_{rz}}{\rho g}\left(\frac{1}{r}\frac{\partial}{\partial z}+\frac{\partial}{\partial r}\frac{\partial}{\partial z}\right)\right.$$

$$\left.+\frac{k_{\theta r}}{\rho g}\frac{1}{r}\frac{\partial}{\partial \theta}\frac{\partial}{\partial r}+\frac{k_{\theta\theta}}{\rho g}\frac{1}{r^2}\frac{\partial^2}{\partial \theta^2}+\frac{k_{\theta z}}{\rho g}\frac{1}{r}\frac{\partial}{\partial \theta}\frac{\partial}{\partial z}+\frac{k_{zr}}{\rho g}\frac{\partial}{\partial z}\frac{\partial}{\partial r}+\frac{k_{z\theta}}{\rho g}\frac{\partial}{\partial z}\frac{1}{r}\frac{\partial}{\partial \theta}+\frac{k_{zz}}{\rho g}\frac{\partial^2}{\partial z^2}\right]$$

Assume $k_{rz} = k_{zr}$ there is no consolidation in the tangential direction, $so\ \frac{\partial}{\partial \theta} and\ k_\theta = 0$. The equation reduces to:

$$-m_v\frac{\partial u_e}{\partial t} = -\left[\frac{k_{rr}}{\rho g}\left(\frac{1}{r}\frac{\partial}{\partial r}+\frac{\partial^2}{\partial r^2}\right)+\frac{k_{rz}}{\rho g}\left(\frac{1}{r}\frac{\partial}{\partial z}\right)+2\frac{k_{rz}}{\rho g}\frac{\partial}{\partial r}\frac{\partial}{\partial z}+\frac{k_{zz}}{\rho g}\frac{\partial^2}{\partial z^2}\right]u_e$$

$$c_v = \frac{k}{m_v \rho g}$$

$$\frac{\partial u_e}{\partial t} = \left[\frac{k_{rr}}{m_v\rho g}\left(\frac{1}{r}\frac{\partial}{\partial r}+\frac{\partial^2}{\partial r^2}\right)+\frac{k_{rz}}{m_v\rho g}\left(\frac{1}{r}\frac{\partial}{\partial z}\right)+2\frac{k_{rz}}{m_v\rho g}\frac{\partial}{\partial r}\frac{\partial}{\partial z}+\frac{k_{zz}}{m_v\rho g}\frac{\partial^2}{\partial z^2}\right]u_e$$

$$\frac{\partial u_e}{\partial t} = \left[c_{rr}\left(\frac{1}{r}\frac{\partial}{\partial r}+\frac{\partial^2}{\partial r^2}\right)+c_{rz}\left(\frac{1}{r}\frac{\partial}{\partial z}\right)+2c_{rz}\frac{\partial}{\partial r}\frac{\partial}{\partial z}+c_{zz}\frac{\partial^2}{\partial z^2}\right]u_e \quad (\mathbf{A.8})$$

APPENDIX B

APPENDIX B: MATLAB CODE

Driven Pile Iteration

The iteration with constant ground-surface temperatures is basically the same as the iteration with transient ground-surface temperatures. Rather than repeat the majority of the functions and main code, the lines of code from the transient ground-surface temperature iteration, that differ from the constant-temperature iteration, will be inserted directly after the functions and main program from the constant-temperature iteration. The lines of code, in context, will be displayed in the next section.

Inputs Function

```
function
[L,R,Th,Tl,Tmed,Tn,krri,krzi,kzzi,cc,gammasat0,e0,Ec,Es,Gs,Krr,Kzz,Krz,Cp5,Cp10,Cp
15,Cp20,Cp25,Cp30,alphas,alphapile,LL,PL,nu,G,cu,Cc,phip,OCR,years]= Inputs()
 %Inputs
%  Specific characteristics of the soil and temperatures

L=15; %input('Length of pile, meters (depth below ground surface): ');

R=0.15; %input('Pile radius, meters: ');

Th=36; %input('Highest average daily air temperature, degrees Celsius: ');

Tl=-4; %input('Lowest average daily air temperature, degrees Celsius: ');

Tmed=16 ;%input('Median annual air temperature, degrees Celsius: ');

Tn=15; %input('Normal average temperature of the soil, degrees Celsius: ');

krri=0.0000007; %input('Hydraulic conductivity in radial (horizontal)...
      %direction at 20 degrees Celsius, m/s: ');
```

```
krzi=0; %input('Hydraulic conductivity in radial (horizontal)and vertical...
   %directions at 20 degrees Celsius, m/s: ');
kzzi=0.0000004; %input('Hydraulic conductivity in vertical direction...
      %at 20 degrees Celsius, m/s: ');
cc=0.5; %input('Concrete cover around pile, fraction of distance between piles: ');

gammasat0=17; %input('Unit weight of soil, kN/m^3: ');

e0=1.1; %input('Initial void ratio, if known: ');

Ec=25e6; %input('Young's Modulus for concrete, kN/m^2: ');

Es=20e3; %input('Young's Modulus for soil, kN/m^2: ');

Gs=2.75; %input('Specific gravity of soil: ');

Krr=365; %input('Conductivity coefficient for saturated clay, radial direction,
         J/day*m*K: ');
Kzz=365; %input('Conductivity coefficient for saturated clay, vertical direction,
         J/day*m*K: ');
Krz=0; %input('Conductivity coefficient for saturated clay, radial and vertical direction,
         W/m*K: ');
Cp5=2471.5; %input('Specific heat for saturated silty clay at 5 deg C, J/kg*
         degrees C: ');
Cp10=2466.6; %input('Specific heat for saturated silty clay at 10 deg C, J/kg*
         degrees C: ');
Cp15=2463.3; %input('Specific heat for saturated silty clay at 15 deg C, J/kg*
         degrees C: ');
Cp20=2462; %input('Specific heat for saturated silty clay at 20 deg C , J/kg*
         degrees C: ');
Cp25=2461.3; %input('Specific heat for saturated silty clay at 25 deg C , J/kg*degrees C:
         ');
Cp30=2460.4; %input('Specific heat for saturated silty clay at 30 deg C , J/kg*degrees C:
         ');
 alphas=0.000033; %input('Coefficient of thermal expansion for soil, 1/deg. C: ');
 alphapile=0.0000145; %input('Coefficient of thermal expansion for concrete pile, 1/deg.
         C: ');
 LL=52; %input('Liquid limit of soil: ');
PL=17; %input('Plastic limit of soil: ');
 nu=0.3; %Poisson's Ratio*
 G=7.69e3; %input('Shear Modulus for soil, kN/m^2: ');
cu=75; %input('undrained shear strength, kN/m^2: ');
 Cc=.28; %input('Compression Index: ');
 phip=20; %input('Angle of effective internal friction, phi prime: ');
 OCR=1.1; %input('Over-consolidation ratio: ');
 years=2; %input('Number of years to run model: ');
```

```
 %tb=182; %input('Number of days between pile installation and HVAC usage: ');
end
```

Constants Function

```
function [W,H,N,M,ccnodes,dr,dz,P,g,dT,dt,Ko,alphast] = Constants(L,cc,phip,OCR)

%Defines grid width, height, and number of nodes, as well as non-input constants

 Ko=(1-sind(phip))*OCR^(sind(phip));
 W=5;% width of zone in radial direction, R=pile radius;
H=2*L+1; %Height of zone, L=length of pile in soil;
N=W*4+1; %# of nodes in radial direction;
M=H; %# of nodes in vertical direction;
ccnodes=(N*cc);
dr=W/((3/2)*(N-1));%distance between radial nodes
dz=(H-1)/(M-1);%distance between vertical nodes
P=M*N;%total # nodes
g=9.81; %gravitational constant m/s^2
dT=1; %change in temperature, degrees Celsius
alphast=-0.5e-4;
dt=1;%time increment in days
end
```

Water Coefficient of Thermal Expansion Function

```
function [alphah2o,rhow] = watercte(P,Told)

%%input temperature, return coefficient of thermal expansion for water

for ii=1:P
if 0<=Told(ii)&& Told(ii)<4
   alphah2o(ii)=0-0.0000125*(4-Told(ii));
   rhow(ii)=.999973/(1+alphah2o(ii)*(4-Told(ii)));

   elseif 4<=Told(ii) && Told(ii)<=10
   alphah2o(ii)=0.00001467*(Told(ii)-4);
   rhow(ii)=.999973/(1+alphah2o(ii)*(Told(ii)-4));

    elseif 10<=Told(ii)&& Told(ii)<=20
   alphah2o(ii)=0.000088+0.0000119*(Told(ii)-10);
   rhow(ii)=.999445/(1+alphah2o(ii)*(Told(ii)-10));

    elseif 20<=Told(ii)&& Told(ii)<=30
   alphah2o(ii)=0.000207+0.0000096*(Told(ii)-20);
```

```
   rhow(ii)=.99738/(1+alphah2o(ii)*(Told(ii)-20));

    elseif 30<=Told(ii)&& Told(ii)<=40
   alphah2o(ii)=0.000303+0.0000082*(Told(ii)-30);
   rhow(ii)=.995184/(1+alphah2o(ii)*(Told(ii)-30));

  elseif 40<=Told(ii)&& Told(ii)<=50
   alphah2o(ii)=0.000385+0.0000072*(Told(ii)-40);
   rhow(ii)=.991368/(1+alphah2o(ii)*(Told(ii)-40));

    else
   alphah2o(ii)=0.000214;
   rhow(ii)=.999973/(1+0.000214*(Told(ii)-4));
  end
end
```

Soil Parameters After Cavity Expansion Function

```
function
[Rp,e1,ued,ds,e2,gammasat,n]=fet(P,R,G,cu,M,W,N,dr,Cc,gammasat0,dz,e0,Gs,g,rhow)

%Calculates changes to plastic zone, void ratio, porosity excess pore-water
%pressure (unused), horizontal stress due to cavity expansion, and
%saturated unit weight as a result of cavity expansion

ued(1:P)=0;     ds(1:P)=0;       e1(1:P)=e0;     n(1:P)=e0/(1+e0);
gammasat(1:P)=gammasat0;
Rp=R*(G/cu)^0.5; %radius of plastic zone

 %void ratio/porosity due to in situ conditions

for d=1:M-1
  for ii=((d-1)*N)+1:((d-1)*N)+N
    e1(ii)=e0-Cc*(log10(0.65*gammasat(ii)*((M-d)*dz))...
      -(log10(0.65*gammasat(ii)*dz)));
    n(ii)=e1/(1+e1);
  end
end
e2=e1;
for d=(M-1)/2:M-2
  for ii=d*N+1:(d*N)+floor((Rp/W)*N)
    r=R+(dr*(ii-(d*N+1)));
    ued(ii)=cu*(log(G/cu)-2*log(r/R));%2*cu*log(Rp/r);
    ds(ii)=cu*(1+log(G/cu)-2*log(r/R)); %horizontal (deviator) stress
     %Change in void ratio and porosity due to cavity expansion
     e2(ii)=e1(ii)-Cc*(log10(0.65*gammasat(ii)*((M-d)*dz)+ds(ii))...
```

```
    -(log10(0.65*gammasat(ii)*(M-d)*dz)));
   n(ii)=e2(ii)/(1+e2(ii));
   gammasat(ii)=(Gs+e2(ii))*rhow(ii)*g/(1+e2(ii)); % post pile installation
  end
 end
```

Permeability and Dynamic Viscosity Function

```
function [muVogel,krriV,kzziV,krziV] = perm(P,Tnew,rhow,krri,kzzi)

%perm provides matrix values for radial and vertical permeability and
%dynamic viscosity at an input temperature for each node.

muVogel(1:P)=0;       krriV(1:P)=0;  kzziV(1:P)=0; krziV(1:P)=0;

for ii=1:P
  muVogel(ii)=0.001*exp(-3.7188+(578.919/(-137.546+(Tnew(ii)+273.15))));
  krriV(ii)=krri*(0.001*(exp(-3.7188+(578.919/(-137.546+(20+273.15))))...
    /(.99738)))*(rhow(ii)/muVogel(ii));
  kzziV(ii)=kzzi*(0.001*(exp(-3.7188+(578.919/(-137.546+(20+273.15))))...
    /(.99738)))*(rhow(ii)/muVogel(ii));
end
end
```

Compressibility, Volumetric Compressibility, and Consolidation Coefficients Function

```
function [avrr,avzz,mvrr,mvzz,CvrriV,CvzziV,CvrziV] =
CvrrT_Driv_Days(P,e0,krriV,kzziV,rhow,g)

%Provides matrix values for coefficients of radial and vertical consolidation for each
%node

CvrziV(1:P)=0;          mvrr(1:P)=0;   avrr(1:P)=0;    mvzz(1:P)=0;
avzz(1:P)=0;   CvrriV(1:P)=0;          CvzziV(1:P)=0;

for ii=1:P
  mvrr(ii)=0.364e-3;  avrr(ii)=mvrr(ii)*(1+e0);
  mvzz(ii)=mvrr(ii);  avzz(ii)=avrr(ii);
  intr(ii)=(krriV(ii)*(g^-1)*86.4)/mvrr(ii); %convert to days
  intz(ii)=(kzziV(ii)*(g^-1)*86.4)/mvzz(ii); %convert to days
  CvrriV(ii)=intr(ii)/rhow(ii);
  CvzziV(ii)=intz(ii)/rhow(ii);%convert to days
end
end
```

Consolidation Node Definition (for consolidation without HVAC)

```
function [a,b]=
Consol_Days_Driv96(P,kzzi,M,N,R,Rp,W,cu,dr,t,CvrriV,CvzziV,dz,dt,CvrziV,uold1)

 %Consol_Nodes
%Consolidation node definition for model run without HVAC

kzz(1:P)=kzzi;

%Interior nodes
 for d=1:(M-2)
   for ii=(d*N)+2:(d+1)*N-1
     r=R+(dr*(ii-(d*N+1)));
     a(ii,ii)=-2*(CvrriV(ii)/(dr^2)+CvzziV(ii)/(dz^2))-1/dt;
     a(ii,ii+1)=CvrriV(ii)/dr^2+CvrriV(ii)/(2*r*dr);
     a(ii,ii-1)=CvrriV(ii)/dr^2-CvrriV(ii)/(2*r*dr);
     a(ii,ii+N)=CvzziV(ii)/dz^2;     a(ii,ii-N)=CvzziV(ii)/dz^2;
     a(ii,ii+N+1)=CvrziV(ii)/(2*dr*dz);     a(ii,ii-N+1)=-CvrziV(ii)/(2*dr*dz);
     a(ii,ii+N-1)=-CvrziV(ii)/(2*dr*dz);     a(ii,ii-N-1)=CvrziV(ii)/(2*dr*dz);
     b(ii)=-uold1(ii)/dt;
  end
 end

 %Boundary conditions
%Pile side
for ii=1:N:((M-3)/2)*N+1;
  %below pile
    a(ii,:)=0;    a(ii,ii)=1;    a(ii,ii+1)=-1;
    b(ii)=0;
end
     for ii=((M-1)/2)*N+1:N:(M-1)*N+1
    %along pile
    a(ii,:)=0;    a(ii,ii)=1;    a(ii,ii+1)=-1;
    b(ii)=4.5*cu*(1-(log(CvrriV(ii)*t/(R^2)))/6);
     if b(ii)<0
      b(ii)=0;
    end
   end

%Bottom
%Sand or clay?
for ii=2:N-1
  %Clay
  if kzz(2)<1e-5
    a(ii,:)=0;    a(ii,ii)=1;    a(ii,ii+N)=-1;
```

```
   b(ii)=0;
   else
  %Sand
   a(ii,:)=0;    a(ii,ii)=1;    a(ii,ii+N)=0;
   b(ii)=0;
  end
end

 %Soil side
for ii=N:N:M*N
  a(ii,:)=0;  a(ii,ii)=1;  a(ii,ii-1)=0;
  b(ii)=0;
end

 %Ground surface under concrete cover next to pile
for ii=(M-1)*N+1:(M-1)*N+11
  a(ii,:)=0;  a(ii,ii)=1;  a(ii,ii-N)=-1;
  b(ii)=0;
end

  %Ground surface from edge of concrete cover to boundary
for ii=(M-1)*N+12:(M-1)*N+N-1
  a(ii,:)=0;  a(ii,ii)=1;  a(ii,ii-N)=0;
  b(ii)=0;
end
end
```

Consolidation Node Definition (with HVAC)

```
function [a,b]=
Consol_Nodes_Driv522(P,kzzi,M,N,R,Rp,W,cu,dr,t,CvrriV,CvzziV,dz,dt,uold,ued,
          CvrziV)

 %Consol_Nodes
%Consolidation node definition
kzz(1:P)=kzzi;

%Interior nodes
 for d=1:(M-2)
   for ii=(d*N)+2:(d+1)*N-1
     r=R+(dr*(ii-(d*N+1)));
     a(ii,ii)=-2*(CvrriV(ii)/(dr^2)+CvzziV(ii)/(dz^2))-1/dt;
     a(ii,ii+1)=CvrriV(ii)/dr^2+CvrriV(ii)/(2*r*dr);
     a(ii,ii-1)=CvrriV(ii)/dr^2-CvrriV(ii)/(2*r*dr);
     a(ii,ii+N)=CvzziV(ii)/dz^2;      a(ii,ii-N)=CvzziV(ii)/dz^2;
```

```
    a(ii,ii+N+1)=CvrziV(ii)/(2*dr*dz);     a(ii,ii-N+1)=-CvrziV(ii)/(2*dr*dz);
    a(ii,ii+N-1)=-CvrziV(ii)/(2*dr*dz);    a(ii,ii-N-1)=CvrziV(ii)/(2*dr*dz);
    b(ii)=-(uold(ii))/dt;
  end
 end

 %Boundary conditions
%Pile side
for ii=1:N:((M-3)/2)*N+1;
  %below pile
   a(ii,:)=0;    a(ii,ii)=1;    a(ii,ii+1)=-1;
   b(ii)=0;
end
 for ii=((M-1)/2)*N+1:N:(M-1)*N+1
  %along pile
  a(ii,:)=0;  a(ii,ii)=1;  a(ii,ii+1)=-1;
  b(ii)=4.5*cu*(1-(log(CvrriV(ii)*t/(R^2)))/6);
end

%Bottom
%Sand or clay?
for ii=2:N-1
  %Clay
  if kzz(2)<1e-5
   a(ii,:)=0;    a(ii,ii)=1;    a(ii,ii+N)=-1;
   b(ii)=0;
   else
  %Sand
   a(ii,:)=0;    a(ii,ii)=1;    a(ii,ii+N)=0;
   b(ii)=0;
  end
end

%Soil side
for ii=N:N:M*N
  a(ii,:)=0;  a(ii,ii)=1;  a(ii,ii-1)=0;
  b(ii)=0;
end
 %Ground surface under concrete cover next to pile
for ii=(M-1)*N+1:(M-1)*N+11
  a(ii,:)=0;  a(ii,ii)=1;  a(ii,ii-N)=-1;
  b(ii)=0;
end

  %Ground surface from edge of concrete cover to boundary
for ii=(M-1)*N+12:(M-1)*N+N-1
```

```
 a(ii,:)=0;  a(ii,ii)=1;  a(ii,ii-N)=0;
 b(ii)=0;
end
end
```

Thermal Expansion of the Pile Function

```
function [R1] = Pilex(P,M,N,R,alphapile,Told,Tn)

%Pilex finds the radius of the energy pile at a given Temp

R1(1:P)=0;
for ii=((M-1)/2)*N+1:N:(M-1)*N+1
        R1(ii)=sqrt(R^2*(1+2*alphapile*(Told(ii)-Tn)));
 end
```

Pile Coefficient of Thermal Expansion Function

```
function [uheat]=ctepile(P,Theatval,R1,R,Es,M,N)

 uhvold(1:P)=0;
 for ii=((M-1)/2)*N+1:N:(M-1)*N+1
  uhvold(ii)=(Theatval*(R1(ii)-R)*Es);%%%This is epwp due to expansion of pile only
  uheat=uhvold';
end
```

Change of Saturated Density and Soil Density with Temperature Change Function

```
function[gammasat,rhoc1]=grammasat(P,Gs,e2,rhow,g,alphas,Told,Tn)

%%%This function recalculates gammasat and clay density as temperature
%%%varies

for ii=1:P
  gammasat(ii)=(Gs+e2(ii))*rhow(ii)*g/(1+e2(ii));
  rhoc1(ii)=(gammasat(ii)/g)/(1+alphas*(Told(ii)-Tn));
end
end
```

Soil Density and Specific Heat with Temperature Change Function

```
%%%Specific Heat and density of soil

function [Cpc]=claycon(P,Cp5,Cp10,Cp20,Cp25,Cp30,Told)

 for ii=1:P
  if Told(ii)>=0 && Told(ii)<5
```

```
    Cpc(ii)=Cp5-((Cp10-Cp5)/5)*(5-Told(ii));

  elseif 5<=Told(ii)&& Told(ii)<=10
    Cpc(ii)=((Cp10-Cp5)/5)*(Told(ii)-5)+Cp5;

  elseif 10<=Told(ii)&& Told(ii)<=20
    Cpc(ii)=((Cp20-Cp10)/10)*(Told(ii)-10)+Cp10;

  elseif 20<=Told(ii)&& Told(ii)<=30
    Cpc(ii)=((Cp30-Cp20)/10)*(Told(ii)-20)+Cp20;

  elseif 30<=Told(ii)
    Cpc(ii)=((Cp30-Cp25)/5)*(Told(ii)-30)+Cp30;

  else
    Cpc(ii)=2462;
  end
end
```

Conduction Node Definition Function

```
function [c,d]=
Conduct_Days_HVAC(M,N,R,Krr,Cpc,rhoc1,dr,Kzz,dz,dt,Krz,Told,Theatval,Tn)

 %Conduction node definition, Constant surface temperature
 %Interior nodes

for f=1:(M-2)
  for ii=(f*N)+2:(f+1)*N-1
    r=R+(dr*(ii-(f*N+1)));
    c(ii,ii)=-2*(Krr/(Cpc(ii)*rhoc1(ii)*dr^2)+Kzz/(Cpc(ii)*rhoc1(ii)*dz^2))-1/dt;
    c(ii,ii+1)=Krr/(Cpc(ii)*rhoc1(ii)*dr^2)+Krr/(2*r*Cpc(ii)*rhoc1(ii)*dr);
    c(ii,ii-1)=(Krr/(Cpc(ii)*rhoc1(ii)*dr^2)-Krr/(2*r*Cpc(ii)*rhoc1(ii)*dr));
    c(ii,ii+N)=Kzz/(Cpc(ii)*rhoc1(ii)*dz^2);
    c(ii,ii-N)=Kzz/(Cpc(ii)*rhoc1(ii)*dz^2);
    c(ii,ii+N+1)=Krz/(2*Cpc(ii)*rhoc1(ii)*dr*dz);
    c(ii,ii-N+1)=-(Krz/(2*Cpc(ii)*rhoc1(ii)*dr*dz));
    c(ii,ii+N-1)=-(Krz/(2*Cpc(ii)*rhoc1(ii)*dr*dz));
    c(ii,ii-N-1)=Krz/(2*Cpc(ii)*rhoc1(ii)*dr*dz);
    d(ii)=-Told(ii)/dt;
  end
end

 %Boundary conditions
%Pile side
for ii=1:N:((M-1)/2)*N+1;
```

```
   c(ii,:)=0;    c(ii,ii)=1;    c(ii,ii+1)=-1;
   d(ii)=0;
end
 for ii=((M-1)/2)*N+1:N:(M-1)*N+1
  c(ii,:)=0;  c(ii,ii)=1;  c(ii,ii+1)=0;
  d(ii)=Told(ii)+Theatval;
end

%Bottom
for ii=2:N-1
  c(ii,:)=0;  c(ii,ii)=1;  c(ii,ii+N)=0;
  d(ii)=Tn;
end

%Soil side
for ii=N:N:M*N
  c(ii,:)=0;    c(ii,ii)=1;    c(ii,ii-1)=-1;
  d(ii)=0;
end

 %Ground surface
%change to building temp for portion and air temp for remainder if needed
for ii=(M-1)*N+2:(M-1)*N+N-1
  c(ii,:)=0;  c(ii,ii)=1;  c(ii,ii-N)=0;
  d(ii)=Tn;%Tl+(Th-Tl)*cos(t/10);
end
end
```

Soil Coefficient of Thermal Expansion Function

```
%%%%Excess Pore-Water Pressure Due to Thermal Expansion of Soil

function[ucte,alphast]=ctesoil(P,n,Tdif,alphas,alphah2o,mvrr)

alphast(1:P)=-0.00005;          Tdif=Tdif';

for ii=1:P
  ucte(ii)=((n(ii)*Tdif(ii)*(alphas-alphah2o(ii)))+alphast(ii)*Tdif(ii))/(-1*mvrr(ii));
end
end
```

Driven Pile Iteration (Constant Surface Temperature) Main File

```
%% %This model will show the change in excess pore-water pressure with
%time and temperature changes for energy piles. This will be used
%show how pile capacity, namely, side friction, varies with time.
```

```
%Daniel P. Zimmerman
%for completion of the requirements of the Master of Science Degree in
%Civil Engineering
%Advisor: Dr. Arvin Farid, PE
%Start date: May 26, 2012
%End date May 21, 2016
clear all;clc;

%%%Inputs
[L,R,Th,Tl,Tmed,Tn,krri,krzi,kzzi,cc,gammasat0,e0,Ec,Es,Gs,Krr,Kzz,Krz,Cp5,Cp10,Cp
15,Cp20,Cp25,Cp30,alphas,alphapile,LL,PL,nu,G,cu,Cc,phip,OCR,years]= Inputs();

 %%%Constants
[W,H,N,M,ccnodes,dr,dz,P,g,dT,dt,Ko,alphast]=Constants(L,cc,phip,OCR);

 Told(1:P)=Tn;          uold(1:P)=0;    uold1(1:P)=0; Tnew=Told;
 sigpr(1:P)=0;          K(1:P)=0;       fs(1:P)=0;       sigpr1(1:P)=0;
 K1(1:P)=0;     fs1(1:P)=0;

 %%%Consolidation of soil after pile installation without temperature
 %%% change

 for t=1:dt:910
   [alphah2o,rhow] = watercte(P,Told);
         %e1alphah2o(t,:)=alphah2o;  %   e1rhow(t,:)=rhow;

         %Initial EPWP, horizontal stress, and void ratio for driven pile
[Rp,e1,ued,ds,e2,gammasat,n]=fet(P,R,G,cu,M,W,N,dr,Cc,gammasat0,dz,e0,Gs,g,rhow);
%e1e1(t,:)=e1;  % e1e2(t,:)=e2;  %e1gammasat(t,:)=gammasat;  % e1n(t,:)=n;
 ds=ds';

   %%%Permeability and dynamic viscosity
  [muVogel,krriV,kzziV,krziV]=perm(P,Tnew,rhow,krri,kzzi);
%e1muVogel(t,:)=muVogel;  %e1krriV(t,:)=krriV;  %e1kzziV(t,:)=kzziV;

%   for ii=1:P
         %e1intrins(ii)=rhow(ii)/muVogel(ii);
%   end
%   e1intrinst(t,:)=e1intrins;

  %%%Compressibility, volumetric compressibility, and consolidation
  %%%coefficients
[avrr,avzz,mvrr,mvzz,CvrriV,CvzziV,CvrziV]=CvrrT_Driv_Days(P,e0,krriV,kzziV,
rhow,g);
%e1CvrriV(t,:)=CvrriV;  %e1CvzziV(t,:)=CvzziV;
```

```
%Consolidation Node definition
[a,b]=Consol_Days_Driv96(P,kzzi,M,N,R,Rp,W,cu,dr,t,CvrriV,CvzziV,dz,dt,CvrziV,
        uold1);
  unew1=(a^-1)*b';   uold1=unew1;
  uexfin1(:,t)=unew1;%substitute t for 1 in uexfin if time step
  unewmax1(:,:)=uexfin1(:,1);

%friction calculation
  for d=(M-1)/2:M-2
   for ii=d*N+1
    K1(ii)=1.5*Ko;
    sigpr1(ii)=Ko*((gammasat(ii)*((M-1)-(d-1)))+(gammasat(ii)-rhow(ii)*g)*0.5);
    fs1(ii)=sigpr1(ii)*(K1(ii)/Ko)*tand(phip*0.8);
   end
  end
  fst1=sum(fs1);
  fsf1(:,t)=fst1*(0.2+0.8*(1-unew1(ii)/(ds(ii)/0.8)));
 end

 Told(1:P)=Tn;          Told=Told';    uold(1:P)=0;    Tnew=Told;
Tfinal(:,1)=Tnew;      TfinalS(:,1)=Tfinal(:,1);       sigpr(1:P)=0;
K(1:P)=0;       fs(1:P)=0;       uheatval=0;

 %%%Consolidation after pile installation. HVAC will be turned on in three
%%%months.
for t=1:dt:182
  %%%Water coefficient of thermal expansion and density due to
     %%%current temp.

  [alphah2o,rhow] = watercte(P,Told);
%ealphah2o(t,:)=alphah2o;    %erhow(t,:)=rhow;

  %%%Initial EPWP, horizontal stress, and void ratio for driven pile
 [Rp,e1,ued,ds,e2,gammasat,n]=fet(P,R,G,cu,M,W,N,dr,Cc,gammasat0,dz,e0,Gs,g,rhow);
%ee1(t,:)=e1;  %ee2(t,:)=e2;  %egammasat(t,:)=gammasat;  %en(t,:)=n;

 %%%Permeability and dynamic viscosity
  [muVogel,krriV,kzziV,krziV]=perm(P,Tnew,rhow,krri,kzzi);
%emuVogel(t,:)=muVogel;
%   for ii=1:P
         %eintrins(ii)=rhow(ii)/muVogel(ii);
%   end
%eintrinst(t,:)=eintrins;          %ekrriV(t,:)=krriV;    %ekzziV(t,:)=kzziV;

  %%%Compressibility, volumetric compressibility, and consolidation
  %%%coefficients
```

```
[avrr,avzz,mvrr,mvzz,CvrriV,CvzziV,CvrziV]=CvrrT_Driv_Days(P,e0,krriV,kzziV,
        rhow,g);
%eCvrriV(t,:)=CvrriV;          % eCvzziV(t,:)=CvzziV;

%%%Consolidation Node definition
[a,b]=Consol_Days_Driv522(P,kzzi,M,N,R,Rp,W,cu,dr,t,CvrriV,CvzziV,dz,dt,CvrziV,
        uold);
 unew=(a^-1)*b';  uold=unew;  uexfin(:,t)=uold;  unewmax(:,:)=uexfin(:,1);

 %%%Calculation of friction
  for d=(M-1)/2:M-2
   for ii=d*N+1
    K(ii)=1.5*Ko;
    sigpr(ii)=Ko*((gammasat(ii)*((M-1)-(d-1)))+(gammasat(ii)-rhow(ii)*g)*0.5);
    fs(ii)=sigpr(ii)*(K(ii)/Ko)*tand(phip*0.8);
   end
  end
  fst=sum(fs);
  fsf(:,t)=fst*(0.2+0.8*(1-unew(ii)/(ds(ii)/0.8)));
end

 uexS(:,1)=uexfin(:,t);   uheatval=0;

aviobj = avifile('Driven_Pile_EPWP_Year_1.avi','compression','Cinepak');
 aviobj.KeyFramePerSec = 0.5;

aviobjt = avifile('Driven_Pile_Temp_Year_1.avi','compression','Cinepak');
aviobjt.KeyFramePerSec = 0.5;

 aviobjtt = avifile('Driven_Pile_EPWP_Year_2.avi','compression','Cinepak');
 aviobjtt.KeyFramePerSec = 0.5;

 aviobjttt = avifile('Driven_Pile_Temp_Year_2.avi','compression','Cinepak');
aviobjttt.KeyFramePerSec = 0.5;

 i=13; j=7;
  uheat(1:P,1)=0;

for y=1:years
   %%%%   SUMMER (Days 0-91(365-455) after HVAC intro)  %%%%
   for w=1:7  %%%w=week
    for dd=1:7 %%%dd=day of the week
     %%%Temp increase based upon hours of heating per day. 40 is
     %%%total temp increase by end of heating. 1344 is total number
     %%%of hours of heating.
     %%%
```

```
Theatval=40/1344*(6+2*(w-1));

for ii=((M-1)/2)*N+1:N:(M-1)*N+1
  Told(ii)=Told(ii)+Theatval;
End

%%%New radius upon change in temperature
[R1]=Pilex(P,M,N,R,alphapile,Told,Tn);
 [uheat]=ctepile(P,Theatval,R1,R,Es,M,N);
     %%%t is days since pile install, h is days since HVAC on.

t=((w-1)*j)+dd+182+((y-1)*364);      h=(t-182);
uheath(:,h)=uheat;

%%%Water coefficient of thermal expansion and density due to
%%%current temp.
[alphah2o,rhow] = watercte(P,Told);
     %ealphah2o(t,:)=alphah2o;   %erhow(t,:)=rhow;

%%%Calculation of gammasat and clay density based upon temp
%%%increase
[gammasat,rhoc1]=grammasat(P,Gs,e2,rhow,g,alphas,Told,Tn);
     %egammasat(t,:)=gammasat;
%%%Clay density and specific heat value due to current temp
[Cpc]=claycon(P,Cp5,Cp10,Cp20,Cp25,Cp30,Told);

for ii=((M-1)/2)*N+1:N:(M-1)*N+1
  Told(ii)=Told(ii)-Theatval;
End

%%%Conduction Node definition
[c,d]=
Conduct_Days_HVAC(M,N,R,Krr,Cpc,rhoc1,dr,Kzz,dz,dt,Krz,Told,Theatval,Tn);

Tnew=(c^-1)*d';      Tdif=Tnew-Told;

for ii=1:P
  if abs(Tdif(ii))<0.001
    Tdif(ii)=0;
  end
end

%%%EPWP due to thermal expansion of clay
[ucte,alphast]=ctesoil(P,n,Tdif,alphas,alphah2o,mvrr);
Told=Tnew;      ucteh(:,h)=ucte';      TfinalS(:,h)=Told;
```

```
    %%%Permeability and dynamic viscosity
    [muVogel,krriV,kzziV,krziV]=perm(P,Tnew,rhow,krri,kzzi);
                % emuVogel(t,:)=muVogel;
        % for ii=1:P
                %eintrins(ii)=rhow(ii)/muVogel(ii);
        %end
        %eintrinst(t,:)=eintrins;        %ekrriV(t,:)=krriV;    %ekzziV(t,:)=kzziV;

    %%%Compressibility, volumetric compressibility, and consolidation
    %%%coefficients
[avrr,avzz,mvrr,mvzz,CvrriV,CvzziV,CvrziV]=CvrrT_Driv_Days(P,e0,krriV,kzziV,
        rhow,g);
%eCvrriV(t,:)=CvrriV;        %eCvzziV(t,:)=CvzziV;

    %%%Consolidation Node definition
[a,b]=Consol_Days_Driv522(P,kzzi,M,N,R,Rp,W,cu,dr,t,CvrriV,CvzziV,dz,dt,CvrziV,
        uold);
 unew=(a^-1)*b';
    %%%EPWP due to consolidation, at pile surface due to expansion
    %%%of the pile, and expansion of the clay
    unew=unew+uheat+ucte';

 %%%Calculation of friction
    for d=(M-1)/2:M-2
      for ii=d*N+1
        K(ii)=1.5*Ko;
        sigpr(ii)=Ko*((gammasat(ii)*((M-1)-(d-1)))+(gammasat(ii)-rhow(ii)*g)*0.5);
        fs(ii)=sigpr(ii)*(K(ii)/Ko)*tand(phip*0.8);
          end
    end
    fst=sum(fs);
    fsf(:,t)=fst*(0.2+0.8*(1-unew(ii)/(ds(ii)/0.8)));
    fsh(:,h)=fst*(0.2+0.8*(1-unew(ii)/(ds(ii)/0.8)));
     uold=unew;     uexS(:,h)=uold;     uexfin(:,t)=uold;
  end
 end

 for w=8:i
   for dd=1:j
    Theatval=40/1344*(6+2*(13-w));

    for ii=((M-1)/2)*N+1:N:(M-1)*N+1
      Told(ii)=Told(ii)+Theatval;
    end

    %New radius upon change in temperature
```

```
    [R1]=Pilex(P,M,N,R,alphapile,Told,Tn);
    [uheat]=ctepile(P,Theatval,R1,R,Es,M,N);
    t=((w-1)*j)+dd+182+((y-1)*364);      h=(t-182);            uheath(:,h)=uheat;

    [alphah2o,rhow] = watercte(P,Told);

     %%%Calculation of gammasat and clay density based upon temp
    %%%increase
    [gammasat,rhoc1]=grammasat(P,Gs,e2,rhow,g,alphas,Told,Tn);
    [Cpc]=claycon(P,Cp5,Cp10,Cp20,Cp25,Cp30,Told);

    for ii=((M-1)/2)*N+1:N:(M-1)*N+1
      Told(ii)=Told(ii)-Theatval;
    End

    %Conduction Node definition
    [c,d]=
Conduct_Days_HVAC(M,N,R,Krr,Cpc,rhoc1,dr,Kzz,dz,dt,Krz,Told,Theatval,Tn);
    Tnew=(c^-1)*d';      Tdif=Tnew-Told;

    for ii=1:P
      if abs(Tdif(ii))<0.001
        Tdif(ii)=0;
      end
    end

    [ucte,alphast]=ctesoil(P,n,Tdif,alphas,alphah2o,mvrr);
    Told=Tnew;      ucteh(:,h)=ucte';   TfinalS(:,h)=Told;

    %%%Permeability and dynamic viscosity
    [muVogel,krriV,kzziV,krziV]=perm(P,Tnew,rhow,krri,kzzi);
    %%%Compressibility, volumetric compressibility, and consolidation
    %%%coefficients
[avrr,avzz,mvrr,mvzz,CvrriV,CvzziV,CvrziV]=CvrrT_Driv_Days(P,e0,krriV,kzziV,
          rhow,g);

%Consolidation Node definition
[a,b]=Consol_Days_Driv522(P,kzzi,M,N,R,Rp,W,cu,dr,t,CvrriV,CvzziV,dz,dt,CvrziV,
          uold);
 unew=(a^-1)*b';      unew=unew+uheat+ucte';

 for d=(M-1)/2:M-2
    for ii=d*N+1
        K(ii)=1.5*Ko;
       sigpr(ii)=Ko*((gammasat(ii)*((M-1)-(d-1)))+(gammasat(ii)-rhow(ii)*g)*0.5);
       fs(ii)=sigpr(ii)*(K(ii)/Ko)*tand(phip*0.8);
```

```
    end
  end
    fst=sum(fs);
    fsf(:,t)=fst*(0.2+0.8*(1-unew(ii)/(ds(ii)/0.8)));
    fsh(:,h)=fst*(0.2+0.8*(1-unew(ii)/(ds(ii)/0.8)));
    uold=unew;      uexS(:,h)=uold;      uexfin(:,t)=uold;
  end
end

  %%%%   FALL  (Days 92-183(456-546) after HVAC intro) %%%%
i=13; j=7;
  for w=1:7
        for dd=1:7
    Theatval=40/1344*(6-(w-1));
    for ii=((M-1)/2)*N+1:N:(M-1)*N+1
      Told(ii)=Told(ii)+Theatval;
    end

    %New radius upon change in temperature
    [R1]=Pilex(P,M,N,R,alphapile,Told,Tn);
         [uheat]=ctepile(P,Theatval,R1,R,Es,M,N);

     t=((w-1)*j)+dd+273+((y-1)*364);      h=(t-182);
     uheath(:,h)=uheat;
    [alphah2o,rhow] = watercte(P,Told);

        %%%Calculation of gammasat and clay density based upon temp
    %%%increase
    [gammasat,rhoc1]=grammasat(P,Gs,e2,rhow,g,alphas,Told,Tn);
         [Cpc]=claycon(P,Cp5,Cp10,Cp20,Cp25,Cp30,Told);

        for ii=((M-1)/2)*N+1:N:(M-1)*N+1
      Told(ii)=Told(ii)-Theatval;
    End

        %Conduction Node definition
    [c,d]=
Conduct_Days_HVAC(M,N,R,Krr,Cpc,rhoc1,dr,Kzz,dz,dt,Krz,Told,Theatval,Tn);
    Tnew=(c^-1)*d';      Tdif=Tnew-Told;
    for ii=1:P
      if abs(Tdif(ii))<0.001
        Tdif(ii)=0;
      end
    end

    [ucte,alphast]=ctesoil(P,n,Tdif,alphas,alphah2o,mvrr);
```

```
    Told=Tnew;      ucteh(:,h)=ucte';      TfinalS(:,h)=Told;

        %%%Permeability and dynamic viscosity
    [muVogel,krriV,kzziV,krziV]=perm(P,Tnew,rhow,krri,kzzi);

        %%%Compressibility, volumetric compressibility, and consolidation
    %%%coefficients
[avrr,avzz,mvrr,mvzz,CvrriV,CvzziV,CvrziV]=CvrrT_Driv_Days(P,e0,krriV,kzziV,
        rhow,g);

%Consolidation Node definition
[a,b]=Consol_Days_Driv522(P,kzzi,M,N,R,Rp,W,cu,dr,t,CvrriV,CvzziV,dz,dt,CvrziV,
        uold);
    unew=(a^-1)*b';      unew=unew+uheat+ucte';

        for d=(M-1)/2:M-2
      for ii=d*N+1
        K(ii)=1.5*Ko;
       sigpr(ii)=Ko*((gammasat(ii)*((M-1)-(d-1)))+(gammasat(ii)-rhow(ii)*g)*0.5);
       fs(ii)=sigpr(ii)*(K(ii)/Ko)*tand(phip*0.8);
      end
    end
    fst=sum(fs);
    fsf(:,t)=fst*(0.2+0.8*(1-unew(ii)/(ds(ii)/0.8)));
    fsh(:,h)=fst*(0.2+0.8*(1-unew(ii)/(ds(ii)/0.8)));
        uold=unew;      uexS(:,h)=uold;      uexfin(:,t)=uold;
        end
 end

  for w=8:i
  for dd=1:j
    Theatval=-((45/1344)*(6-(13-w)));
    for ii=((M-1)/2)*N+1:N:(M-1)*N+1
      Told(ii)=Told(ii)+Theatval;
    end

    %New radius upon change in temperature
    [R1]=Pilex(P,M,N,R,alphapile,Told,Tn);
    [uheat]=ctepile(P,Theatval,R1,R,Es,M,N);
        t=((w-1)*j)+dd+273+((y-1)*364);      h=(t-182);
     uheath(:,h)=uheat;

    [alphah2o,rhow] = watercte(P,Told);

    %%%Calculation of gammasat and clay density based upon temp
    %%%increase
```

```
    [gammasat,rhoc1]=grammasat(P,Gs,e2,rhow,g,alphas,Told,Tn);
    [Cpc]=claycon(P,Cp5,Cp10,Cp20,Cp25,Cp30,Told);
    for ii=((M-1)/2)*N+1:N:(M-1)*N+1
     Told(ii)=Told(ii)-Theatval;
    end

    %Conduction Node definition
    [c,d]=
Conduct_Days_HVAC(M,N,R,Krr,Cpc,rhoc1,dr,Kzz,dz,dt,Krz,Told,Theatval,Tn);
    Tnew=(c^-1)*d';     Tdif=Tnew-Told;
    for ii=1:P
     if abs(Tdif(ii))<0.001
       Tdif(ii)=0;
     end
    end
    [ucte,alphast]=ctesoil(P,n,Tdif,alphas,alphah2o,mvrr);
    Told=Tnew;     ucteh(:,h)=ucte';     TfinalS(:,h)=Told;
    %%%Permeability and dynamic viscosity

    [muVogel,krriV,kzziV,krziV]=perm(P,Tnew,rhow,krri,kzzi);
    %%%Compressibility, volumetric compressibility, and consolidation
    %%%coefficients
[avrr,avzz,mvrr,mvzz,CvrriV,CvzziV,CvrziV]=CvrrT_Driv_Days(P,e0,krriV,kzziV,
        rhow,g);

%ConsolidationNode definition
[a,b]=Consol_Days_Driv522(P,kzzi,M,N,R,Rp,W,cu,dr,t,CvrriV,CvzziV,dz,dt,CvrziV,
        uold);
    unew=(a^-1)*b';     unew=unew+uheat+ucte';

    for d=(M-1)/2:M-2
     for ii=d*N+1
       K(ii)=1.5*Ko;
      sigpr(ii)=Ko*((gammasat(ii)*((M-1)-(d-1)))+(gammasat(ii)-rhow(ii)*g)*0.5);
      fs(ii)=sigpr(ii)*(K(ii)/Ko)*tand(phip*0.8);
     end
    end
    fst=sum(fs);
    fsf(:,t)=fst*(0.2+0.8*(1-unew(ii)/(ds(ii)/0.8)));
    fsh(:,h)=fst*(0.2+0.8*(1-unew(ii)/(ds(ii)/0.8)));
    uold=unew;     uexS(:,h)=uold;     uexfin(:,t)=uold;
  end
 end

 %%%%  WINTER (Days 184-275(547-637) after HVAC intro)  %%%%
 i=13; j=7;
```

```
for w=1:7

  for dd=1:7
    Theatval=-((45/1344)*(6+2*(w-1)));
    for ii=((M-1)/2)*N+1:N:(M-1)*N+1
      Told(ii)=Told(ii)+Theatval;
    end
    %New radius upon change in temperature
    [R1]=Pilex(P,M,N,R,alphapile,Told,Tn);

    [uheat]=ctepile(P,Theatval,R1,R,Es,M,N);

    t=((w-1)*j)+dd+364+((y-1)*364);      h=(t-182);

    uheath(:,h)=uheat;
    [alphah2o,rhow] = watercte(P,Told);

    %%%Calculation of gammasat and clay density based upon temp
    %%%increase
    [gammasat,rhoc1]=grammasat(P,Gs,e2,rhow,g,alphas,Told,Tn);

    [Cpc]=claycon(P,Cp5,Cp10,Cp20,Cp25,Cp30,Told);

    for ii=((M-1)/2)*N+1:N:(M-1)*N+1
      Told(ii)=Told(ii)-Theatval;
    end

    %Conduction Node definition
    [c,d]=
Conduct_Days_HVAC(M,N,R,Krr,Cpc,rhoc1,dr,Kzz,dz,dt,Krz,Told,Theatval,Tn);
    Tnew=(c^-1)*d';
    Tdif=Tnew-Told;
    for ii=1:P
      if abs(Tdif(ii))<0.001
        Tdif(ii)=0;
      end
    end
    [ucte,alphast]=ctesoil(P,n,Tdif,alphas,alphah2o,mvrr);
    Told=Tnew;      ucteh(:,h)=ucte';      TfinalS(:,h)=Told;

    %%%Permeability and dynamic viscosity
    [muVogel,krriV,kzziV,krziV]=perm(P,Tnew,rhow,krri,kzzi);

    %%%Compressibility, volumetric compressibility, and consolidation
    %%%coefficients
```

```
    [avrr,avzz,mvrr,mvzz,CvrriV,CvzziV,CvrziV]=CvrrT_Driv_Days(P,e0,krriV,kzziV,
        rhow,g);

    %ConsolidationNode definition

[a,b]=Consol_Days_Driv522(P,kzzi,M,N,R,Rp,W,cu,dr,t,CvrriV,CvzziV,dz,dt,CvrziV,
        uold);
    unew=(a^-1)*b';      unew=unew+uheat+ucte';

    for d=(M-1)/2:M-2
      for ii=d*N+1
        K(ii)=1.5*Ko;
       sigpr(ii)=Ko*((gammasat(ii)*((M-1)-(d-1)))+(gammasat(ii)-rhow(ii)*g)*0.5);
       fs(ii)=sigpr(ii)*(K(ii)/Ko)*tand(phip*0.8);
      end
    end
    fst=sum(fs);
    fsf(:,t)=fst*(0.2+0.8*(1-unew(ii)/(ds(ii)/0.8)));
    fsh(:,h)=fst*(0.2+0.8*(1-unew(ii)/(ds(ii)/0.8)));

    uold=unew;
    uexS(:,h)=uold;
    uexfin(:,t)=uold;

   end
 end

 for w=8:i
   for dd=1:j
    Theatval=-((45/1344)*(6+2*(13-w)));
    for ii=((M-1)/2)*N+1:N:(M-1)*N+1
      Told(ii)=Told(ii)+Theatval;
    end
    %New radius upon change in temperature
    [R1]=Pilex(P,M,N,R,alphapile,Told,Tn);

    [uheat]=ctepile(P,Theatval,R1,R,Es,M,N);

    t=((w-1)*j)+dd+364+((y-1)*364);      h=(t-182);

    uheath(:,h)=uheat;
    [alphah2o,rhow] = watercte(P,Told);

    %%%Calculation of gammasat and clay density based upon temp
    %%%increase
    [gammasat,rhoc1]=grammasat(P,Gs,e2,rhow,g,alphas,Told,Tn);
```

```
[Cpc]=claycon(P,Cp5,Cp10,Cp20,Cp25,Cp30,Told);

for ii=((M-1)/2)*N+1:N:(M-1)*N+1
  Told(ii)=Told(ii)-Theatval;
end

%Conduction Node definition
[c,d]=
Conduct_Days_HVAC(M,N,R,Krr,Cpc,rhoc1,dr,Kzz,dz,dt,Krz,Told,Theatval,Tn);
Tnew=(c^-1)*d';      Tdif=Tnew-Told;

for ii=1:P
  if abs(Tdif(ii))<0.001
    Tdif(ii)=0;
  end
end
[ucte,alphast]=ctesoil(P,n,Tdif,alphas,alphah2o,mvrr);
Told=Tnew;      ucteh(:,h)=ucte';  TfinalS(:,h)=Told;

%%%Permeability and dynamic viscosity
[muVogel,krriV,kzziV,krziV]=perm(P,Tnew,rhow,krri,kzzi);

%%%Compressibility, volumetric compressibility, and consolidation
%%%coefficients
[avrr,avzz,mvrr,mvzz,CvrriV,CvzziV,CvrziV]=CvrrT_Driv_Days(P,e0,krriV,kzziV,
     rhow,g);

%Consolidation Node definition

[a,b]=Consol_Days_Driv522(P,kzzi,M,N,R,Rp,W,cu,dr,t,CvrriV,CvzziV,dz,dt,CvrziV,uo
ld);
unew=(a^-1)*b';      unew=unew+uheat+ucte';

for d=(M-1)/2:M-2
  for ii=d*N+1
    K(ii)=1.5*Ko;
   sigpr(ii)=Ko*((gammasat(ii)*((M-1)-(d-1)))+(gammasat(ii)-rhow(ii)*g)*0.5);
   fs(ii)=sigpr(ii)*(K(ii)/Ko)*tand(phip*0.8);
  end
end
fst=sum(fs);
fsf(:,t)=fst*(0.2+0.8*(1-unew(ii)/(ds(ii)/0.8)));
fsh(:,h)=fst*(0.2+0.8*(1-unew(ii)/(ds(ii)/0.8)));

uold=unew;      uexS(:,h)=uold;      uexfin(:,t)=uold;
```

```
  end
end

%%%%   SPRING (Days 276-364(638-728) after HVAC intro)  %%%%
i=13; j=7;

for w=1:7

  for dd=1:7
    Theatval=-((45/1344)*(6-(w-1)));
    for ii=((M-1)/2)*N+1:N:(M-1)*N+1
      Told(ii)=Told(ii)+Theatval;
    end
    %New radius upon change in temperature
    [R1]=Pilex(P,M,N,R,alphapile,Told,Tn);

    [uheat]=ctepile(P,Theatval,R1,R,Es,M,N);

    t=((w-1)*j)+dd+455+((y-1)*364);      h=(t-182);

    uheath(:,h)=uheat;
    [alphah2o,rhow] = watercte(P,Told);

    %%%Calculation of gammasat and clay density based upon temp
    %%%increase
    [gammasat,rhoc1]=grammasat(P,Gs,e2,rhow,g,alphas,Told,Tn);

    [Cpc]=claycon(P,Cp5,Cp10,Cp20,Cp25,Cp30,Told);

    for ii=((M-1)/2)*N+1:N:(M-1)*N+1
      Told(ii)=Told(ii)-Theatval;
    end

    %Conduction Node definition
    [c,d]=
Conduct_Days_HVAC(M,N,R,Krr,Cpc,rhoc1,dr,Kzz,dz,dt,Krz,Told,Theatval,Tn);
    Tnew=(c^-1)*d';      Tdif=Tnew-Told;

    for ii=1:P
      if abs(Tdif(ii))<0.001
        Tdif(ii)=0;
      end
    end
    [ucte,alphast]=ctesoil(P,n,Tdif,alphas,alphah2o,mvrr);
    Told=Tnew;      ucteh(:,h)=ucte';      TfinalS(:,h)=Told;
```

```
    %%%Permeability and dynamic viscosity
    [muVogel,krriV,kzziV,krziV]=perm(P,Tnew,rhow,krri,kzzi);

    %%%Compressibility, volumetric compressibility, and consolidation
    %%%coefficients
    [avrr,avzz,mvrr,mvzz,CvrriV,CvzziV,CvrziV]=CvrrT_Driv_Days(P,e0,krriV,kzziV,
        rhow,g);

    %ConsolidationNode definition

[a,b]=Consol_Days_Driv522(P,kzzi,M,N,R,Rp,W,cu,dr,t,CvrriV,CvzziV,dz,dt,CvrziV,uo
ld);
    unew=(a^-1)*b';     unew=unew+uheat+ucte';

    for d=(M-1)/2:M-2
      for ii=d*N+1
        K(ii)=1.5*Ko;
        sigpr(ii)=Ko*((gammasat(ii)*((M-1)-(d-1)))+(gammasat(ii)-rhow(ii)*g)*0.5);
        fs(ii)=sigpr(ii)*(K(ii)/Ko)*tand(phip*0.8);
      end
    end
    fst=sum(fs);
    fsf(:,t)=fst*(0.2+0.8*(1-unew(ii)/(ds(ii)/0.8)));
    fsh(:,h)=fst*(0.2+0.8*(1-unew(ii)/(ds(ii)/0.8)));

    uold=unew;     uexS(:,h)=uold;     uexfin(:,t)=uold;

  end
 end

 for w=8:i
  for dd=1:j
    Theatval=40/1344*(6-(13-w));
    for ii=((M-1)/2)*N+1:N:(M-1)*N+1
      Told(ii)=Told(ii)+Theatval;
    end
    %New radius upon change in temperature
    [R1]=Pilex(P,M,N,R,alphapile,Told,Tn);

    [uheat]=ctepile(P,Theatval,R1,R,Es,M,N);

    t=((w-1)*j)+dd+455+((y-1)*364);     h=(t-182);

    uheath(:,h)=uheat;
    [alphah2o,rhow] = watercte(P,Told);
```

```
%%%Calculation of gammasat and clay density based upon temp
%%%increase
[gammasat,rhoc1]=grammasat(P,Gs,e2,rhow,g,alphas,Told,Tn);

[Cpc]=claycon(P,Cp5,Cp10,Cp20,Cp25,Cp30,Told);

for ii=((M-1)/2)*N+1:N:(M-1)*N+1
  Told(ii)=Told(ii)-Theatval;
end

%Conduction Node definition
[c,d]=
Conduct_Days_HVAC(M,N,R,Krr,Cpc,rhoc1,dr,Kzz,dz,dt,Krz,Told,Theatval,Tn);
Tnew=(c^-1)*d';      Tdif=Tnew-Told;

for ii=1:P
  if abs(Tdif(ii))<0.001
    Tdif(ii)=0;
  end
end
[ucte,alphast]=ctesoil(P,n,Tdif,alphas,alphah2o,mvrr);
Told=Tnew;      ucteh(:,h)=ucte';   TfinalS(:,h)=Told;

%%%Permeability and dynamic viscosity
[muVogel,krriV,kzziV,krziV]=perm(P,Tnew,rhow,krri,kzzi);

%%%Compressibility, volumetric compressibility, and consolidation
%%%coefficients
[avrr,avzz,mvrr,mvzz,CvrriV,CvzziV,CvrziV]=CvrrT_Driv_Days(P,e0,krriV,kzziV,
     rhow,g);

%ConsolidationNode definition

[a,b]=Consol_Days_Driv522(P,kzzi,M,N,R,Rp,W,cu,dr,t,CvrriV,CvzziV,dz,dt,CvrziV,
      uold);
unew=(a^-1)*b';      unew=unew+uheat+ucte';

for d=(M-1)/2:M-2
  for ii=d*N+1
    K(ii)=1.5*Ko;
   sigpr(ii)=Ko*((gammasat(ii)*((M-1)-(d-1)))+(gammasat(ii)-rhow(ii)*g)*0.5);
   fs(ii)=sigpr(ii)*(K(ii)/Ko)*tand(phip*0.8);
   %       F=sum(fs)*2*pi*R*L;
  end
end
```

```
      fst=sum(fs);
      fsf(:,t)=fst*(0.2+0.8*(1-unew(ii)/(ds(ii)/0.8)));
      fsh(:,h)=fst*(0.2+0.8*(1-unew(ii)/(ds(ii)/0.8)));

      uold=unew;      uexS(:,h)=uold;      uexfin(:,t)=uold;

    end
  end
end


  ff=1:10:t;
  pp=fsf(:,1:10:t);

  plot(ff,pp,':*');

  text(183,150,' \leftarrow Begin HVAC','Rotation',90.0)
  text(183,100,' \leftarrow Summer, Year 1','Rotation',90.0)
  text(274,100,' \leftarrow Fall, Year 1','Rotation',90.0)
  text(323,100,' \leftarrow Soil Cooling','Rotation',90.0)
  text(365,100,' \leftarrow Winter, Year 1','Rotation',90.0)
  text(456,100,' \leftarrow Spring, Year 1','Rotation',90.0)
  text(505,100,' \leftarrow Soil Heating','Rotation',90.0)
  text(547,100,' \leftarrow Summer, Year 2','Rotation',90.0)
  text(687,100,' \leftarrow Soil Cooling','Rotation',90.0)
  text(638,100,' \leftarrow Fall, Year 2','Rotation',90.0)
  text(729,100,' \leftarrow Winter, Year 2','Rotation',90.0)
  text(869,100,' \leftarrow Soil Heating','Rotation',90.0)
  text(820,100,' \leftarrow Spring, Year 2','Rotation',90.0)
  xlabel('Elapsed Time, Days', 'FontSize',24)
  ylabel('Unit Friction, (kN/m)','FontSize',24)
  title({'Unit Friction Values at Depth, After HVAC'},'FontSize',24)


fig1=figure;
for k=1:10:371
  for ii=1:M
    for jj=1:N
      r=(jj-1)*dr;
      z=(ii-1)*dz;
      uplot(ii,jj)=uexfin((ii-1)*N+jj,k);

    end
  end

  contourf(uplot,9,'b');
```

```
  axis ([1 N*dr 1 M*dz+1]);

  caxis([0 550]);
  %% 9 Level Color Scale Colormap with Mapping to Grayscale for Publications.
%
CMRmap=[0 0 0;.15 .15 .5;.3 .15 .75;.6 .2 .50;1 .25 .15;.9 .5 0;.9 .75 .1;.9 .9 .5;1 1 1];
colormap(CMRmap)
colorbar

  xlabel('Distance from Pile (m)', 'FontSize',14)
  ylabel('Depth (m)','FontSize',14)
  title({'EPWP: Days Elapsed Since Pile Driven: ',int2str(k)},'FontSize',18)%,
  drawnow
  hold on
  pause(2);
  aviobj = addframe(aviobj,gcf);
end

aviobj = close(aviobj);
fig2=figure;
for k=1:10:371
  for ii=1:M
    for jj=1:N
      r(ii,jj) = (jj-1)*dr;
      z(ii,jj) = (ii-1)*dz;
      Tplot(ii,jj)=TfinalS((ii-1)*N+jj,k);

    end
  end

  contourf(Tplot,9, 'b');
  axis ([1 N*dr 1 M*dz+1]);

  caxis([-1 51]);
  %% 9 Level Color Scale Colormap with Mapping to Grayscale for Publications.
%
CMRmap=[0 0 0;.15 .15 .5;.3 .15 .75;.6 .2 .50;1 .25 .15;.9 .5 0;.9 .75 .1;.9 .9 .5;1 1 1];
colormap(CMRmap)
colorbar

  xlabel('Distance from Pile (m)', 'FontSize',14)
  ylabel('Depth (m)','FontSize',14)
  title({'Temperature: Days Elapsed Since Pile Driven: ',int2str(k)},'FontSize',18)
  drawnow
  hold on
  pause(2);
```

```
  aviobjt = addframe(aviobjt,gcf);

end

aviobjt = close(aviobjt);
fig3=figure;
for k=371:10:721
  for ii=1:M
    for jj=1:N
      r(ii,jj) = (jj-1)*dr;
      z(ii,jj) = (ii-1)*dz;
      uplot(ii,jj)=uexfin((ii-1)*N+jj,k);

    end
  end

  contourf(uplot,9,'b');
  axis ([1 N*dr 1 M*dz+1]);

  caxis([-1 95]);
  %% 9 Level Color Scale Colormap with Mapping to Grayscale for Publications.
%
CMRmap=[0 0 0;.15 .15 .5;.3 .15 .75;.6 .2 .50;1 .25 .15;.9 .5 0;.9 .75 .1;.9 .9 .5;1 1 1];
colormap(CMRmap)
colorbar
  xlabel('Distance from Pile (m)', 'FontSize',14)
  ylabel('Depth (m)','FontSize',14)
  title({'EPWP: Days Elapsed Since Pile Driven: ',int2str(k)},'FontSize',18)%,
  drawnow
  hold on
  pause(2);
  aviobjtt = addframe(aviobjtt,gcf);
end

aviobjtt = close(aviobjtt);
fig4=figure;
for k=371:10:721
  for ii=1:M
    for jj=1:N
      r(ii,jj) = (jj-1)*dr;
      z(ii,jj) = (ii-1)*dz;
      Tplot(ii,jj)=TfinalS((ii-1)*N+jj,k);

    end
  end
```

```
  contourf(Tplot,9, 'b');
  axis ([1 N*dr 1 M*dz+1]);

  caxis([-1 51]);
  %% 9 Level Color Scale Colormap with Mapping to Grayscale for Publications.
%
CMRmap=[0 0 0;.15 .15 .5;.3 .15 .75;.6 .2 .50;1 .25 .15;.9 .5 0;.9 .75 .1;.9 .9 .5;1 1 1];
colormap(CMRmap)
colorbar

  xlabel('Distance from Pile (m)', 'FontSize',14)
  ylabel('Depth (m)','FontSize',14)
  title({'Temperature: Days Elapsed Since Pile Driven: ',int2str(k)},'FontSize',18)
  drawnow
  hold on
  pause(2);
  aviobjttt = addframe(aviobjttt,gcf);

end

aviobjttt = close(aviobjttt);
```

Driven Pile Iteration with Transient Ground-Surface Temperatures

The "Trans_Surf_Temp_Conduct.m" function file takes the place of the "Conduct_Days_HVAC.m" function file that is used in the constant surface temperature iteration.

Conduction Node Definition Function

```
function
[c,d]=Trans_Surf_Temp_Conduct(M,N,R,Krr,Cpc,rhoc1,dr,Kzz,dz,dt,Krz,Told,Th,Tl,Tm
ed,Tn,t)

%Conduction node definition with transient surface temperatures

%Interior nodes
for f=1:(M-2)
  for ii=(f*N)+2:(f+1)*N-1
    r=R+(dr*(ii-(f*N+1)));
    c(ii,ii)=-2*(Krr/(Cpc(ii)*rhoc1(ii)*dr^2)+Kzz/(Cpc(ii)*rhoc1(ii)*dz^2))-1/dt;
```

```
   c(ii,ii+1)=Krr/(Cpc(ii)*rhoc1(ii)*dr^2)+Krr/(2*r*Cpc(ii)*rhoc1(ii)*dr);
   c(ii,ii-1)=(Krr/(Cpc(ii)*rhoc1(ii)*dr^2)-Krr/(2*r*Cpc(ii)*rhoc1(ii)*dr));
   c(ii,ii+N)=Kzz/(Cpc(ii)*rhoc1(ii)*dz^2);
   c(ii,ii-N)=Kzz/(Cpc(ii)*rhoc1(ii)*dz^2);
   c(ii,ii+N+1)=Krz/(2*Cpc(ii)*rhoc1(ii)*dr*dz);
   c(ii,ii-N+1)=-(Krz/(2*Cpc(ii)*rhoc1(ii)*dr*dz));
   c(ii,ii+N-1)=-(Krz/(2*Cpc(ii)*rhoc1(ii)*dr*dz));
   c(ii,ii-N-1)=Krz/(2*Cpc(ii)*rhoc1(ii)*dr*dz);
   d(ii)=-Told(ii)/dt;
  end
end

%Boundary conditions
%Pile side
%Below Pile
for ii=1:N:((M-3)/2)*N+1;

   c(ii,:)=0;    c(ii,ii)=1;    c(ii,ii+1)=-1;
   d(ii)=0;
end

%Along Pile
 for ii=((M-1)/2)*N+1:N:(M-1)*N+1
  c(ii,:)=0;  c(ii,ii)=1;  c(ii,ii+1)=-1;
  d(ii)=0;
end

%Bottom
for ii=2:N-1
  c(ii,:)=0;  c(ii,ii)=1;  c(ii,ii+N)=0;
  d(ii)=Tn;
end

%Soil side
for ii=N:N:M*N
  c(ii,:)=0;  c(ii,ii)=1;  c(ii,ii-1)=-1;
  d(ii)=0;
end

%Ground surface under concrete cover next to pile
for ii=(M-1)*N+2:(M-1)*N+11
  c(ii,:)=0;  c(ii,ii)=1;  c(ii,ii-N)=0;
  d(ii)=19;
end

%Ground surface from edge of concrete cover to boundary
```

```
 for ii=(M-1)*N+12:M*N-1
  c(ii,:)=0;  c(ii,ii)=1;  c(ii,ii-N)=0;
  d(ii)=Tmed+((Th-Tl)/2)*cos(2*pi/364*(t-212));
end
end
```

Driven Pile Iteration (Transient Ground-Surface Temperature) Main File (partial)

```
%This model will show the change in excess pore-water pressure with
%time and temperature changes for energy piles. The temperature at the
%surface will fluctuate sinusoidally. This will be used
%show how pile capacity, namely, side friction, varies with time.
%Daniel P. Zimmerman
%for completion of the requirements of the Master of Science Degree in
%Civil Engineering
%Advisor: Dr. Arvin Farid, PE
%Start date: May 26, 2012
clear all;clc;

%%%Inputs
[L,R,Th,Tl,Tmed,Tn,krri,krzi,kzzi,cc,gammasat0,e0,Ec,Es,Gs,Krr,Kzz,Krz,Cp5,Cp10,Cp
15,Cp20,Cp25,Cp30,alphas,alphapile,LL,PL,nu,G,cu,Cc,phip,OCR,years]= Inputs();

%%%Constants
[W,H,N,M,ccnodes,dr,dz,P,g,dT,dt,Ko,alphast]=Constants(L,cc,phip,OCR);

Told(1:P)=Tn;           Told=Told';     Tnew=Told;
uold(1:P)=0;    uold1(1:P)=0;

 sigpr(1:P)=0;   K(1:P)=0;       fs(1:P)=0;       sigpr1(1:P)=0;
 K1(1:P)=0;      fs1(1:P)=0;

 %%%Consolidation of soil after pile installation without temperature
 %%% change

 for t=1:dt:910

   [alphah2o,rhow] = watercte(P,Told);
%   e1alphah2o(t,:)=alphah2o;
%   e1rhow(t,:)=rhow;
   %Initial EPWP, horizontal stress, and void ratio for driven pile

[Rp,e1,ued,ds,e2,gammasat,n]=fet(P,R,G,cu,M,W,N,dr,Cc,gammasat0,dz,e0,Gs,g,rhow);
%e1e1(t,:)=e1;  e1e2(t,:)=e2;   e1gammasat(t,:)=gammasat;  e1n(t,:)=n;
 ds=ds';
```

```
  %%%Permeability and dynamic viscosity
 [muVogel,krriV,kzziV,krziV]=perm(P,Tnew,rhow,krri,kzzi);
%e1muVogel(t,:)=muVogel;  e1krriV(t,:)=krriV;  e1kzziV(t,:)=kzziV;

%for ii=1:P
%e1intrins(ii)=rhow(ii)/muVogel(ii);
%end
%e1intrinst(t,:)=e1intrins;

 %%%Compressibility, volumetric compressibility, and consolidation
 %%%coefficients
 [avrr,avzz,mvrr,mvzz,CvrriV,CvzziV,CvrziV]=CvrrT_Driv_Days(P,e0,krriV,kzziV,
        rhow,g);
%   e1CvrriV(t,:)=CvrriV;   e1CvzziV(t,:)=CvzziV;

 %%%Calculation of gammasat and clay density based upon temp
    %%%increase
    [gammasat,rhoc1]=grammasat(P,Gs,e2,rhow,g,alphas,Told,Tn);

    [Cpc]=claycon(P,Cp5,Cp10,Cp20,Cp25,Cp30,Told);

 %Conduction Node definition

[c,d]=Trans_Surf_Temp_Conduct(M,N,R,Krr,Cpc,rhoc1,dr,Kzz,dz,dt,Krz,Told,Th,Tl,Tm
ed,Tn,t);
    Tnew=(c^-1)*d';      Tdif=Tnew-Told;

    for ii=1:P
      if abs(Tdif(ii))<0.001
        Tdif(ii)=0;
      end
    end

    [ucte,alphast]=ctesoil(P,n,Tdif,alphas,alphah2o,mvrr);
    Told=Tnew;      uctet1(:,t)=ucte';      TfinalS1(:,t)=Told;

  %Consolidation Node definition

[a,b]=Consol_Days_Driv96(P,kzzi,M,N,R,Rp,W,cu,dr,t,CvrriV,CvzziV,dz,dt,CvrziV,uol
d1);
  unew1=(a^-1)*b';   unew1=unew1+ucte';   uold1=unew1;

  uexfin1(:,t)=unew1;%substitute t for 1 in uexfin if time step

  for d=(M-1)/2:M-2
    for ii=d*N+1
```

```
      K1(ii)=1.5*Ko;
      sigpr1(ii)=Ko*((gammasat(ii)*((M-1)-(d-1)))+(gammasat(ii)-rhow(ii)*g)*0.5);
      fs1(ii)=sigpr1(ii)*(K1(ii)/Ko)*tand(phip*0.8);
    end
  end
  fst1=sum(fs1);
  fsf1(:,t)=fst1*(0.2+0.8*(1-unew1(ii)/(ds(ii)/0.8)));
 end

Told(1:P)=Tn;%Told=Told';
uold(1:P)=0;

Tnew=Told;    Tfinal(:,1)=Tnew;       TfinalS(:,1)=Tfinal(:,1);
sigpr(1:P)=0;   K(1:P)=0;       fs(1:P)=0;       uheatval=0;

%%%Consolidation after pile installation. HVAC will be turned on in three
%%%months.

for t=1:dt:182
  %%%Water coefficient of thermal expansion and density due to
     %%%current temp.

  [alphah2o,rhow] = watercte(P,Told);
% ealphah2o(t,:)=alphah2o;   erhow(t,:)=rhow;

  %%%Initial EPWP, horizontal stress, and void ratio for driven pile

[Rp,e1,ued,ds,e2,gammasat,n]=fet(P,R,G,cu,M,W,N,dr,Cc,gammasat0,dz,e0,Gs,g,rhow);
  % ee1(t,:)=e1;   ee2(t,:)=e2;   egammasat(t,:)=gammasat;   en(t,:)=n;
    ds=ds';

  %%%Permeability and dynamic viscosity
  [muVogel,krriV,kzziV,krziV]=perm(P,Tnew,rhow,krri,kzzi);
%   emuVogel(t,:)=muVogel;
%   for ii=1:P
%   eintrins(ii)=rhow(ii)/muVogel(ii);
%   end
%   eintrinst(t,:)=eintrins;   ekrriV(t,:)=krriV;   ekzziV(t,:)=kzziV;

  %%%Compressibility, volumetric compressibility, and consolidation
  %%%coefficients
  [avrr,avzz,mvrr,mvzz,CvrriV,CvzziV,CvrziV]=CvrrT_Driv_Days(P,e0,krriV,kzziV,
          rhow,g);
%   eCvrriV(t,:)=CvrriV;   eCvzziV(t,:)=CvzziV;

  [gammasat,rhoc1]=grammasat(P,Gs,e2,rhow,g,alphas,Told,Tn);
```

```
 [Cpc]=claycon(P,Cp5,Cp10,Cp20,Cp25,Cp30,Told);

 %Conduction Node definition

[c,d]=Trans_Surf_Temp_Conduct(M,N,R,Krr,Cpc,rhoc1,dr,Kzz,dz,dt,Krz,Told,Th,Tl,Tm
ed,Tn,t);
    Tnew=(c^-1)*d';     Tdif=Tnew-Told;

    for ii=1:P
     if abs(Tdif(ii))<0.001
       Tdif(ii)=0;
     end
    end
    [ucte,alphast]=ctesoil(P,n,Tdif,alphas,alphah2o,mvrr);
    Told=Tnew;     ucteh(:,t)=ucte';     TfinalS(:,t)=Told;

 %%%Consolidation Node definition
 [a,b]=Consol_Days_Driv522(P,kzzi,M,N,R,Rp,W,cu,dr,t,CvrriV,CvzziV,dz,dt,CvrziV,
         uold);
 unew=(a^-1)*b';  unew=unew+ucte';  uold=unew;  uexfin(:,t)=uold;

 %%%Calculation of friction
 for d=(M-1)/2:M-2
    for ii=d*N+1
     K(ii)=1.5*Ko;
     sigpr(ii)=Ko*((gammasat(ii)*((M-1)-(d-1)))+(gammasat(ii)-rhow(ii)*g)*0.5);
     fs(ii)=sigpr(ii)*(K(ii)/Ko)*tand(phip*0.8);
    end
  end
  fst=sum(fs);
  fsf(:,t)=fst*(0.2+0.8*(1-unew(ii)/(ds(ii)/0.8)));
end

uexS(:,1)=uexfin(:,t);            uheatval=0;

aviobj =
avifile('Pile_EPWP_Year_1_with_Cyclic_Surf_Temp.avi','compression','Cinepak');
 aviobj.KeyFramePerSec = 0.5;


aviobjt =
avifile('Pile_Temp_Year_1_with_Cyclic_Surf_Temp.avi','compression','Cinepak');
aviobjt.KeyFramePerSec = 0.5;
```

```
aviobjtt =
avifile('Pile_EPWP_Year_2_with_Cyclic_Surf_Temp.avi','compression','Cinepak');
  aviobjtt.KeyFramePerSec = 0.5;


aviobjttt =
avifile('Pile_Temp_Year_2_with_Cyclic_Surf_Temp.avi','compression','Cinepak');
aviobjttt.KeyFramePerSec = 0.5;
```

****

The constant-ground-surface-temperature iteration and the transient-ground-surface-temperature iteration are the same from this point, which is right before the loop that introduces HVAC. The only exception is that the conduction node definitions function files are different, as described above.

Drilled Shaft Iteration

Inputs Function

```
function
[L,R,Th,Tl,Tmed,Tn,krri,krzi,kzzi,cc,gammasat0,e0,Ec,Es,Gs,Krr,Kzz,Krz,Cp5,Cp10,Cp
15,Cp20,Cp25,Cp30,alphas,alphapile,LL,PL,nu,G,cu,Cc,phip,OCR,years]= DS_Inputs()

%Inputs
% Soil characteristics, drilled shaft length and radius

L=15; %input('Length of drilled shaft, meters (depth below ground surface): ');

R=0.45; %input('Drilled Shaft radius, meters: ');

Th=32; %input('Highest average daily air temperature, degrees Celsius: ');

Tl=-4; %input('Lowest average daily air temperature, degrees Celsius: ');

Tmed=16; %input('Median annual air temperature, degrees Celsius: ');

Tn=15; %input('Normal average temperature of the soil, degrees Celsius: ');

krri=0.0000007; %input('Hydraulic conductivity in radial (horizontal)...
      %direction at 20 degrees Celsius, m/s: ');

krzi=0; %input('Hydraulic conductivity in radial (horizontal)and vertical...
   %directions at 20 degrees Celsius, m/s: ');
```

```
kzzi=0.0000004; %input('Hydraulic conductivity in vertical direction...
      %at 20 degrees Celsius, m/s: ');

cc=0.5; %input('Concrete cover around drilled shaft, fraction of distance between drilled
        shafts: ');

gammasat0=17; %input('Unit weight of soil, kN/m^3: ');

e0=1.1; %input('Initial void ratio, if known: ');

Ec=25e6; %input('Young's Modulus for concrete, kN/m^2: ');

Es=20e3; %input('Young's Modulus for soil, kN/m^2: ');

Gs=2.75; %input('Specific gravity of soil: ');

Krr=365; %input('Conductivity coefficient for saturated clay, radial direction,
        J/day*m*K: ');

Kzz=365; %input('Conductivity coefficient for saturated clay, vertical direction,
        J/day*m*K: ');

Krz=0; %input('Conductivity coefficient for saturated clay, radial and vertical direction,
        W/m*K: ');

Cp5=2471.5; %input('Specific heat for saturated silty clay at 5 deg C, J/kg
        *degrees C: ');

Cp10=2466.6; %input('Specific heat for saturated silty clayat 10 deg C , J/kg
        *degrees C: ');

Cp15=2463.3; %input('Specific heat for saturated silty clayat 15 deg C, J/kg
        *degrees C: ');

Cp20=2462; %input('Specific heat for saturated silty clayat 20 deg C , J/kg
        *degrees C: ');

Cp25=2461.3; %input('Specific heat for saturated silty clayat 25 deg C , J/kg
        *degrees C: ');

Cp30=2460.4; %input('Specific heat for saturated silty clayat 30 deg C , J/kg
        *degrees C: ');

alphas=0.000033; %input('Coefficient of thermal expansion for soil, 1/deg. C: ');
```

```
alphapile=0.0000145; %input('Coefficient of thermal expansion for concrete
        drilled shaft, 1/deg. C: ');

LL=52; %input('Liquid limit of soil: ');

PL=17; %input('Plastic limit of soil: ');

nu=0.3; %Poisson's Ratio*

G=7.69e3; %input('Shear Modulus for soil, kN/m^2: ');

cu=75; %input('undrained shear strength, kN/m^2: ');

Cc=.28; %input('Compression Index: ');

phip=20; %input('Angle of effective internal friction, phi prime: ');

OCR=1.1; %input('Over-consolidation ratio: ');

years=2; %input('Number of years to run model: ');

end
```

Drilled Shaft Soil Conditions Function

```
function [e1,gammasat,n]=DS_fet(P,M,N,Cc,gammasat0,dz,e0,rhow,Gs,g)
%Establishes insitu void ratio, porosity and saturated unit weight values
%for each node

e1(1:P)=e0;     n(1:P)=e0/(1+e0);       gammasat(1:P)=gammasat0;

for d=1:M-1
  for ii=((d-1)*N)+1:((d-1)*N)+N
    e1(ii)=e0-Cc*(log10(0.55*gammasat(ii)*((M-d)*dz))...
      -(log10(0.55*gammasat(ii)*dz)));
     n(ii)=e1/(1+e1);
     gammasat(ii)=(Gs+e1(ii))*rhow(ii)*g/(1+e1(ii));
  end
end
end
```

Saturated Unit Weight Function

```
function[gammasat,rhoc1]=DS_grammasat(P,Gs,e1,rhow,g,alphas,Told,Tn)
%%%This function recalculates gammasat and clay density as temperature
%%%varies
```

```
for ii=1:P
  gammasat(ii)=(Gs+e1(ii))*rhow(ii)*g/(1+e1(ii));
  rhoc1(ii)=(gammasat(ii)/g)/(1+alphas*(Told(ii)-Tn));
end
end
```

Consolidation Node Definition Function

```
function [a,b]= Consol_Days_DS(P,kzzi,M,N,R,dr,CvrriV,CvzziV,dz,dt,CvrziV,uold)

%Consol_Nodes
%Consolidation node definition

kzz(1:P)=kzzi;
%Interior nodes
 for d=1:(M-2)
   for ii=(d*N)+2:(d+1)*N-1
     r=R+(dr*(ii-(d*N+1)));
     a(ii,ii)=-2*(CvrriV(ii)/(dr^2)+CvzziV(ii)/(dz^2))-1/dt;
     a(ii,ii+1)=CvrriV(ii)/dr^2+CvrriV(ii)/(2*r*dr);
     a(ii,ii-1)=CvrriV(ii)/dr^2-CvrriV(ii)/(2*r*dr);
     a(ii,ii+N)=CvzziV(ii)/dz^2;     a(ii,ii-N)=CvzziV(ii)/dz^2;
     a(ii,ii+N+1)=CvrziV(ii)/(2*dr*dz);     a(ii,ii-N+1)=-CvrziV(ii)/(2*dr*dz);
     a(ii,ii+N-1)=-CvrziV(ii)/(2*dr*dz);     a(ii,ii-N-1)=CvrziV(ii)/(2*dr*dz);
     b(ii)=-(uold(ii))/dt;
  end
 end

%Boundary conditions
%Pile side
for ii=1:N:((M-3)/2)*N+1;
  %below pile
    a(ii,:)=0;    a(ii,ii)=1;    a(ii,ii+1)=-1;
    b(ii)=0;
end

for ii=((M-1)/2)*N+1:N:(M-1)*N+1
    %along pile
    a(ii,:)=0;    a(ii,ii)=1;    a(ii,ii+1)=-1;
    b(ii)=0;
end

%Bottom
%Sand or clay?
for ii=2:N-1
```

```
 %Clay
 if kzz(2)<1e-5
  a(ii,:)=0;    a(ii,ii)=1;    a(ii,ii+N)=-1;
  b(ii)=0;
  else
 %Sand
  a(ii,:)=0;    a(ii,ii)=1;    a(ii,ii+N)=0;
  b(ii)=0;
 end
end

%Soil side
for ii=N:N:M*N
 a(ii,:)=0;  a(ii,ii)=1;  a(ii,ii-1)=0;
 b(ii)=0;
end

%Ground surface under concrete cover next to pile
for ii=(M-1)*N+1:(M-1)*N+11
 a(ii,:)=0;  a(ii,ii)=1;  a(ii,ii-N)=-1;
 b(ii)=0;
end

 %Ground surface from edge of concrete cover to boundary
for ii=(M-1)*N+12:(M-1)*N+N-1
 a(ii,:)=0;  a(ii,ii)=1;  a(ii,ii-N)=0;
 b(ii)=0;
end
end
```

Drilled Shaft Main File

```
%This model will show the change in excess pore-water pressure with
%time and temperature changes for energy piles. This will be used
%show how pile capacity, namely, side friction, varies with time.
%Daniel P. Zimmerman
%for completion of the requirements of the Master of Science Degree in
%Civil Engineering
%Advisor: Dr. Arvin Farid, PE
%Start date: May 26, 2012

clear all;clc;

%Inputs
[L,R,Th,Tl,Tmed,Tn,krri,krzi,kzzi,cc,gammasat0,e0,Ec,Es,Gs,Krr,Kzz,Krz,Cp5,Cp10,Cp
15,Cp20,Cp25,Cp30,alphas,alphapile,LL,PL,nu,G,cu,Cc,phip,OCR,years]= DS_Inputs();
```

```
%%%Constants
[W,H,N,M,ccnodes,dr,dz,P,g,dT,dt,Ko,alphast]=Constants(L,cc,phip,OCR);

Told(1:P)=Tn;          Told=Told';    uold(1:P)=0;   Tnew=Told;   sigpr(1:P)=0;
K(1:P)=0;      fs(1:P)=0;      Tfinal(:,1)=Tnew;      TfinalS(:,1)=Tfinal(:,1);

aviobj = avifile('Drilled_Shaft_EPWP_Year_1.avi','compression','Cinepak');
 aviobj.KeyFramePerSec = 0.5;

aviobjt = avifile('Drilled_Shaft_Temp_Year_1.avi','compression','Cinepak');
 aviobjt.KeyFramePerSec = 0.5;

aviobjtt = avifile('Drilled_Shaft_EPWP_Year_2.avi','compression','Cinepak');
 aviobjtt.KeyFramePerSec = 0.5;

aviobjttt = avifile('Drilled_Shaft_Temp_Year_2.avi','compression','Cinepak');
 aviobjttt.KeyFramePerSec = 0.5;

i=13; j=7;
uheat(1:P,1)=0;          sigpr(1:P)=0;   K(1:P)=0;      fs(1:P)=0;

 for y=1:years

 %%%%   SUMMER (Days 1-91(365-455) after HVAC intro)  %%%%

 for w=1:7

   for dd=1:7
    Theatval=40/1344*(6+2*(w-1));
    for ii=((M-1)/2)*N+1:N:(M-1)*N+1
     Told(ii)=Told(ii)+Theatval;
    end

    %%%Water coefficient of thermal expansion and density due to
    %%%current temp.
    [alphah2o,rhow] = watercte(P,Told);

    %%%Initial EPWP, horizontal stress, and void ratio for driven pile
    [e1,gammasat,n]=DS_fet(P,M,N,Cc,gammasat0,dz,e0,rhow,Gs,g);

    %%%New radius upon change in temperature
    [R1]=Pilex(R,alphapile,Told,Tn);

    [uheat]=ctepile(P,Theatval,R1,R,Es,M,N);
```

```
    %%%t is days since drilled shaft install and days since HVAC on.
    t=((w-1)*j)+dd+((y-1)*364);

    uheatt(:,t)=uheat;

%     ealphah2o(t,:)=alphah2o;      erhow(t,:)=rhow;

    %%%Calculation of gammasat and clay density based upon temp
    %%%increase
    [gammasat,rhoc1]=DS_grammasat(P,Gs,e1,rhow,g,alphas,Told,Tn);
%     egammasat(t,:)=gammasat;

    %%%Clay density and specific heat value due to current temp
    [Cpc]=claycon(P,Cp5,Cp10,Cp20,Cp25,Cp30,Told);

    for ii=((M-1)/2)*N+1:N:(M-1)*N+1
     Told(ii)=Told(ii)-Theatval;
    end

    %Conduction Node definition
    [c,d]=
Conduct_Days_HVAC(M,N,R,Krr,Cpc,rhoc1,dr,Kzz,dz,dt,Krz,Told,Theatval,Tn);
    Tnew=(c^-1)*d';      Tdif=Tnew-Told;

    for ii=1:P
     if abs(Tdif(ii))<0.001
       Tdif(ii)=0;
     end
    end

    %%%Permeability and dynamic viscosity
    [muVogel,krriV,kzziV,krziV]=perm(P,Tnew,rhow,krri,kzzi);

    %%%Compressibility, volumetric compressibility, and consolidation
    %%%coefficients
    [avrr,avzz,mvrr,mvzz,CvrriV,CvzziV,CvrziV]=CvrrT_Driv_Days(P,e0,krriV,kzziV,
        rhow,g);

    %%%EPWP due to thermal expansion of clay
    [ucte,alphast]=ctesoil(P,n,Tdif,alphas,alphah2o,mvrr);
    Told=Tnew;      uctet(:,t)=ucte';    TfinalS(:,t)=Told;

    %Consolidation Node definition
    [a,b]=Consol_Days_DS(P,kzzi,M,N,R,dr,CvrriV,CvzziV,dz,dt,CvrziV,uold);
    unew=(a^-1)*b';      unew=unew+uheat+ucte';
```

```
    for d=(M-1)/2:M-2
      for ii=d*N+1
        sigpr(ii)=((gammasat(ii)*((M-1)-(d+1)))+
                  (gammasat(ii)-rhow(ii)*g)*0.5)-unew(ii);
        K(ii)=tand(phip);
        fs(ii)=Ko*sigpr(ii)*K(ii);
      end
    end

     fst=sum(fs(1,337:21:589));
    fsf(:,t)=fst;

    uold=unew;      uexS(:,t)=uold;

  end
 end


for w=8:i
  for dd=1:j
    Theatval=40/1344*(6+2*(13-w));
    for ii=((M-1)/2)*N+1:N:(M-1)*N+1
      Told(ii)=Told(ii)+Theatval;
    end

    %%%Water coefficient of thermal expansion and density due to
    %%%current temp.
    [alphah2o,rhow] = watercte(P,Told);

    %%%Initial EPWP, horizontal stress, and void ratio for driven pile
    [e1,gammasat,n]=DS_fet(P,M,N,Cc,gammasat0,dz,e0,rhow,Gs,g);

    %%%New radius upon change in temperature
    [R1]=Pilex(R,alphapile,Told,Tn);

    [uheat]=ctepile(P,Theatval,R1,R,Es,M,N);

    t=((w-1)*j)+dd+((y-1)*364);

    uheatt(:,t)=uheat;

    %%%Calculation of gammasat and clay density based upon temp
    %%%increase
    [gammasat,rhoc1]=DS_grammasat(P,Gs,e1,rhow,g,alphas,Told,Tn);
%       egammasat(t,:)=gammasat;
```

```
%%%Clay density and specific heat value due to current temp
[Cpc]=claycon(P,Cp5,Cp10,Cp20,Cp25,Cp30,Told);

for ii=((M-1)/2)*N+1:N:(M-1)*N+1
  Told(ii)=Told(ii)-Theatval;
end

%Conduction Node definition
[c,d]=
Conduct_Days_HVAC(M,N,R,Krr,Cpc,rhoc1,dr,Kzz,dz,dt,Krz,Told,Theatval,Tn);
Tnew=(c^-1)*d';      Tdif=Tnew-Told;

for ii=1:P
  if abs(Tdif(ii))<0.001
    Tdif(ii)=0;
  end
end

%%%Permeability and dynamic viscosity
[muVogel,krriV,kzziV,krziV]=perm(P,Tnew,rhow,krri,kzzi);

%%%Compressibility, volumetric compressibility, and consolidation
%%%coefficients
[avrr,avzz,mvrr,mvzz,CvrriV,CvzziV,CvrziV]=CvrrT_Driv_Days(P,e0,krriV,kzziV,
     rhow,g);

%%%EPWP due to thermal expansion of clay
[ucte,alphast]=ctesoil(P,n,Tdif,alphas,alphah2o,mvrr);
Told=Tnew;      uctet(:,t)=ucte';    TfinalS(:,t)=Told;

%Consolidation Node definition
[a,b]=Consol_Days_DS(P,kzzi,M,N,R,dr,CvrriV,CvzziV,dz,dt,CvrziV,uold);
unew=(a^-1)*b';      unew=unew+uheat+ucte';

 for d=(M-1)/2:M-2
  for ii=d*N+1
    sigpr(ii)=((gammasat(ii)*((M-1)-(d+1)))+
              (gammasat(ii)-rhow(ii)*g)*0.5)-unew(ii);
    K(ii)=tand(phip);
    fs(ii)=Ko*sigpr(ii)*K(ii);
  end
end

 fst=sum(fs(1,337:21:589));
fsf(:,t)=fst;
```

```
    uold=unew;      uexS(:,t)=uold;
  end
end


%%%%   FALL  (Days 92-183(456-546) after HVAC intro) %%%%
i=13; j=7;

for w=1:7

  for dd=1:7
    Theatval=40/1344*(6-(w-1));
    for ii=((M-1)/2)*N+1:N:(M-1)*N+1
      Told(ii)=Told(ii)+Theatval;
    end

    %%%Water coefficient of thermal expansion and density due to
    %%%current temp.
    [alphah2o,rhow] = watercte(P,Told);

    %%%Initial EPWP, horizontal stress, and void ratio for driven pile
    [e1,gammasat,n]=DS_fet(P,M,N,Cc,gammasat0,dz,e0,rhow,Gs,g);

    %%%New radius upon change in temperature
    [R1]=Pilex(R,alphapile,Told,Tn);

    [uheat]=ctepile(P,Theatval,R1,R,Es,M,N);

    t=((w-1)*j)+dd+91+((y-1)*364);
    uheatt(:,t)=uheat;

    %%%Calculation of gammasat and clay density based upon temp
    %%%increase
    [gammasat,rhoc1]=DS_grammasat(P,Gs,e1,rhow,g,alphas,Told,Tn);
%       egammasat(t,:)=gammasat;

    %%%Clay density and specific heat value due to current temp
    [Cpc]=claycon(P,Cp5,Cp10,Cp20,Cp25,Cp30,Told);

    for ii=((M-1)/2)*N+1:N:(M-1)*N+1
      Told(ii)=Told(ii)-Theatval;
    end

    %Conduction Node definition
    [c,d]=
Conduct_Days_HVAC(M,N,R,Krr,Cpc,rhoc1,dr,Kzz,dz,dt,Krz,Told,Theatval,Tn);
```

```
    Tnew=(c^-1)*d';      Tdif=Tnew-Told;

    for ii=1:P
     if abs(Tdif(ii))<0.001
       Tdif(ii)=0;
     end
    end

    %%%Permeability and dynamic viscosity
    [muVogel,krriV,kzziV,krziV]=perm(P,Tnew,rhow,krri,kzzi);

    %%%Compressibility, volumetric compressibility, and consolidation
    %%%coefficients

[avrr,avzz,mvrr,mvzz,CvrriV,CvzziV,CvrziV]=CvrrT_Driv_Days(P,e0,krriV,kzziV,rhow
,g);

    %%%EPWP due to thermal expansion of clay
    [ucte,alphast]=ctesoil(P,n,Tdif,alphas,alphah2o,mvrr);
    Told=Tnew;      uctet(:,t)=ucte';    TfinalS(:,t)=Told;

    %Consolidation Node definition
    [a,b]=Consol_Days_DS(P,kzzi,M,N,R,dr,CvrriV,CvzziV,dz,dt,CvrziV,uold);
    unew=(a^-1)*b';      unew=unew+uheat+ucte';

     for d=(M-1)/2:M-2
      for ii=d*N+1
        sigpr(ii)=((gammasat(ii)*((M-1)-(d+1)))+
                  (gammasat(ii)-rhow(ii)*g)*0.5)-unew(ii);
        K(ii)=tand(phip);
        fs(ii)=Ko*sigpr(ii)*K(ii);
      end
    end

     fst=sum(fs(1,337:21:589));
    fsf(:,t)=fst;

    uold=unew;      uexS(:,t)=uold;
  end
 end

 for w=8:i
  for dd=1:j
    Theatval=-((41/1344)*(6-(13-w)));
    for ii=((M-1)/2)*N+1:N:(M-1)*N+1
      Told(ii)=Told(ii)+Theatval;
```

```
    end

    %%%Water coefficient of thermal expansion and density due to
    %%%current temp.
    [alphah2o,rhow] = watercte(P,Told);

    %%%Initial EPWP, horizontal stress, and void ratio for driven pile
    [e1,gammasat,n]=DS_fet(P,M,N,Cc,gammasat0,dz,e0,rhow,Gs,g);

    %%%New radius upon change in temperature
    [R1]=Pilex(R,alphapile,Told,Tn);

    [uheat]=ctepile(P,Theatval,R1,R,Es,M,N);

    t=((w-1)*j)+dd+91+((y-1)*364);
     uheatt(:,t)=uheat;

    [gammasat,rhoc1]=DS_grammasat(P,Gs,e1,rhow,g,alphas,Told,Tn);
%      egammasat(t,:)=gammasat;

    %%%Clay density and specific heat value due to current temp
    [Cpc]=claycon(P,Cp5,Cp10,Cp20,Cp25,Cp30,Told);

    for ii=((M-1)/2)*N+1:N:(M-1)*N+1
      Told(ii)=Told(ii)-Theatval;
    end

    %Conduction Node definition
    [c,d]=
Conduct_Days_HVAC(M,N,R,Krr,Cpc,rhoc1,dr,Kzz,dz,dt,Krz,Told,Theatval,Tn);
    Tnew=(c^-1)*d';      Tdif=Tnew-Told;

    for ii=1:P
      if abs(Tdif(ii))<0.001
        Tdif(ii)=0;
      end
    end

    %%%Permeability and dynamic viscosity
    [muVogel,krriV,kzziV,krziV]=perm(P,Tnew,rhow,krri,kzzi);

    %%%Compressibility, volumetric compressibility, and consolidation
    %%%coefficients
    [avrr,avzz,mvrr,mvzz,CvrriV,CvzziV,CvrziV]=CvrrT_Driv_Days(P,e0,krriV,kzziV,
         rhow,g);
```

```
   %%%EPWP due to thermal expansion of clay
   [ucte,alphast]=ctesoil(P,n,Tdif,alphas,alphah2o,mvrr);
   Told=Tnew;      uctet(:,t)=ucte';    TfinalS(:,t)=Told;

   %Consolidation Node definition
   [a,b]=Consol_Days_DS(P,kzzi,M,N,R,dr,CvrriV,CvzziV,dz,dt,CvrziV,uold);
   unew=(a^-1)*b';      unew=unew+uheat+ucte';

    for d=(M-1)/2:M-2
     for ii=d*N+1
       sigpr(ii)=((gammasat(ii)*((M-1)-(d+1)))+
                  (gammasat(ii)-rhow(ii)*g)*0.5)-unew(ii);
       K(ii)=tand(phip);
       fs(ii)=Ko*sigpr(ii)*K(ii);
     end
   end

    fst=sum(fs(1,337:21:589));
   fsf(:,t)=fst;

   uold=unew;      uexS(:,t)=uold;
  end
end


%%%%   WINTER (Days 184-275(547-637) after HVAC intro)  %%%%
i=13; j=7;

for w=1:7

  for dd=1:7
   Theatval=-((41/1344)*(6+2*(w-1)));
   for ii=((M-1)/2)*N+1:N:(M-1)*N+1
     Told(ii)=Told(ii)+Theatval;
   end

   %%%Water coefficient of thermal expansion and density due to
   %%%current temp.
   [alphah2o,rhow] = watercte(P,Told);

   %%%Initial EPWP, horizontal stress, and void ratio for driven pile
   [e1,gammasat,n]=DS_fet(P,M,N,Cc,gammasat0,dz,e0,rhow,Gs,g);

   %%%New radius upon change in temperature
   [R1]=Pilex(R,alphapile,Told,Tn);
```

```
    [uheat]=ctepile(P,Theatval,R1,R,Es,M,N);

    t=((w-1)*j)+dd+182+((y-1)*364);
    uheatt(:,t)=uheat;

    [gammasat,rhoc1]=DS_grammasat(P,Gs,e1,rhow,g,alphas,Told,Tn);
%     egammasat(t,:)=gammasat;

    %%%Clay density and specific heat value due to current temp
    [Cpc]=claycon(P,Cp5,Cp10,Cp20,Cp25,Cp30,Told);

    for ii=((M-1)/2)*N+1:N:(M-1)*N+1
      Told(ii)=Told(ii)-Theatval;
    end

    %Conduction Node definition
    [c,d]=
Conduct_Days_HVAC(M,N,R,Krr,Cpc,rhoc1,dr,Kzz,dz,dt,Krz,Told,Theatval,Tn);
    Tnew=(c^-1)*d';     Tdif=Tnew-Told;

    for ii=1:P
      if abs(Tdif(ii))<0.001
        Tdif(ii)=0;
      end
    end

    %%%Permeability and dynamic viscosity
    [muVogel,krriV,kzziV,krziV]=perm(P,Tnew,rhow,krri,kzzi);

    %%%Compressibility, volumetric compressibility, and consolidation
    %%%coefficients
    [avrr,avzz,mvrr,mvzz,CvrriV,CvzziV,CvrziV]=CvrrT_Driv_Days(P,e0,krriV,kzziV,
        rhow,g);

    %%%EPWP due to thermal expansion of clay
    [ucte,alphast]=ctesoil(P,n,Tdif,alphas,alphah2o,mvrr);
    Told=Tnew;     uctet(:,t)=ucte';   TfinalS(:,t)=Told;

    %Consolidation Node definition
    [a,b]=Consol_Days_DS(P,kzzi,M,N,R,dr,CvrriV,CvzziV,dz,dt,CvrziV,uold);
    unew=(a^-1)*b';     unew=unew+uheat+ucte';

    for d=(M-1)/2:M-2
      for ii=d*N+1
        sigpr(ii)=((gammasat(ii)*((M-1)-(d+1)))+
                  (gammasat(ii)-rhow(ii)*g)*0.5)-unew(ii);
```

```
        K(ii)=tand(phip);
        fs(ii)=Ko*sigpr(ii)*K(ii);
       end
     end

      fst=sum(fs(1,337:21:589));
     fsf(:,t)=fst;

     uold=unew;      uexS(:,t)=uold;
   end
 end

 for w=8:i
   for dd=1:j
     Theatval=-((41/1344)*(6+2*(13-w)));
     for ii=((M-1)/2)*N+1:N:(M-1)*N+1
       Told(ii)=Told(ii)+Theatval;
     end

     %%%Water coefficient of thermal expansion and density due to
     %%%current temp.
     [alphah2o,rhow] = watercte(P,Told);

     %%%Initial EPWP, horizontal stress, and void ratio for driven pile
     [e1,gammasat,n]=DS_fet(P,M,N,Cc,gammasat0,dz,e0,rhow,Gs,g);

     %%%New radius upon change in temperature
     [R1]=Pilex(R,alphapile,Told,Tn);

     [uheat]=ctepile(P,Theatval,R1,R,Es,M,N);

     t=((w-1)*j)+dd+182+((y-1)*364);
     uheatt(:,t)=uheat;

     [gammasat,rhoc1]=DS_grammasat(P,Gs,e1,rhow,g,alphas,Told,Tn);
%       egammasat(t,:)=gammasat;

     %%%Clay density and specific heat value due to current temp
     [Cpc]=claycon(P,Cp5,Cp10,Cp20,Cp25,Cp30,Told);

     for ii=((M-1)/2)*N+1:N:(M-1)*N+1
       Told(ii)=Told(ii)-Theatval;
     end

     %Conduction Node definition
```

```
    [c,d]=
Conduct_Days_HVAC(M,N,R,Krr,Cpc,rhoc1,dr,Kzz,dz,dt,Krz,Told,Theatval,Tn);
    Tnew=(c^-1)*d';      Tdif=Tnew-Told;

    for ii=1:P
     if abs(Tdif(ii))<0.001
       Tdif(ii)=0;
     end
    end

    %%%Permeability and dynamic viscosity
    [muVogel,krriV,kzziV,krziV]=perm(P,Tnew,rhow,krri,kzzi);

    %%%Compressibility, volumetric compressibility, and consolidation
    %%%coefficients
    [avrr,avzz,mvrr,mvzz,CvrriV,CvzziV,CvrziV]=CvrrT_Driv_Days(P,e0,krriV,kzziV,
         rhow,g);

    %%%EPWP due to thermal expansion of clay
    [ucte,alphast]=ctesoil(P,n,Tdif,alphas,alphah2o,mvrr);
    Told=Tnew;      uctet(:,t)=ucte';    TfinalS(:,t)=Told;

    %Consolidation Node definition
    [a,b]=Consol_Days_DS(P,kzzi,M,N,R,dr,CvrriV,CvzziV,dz,dt,CvrziV,uold);
    unew=(a^-1)*b';      unew=unew+uheat+ucte';

    for d=(M-1)/2:M-2
     for ii=d*N+1
       sigpr(ii)=((gammasat(ii)*((M-1)-(d+1)))+
                  (gammasat(ii)-rhow(ii)*g)*0.5)-unew(ii);
       K(ii)=tand(phip);
       fs(ii)=Ko*sigpr(ii)*K(ii);
     end
    end

     fst=sum(fs(1,337:21:589));
    fsf(:,t)=fst;

    uold=unew;      uexS(:,t)=uold;

   end
 end

 %%%%   SPRING (Days 276-364(638-728) after HVAC intro)  %%%%
 i=13; j=7;
```

```
 for w=1:7

  for dd=1:7
   Theatval=-((41/1344)*(6-(w-1)));
   for ii=((M-1)/2)*N+1:N:(M-1)*N+1
    Told(ii)=Told(ii)+Theatval;
   end

   %%%Water coefficient of thermal expansion and density due to
   %%%current temp.
   [alphah2o,rhow] = watercte(P,Told);

   %%%Initial EPWP, horizontal stress, and void ratio for driven pile
   [e1,gammasat,n]=DS_fet(P,M,N,Cc,gammasat0,dz,e0,rhow,Gs,g);

   %%%New radius upon change in temperature
   [R1]=Pilex(R,alphapile,Told,Tn);

   [uheat]=ctepile(P,Theatval,R1,R,Es,M,N);

   t=((w-1)*j)+dd+273+((y-1)*364);
   uheatt(:,t)=uheat;

   [gammasat,rhoc1]=DS_grammasat(P,Gs,e1,rhow,g,alphas,Told,Tn);
%     egammasat(t,:)=gammasat;

   %%%Clay density and specific heat value due to current temp
   [Cpc]=claycon(P,Cp5,Cp10,Cp20,Cp25,Cp30,Told);

   for ii=((M-1)/2)*N+1:N:(M-1)*N+1
    Told(ii)=Told(ii)-Theatval;
   end

   %Conduction Node definition
   [c,d]=
Conduct_Days_HVAC(M,N,R,Krr,Cpc,rhoc1,dr,Kzz,dz,dt,Krz,Told,Theatval,Tn);
   Tnew=(c^-1)*d';     Tdif=Tnew-Told;

   for ii=1:P
    if abs(Tdif(ii))<0.001
     Tdif(ii)=0;
    end
   end

   %%%Permeability and dynamic viscosity
   [muVogel,krriV,kzziV,krziV]=perm(P,Tnew,rhow,krri,kzzi);
```

```
    %%%Compressibility, volumetric compressibility, and consolidation
    %%%coefficients
    [avrr,avzz,mvrr,mvzz,CvrriV,CvzziV,CvrziV]=CvrrT_Driv_Days(P,e0,krriV,kzziV,
        rhow,g);

    %%%EPWP due to thermal expansion of clay
    [ucte,alphast]=ctesoil(P,n,Tdif,alphas,alphah2o,mvrr);
    Told=Tnew;      uctet(:,t)=ucte';    TfinalS(:,t)=Told;

    %Consolidation Node definition
    [a,b]=Consol_Days_DS(P,kzzi,M,N,R,dr,CvrriV,CvzziV,dz,dt,CvrziV,uold);
    unew=(a^-1)*b';      unew=unew+uheat+ucte';

     for d=(M-1)/2:M-2
      for ii=d*N+1
        sigpr(ii)=((gammasat(ii)*((M-1)-(d+1)))+
                  (gammasat(ii)-rhow(ii)*g)*0.5)-unew(ii);
        K(ii)=tand(phip);
        fs(ii)=Ko*sigpr(ii)*K(ii);
      end
    end

     fst=sum(fs(1,337:21:589));
    fsf(:,t)=fst;

    uold=unew;      uexS(:,t)=uold;
  end
end

for w=8:i
  for dd=1:j
    Theatval=41/1344*(6-(13-w));
    for ii=((M-1)/2)*N+1:N:(M-1)*N+1
      Told(ii)=Told(ii)+Theatval;
    end

    %%%Water coefficient of thermal expansion and density due to
    %%%current temp.
    [alphah2o,rhow] = watercte(P,Told);

    %%%Initial EPWP, horizontal stress, and void ratio for driven pile
    [e1,gammasat,n]=DS_fet(P,M,N,Cc,gammasat0,dz,e0,rhow,Gs,g);

    %%%New radius upon change in temperature
    [R1]=Pilex(R,alphapile,Told,Tn);
```

```
    [uheat]=ctepile(P,Theatval,R1,R,Es,M,N);

    t=((w-1)*j)+dd+273+((y-1)*364);
    uheatt(:,t)=uheat;

    [gammasat,rhoc1]=DS_grammasat(P,Gs,e1,rhow,g,alphas,Told,Tn);
%     egammasat(t,:)=gammasat;

    %%%Clay density and specific heat value due to current temp
    [Cpc]=claycon(P,Cp5,Cp10,Cp20,Cp25,Cp30,Told);

    for ii=((M-1)/2)*N+1:N:(M-1)*N+1
     Told(ii)=Told(ii)-Theatval;
    end

    %Conduction Node definition
    [c,d]=
Conduct_Days_HVAC(M,N,R,Krr,Cpc,rhoc1,dr,Kzz,dz,dt,Krz,Told,Theatval,Tn);
    Tnew=(c^-1)*d';     Tdif=Tnew-Told;

    for ii=1:P
     if abs(Tdif(ii))<0.001
       Tdif(ii)=0;
     end
    end

    %%%Permeability and dynamic viscosity
    [muVogel,krriV,kzziV,krziV]=perm(P,Tnew,rhow,krri,kzzi);

    %%%Compressibility, volumetric compressibility, and consolidation
    %%%coefficients
    [avrr,avzz,mvrr,mvzz,CvrriV,CvzziV,CvrziV]=CvrrT_Driv_Days(P,e0,krriV,kzziV,
        rhow,g);

    %%%EPWP due to thermal expansion of clay
    [ucte,alphast]=ctesoil(P,n,Tdif,alphas,alphah2o,mvrr);
    Told=Tnew;     uctet(:,t)=ucte';   TfinalS(:,t)=Told;

    %Consolidation Node definition
    [a,b]=Consol_Days_DS(P,kzzi,M,N,R,dr,CvrriV,CvzziV,dz,dt,CvrziV,uold);
    unew=(a^-1)*b';     unew=unew+uheat+ucte';

    for d=(M-1)/2:M-2
     for ii=d*N+1
       sigpr(ii)=((gammasat(ii)*((M-1)-(d+1)))+
```

```
                    (gammasat(ii)-rhow(ii)*g)*0.5)-unew(ii);
          K(ii)=tand(phip);
          fs(ii)=Ko*sigpr(ii)*K(ii);
        end
      end

       fst=sum(fs(1,337:21:589));
      fsf(:,t)=fst;

      uold=unew;      uexS(:,t)=uold;
    end
  end
end

  ff=1:10:t;
  pp=fsf(:,1:10:t);

  plot(ff,pp,':*');

  text(1,290,' \leftarrow Begin HVAC','Rotation',0.0)
  text(1,280,' \leftarrow Summer, Year 1','Rotation',0.0)
  text(91,260,' \leftarrow Fall, Year 1','Rotation',90.0)
  text(140,260,' \leftarrow Soil Cooling','Rotation',90.0)
  text(183,260,' \leftarrow Winter, Year 1','Rotation',90.0)
  text(274,260,' \leftarrow Spring, Year 1','Rotation',90.0)
  text(323,260,' \leftarrow Soil Heating','Rotation',90.0)
  text(365,260,' \leftarrow Summer, Year 2','Rotation',90.0)
  text(419,260,' \leftarrow Soil Cooling','Rotation',90.0)
  text(456,260,' \leftarrow Fall, Year 2','Rotation',90.0)
  text(547,260,' \leftarrow Winter, Year 2','Rotation',90.0)
  text(687,260,' \leftarrow Soil Heating','Rotation',90.0)
  text(638,260,' \leftarrow Spring, Year 2','Rotation',90.0)
  xlabel('Elapsed Time, Days', 'FontSize',24)
  ylabel('Unit Friction (kN/m)','FontSize',24)
  title({'Unit Friction Values at Depth, After HVAC'},'FontSize',24)


fig1=figure;
for k=1:10:371
  for ii=1:M
    for jj=1:N
      r(ii,jj) = (jj-1)*dr;
      z(ii,jj) = (ii-1)*dz;
      uplot(ii,jj)=uexS((ii-1)*N+jj,k);

    end
```

```
  end

  contourf(uplot,9,'b');
  axis ([1 N*dr 1 M*dz+1]);

  caxis([-5 7]);
  CMRmap=[0 0 0;.15 .15 .5;.3 .15 .75;.6 .2 .50;1 .25 .15;.9 .5 0;.9 .75 .1;.9 .9 .5;1 1 1];
  colormap(CMRmap)
  colorbar
  xlabel('Distance from Drilled Shaft (m)', 'FontSize',14)
  ylabel('Depth (m)','FontSize',14)
  title({'EPWP: Number of Days Elapsed: ',int2str(k)},'FontSize',18)%,
  drawnow
  hold on
  pause(2);
  aviobj = addframe(aviobj,gcf);
end

aviobj = close(aviobj);
fig2=figure;
for k=1:10:371
  for ii=1:M
    for jj=1:N
      r(ii,jj) = (jj-1)*dr;
      z(ii,jj) = (ii-1)*dz;
      Tplot(ii,jj)=TfinalS((ii-1)*N+jj,k);

    end
  end

  contourf(Tplot,9, 'b');
  axis ([1 N*dr 1 M*dz+1]);

  caxis([7 52]);
  CMRmap=[0 0 0;.15 .15 .5;.3 .15 .75;.6 .2 .50;1 .25 .15;.9 .5 0;.9 .75 .1;.9 .9 .5;1 1 1];
  colormap(CMRmap)
  colorbar;
  xlabel('Distance from Drilled Shaft (m)', 'FontSize',14)
  ylabel('Depth (m)','FontSize',14)
  title({'Temperature: Number of Days Elapsed: ',int2str(k)},'FontSize',18)
  drawnow
  hold on
  pause(2);
  aviobjt = addframe(aviobjt,gcf);

end
```

```
aviobjt = close(aviobjt);
fig3=figure;
for k=371:10:t
  for ii=1:M
    for jj=1:N
      r(ii,jj) = (jj-1)*dr;
      z(ii,jj) = (ii-1)*dz;
      uplot(ii,jj)=uexS((ii-1)*N+jj,k);

    end
  end

  contourf(uplot,9,'b');
  axis ([1 N*dr 1 M*dz+1]);

  caxis([-5 7]);
  CMRmap=[0 0 0;.15 .15 .5;.3 .15 .75;.6 .2 .50;1 .25 .15;.9 .5 0;.9 .75 .1;.9 .9 .5;1 1 1];
  colormap(CMRmap)
  colorbar;
  xlabel('Distance from Drilled Shaft (m)', 'FontSize',14)
  ylabel('Depth (m)','FontSize',14)
  title({'EPWP: Number of Days Elapsed: ',int2str(k)},'FontSize',18)%,
  drawnow
  hold on
  pause(2);
  aviobjtt = addframe(aviobjtt,gcf);
end

aviobjtt = close(aviobjtt);
fig4=figure;
for k=371:10:t
  for ii=1:M
    for jj=1:N
      r(ii,jj) = (jj-1)*dr;
      z(ii,jj) = (ii-1)*dz;
      Tplot(ii,jj)=TfinalS((ii-1)*N+jj,k);

    end
  end

  contourf(Tplot,9, 'b');
  axis ([1 N*dr 1 M*dz+1]);

  caxis([7 52]);
  CMRmap=[0 0 0;.15 .15 .5;.3 .15 .75;.6 .2 .50;1 .25 .15;.9 .5 0;.9 .75 .1;.9 .9 .5;1 1 1];
```

```
  colormap(CMRmap)
  colorbar;
  xlabel('Distance from Drilled Shaft (m)', 'FontSize',14)
  ylabel('Depth (m)','FontSize',14)
  title({'Temperature: Number of Days Elapsed: ',int2str(k)},'FontSize',18)
  drawnow
  hold on
  pause(2);
  aviobjttt = addframe(aviobjttt,gcf);

end

aviobjttt = close(aviobjttt);
```

APPENDIX C

APPENDIX C: MODEL DATA at 5 m, 10 m, and 15 m

Variations of Temperature and EPWP at Depths of 5 m, 10 m, and 15 m at Various Lateral Distances from a Driven Energy Pile

This section presents model results at various lateral distances (as indicated in Table 5.1) from the pile face. These results do not contain additional information to the results presented above; rather, the information is presented here to show how EPWP and temperature vary by lateral distance from the pile instead of by depth. The figures are grouped by depth.

Variations of Temperature and EPWP at a Depth of 5 m

The temperatures presented in Figures C.1 and C.2 show that the highest and lowest extremes occur at the pile face. The peak temperature at the pile face is slightly lower for the transient ground-surface case. The temperature of the pile is closer to 14 °C when HVAC is introduced. As the distance from the pile increases, the range of variations in temperature decreases and occurs later. Transient ground-surface temperatures appear to only slightly penetrate to this depth.

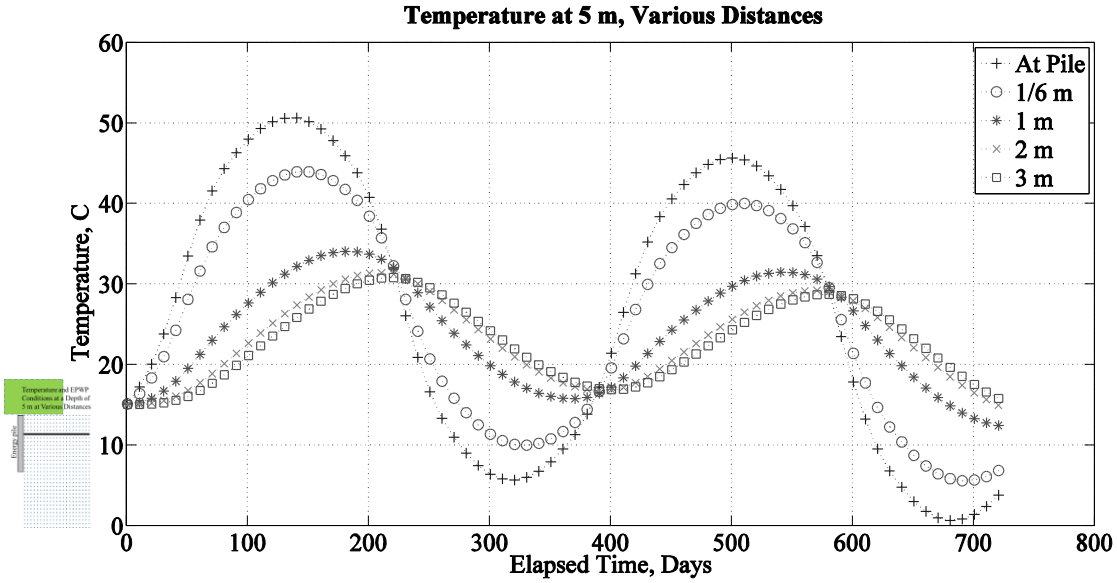

Figure C.1. Temperature values at a depth of 5 m at various distances from the pile, from the time of pile installation to the end of the model run. The ground-surface temperature is a constant 15 °C.

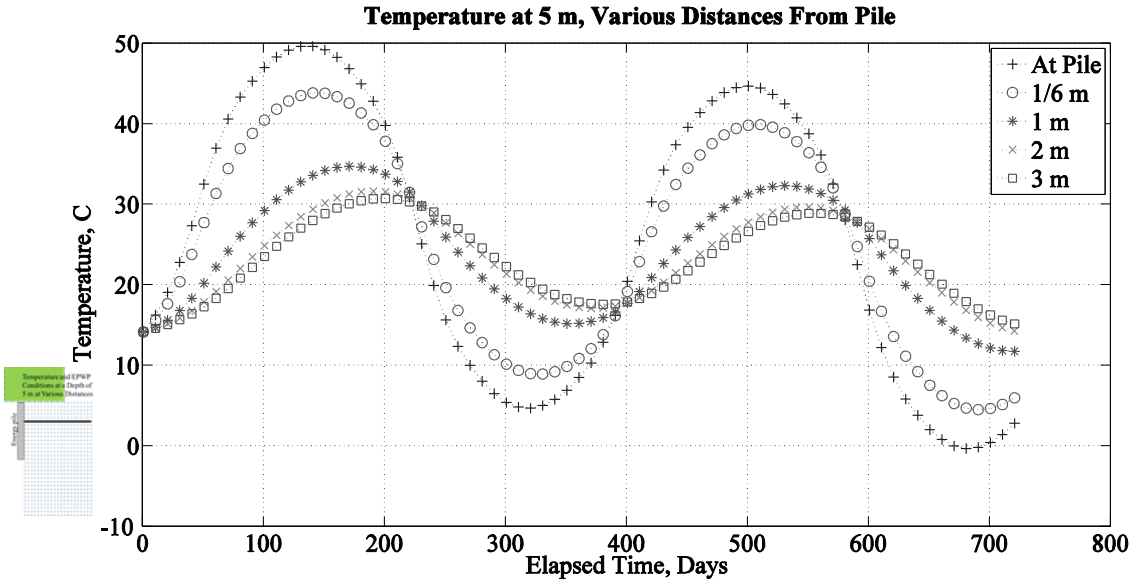

Figure C.2. Temperature values at a depth of 5 m at various distances from the pile, from the time of pile installation to the end of the model run, with transient ground-surface temperatures.

Figures C.3 and C.4 and Figures C.11 and C.12 present EPWP data at various lateral distances from the pile at a depth of 5 m and 10 m below the ground surface, respectively. Figures C.3 and C.4 show that transient ground-surface temperatures

minimally affect EPWP values at depths below 5 m. Figures C.11 and C.12 are very similar to Figures C.3 and C.4.

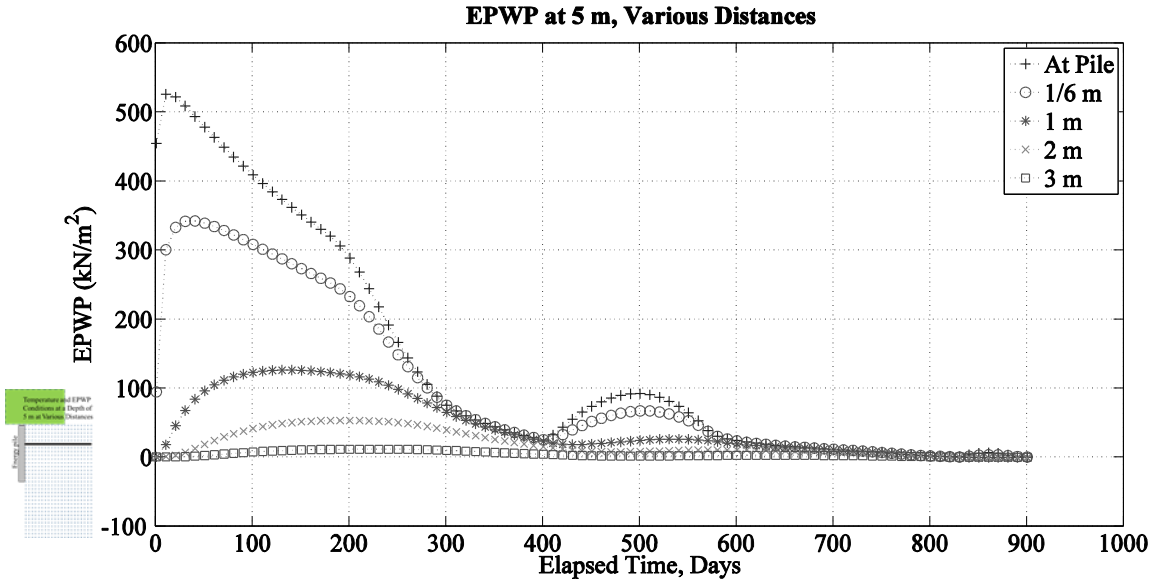

Figure C.3. EPWP at a depth of 5 m at the various distances from the pile, from the time of pile installation to the end of the model run. The ground-surface temperature is a constant 15 °C.

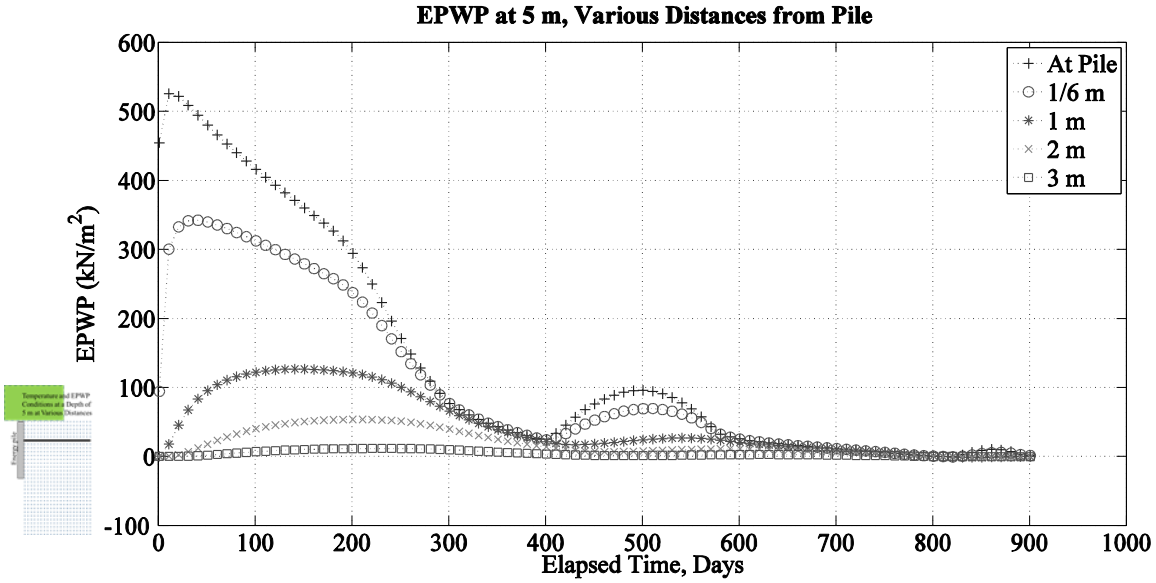

Figure C.4. EPWP at a depth of 5 m at various distances from the pile, from the time of pile installation to the end of the model run, with transient ground-surface temperatures.

As was the case for EPWP values at depths of 5 m, 10 m, and 15 m, as seen in Figures C.3, C.11, and C.19, the EPWP differential presented at these same depths in Figures C.5, C.13 and C.21 are very similar. As was the case for the EPWP values, the differential EPWP values presented in Figures C.6 and C.14 are very similar but slightly lower in value at 15 m, as seen in Figure C.22. The absolute value of the differential at all three depths is greatest at the pile face and decreases with increasing lateral distance away from the pile. The differential only becomes positive for lateral distances less than 1 m away from the pile.

There are differences between the differential values with and without transient ground-surface temperatures. The peak negative values in Figure C.6 are approximately 20 kN/m^2 higher for the differential values next to and near the pile. At a lateral distance of 1 m, the difference is negligible. The peak positive value on the pile face after Day 500 for the variable ground-surface temperatures is slightly lower in Figure C.6 than the one

for a constant 15 ºC ground-surface temperature in Figure C.5, and the peak positive differential value at the pile after Day 860 is slightly greater.

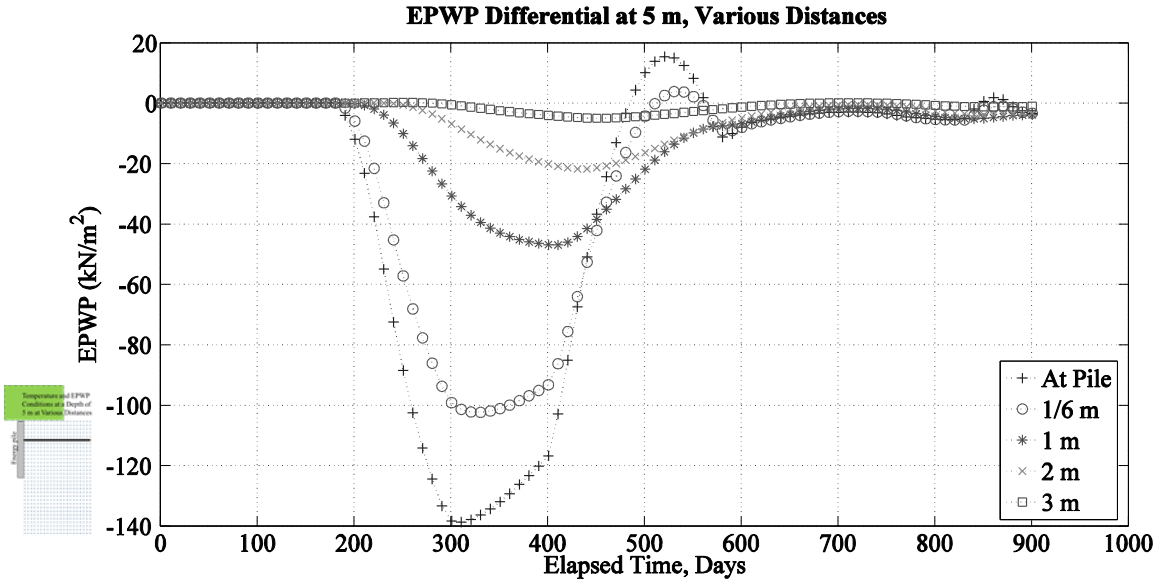

Figure C.5. EPWP differential between model runs with and without HVAC introduction, at a depth of 5 m at various lateral distances from the pile surface. The ground-surface temperature is a constant 15 °C.

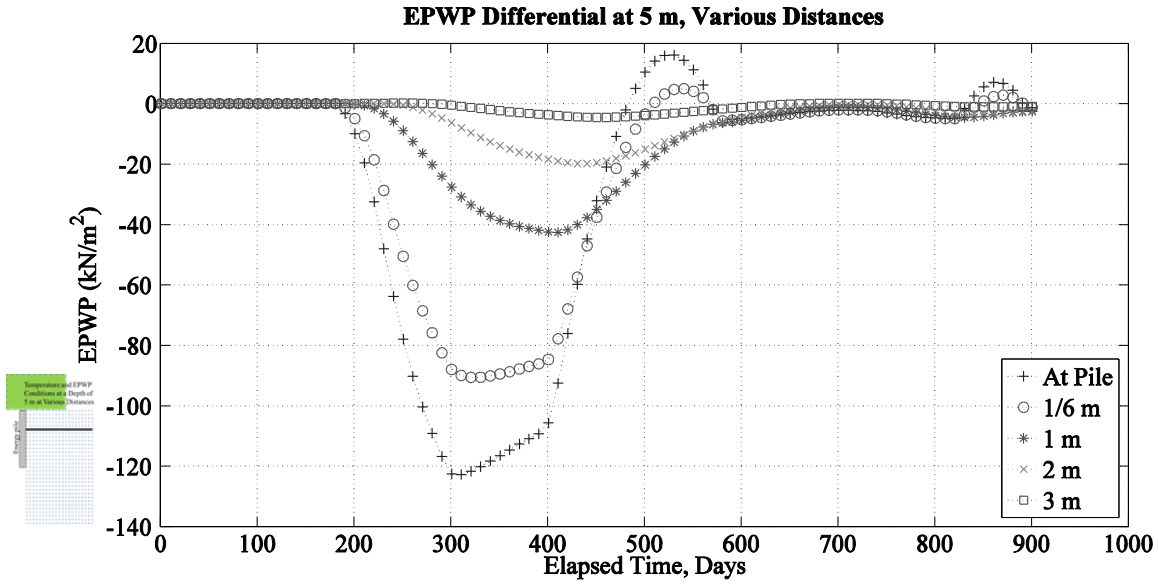

Figure C.6. EPWP differential between model runs with and without HVAC introduction, at a depth of 5 m at various lateral distances from the pile surface, with transient ground-surface temperatures.

Figures C.7 and C.8, Figures C.15 and C.16, and Figures C.22 and C.23 present the normalized EPWP at depths of 5 m, 10 m, and 15 m below the ground surface at various lateral distances from the pile face, respectively. It is easy to see the effects that the distance to the pile has on the time to reach the peak EPWP and how the EPWP dissipates differently at each distance in these figures.

The differences between Figures C.7 and C.8 are minimal.

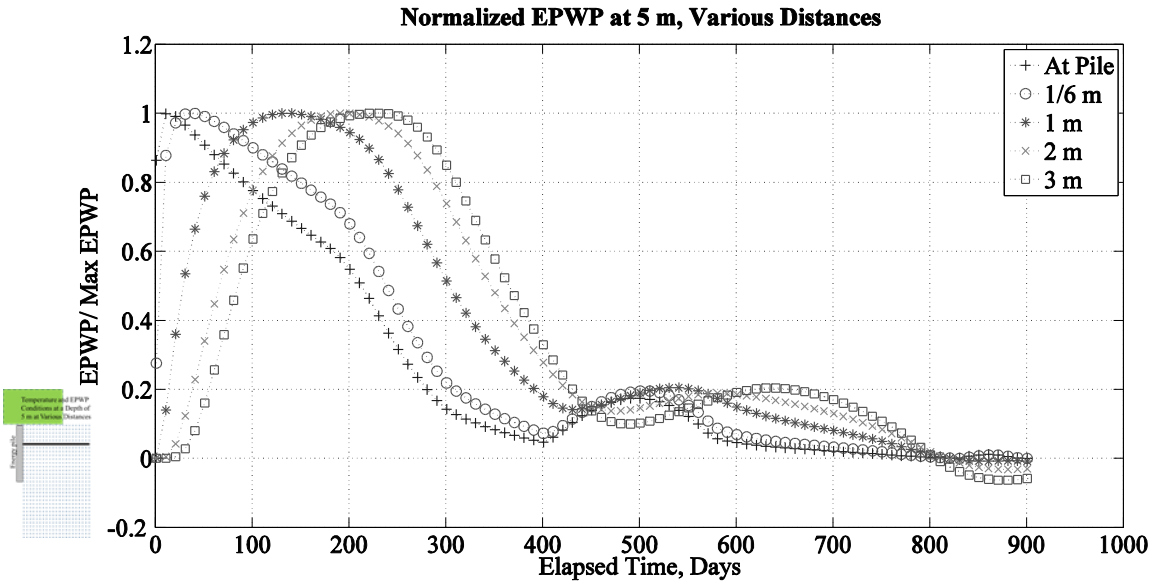

Figure C.7. EPWP, normalized to the peak EPWP, at a depth of 5 m at various lateral distances from the pile surface, from the time of pile installation to the end of the model run. The ground-surface temperature is a constant 15 °C.

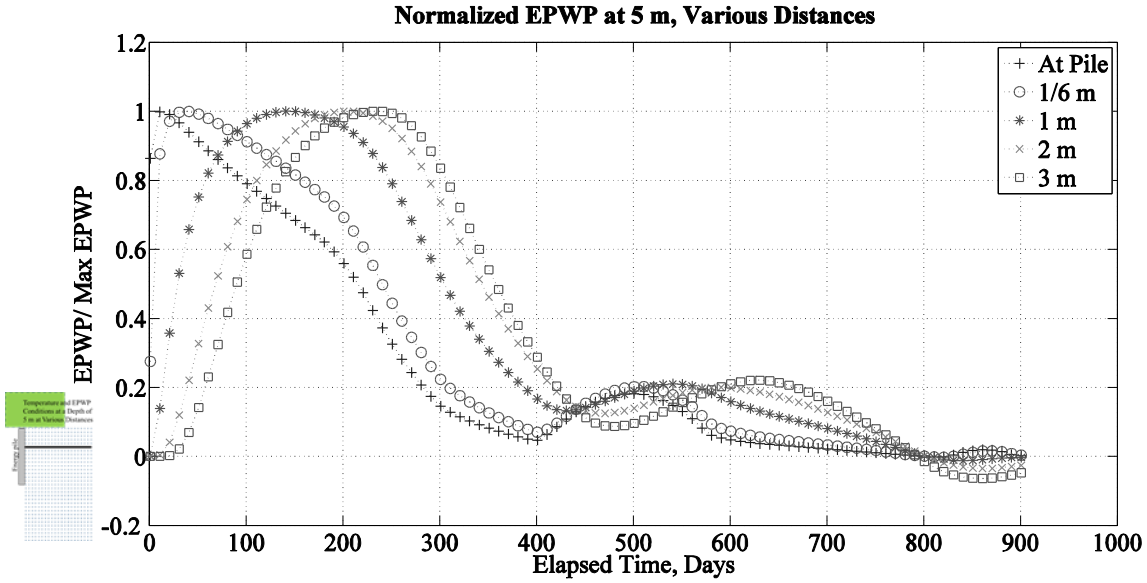

Figure C.8. EPWP, normalized to the peak EPWP, at a depth of 5 m at various lateral distances from the pile surface, from the time of pile installation to the end of the model run, with transient ground-surface temperatures.

Variations of Temperature and EPWP at a Depth of 10 m

The temperature values shown in Figures C.9 and C.10 are very similar to the values shown in Figures C.1 and C.2.

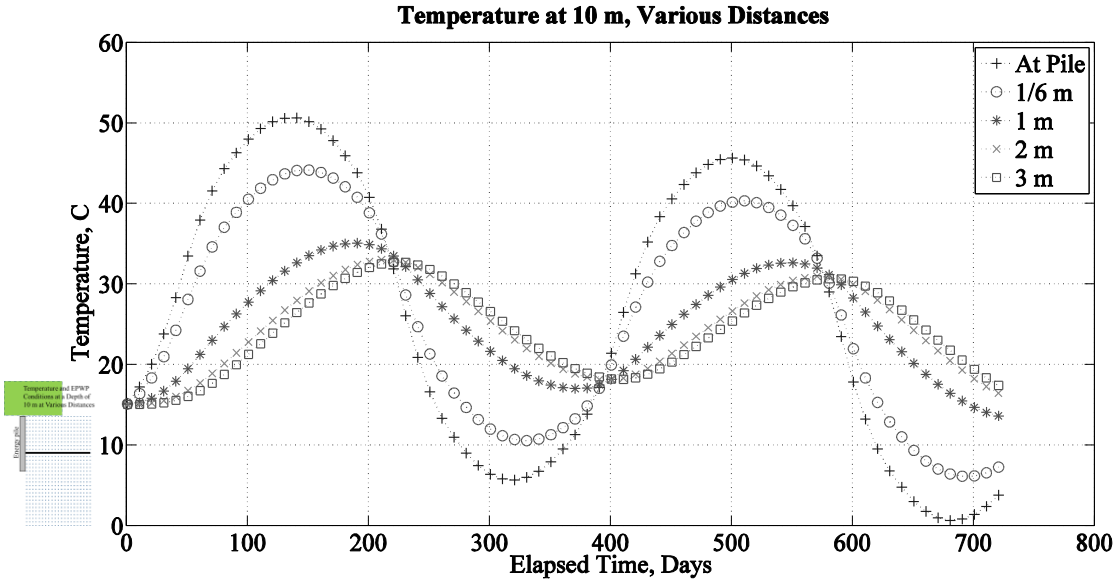

Figure C.9. Temperature values at a depth of 10 m at various distances from the pile, from the time of pile installation to the end of the model run. The ground-surface temperature is a constant 15 °C.

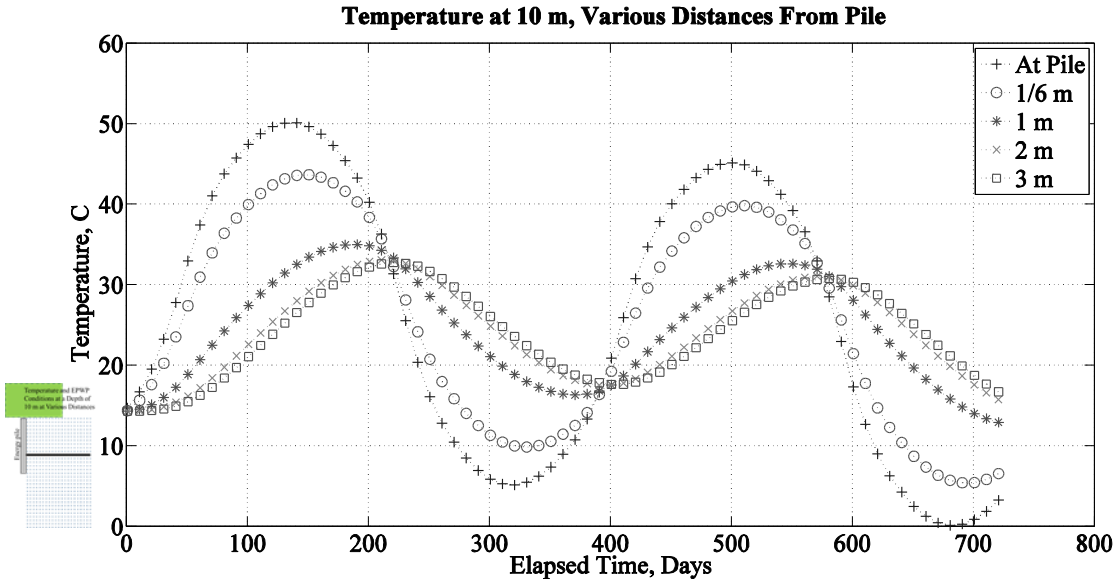

Figure C.10. Temperature values at a depth of 10 m at various distances from the pile, from the time of pile installation to the end of the model run, with transient ground-surface temperatures.

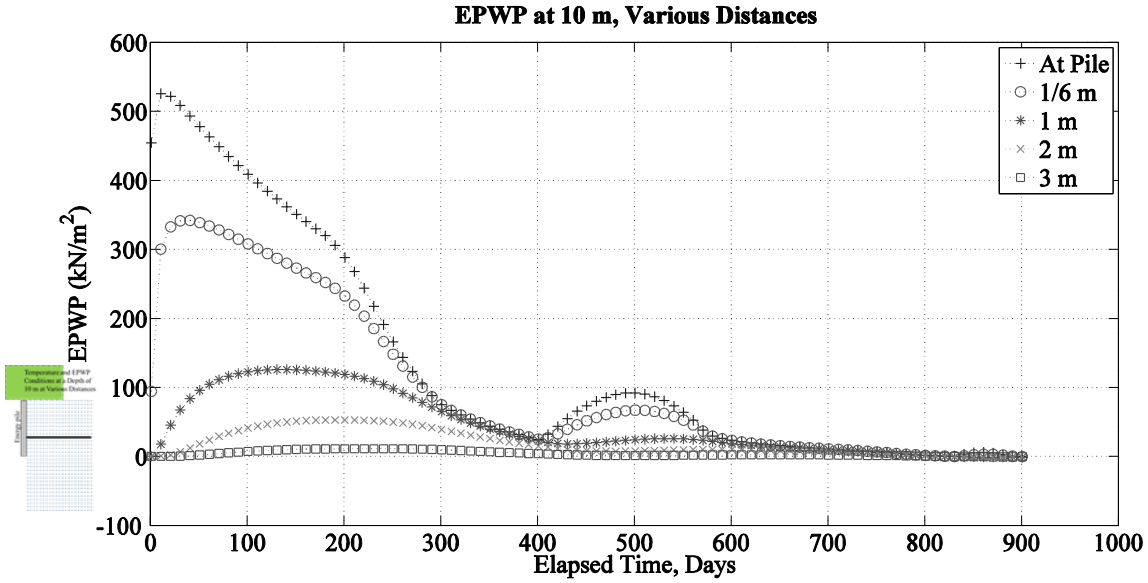

Figure C.11. EPWP at a depth of 10 m at various distances from the pile, from the time of pile installation to the end of the model run. The ground-surface temperature is a constant 15 °C.

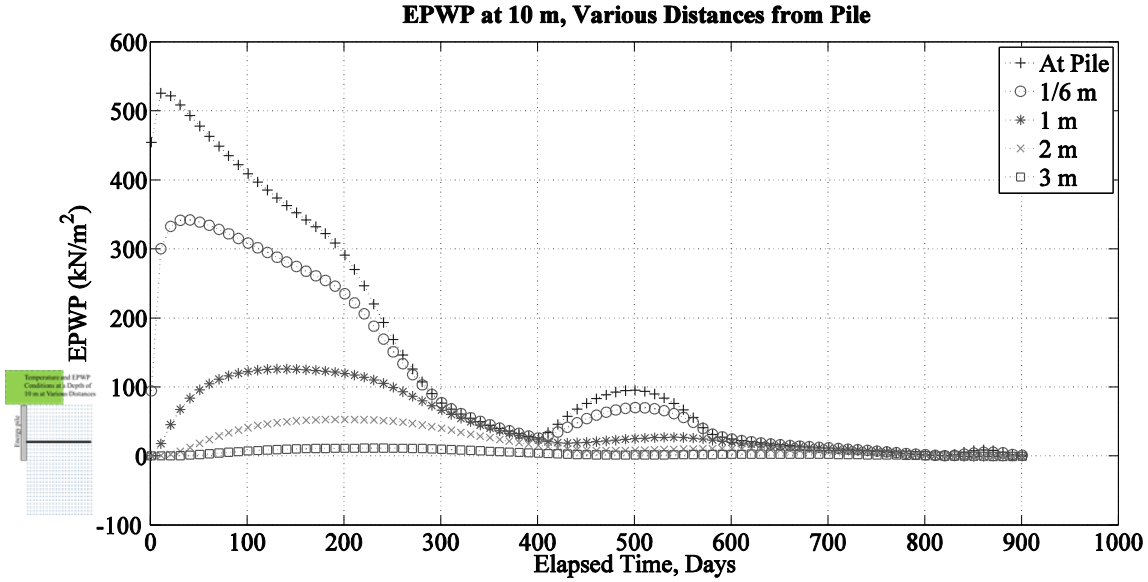

Figure C.12. EPWP at a depth of 10 m at various distances from the pile, from the time of pile installation to the end of the model run, with transient ground-surface temperatures.

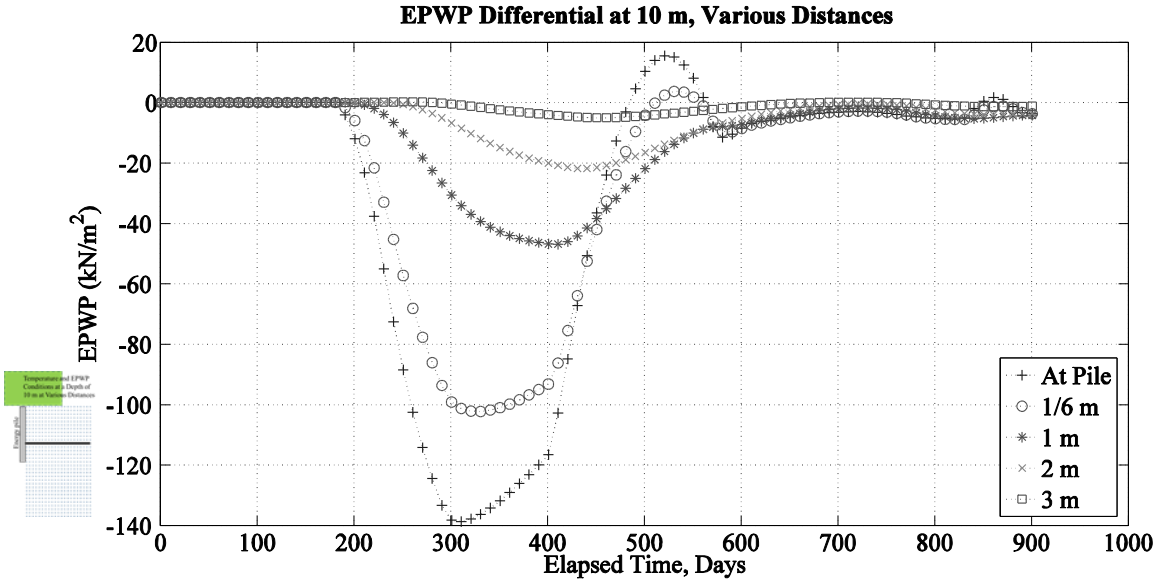

Figure C.13. EPWP differential between model runs with and without HVAC introduction, at a depth of 10 m at various lateral distances from the pile surface. The ground-surface temperature is a constant 15 °C.

The differences between Figure C.13 and Figure C.14 are negligible with the exception of the spike at the pile around Day 860. Figures C.5 and C.13 are very similar to each other.

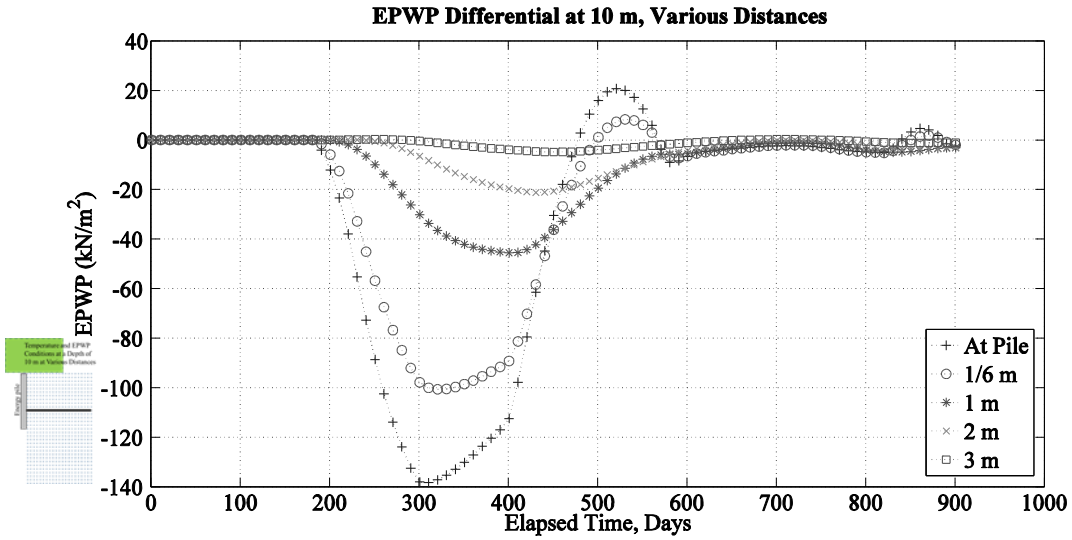

Figure C.14. EPWP differential between model runs with and without HVAC introduction, at a depth of 10 m at various lateral distances from the pile surface, from the time of pile installation to the end of the model run, with transient ground-surface temperatures.

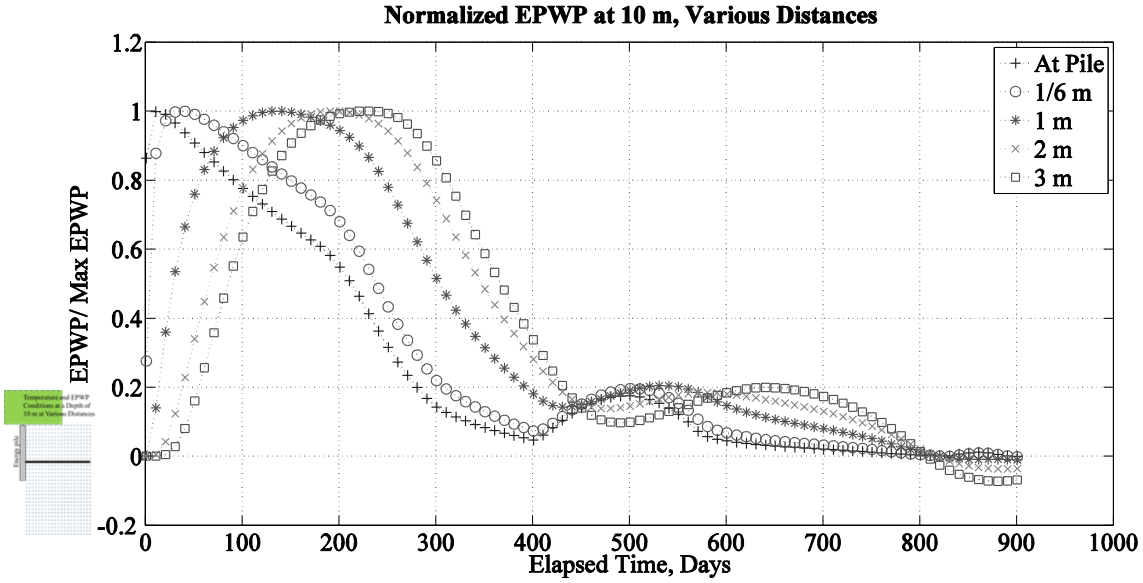

Figure C.15. EPWP, normalized to the peak EPWP, at a depth of 10 m at various lateral distances from the pile surface, from the time of pile installation to the end of the model run. The ground-surface temperature is a constant 15 °C.

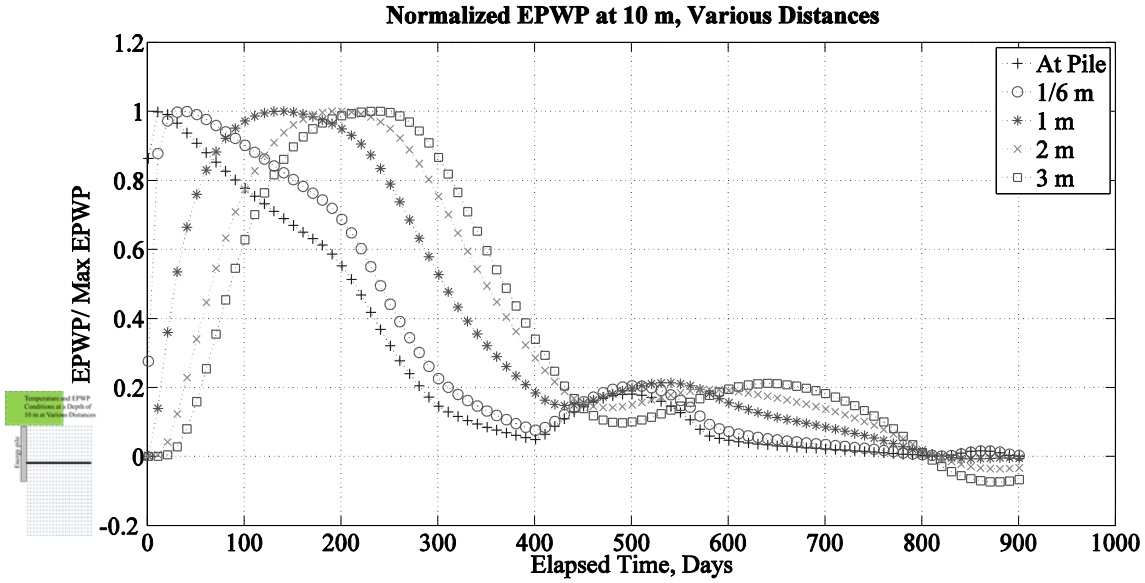

Figure C.16. EPWP, normalized to the peak EPWP, at a depth of 10 m at various lateral distances from the pile surface, from the time of pile installation to the end of the model run, with transient ground-surface temperatures.

Variations of Temperature and EPWP at a Depth of 15 m

The temperatures shown in Figures C.17 and C.18 are similar to those in Figures C.1, C.2, C.9, and C.10 at the pile face, but are lower for the other corresponding lateral distances from the pile, due to their proximity to the soil below the pile which remains at or near 15 °C.

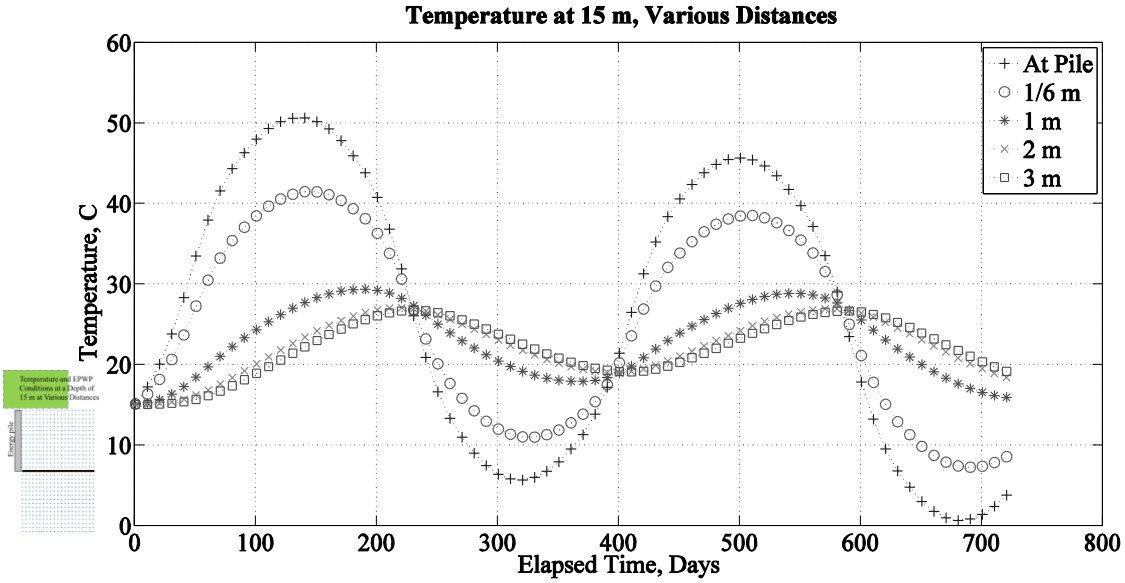

Figure C.17. Temperature values at a depth of 15 m at various distances from the pile, from the time of pile installation to the end of the model run. The ground-surface temperature is a constant 15 °C.

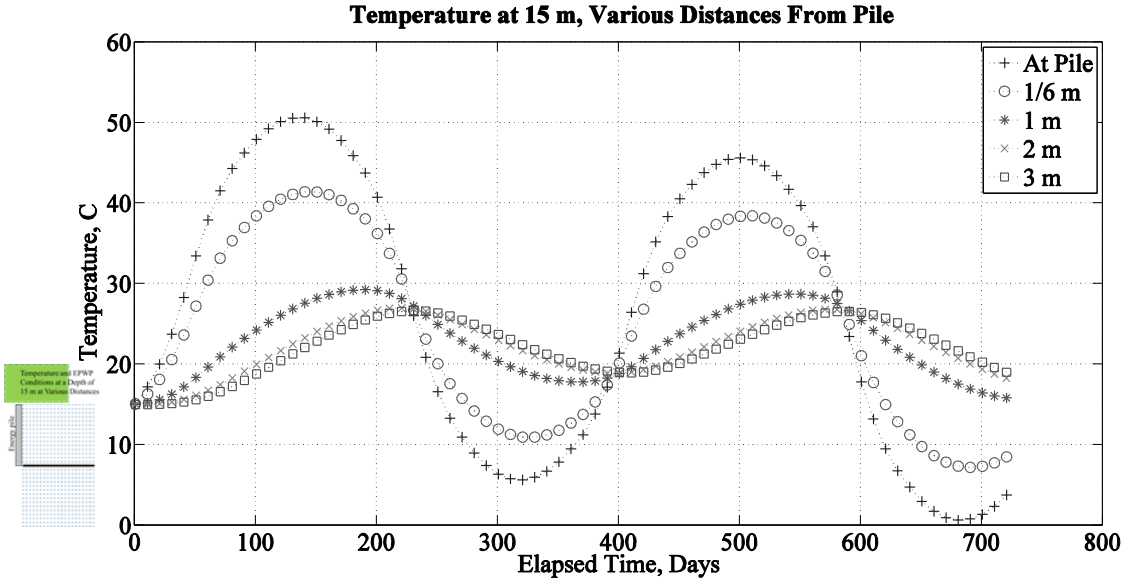

Figure C.18. Temperature values at a depth of 15 m at various distances from the pile, from the time of pile installation to the end of the model run, with transient ground-surface temperatures.

The EPWP values shown at a depth of 15 m in Figures C.19 and C.20 are slightly lower than those at the previous depths, but the EPWP values are similar to the values shown in Figures C.3, C.4, C.11 and C.12.

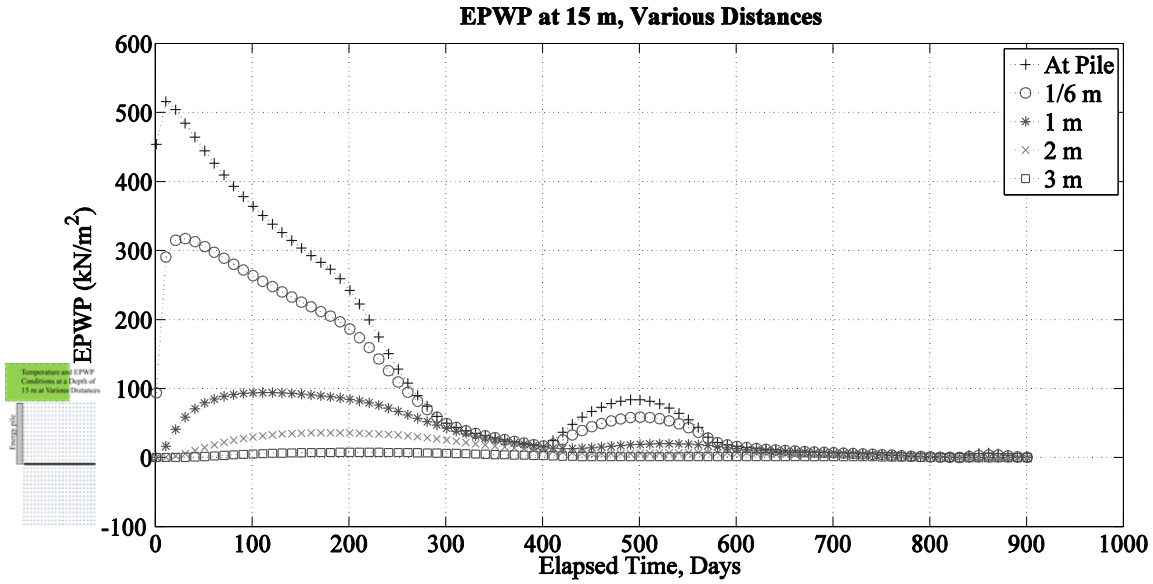

Figure C.19. EPWP at a depth of 15 m at various distances from the pile, from the time of pile installation to the end of the model run. The ground-surface temperature is a constant 15 °C.

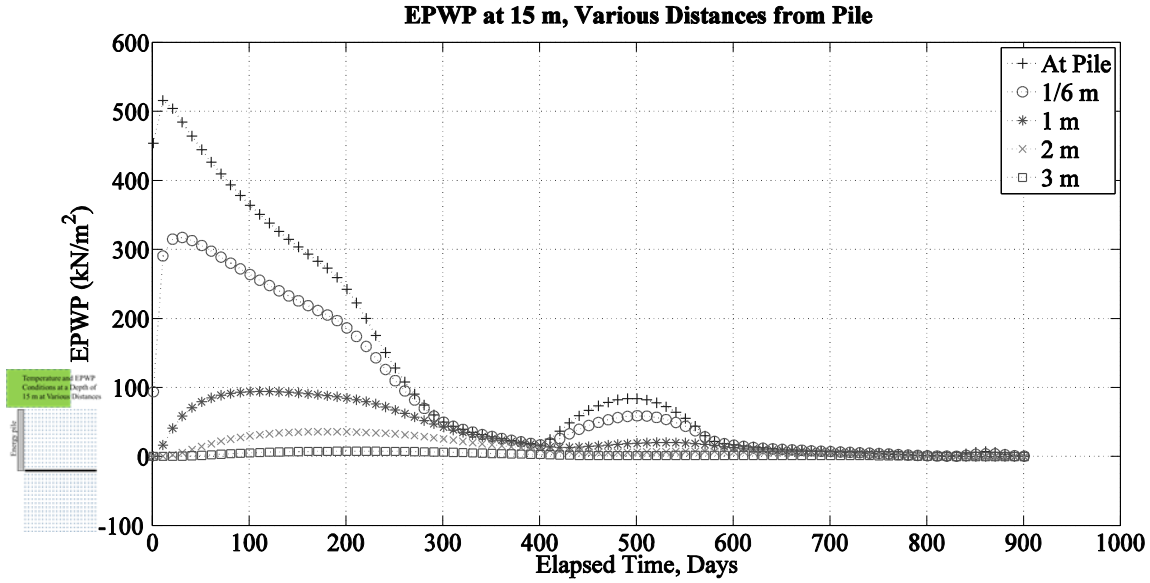

Figure C.20. EPWP at a depth of 15 m at various distances from the pile, from the time of pile installation to the end of the model run, with transient ground-surface temperatures.

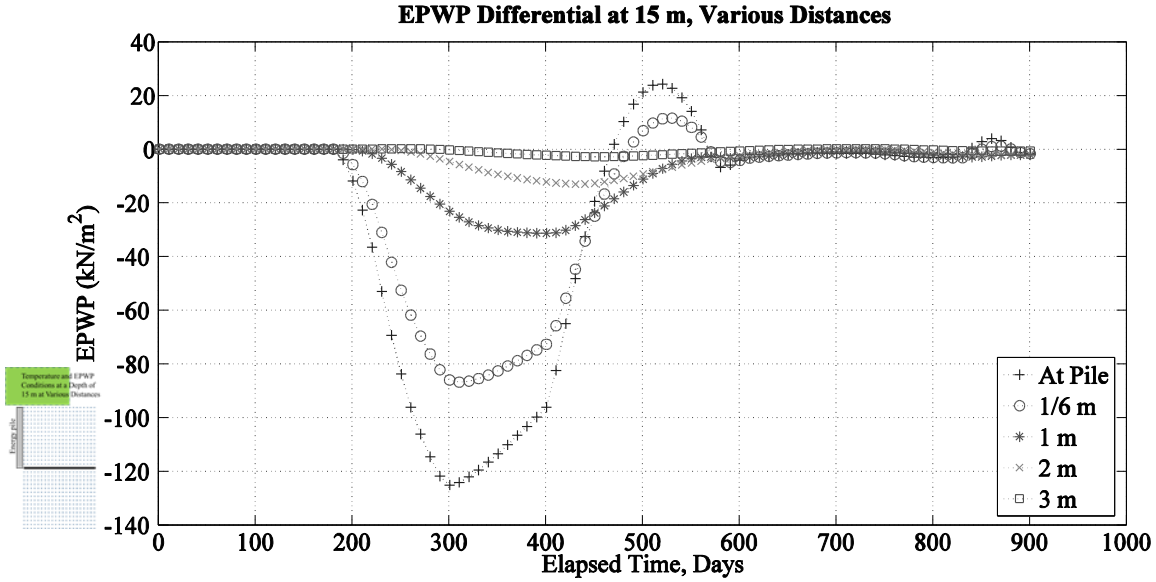

Figure C.21. EPWP differential between model runs with and without HVAC introduction, at a depth of 15 m at various lateral distances from the pile surface. The ground-surface temperature is a constant 15 °C.

The differences between Figure C.21 and Figure C.22 are negligible.

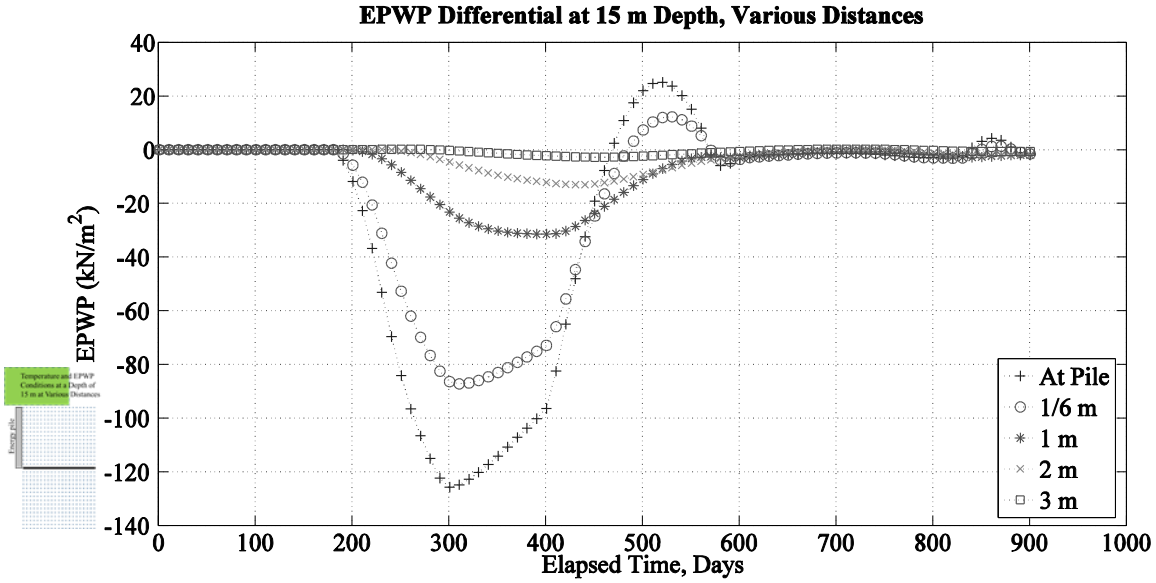

Figure C.22. EPWP differential between model runs with and without HVAC introduction, at a depth of 15 m at various lateral distances from the pile surface, with transient ground-surface temperatures.

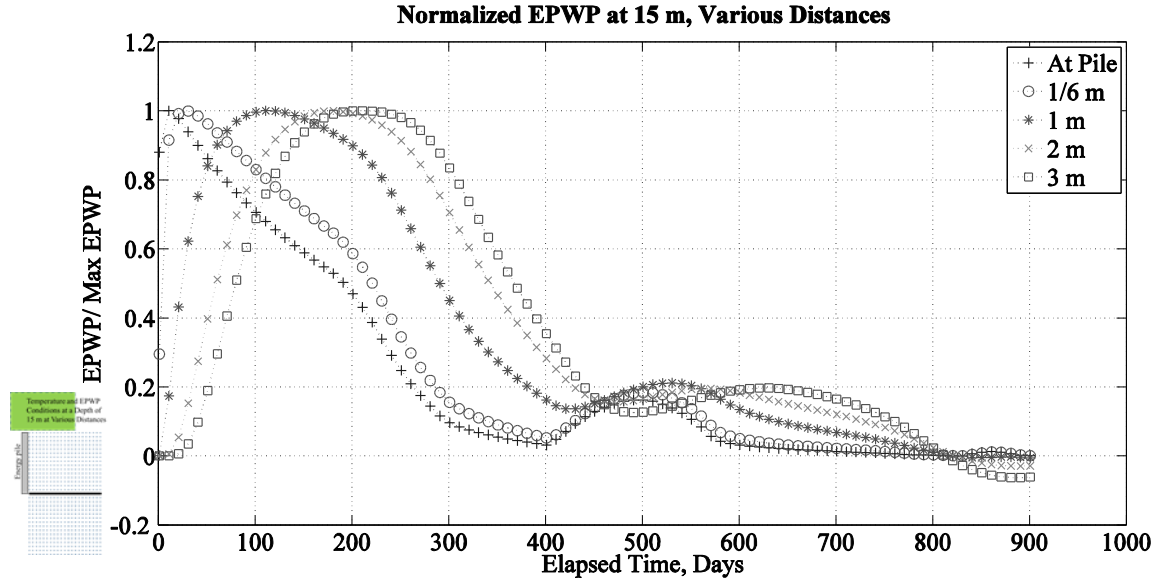

Figure C.23. EPWP, normalized to the peak EPWP, at a depth of 15 m at various lateral distances from the pile surface, from the time of pile installation to the end of the model run. The ground-surface temperature is a constant 15 °C.

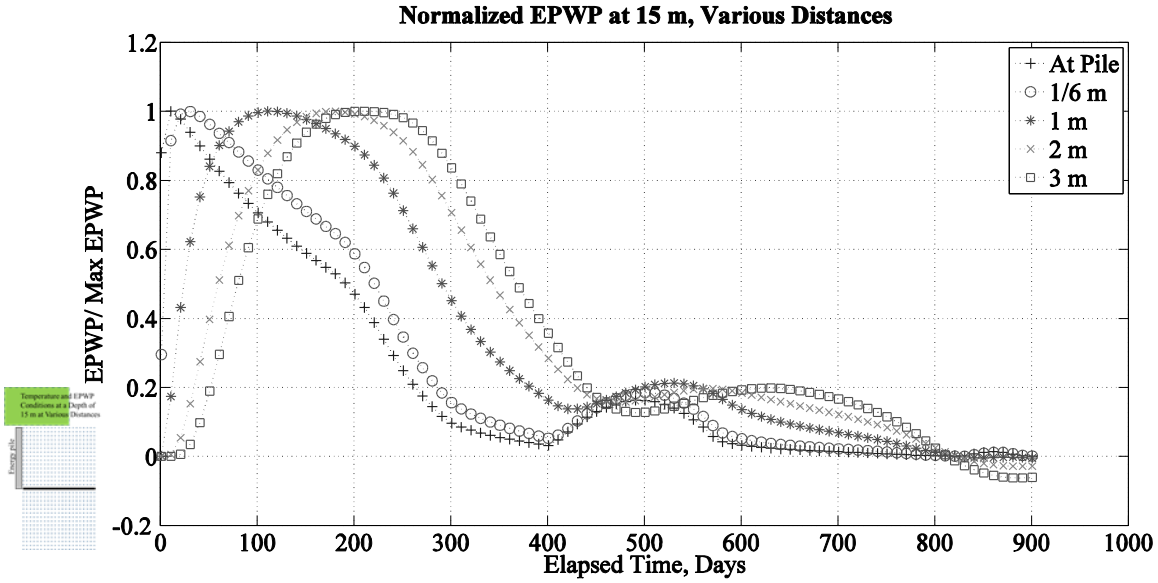

Figure C.24. EPWP, normalized to the peak EPWP, at a depth of 15 m at various lateral distances from the pile surface, from the time of pile installation to the end of the model run, with transient ground-surface temperatures.

Variations of Temperature and Excess Pore-Water Pressure Results at Variations of Temperature and EPWP at Depths of 5 m, 10 m, and 15 m at Various Lateral Distances from a Drilled-Shaft Energy-Pile

The following figures present data that has been previously presented from a different perspective.

Figures C.25, C.28, and C.31 present the temperature effects at depths of 5 m, 10 m, and 15 m, respectively, at various lateral distances from the drilled shaft. EPWP is, however, presented in Figures C.26, C.29, and C.32 in the same way. Generally, temperature and EPWP values decrease and peak later as the lateral distance from the drilled shaft increases. Abrupt changes in the EPWP and temperature values along the drilled shaft occur at the time the heating-variation pattern (i.e., equation in the model) is changed, either due to changing seasons or changing from heating to cooling. EPWP and temperature values are generally lower at the 15m depth than at 5m and 10m ones.

Although as shown in Figure C.1, all the temperatures along the drilled shaft are equal to each other.

Variations of Temperature and EPWP at a 5m Depth

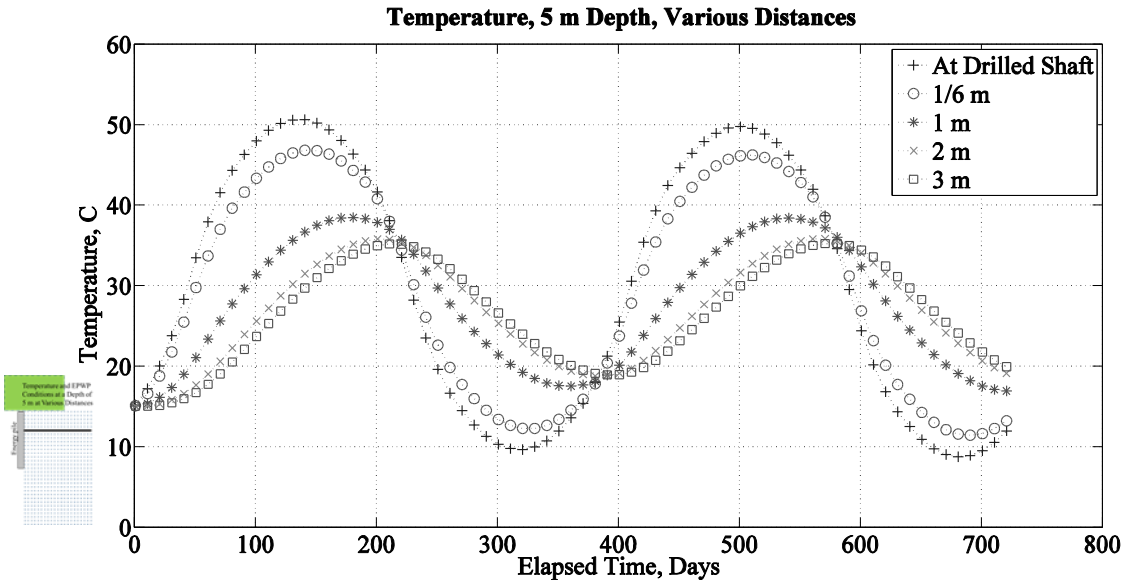

Figure C.25. Temperature at a depth of 5 m at the distances shown for the two-year model run.

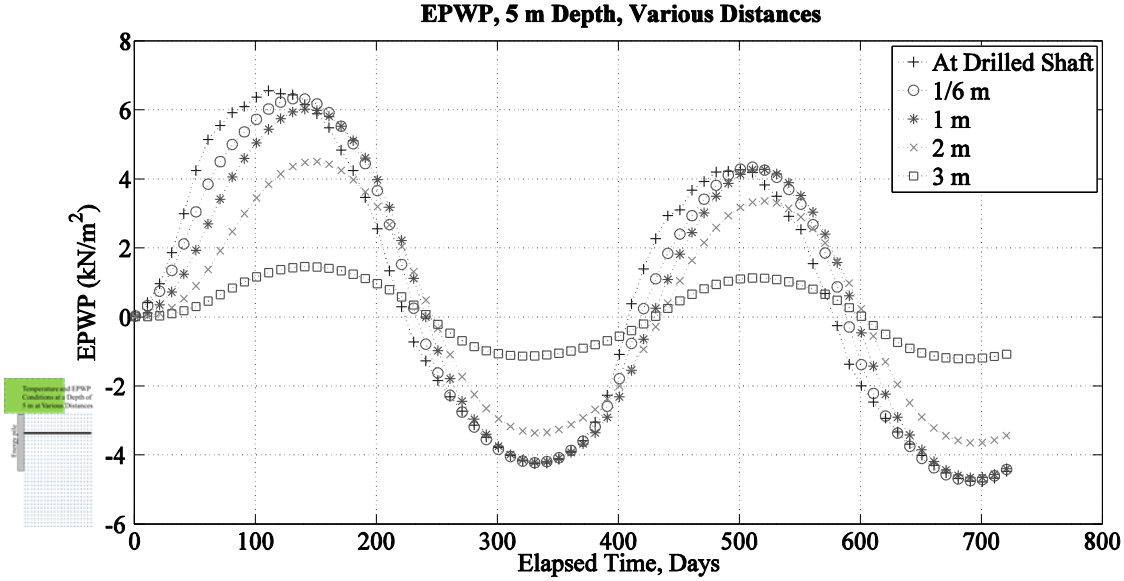

Figure C.26. EPWP at a depth of 5 m at the distances shown for the two-year model run.

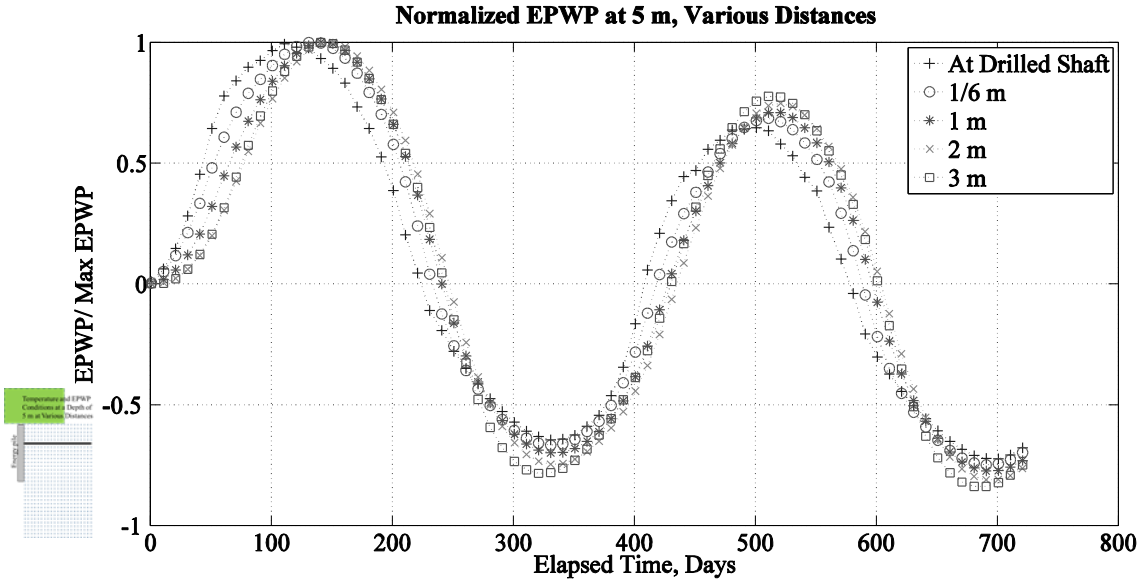

Figure C.27. EPWP, normalized to the peak EPWP, at a depth of 5 m at the distances shown for the two-year model run.

Variations of Temperature and EPWP at a 10m Depth

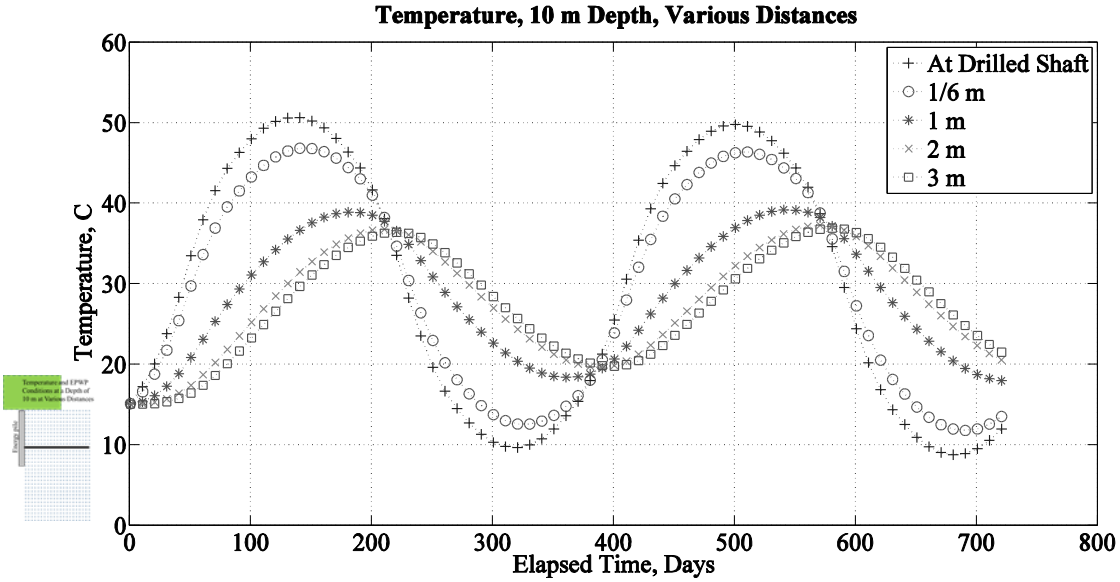

Figure C.28. Temperature at a depth of 10 m at the distances shown for the two-year model run.

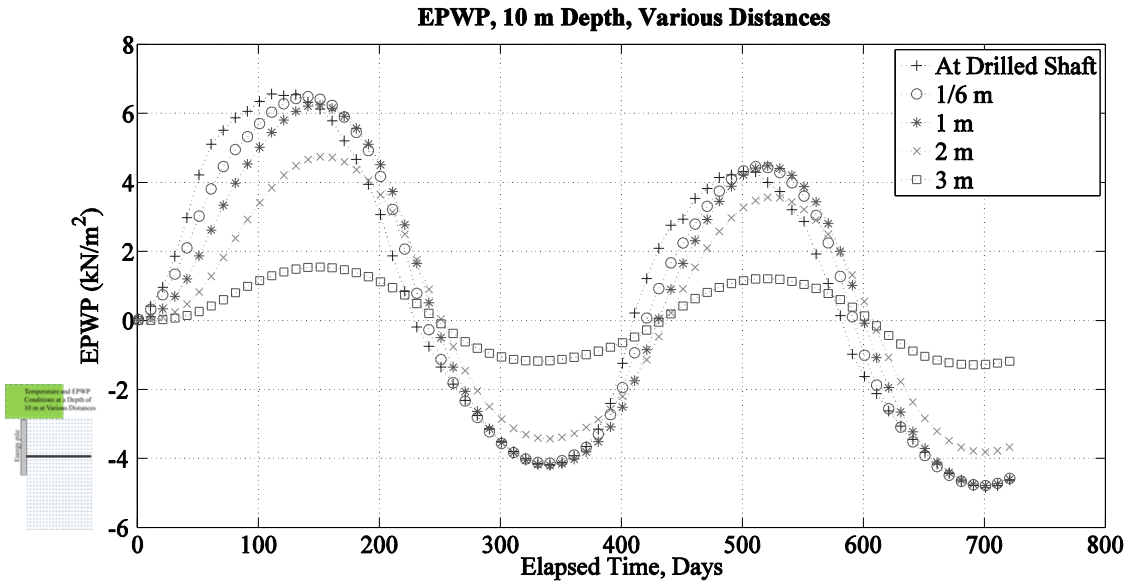

Figure C.29. EPWP at a depth of 10 m at the distances shown for the two-year model run.

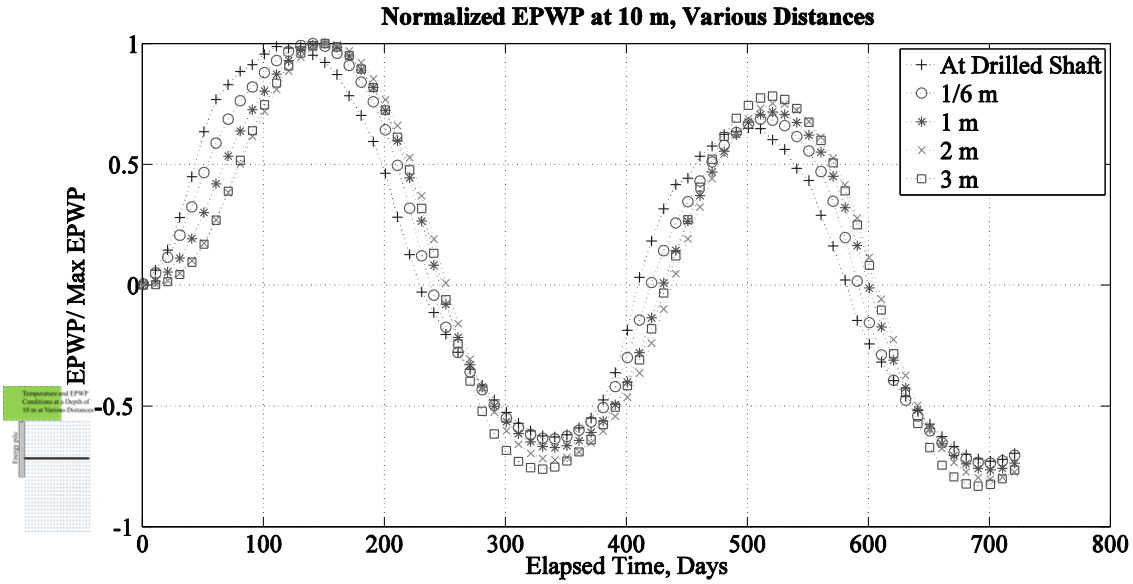

Figure C.30. EPWP, normalized to the peak EPWP, at a depth of 10 m at the distances shown for the two-year model run.

Variations of Temperature and EPWP at a 15m Depth

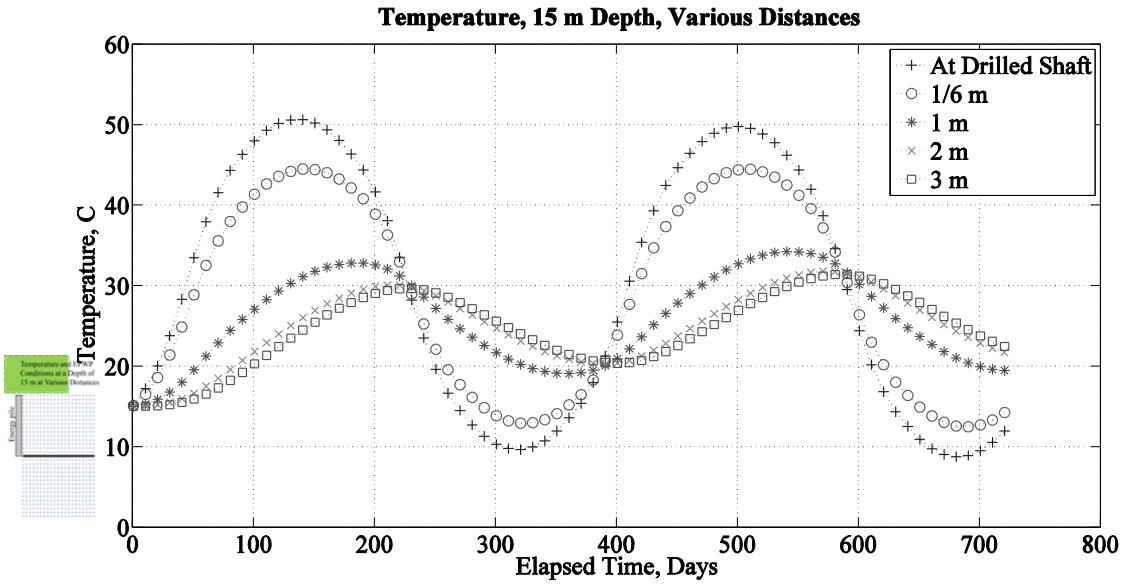

Figure C.31. Temperature at a depth of 15 m at the distances shown for the two-year model run.

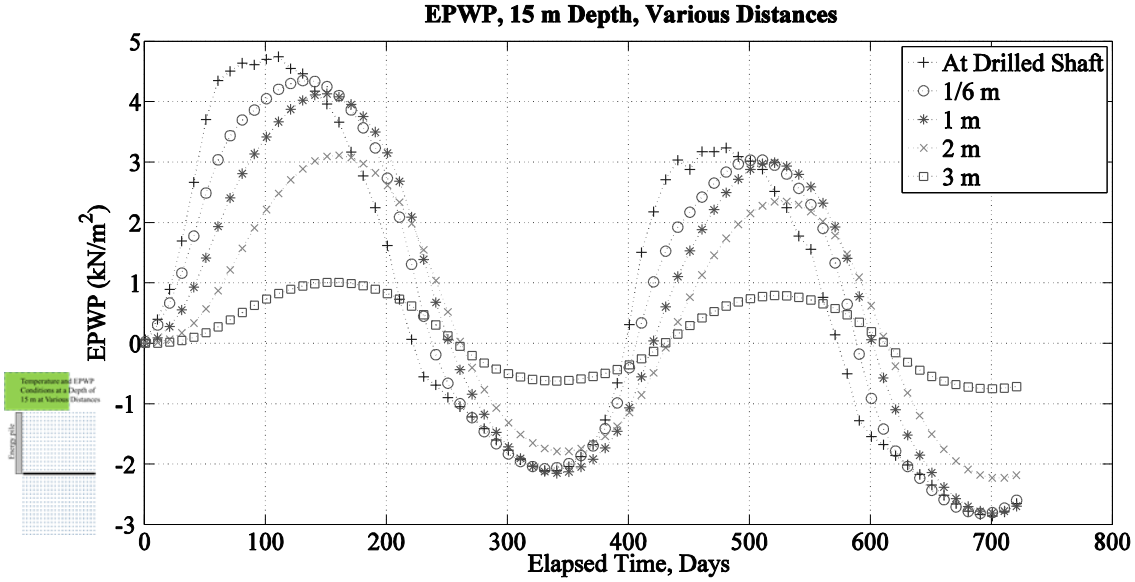

Figure C.32. EPWP at a depth of 15 m at the distances shown for the two-year model run.

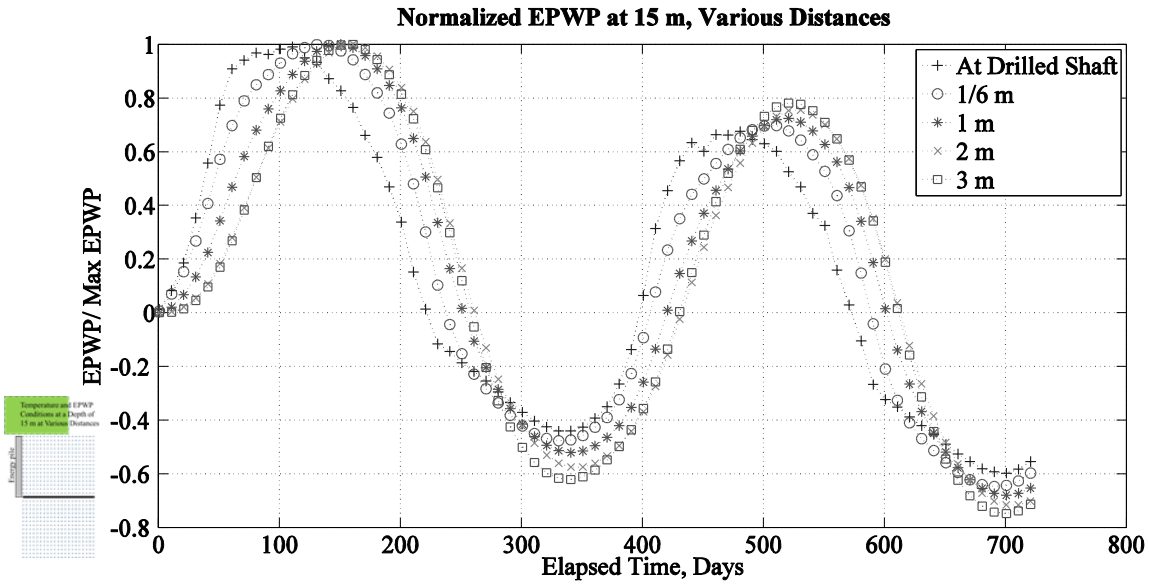

Figure C.33. EPWP, normalized to the peak EPWP, at a depth of 15 m at the distances shown for the two-year model run.